JOURNAL OF

# METALS

IN 2 SECTIONS—SECTION 1

November 1955

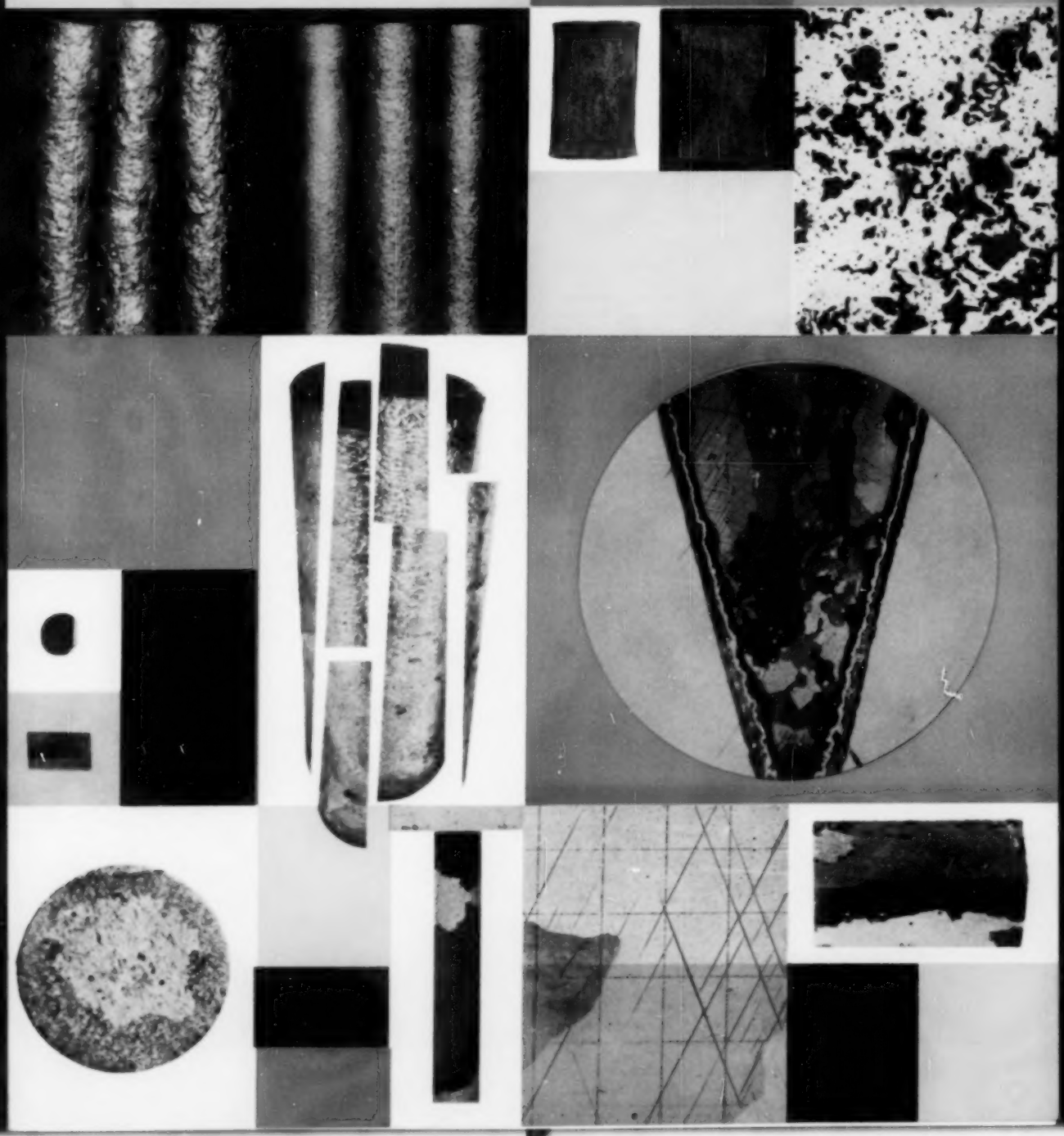

# Bailey EQUIPMENT

contributes to

# STEEL PLANT

## Safety and Efficiency

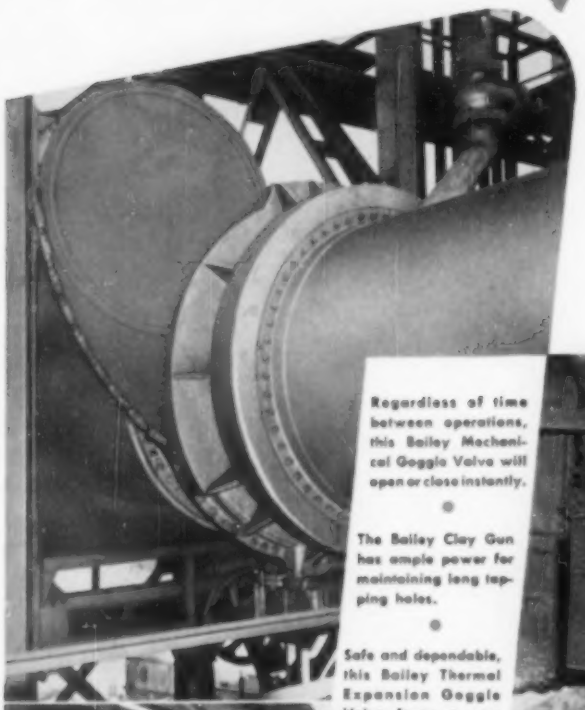

Regardless of time between operations, this Bailey Mechanical Goggle Valve will open or close instantly.

The Bailey Clay Gun has ample power for maintaining long tapping holes.

Safe and dependable, this Bailey Thermal Expansion Goggle Valve forms a gas-tight leakproof seal.

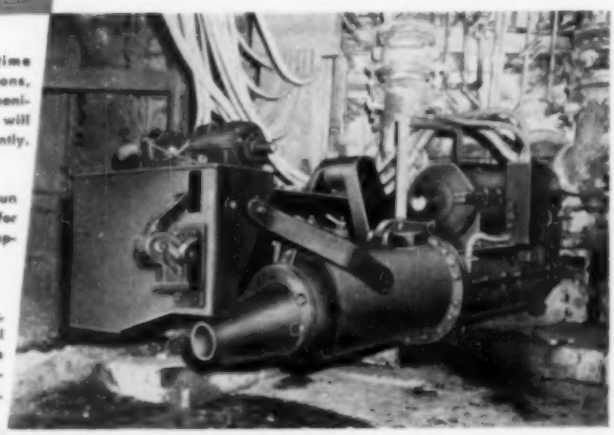

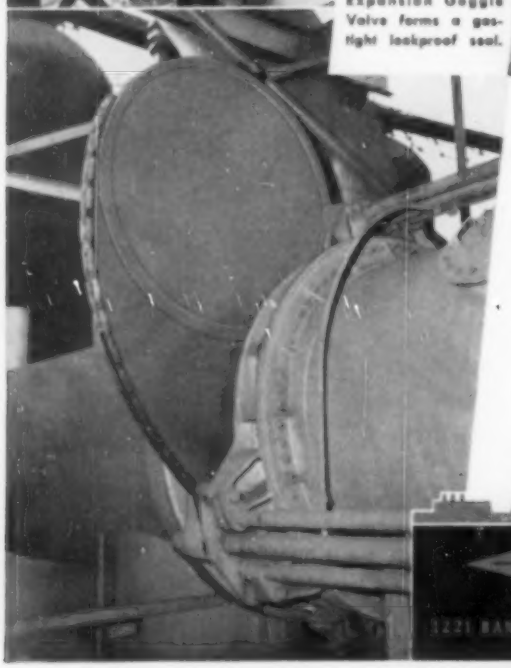

The dependability of Bailey Equipment plays a part in the safe, efficient operation of many major steel plants. All Bailey Equipment is designed and manufactured with two basic considerations in mind—protection for men and equipment, and operation that is dependable and economical.

WILLIAM E. Bailey COMPANY

ENGINEERS

EXPANSION THROUGH QUALITY

3221 BANKSVILLE ROAD PITTSBURGH 16, PA

JOURNAL OF

# METALS

**Published to provide a continuing, authoritative, and up-to-date record of technological, engineering, and economic progress in all branches of the metals industry by the Metals Branch American Institute of Mining and Metallurgical Engineers, Inc. 29 West 39th Street, New York 18**

ALVIN S. COHAN
Manager of Publications
Editor, JOURNAL OF METALS

EDWIN M. WEISS
Associate Editor

M. SNEDEKER — G. M. ZILL
Assistant Editors

GRACE PUGSLEY — Production Manager
W. J. SEWING — Asst. Prod. Mgr.

METALS BRANCH COUNCIL

J. H. Scaff — Chairman
R. W. Shearman — Secretary
J. S. Smart, Jr. — IMD Chairman
A. W. Thornton — ISD Chairman
A. W. Schlechten — EMD Chairman
P. T. Stroup — M. E. Volin
J. S. Marsh — D. S. Eppelsheimer

EDITORIAL ADVISORY COMMITTEE

J. S. Smart, Jr. — Chairman
W. A. Dean — Evan Just
J. C. Kinnear, Jr. — John Marsh
T. D. Jones — M. Tenenbaum

TECHNICAL PUBLICATIONS COMMITTEES

N. Arbiter — AIME Chairman
H. B. Emerick — ISD Chairman
S. J. Dickinson — EMD Chairman
P. A. Beck — IMD Chairman
E. J. Kennedy, Jr. — Secretary

WARREN V. SMITH
Eastern Advertising Manager

BOB WILSON
Western Advertising Manager
Millard Ave., Fox River Grove, Ill.

**The AIME Publishes:**
Journal of Metals
Mining Engineering
Journal of Petroleum Technology

VOL. 7, NO. 11 — NOVEMBER, 1955

COVER

**Harry Brocke points up the growing importance of nuclear metallurgy in his design for this month's cover.**

NEWS

| | | | |
|---|---|---|---|
| **Books for Engineers** | **1143** | **Trends** | **1152** |
| **Employment Service** | **1146** | **Reporter** | **1155** |
| **Coming Events** | **1148** | **Drift of Things** | **1156** |
| **Industrial Notes** | **1150** | **AIME News** | **1195** |

TECHNICAL FEATURES

**Uniform Density and Structure Possible with Simultaneous High Pressure and Temperature** — R. Humphrey, M. Vitella, L. W. Tomarkin **1159**

**Iodide Process Produces Ductile Hafnium for Fabrication** — J. G. Goodwin, W. J. Hurford **1162**

**Efficiencies of Electric Furnaces Can Be Increased by Using Higher Voltages** — E. L. French **1169**

**Short Cycle Heat Treatment Improves Low Alloy Pipe Production** — J. Kniveton **1172**

**Box Car Roof Design for Open Hearths Evaluated at Inland Steel Co.** — P. W. Nutting **1178**

TRANSACTIONS

**Effect of Sinter Mix Composition and Additives on the Quality of Blast Furnace Sinter** — E. C. Rudolphy, C. W. Baquist, D. J. Carney **1179**

**Production and Purification of $TiCl_4$** — L. W. Rowe, W. R. Opie **1189**

TECHNICAL NOTE

**Residual Lattice Strains in Sectioned Bars of Plastically Deformed Iron** — C. J. Newton, H. C. Vacher **1193**

**This issue of JOURNAL OF METALS is in two Sections:**
**Section 1—Magazine** **Section 2—Transactions Section**

Published the first day of each month by the American Institute of Mining and Metallurgical Engineers, Inc., 29 West 39th Street, New York 18, N. Y. Telephone: PEnnsylvania 6-9220. Subscription $8 per year for non-AIME members in United States and North, South and Central America; $10, foreign; $6 for AIME members, or $4 additional in combination with a subscription to "Mining Engineering" or "Journal of Petroleum Technology." Single copies, 75 cents; single copies foreign, $1.00; special issues, $1.50 . . . The AIME is not responsible for any statement made or opinion expressed in its publications . . . Copyright 1955 by the American Institute of Mining and Metallurgical Engineers, Inc. . . . Registered cable address, AIME New York . . . Indexed in Engineering Index, Industrial Arts Index and Chemical Abstracts . . . Reentered as second-class matter Sept. 21, 1949, at the post office at New York, N. Y., under the Act of March 3, 1879. Additional entry established at Manchester, N. H.

# General Electric announces a versatile *new x-ray diffraction unit*

## Featuring one or two tube operation

Here's the latest advance in x-ray diffraction apparatus. It's the new General Electric XRD-5, the unit that's designed with special care to fit any analysis program.

As shown in the box at right — you can start with a simple film set-up. Build up facilities as needed. Possibilities include: film technics for up to six instruments at a time, simultaneous film and direct measurement technics on two different tubes, and fluorescence analysis.

Whatever your analysis requirements — research, raw materials or quality control — this General Electric diffraction unit can be adapted to your exact needs. Get full information from your G-E x-ray representative, or write X-Ray Department, General Electric Company, Milwaukee 1, Wis., for Pub. AY-114.

### *XRD-5 lets you build as your needs grow*

1. Basic XRD-5 includes simple table, one tube, camera and camera tracks, one kv panel, one ma panel, one timer panel, with choice of three cooling methods. You are equipped for film technics.
2. Add a tube unit, another ma panel, a tube selector panel — and you're equipped for two-tube film technic.
3. Add a spectrogoniometer, a horizontal tube support, a direct measurement attachment (No. 2 SPG detector that includes power supply, linear and logarithmic ratemeter, 8-decade scaler) — and you're equipped for simultaneous film and direct measurement technics.
4. Add a spectrometer — and you're fully equipped for fluorescence analysis.
5. Add a helium tunnel assembly — and you're equipped for fluorescent detection of any material down to Atomic No. 15.

*Progress Is Our Most Important Product*

GENERAL ELECTRIC

# Books for Engineers

ORDER YOUR BOOKS THROUGH AIME—Address Irene K. Sharp, Book Dept. AIME members given 10 pct discount whenever possible. Please order Government publications direct from the agency concerned.

**Review of Current Research and Directory of Member Institutions,** *Engineering College Research Council,* American Society for Engineering Education, $2.00, 352 pp., 1955.—This volume reviews current research programs in engineering colleges. It should be of interest to faculty members in determining where the work they are most interested in is being carried out. It is also a help to students in planning their education in institutions which are active in the type of education most suited to their life plans. A comprehensive index to research projects rounds out the volume.

**Comprehensive Inorganic Chemistry,** edited by M. Cannon Sneed and Robert C. Brasted, Vol. 4, **Zinc, Cadmium, and Mercury,** by Howard M. Cyr and the editors and **Scandium, Yttrium, and the Lanthanide Series,** by Thomas D. O'Brien and the editors, *D. Van Nostrand Co. Inc.,* $5.00, 193 pp., 1955.—A part of the 11 volume reference work on chemical elements generally entitled *Comprehensive Inorganic Chemistry,* this volume treats the chemistry of the rare earth elements in detail. It also gives an up-to-date and thorough coverage of zinc, cadmium, and mercury.

**The Inspection and Testing of Metals,** *The Institution of Metallurgists,* 119 pp., 1955.—This collection of papers contains the lectures delivered at the refresher course held in 1954. Contributors are well known experts in the fields with which their lectures deal. The volume is fully illustrated.

**Handbook of Engineering Materials,** edited by Douglas F. Miner and John B. Seastone, *John Wiley & Sons, Inc.,* $17.50, 1111 pp., 1955.—This volume is designed to be a single source of authentic and useful information on materials of manufacturing and construction. Prepared by a staff of specialists, the handbook is arranged by classes of related or similar materials. It has been compiled at a professional level understandable to engineering designers of products or construction projects, research workers, and advanced students. In scope it is more complete than a technical dictionary but less detailed than special textbooks. A comprehensive index is included.

**The Principles of Electromagnetism,** by E. B. Moullin, third edition, *Oxford University Press,* $7.20, 438 pp., 1955—Four major sections of the book cover elements of magnetism, the second law of electrodynamics, iron in magnetic fields, and two groups of special electromagnetic equations. New material has been included on high frequency resistance of rods and coils and a set of 20 worked examples on cylinders and tubes in magnetic fields added.

**Industrial Furnaces,** by W. Trinks, Vol. 2, third edition, *John Wiley & Sons Inc.,* $10.00, 358 pp., 1955.—In this edition advances in the industrial furnace field since 1941 are brought to the attention of the reader. The book discusses and describes practically everything of value required for efficient furnace operation. The general arrangement of the previous edition has been retained, but important changes and revisions have been made.

Testing of metals made easy
...with fine accuracy assured
To test-best with mechanical ease, yet assured accuracy, for any given physical property—it is important you have *exactly the right* machine. For more than 40 years Steel City has designed and built the correct machines for various types of work, with the customers' requirements utmost in mind.
Illustrated Model UK-300-M is the *right* machine for testing Brinell Hardness where application requires limited production rate and fine accuracy. Machine is motorized, floor mounted and has wide range of application. Minimum maintenance needed.
Steel City has qualified sales representatives in major metal-working areas for your convenience. Write today for name of nearest representative . . . and detail information on complete line.
Manufacturers of machines for testing physical properties of metals, including:
Steel City Testing Machines Inc.
Brinell Hardness
Ductility
Tensile
Compression
Transverse
Hydrostatic
Proving Instruments
Flex-Tester
8825 Lyndon Ave. Detroit 38, Mich.
. . . and Special Testing Machines.

*Books, continued—*

**Principles of Mass and Flow Production,** by Frank G. Woollard, *Philosophical Library, Inc.*, $7.50, 195 pp., 1955.—Describing economical means for increasing production, the book is of value to students of engineering economics because it is a practical exposition of the laws that lie behind modern manufacturing. The principles and methods described are suitable for the manufacture of almost every article that is continuously saleable. The book also deals with some of the problems arising from the increased use of automation.

**Machine Design,** by Paul H. Black, second edition, *McGraw Hill Book Co., Inc.*, $7.50, 471 pp., 1955—Intended both as text and a reference book for design offices, this book covers the fundamentals of the design of machine elements and the design and selection of units of power transmission, of strength, rigidity, wear, and economy of manufacture and operation. The practical aspects are emphasized including the important factors leading to failure and the latest treatment of stress concentration.

**Chemical Engineering Cost Estimation,** by R. S. Aries and R. D. Newton, *McGraw-Hill Book Co. Inc.*, $6.00, 263 pp., 1955—The subjects covered include methods for determining capital investment, equipment and other components of physical plant cost, manufacturing and general expenses, profit, effect of plant size and operating level, plant location, and the economic evaluation of projects. The principles and extensive qualitative data are applicable in fields other than chemical engineering.

**Handbook of Industrial Engineering and Management,** edited by W. G. Ireson and E. L. Grant, *Prentice-Hall, Inc.*, $16.00, 1203 pp., 1955—In addition to covering the traditional subjects such as time study, plant layout, etc., this new handbook contains sections on engineering economy, budgeting, standardization, safety engineering, industrial hygiene, quality control, industrial statistics, and operations research. Treatment stresses general principles and the best current practice.

**Fundamentals of Friction and Lubrication in Engineering,** *American Society of Lubrication Engineers*, $3.50, 196 pp., 1954—The 12 papers presented in this first ASLE National Symposium cover many aspects from historical and general surveys of the hydrodynamics of lubrication to specialized treatments of various bearing types, constitution of lubricants, friction problems, and wear.

**Powder Metallurgy,** Technical Assistance Mission No. 141, *Organisation for European Economic Cooperation*, $3.00, 309 pp., 1955.—This comprehensive book is the result of the work of a technical assistance mission that recently visited the United States. The mission visited 43 factories, universities, and research centers. The book covers electrical and magnetic materials, hard metals, refractory materials, and engineering and structural parts. Please order from: O. E. E. C. Mission, Publications Office, 2000 P St., N. W., Washington 6, D. C.

**Principles of Flotation,** by K. L. Sutherland and I. W. Wark, *Australasian Institute of Mining & Metallurgy*, 489 pp., 1955.—The original edition of this book, published in 1938, was written by I. W. Wark. The demand for it persisted long after the original edition was exhausted. This revised and enlarged version is the joint work of Mr. Wark, chief, Div. of Industrial Chemistry of the Commonwealth Scientific & Industrial Research Organization, and Mr. Sutherland, assistant chief of that Division. An excellent reference and text it will be of value to those in the fields of mineral dressing, surface chemistry, and industrial chemistry. Please order direct from 399 Little Collins St., Melbourne, Australia.


*Another "must" for proper Metallographic Control*

**The AB MICROMET ETCHER**

A self-contained variable d.c. power supply for electrolytic etching of prepared metallographic specimens.

This neat compact unit is always ready to operate eliminating time consuming hook ups and delays due to battery failure.

All controls are advantageously located for fingertip adjustment. Twin type voltmeter and ammeter are positioned for ready and easy observation.

Properly identified leads for the cathode and the anode with forceps for contacting or holding the specimen are supplied. A replaceable beaker and fitted cathode clip to support either the vertical or horizontal stainless steel cathode are furnished.

*Buehler Ltd.*

METALLURGICAL APPARATUS
2120 GREENWOOD STREET
EVANSTON, ILL., U.S.A.

# GA&F

## Carbonyl Iron Powders

These are spherical iron powders—as shown in the surrounding photomicrograph. Diameters run from 3 to 20 microns; in some types the iron content is as high as 99.6% to 99.9% . . . New types have recently been developed; there are today a total of 10—which may be classified as shown in this table.

| FIRMNESS / PARTICLE SIZE RANGE | SOFT (EASILY COMPRESSIBLE TO HIGH DENSITIES) | | HARD (PRESERVE SPHERICAL SHAPE UNDER PRESSURE) | |
|---|---|---|---|---|
| | "NORMAL" | SPECIAL FOR HIGH Q | "NORMAL" | SPECIAL FOR HIGH Q |
| COARSE | L | GQ-4 | E | J |
| MEDIUM | HP | GS-6 | TH | – |
| FINE | C* | – | SF | W |

*C HAS MEDIUM PARTICLE SIZE RANGE, BUT IS HARDER THAN HP.

Let us send you a 32-page book giving characteristics and applications . . . We invite you to call upon our research facilities and Technical Service Department for assistance in developing new applications or new products involving the use of any of these powders. We also invite inquiries for powders whose performance characteristics are different from those exhibited by any of our existing types . . . Kindly address Department 44.

*from Research to Reality . . .*

ANTARA CHEMICALS

A SALES DIVISION OF GENERAL ANILINE & FILM CORPORATION

435 HUDSON STREET • NEW YORK 14, N. Y.

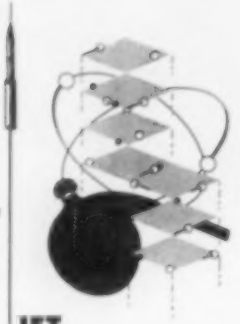

*Developers of the Corporal Guided Missile*

**JET PROPULSION LABORATORY**

CALIFORNIA INSTITUTE OF TECHNOLOGY

*Active in all phases of propulsion and related materials research.*

The nation's foremost guided-missile research and development facility, established in 1940, offers exceptional opportunities for engineers and research scientists in a broad range of propulsion and materials research problems. Special interests include polymer chemistry, solid-state physics, heat transfer, propellant research, metallurgy, and high-temperature technology. The Laboratory offers a stimulating blend of academic and industrial environments. Attractive salaries are offered.

*A brochure describing opportunities and activities at the Laboratory will be sent upon request.*

JET PROPULSION LABORATORY
CALIFORNIA INSTITUTE OF TECHNOLOGY
4800 OAK GROVE DRIVE
PASADENA 3, CALIFORNIA


## —Personnel Service—

THE following employment items are made available to AIME members on a nonprofit basis by the Engineering Societies Personnel Service Inc., operating in cooperation with the Four Founder Societies. Local offices of the Personnel Service are at 8 W. 40th St., **New York 18;** 100 Farnsworth Ave., **Detroit;** 57 Post St., **San Francisco;** 84 E. Randolph St., **Chicago 1.** Applicants should address all mail to the proper key numbers in care of the New York office and include 6c in stamps for forwarding and returning application. The applicant agrees, if placed in a position by means of the Service, to pay the placement fee listed by the Service. AIME members may secure a weekly bulletin of positions available for $3.50 a quarter, $12 a year.

### —— POSITIONS OPEN ——

**Metallurgist,** ceramist, to lead programs of materials and process development in field of cemented tungsten carbides. Degree and five years' experience desired in powder metallurgy processes or refractory alloy development. Strong theoretical background preferred plus familiarity with powder metal processing technique and equipment. Location, Michigan. W2283D.

**Assistant Metallurgists,** B.S. engineering, 22 to 32, for the development, piloting through production, and production control of automatic and semiautomatic welding rods and/or their fluxes. Must have had some experience with welding and knowledge of metallurgy and welding. Salary, $4800 to $6000 a year. Employer will negotiate placement fee. Location, South Chicago. C3907.


**METALLURGISTS**
**PHYSICISTS**
**MECHANICAL ENGINEERS**

Expansion plans for our Metallurgical Research Laboratories have resulted in several openings with excellent opportunities for advancement. Well equipped laboratory is located in Pacific Northwest amid attractive surroundings and ideal climate. Liberal policy on publications. Among positions to be filled are:

1. X-Ray Diffractionist interested in metallurgical problems.
2. Metallurgist to study phase diagrams and metallographic structures.
3. Mechanical Engineer or Physicist interested in strength of materials, vibration, plasticity, etc. Must have advanced degree and research experience in these fields.
4. Mechanical Engineer or Physicist interested in analytical mechanics as applied to uses of light metals.

Salaries depend on experience and past record. Replies will be held in strict confidence. Send full details of experience and salary requirements to:

S. E. Maddigan, Assistant Director
Department of Metallurgical Research
**Kaiser Aluminum & Chemical Corporation**
**Spokane 69, Washington**


**Metallurgists,** young, B.S., M.S. and Ph.D. degrees. Experience desirable for company engaged in all phases of semiconductor work; research, development, pilot production, and regular production. Salaries open. Location, Massachusetts. W2258.

**Assistant Mill Superintendent** for large base metal mine in South West Africa. Should be technical graduate, with at least five years base metal flotation experience. Three year contract, transportation for self and family and salary while traveling. House furnished for married man. Climate and living conditions excellent. F2163.

**Metallurgical Engineer,** young, graduate, with at least three years experience covering welding, heat treating, testing and/or manufacturing of ferrous and nonferrous equipment. Location, upstate New York. W2147(a).

**Field Engineer,** young, with equipment experience in chemical, metallurgical or process industry for service work covering equipment improvements. Considerable traveling. Salary, $4800 to $6000 a year. Location, eastern states. W2144.

**Junior Metallurgist,** degree in metallurgy, mining or chemical engineering, to perform control work and ore dressing research in a 5000 ton magnetic gravity flotation mill. Excellent opportunity for recent graduate to learn many phases of milling. Salary open. Location, Northeast. W2127.

**Production Engineer,** young, M.E. graduate, with metal mill processing experience for rolling mill production duties on shift basis. Salary, $4800 to $6000 a year. Location, Midwest. W2136.

**Metallurgical Engineer,** graduate, with minimum of five years experience. Salaries, $6000 to $10,000 a year. Location, Midwest. W2135C(c).


**METALLURGICAL RESEARCH OPPORTUNITIES**

Battelle's extensive metallurgical research program is growing. Additional career opportunities have, therefore, developed for B.S., M.S., and Ph.D. graduates with appropriate training, experience, or interests in any of the following fields: physical, process, foundry, high-temperature, mechanical and extractive metallurgy; light-alloy development; minerals processing; welding and reactor technology. Excellent technical facilities, informal teamwork operational method, merit promotional policy, liberal staff benefits and many other advantages. For additional information please write today to:

The Personnel Manager
**BATTELLE MEMORIAL INSTITUTE**
505 King Avenue
Columbus 1, Ohio

**Metallurgist,** 26 to 40, M.A. or B.A. in metallurgy, to assist in development and trouble shooting program, to conduct metallurgical tests relating to design and operating problems and the investigation of processes and to advise personnel of the various divisions on the solution of metallurgical problems. Salary, $6838 a year to start. Must be U.S.A. citizen. Location, New York Metropolitan area. W2255(a).

**Metallurgical Engineer,** young, with steel products experience for analytical and application engineering duties with steel converter. Salary, $4800 to $5400 a year. Location, northern New Jersey. W2235.

**Metallurgical Engineer** with melting experience, including vacuum techniques for application engineering and development work with equipment manufacturer. Salary, $8000 to $10,000 a year. Location, Massachusetts. W2194.

**Metallurgical Engineer**, with B.S. in chemical, metallurgical, or mechanical engineering, and at least five years ferrous, furnace, and foundry experience for field development with process equipment manufacturer. Considerable traveling in East and Midwest. Salary, $7200 to $8400 a year. Headquarters, New York, N. Y. W2179.

## PROFESSIONAL SERVICES

**Limited to AIME members, or to companies that have at least one AIME member on their staffs. Rates $40 per year per inch.**

**DR. B. EGEBERG**
*Metallurgical Consultant*
Reg. Prof. Engr.
Steel & Metals
Operations — Research
**Meriden, Conn.**

**LEDOUX & COMPANY**
Chemists Assayers Spectroscopists
**SHIPPERS REPRESENTATIVES**
Mine Examination Analyses
**359 Alfred Ave. Teaneck, New Jersey**

**MAX STERN**
**Consulting Engineer**
Expert for Scrap Recovery and Shipwrecking — Modernization of Plants and Yards for Ferrous and Nonferrous Metal Scrap
**149 Broadway New York 6, N. Y.**

**H. L. TALBOT**
**Consulting Metallurgical Engineer**
Extraction and Refining of Base Metals
Specializing in Cobalt and Copper
**Room 330, 84 State St., Boston 9, Mass.**


**TAM**
Zirconium-Magnesium
**MASTER ALLOY**

## Easy, Economical Alloying

Readily soluble in production heats of magnesium, TAM's Master Alloy is a most efficient method of alloying zirconium with magnesium. Recoveries of zirconium are high. Fuming in the foundry is minimized and, as a plus feature, the material is easy to store and handle.

The resulting magnesium alloys are known for their retention of high strength at elevated temperatures, fine grained structure, freedom from microporosity and microshrinkage, and minimized contamination. As a result, extruding and casting are improved... useful applications expanded.

TAM Master Alloy has been proved in use by both large and small foundries. Complete detailed information can be obtained through our field engineers and by writing our N.Y.C. office.

**TAM PRODUCTS**
Registered U.S. Pat. Off.

**TITANIUM ALLOY MFG. DIVISION**
**NATIONAL LEAD COMPANY**
*Executive and Sales Offices:*
111 Broadway, New York City
*General Offices, Works and Research Laboratories:*
Niagara Falls, New York

TAM is a registered trademark.

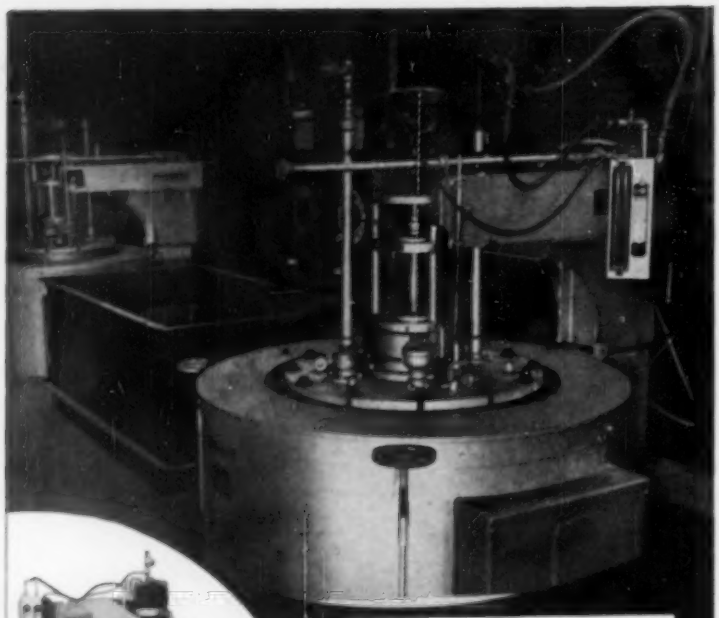

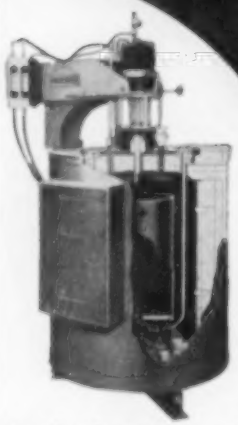

HEVI DUTY®

Pressure Carburizing FURNACES

Hevi Duty Construction — Return Bend Heating Coils — Graded layers of insulation.

## Simplify Control of the Carbon Case

Carburizing with a positive pressure inside the retort has simplified the obtaining of exact carbon concentrations on the surface of the work and to specified case depths. Close case tolerances and shorter carburizing cycles are additional advantages.

Identical results are assured from heat to heat because conditions in the retort can easily be duplicated. Forced atmosphere circulation assures uniform cases in the densest loads. You, too, can produce consistently uniform results if you specify Hevi Duty Verticle Retort Furnaces for Carburizing, Nitriding, Dry Cyaniding, and Bright Annealing.

Write for Bulletin HD - 646R.

**Consult your nearest Hevi Duty Office for more information —**

Eastern District
50 Journal Square
Jersey City 6, N. J.

Cleveland District
1979 Union Commerce Bldg.
Cleveland 14, Ohio

Chicago District
205 W. Wacker Drive
Chicago 6, Illinois

California District
15026 Oxnard St.
Van Nuys, Calif.

**HEVI DUTY ELECTRIC COMPANY**

MILWAUKEE 1, WISCONSIN

*Heat Treating Furnaces... Electric Exclusively*
*Dry Type Transformers* *Constant Current Regulators*


## — Coming Events —

**Oct. 31-Nov. 2, National Lubricating Grease Institute**, annual meeting, Edgewater Beach Hotel, Chicago.

**Nov. 1-3, Investment Casting Institute**, annual meeting, Detroit.

**Nov. 1-5, World Symposium on Applied Solar Energy**, Westward-Ho, Phoenix.

**Nov. 2, SAE**, The Chase, St. Louis.

**Nov. 3-4, Society for Advancement of Management**, measurement of management conference, Hotel Statler, New York.

**Nov. 4, AIME**, Pittsburgh Local Section, and Pittsburgh NOHC Local Section, off-the-record meeting, William Penn Hotel, Pittsburgh.

**Nov. 7-8, Western Governors Mineral Policies Conference**, Sacramento.

**Nov. 7-9, Eastern Joint Computer Conference**, Hotel Statler, Boston, Mass.

**Nov. 9, Stanford Research Institute**, associates' day, Stanford, Calif.

**Nov. 9-11, Industrial Management Society**, time and motion study and management clinic, Sherman Hotel, Chicago.

**Nov. 13-18, ASME**, annual meeting, Congress, Conrad Hilton, and Sheraton-Blackstone Hotels, Chicago.

**Nov. 15, AIME, NOHC**, Buffalo Section, Royal Connaught Hotel, Hamilton, Ont.

**Nov. 16, AIME**, NOHC, Western Section, Rodger Young Auditorium, 936 W. Washington Blvd., Los Angeles.

**Nov. 16, AIME**, NOHC, Northern Ohio Section.

**Nov. 16-17, Industrial Hygiene Foundation**, annual meeting, Mellon Institute, Pittsburgh.

**Nov. 16-18, Steel Founders' Society of America**, annual technical and operating conference, Hotel Carter, Cleveland.

**Nov. 17-18, American Mining Congress**, coal div. conference, William Penn Hotel, Pittsburgh.

**Nov. 17-18, American Society for Quality Control**, midwest conference, Schroeder Hotel, Milwaukee.

**Nov. 27-30, American Institute of Chemical Engineers**, annual meeting, Statler Hotel, Detroit.

**Nov. 28-Dec. 1, Air Conditioning and Refrigeration Institute**, exposition, Auditorium, Atlantic City.

**Dec. 7, AIME**, New York Powder Metallurgy group, Brass Rail Restaurant, New York.

**Dec. 7-9, AIME, Electric Furnace Steel Conference**, William Penn Hotel, Pittsburgh.

**Dec. 10-16, International Atomic Exposition**, Cleveland Public Auditorium, Cleveland.

**Dec. 12-16, Nuclear Engineering and Science Congress**, EJC, Cleveland Public Auditorium, Cleveland.

**Dec. 20-22, Indian Institute of Metals**, general meeting, Calcutta, India.

**Jan. 18, 1956, AIME**, NOHC, Western Section, Rodger Young Auditorium, 936 W. Washington Blvd., Los Angeles.

**Jan. 27, AIME**, Blast Furnace & Coke Assn., Del Prado Hotel, Chicago.

**Feb. 20-23, AIME**, annual meeting, Statler and New Yorker hotels, New York.

**Mar. 19-21, AIME**, Niagara Frontier Local Section, Regional Meeting on Reactive Metals, Hotel Statler, Buffalo.

**Mar. 21, AIME**, NOHC, Western Section, Rodger Young Auditorium, Los Angeles.

**Mar. 29-30, AIME**, Southern California Local Section, Symposium on Physical Metallurgy of Titanium, University of California, Los Angeles.

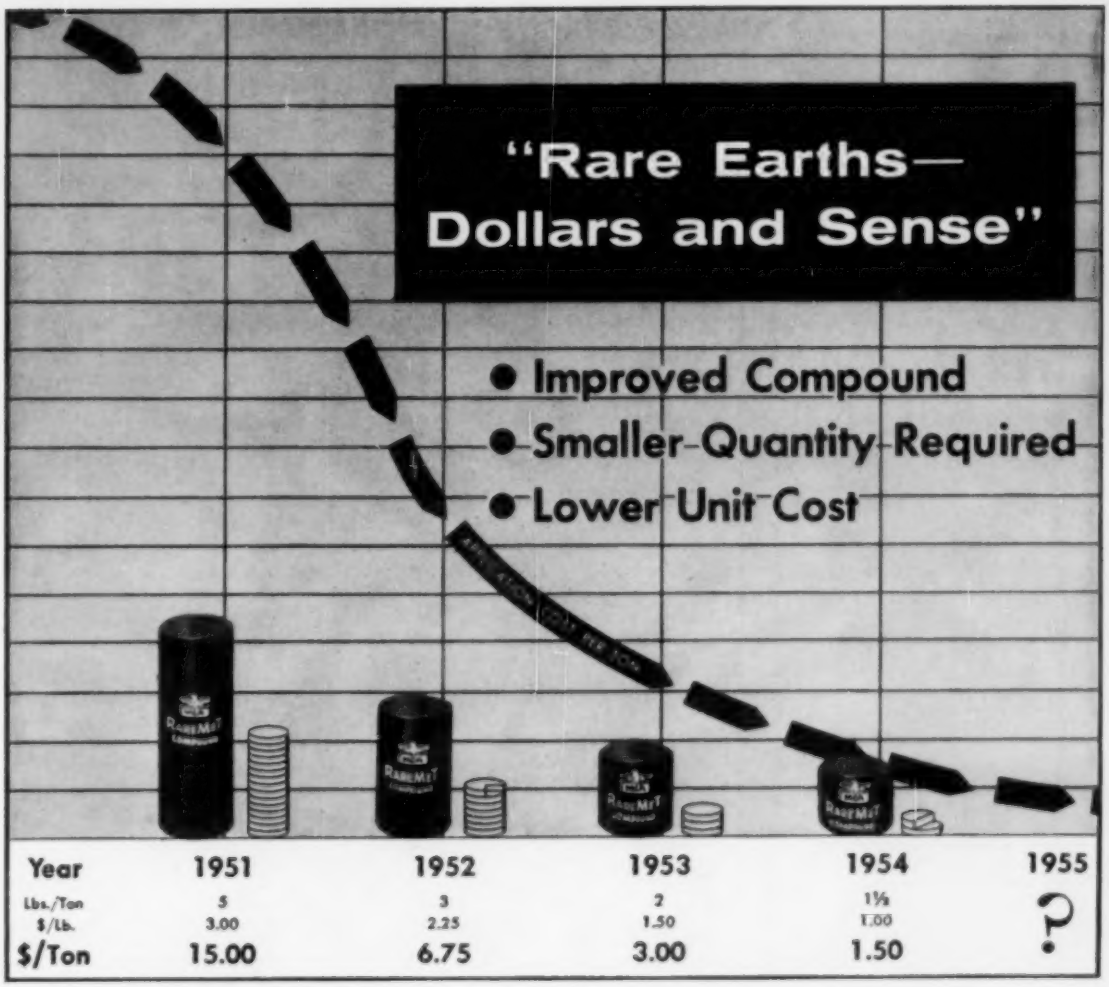


So rapid has been the advance in technical progress and use of rare earths (Trade Name: MCA RareMeT Compound) that in the brief span of four years, about one-fourth as much is needed to accomplish the desired results, at one-third the cost per pound. Now, the economics in favor of rare earths are ten times as great as they were four years ago.

In OPEN HEARTH STEELS, the improvement in addition practice is making rare earths more and more economical, actually cutting production costs. Excellent results with STAINLESS STEEL in hot workability and increased yield have been verified consistently.

Most steel producers, conscious of their customers' increasing demands for better quality, greater uniformity, and consistently good iron and steel are actively engaged in research employing rare earths. If the cost of iron and steel producing is at all interesting to you, or if customer rejections play any part in your operations, it will pay you to investigate the intelligent use of MCA RareMeT Compound. A letter addressed to any office will bring prompt and confidential response.

MCA

**MOLYBDENUM**

CORPORATION OF AMERICA

Grant Building Pittsburgh 19, Pa.

Offices: Pittsburgh, Chicago, Detroit, Los Angeles, New York, San Francisco
Sales Representatives: Edgar L. Fink, Detroit; Brumley-Donaldson Co., Los Angeles, San Francisco
Subsidiary: Cleveland-Tungsten, Inc., Cleveland Plants: Washington, Pa., York, Pa.

SHIELDALLOY

PRODUCTS for the

STEEL, FOUNDRY and NON-FERROUS

METALLURGICAL INDUSTRIES

- CHROMIUM METAL "98" (min. 98% Cr)
- CHROMIUM METAL "99" (min. 99% Cr)
- FERRO COLUMBIUM
- MELTING BASE ALLOY (30% W LOW-MELTING PT. Fe-BASE ALLOY)
- ZIRCON SAND AND FLOUR

SHIELDALLOY

CORPORATION

EXECUTIVE OFFICES:
99 PARK AVENUE, NEW YORK 16, N. Y.
PLANT:
NEWFIELD, NEW JERSEY

SHIELDALLOY

## Industrial Notes

• *An illustrated booklet giving up-to-date data on the properties of titanium and discussing methods of fabricating the metal has been issued by duPont's pigments dept. The booklet includes tables giving the mechanical properties of both alloyed and unalloyed grades of the metal and comparative properties of titanium and other pure metals. Copies can be obtained from Public Relations Dept., E. I. duPont deNemours & Co. Inc., Wilmington 98, Del.*

• **A booklet issued by Johns-Manville describes the hydraulic setting refractories firecrete and blazecrete which are used through 3000°F. Containing tables on properties, the booklet is available from Johns-Manville, 22 E. 40th St., New York 16.**

• Applications of a relatively new surface alloying technique for increasing the heat, wear, and corrosion resistance of ferrous metals by diffusing chromium into the surface at high temperatures are described in a bulletin entitled *Applications of Chromizing*, available from the Chromalloy Corp., 109 W. 64th St., New York.

• J. B. Arthur, founder and president of the Mexico Refractories Co., Mexico, Mo., received a bronze plaque commemorative of his leadership in the industry. The honor was conferred on Sept. 17 on the occasion of the company's 25th anniversary. The plaque was presented by 16 men who have been continuously associated with him in the firm since 1930.

• A 15 min sound color film, *Ductile Cast Iron*, graphically illustrates the fact that this new engineering material can be cast like gray iron yet has the properties of steel. The ductility of the iron is shown by bending, twisting, impact, and tensile tests. The film is available for use by industry, technical societies, and educational institutions and was released by The International Nickel Co. Inc., New York.

• **Assembly and prototype fabrication costs are reduced as much as 80 pct by Superwelding, an improved high temperature, high production copper brazing process developed by Superweld Corp. The process permanently bonds together ferrous metal parts in a controlled, nonoxidizing atmosphere. Safe operating temperatures for parts Superwelded with copper range from −100°F to +800°F for continuous service, or to 1800°F for short periods of time. For application engineering information write R. E. Jones, Superweld Corp., 6840 Vineland Ave., North Hollywood, Calif.**

• A metal protective paint containing 100 pct zinc dust and possessing rust inhibitive properties similar to those of the zinc coating on galvanized steel is announced by the New Jersey Zinc Co. The zinc rich paint is capable of making metallic contact with the underlying metal.

• *A new high speed radiation detector five times faster than existing models has been developed by the industrial div. of Minneapolis-Honeywell Regulator Co. The new unit responds to 98 pct of any temperature change in less than half second. Measurement can be accomplished without physical contact. It is especially suited for temperature measurement of fast-moving bars, billets, and sheets which are on target for less than a second. It is also designed for applications where profile measurements determine temperature distribution along a moving slab, strip, or sheet.*

• **Linde Air Products Co. has developed Heliarc cutting for the cutting, shaping and sizing of nonferrous materials. Heliarc cutting can be done either manually or mechanically. Saw like quality edges are obtained in ¼ in. thick aluminum plate by mechanized cutting at a speed of 300 ipm. This new tool can be used for bevel cutting, pattern cutting, and circle cutting.**

• *Two new steel cutting carbide grades called CA-606 and CA-609 were announced today by the Carmet Div. of Allegheny Ludlum Steel Corp. These new cemented carbide grades were developed to give greater edge wear without loss of shock resistance. These grades are made with the new anti-cratering ingredient called Crystalloy. Crystalloy uses titanium metal in place of titanium oxide to gain greater impact strength.*

• An improved blast furnace cooling plate holder has been developed by William M. Bailey Co., Pittsburgh. Unit has two main parts, the cooling plate and its holder, and the nozzle through which the cooling plate is inserted into the furnace brickwork. The Bailey Cooling Plate Holder is adaptable for new or relined furnaces. The holder is described in a bulletin that can be obtained from William M. Bailey Co., 1221 Banksville Rd., Pittsburgh 16.

• *Harbison-Walker Refractories Co. has opened a new silica refractories plant at Leslie, Md. The site was selected for its proximity to raw material and to important consuming industries. The new operation includes all the latest operating techniques as well as the latest improvements in machine design.*

# Research dollars working for you... a continuing aid to industry from ELECTROMET

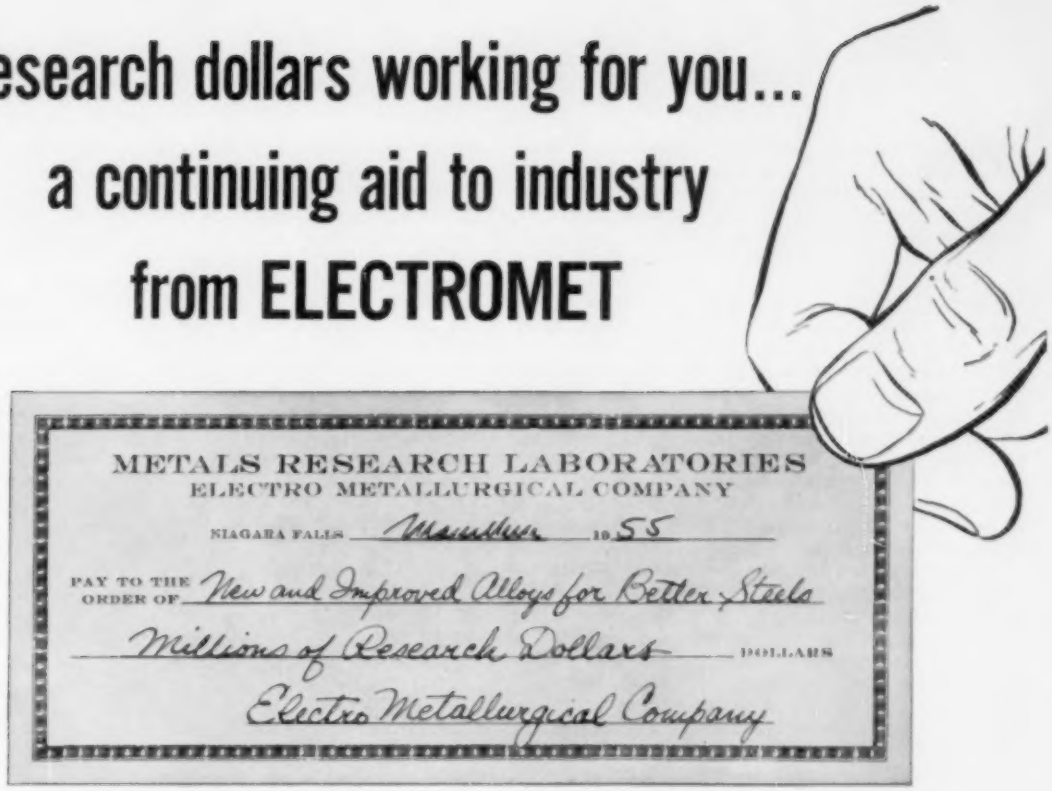
METALS RESEARCH LABORATORIES
ELECTRO METALLURGICAL COMPANY
NIAGARA FALLS March 10 55
PAY TO THE ORDER OF New and Improved Alloys for Better Steels
Millions of Research Dollars DOLLARS
Electro Metallurgical Company

**ELECTROMET's** *research laboratories spend millions of dollars to develop new and improved alloys for better steels—and you receive the benefits.*

More than 300 skilled research scientists, engineers, and technicians work in ELECTROMET's Metals Research Laboratories on the solution of metallurgical problems. They develop new and improved ferro-alloys and metals, better ways of using them, and new and improved alloy steels and irons.

ELECTROMET conducts this continuing research program as a bonus for you, to provide high-quality ferro-alloys and valuable technical service.

You can profit from this continuing research program. For help on your problems in the use of ferro-alloys or the metallurgy of alloy steels or irons, please contact the nearest ELECTROMET office listed below.

*The term "Electromet" is a registered trade-mark of Union Carbide and Carbon Corporation.*

**ELECTRO METALLURGICAL COMPANY**
A Division of Union Carbide and Carbon Corporation
30 East 42nd Street UCC New York 17, N. Y.
OFFICES: Birmingham • Chicago • Cleveland • Detroit
Houston • Los Angeles • New York • Pittsburgh • San Francisco
In Canada: Electro Metallurgical Company, Division of Union Carbide Canada Limited, Welland, Ontario

**Electromet**
TRADE-MARK
Ferro-Alloys and Metals

# Journal of Metals

GLAMOUR comes naturally to electric furnace steel operators. This is illustrated in a research program just completed for the Committee of Stainless Steel Producers, AISI. R. W. McLaughlin of Princeton University predicted that more and more buildings will be constructed of metal walls, in particular stainless steel.

Big city skyscrapers like New York's Lever House and the Socony-Mobil Building are accomplished facts. But Mr. McLaughlin predicts that small towns will also begin to use the outer wall materials that give these giant structures their glamour—glass, stainless steel, and other metals.

"Stainless steel," said Mr. McLaughlin, "combines two fundamental and highly desirable qualities that make it an excellent building material—strength and durability. So outstanding are its combination of these qualities that stainless steel, alone among building materials, can be used for permanent and complete exterior wall surfaces in thicknesses measurable in a few hundredths of an inch. We know of no other material with which this is feasible."

During the two year research program, the Princeton project staff examined scores of installations of stainless steel on the facades of buildings throughout the U. S. No examples were found where corrosion had occurred to an extent visible to the naked eye. The vertical mullions on the Empire State Building and the finials on the Chrysler Building are black with dirt but neither has been cleaned since built in 1931. These structural parts do not, however, show signs of corrosion, and when the dirt is removed the metal appears substantially in its original condition. Even though the parts are dirty, they look bright when seen from the sidewalk.

Other factors that make a case for the use of stainless steel are: speed of erection, more useable floor space because of thinner walls, and costs comparable to brickwork with the added advantage of beauty and contemporary design.

R. E. Paret, stainless steel specialist AISI, pointed out that there are many technical problems to be overcome. "Many fabricators," Mr. Paret observed, "have hesitated to enter this field largely because of unfamiliarity with its requirements." In many cases the fabricating equipment required to form metal curtain wall panels need not be huge or elaborate. One curtain wall design proposed in the Princeton report, for example, uses a standard standing seam type joint which can be formed on a simple press brake found in virtually every metalworking shop.

Mr. Paret concluded, "Many of the technical problems that loomed as serious deterrents to the use of metal curtain walls in the eyes of architects are problems that can be quite easily solved by experienced fabricators in the metalworking industry."

A new experimental process for adding color to stainless steel involves the application of glazes, retaining in view as much natural metallic quality as possible.

New York's newest office building, the Socony-Mobil Building, uses 750,000 lb of stainless steel. The preformed panels would cover 11 acres.

SELECTING the supervisor or management trainee is a complex and hazardous business. In a survey of management development activities in 460 companies, the American Management Assn. developed a series of conclusions.

Managers cannot be developed, but they can be inspired to improve and develop themselves. They are best developed by becoming absorbed in a task, a challenge, that enlists all their abilities, energies, and determination. Through such a task, they will turn to the development and educational aids that the company offers in the training program. The salary motivation is a poor one to emphasize in management development. Rather the individual must satisfy senses of trust, initiative, duty, accomplishment, identity, and integrity. The management trainee must participate in the planning activities and be given as much responsibility as possible.

Most of the conclusions given in the survey refer largely to the psychological growth of the trainee. The major question then in selecting supervisory or management trainees is whether they have the basic psychological potential to learn, grow, and develop as managers.

Many of these desirable traits can be spotted in advance by utilizing standard psychological practices. The first step for the company is the development of good recruiting techniques followed up by adequate intelligence testing. The personality of the candidate plus his past history are also pertinent to satisfactory selection.

Approaching the problems of selecting management trainees on a scientific or objective basis results not only in a cost savings for the company, but also tends to decrease the disappointment and frustration of the unsuccessful trainee. Industrial Psychology, Inc., a national psychological research organization, points out that, "while the rank-and-file employee in a company is an investment of about $300, the supervisor or management trainee runs between $1000 and $5000."

◆◆◆◆◆◆◆

UTILIZING the principle of magnetic cooling, a new refrigerator has come to within a degree of absolute zero, −559.6°F. Developed by Arthur D. Little Inc. the design is based on a cyclic principle of magnetic cooling originated by J. G. Daunt and C. V. Heer of Ohio State University.

There are no moving parts or flowing fluids in the cooling system. It uses, instead, a plastic capsule 3 in. long containing a special chemical salt as the refrigerant. Operation of the refrigerator is controlled entirely by external magnetic fields.

The fact that certain materials will warm up when magnetized and cool when demagnetized has been used for several years in a few cryogenic (low temperature) laboratories for achieving extremely low temperatures in the range of absolute zero. The new apparatus is the first that has been able to produce these extreme low temperatures and to maintain them for long periods of time. Previous equipment would immediately begin to warm up as soon as the low temperatures had been reached.

In the new refrigerator the phenomenon of *superconductivity* is utilized. This is a change that certain metals undergo at very low temperatures in which they lose all resistance to an electric current. At the same time metals in the superconducting state act essentially as thermal insulators but conduct heat readily when not showing the superconducting effect. It is this thermal phenomenon of superconductors that is employed in the ADL machine.

The magnetic refrigerator will enable metallurgists to carry out many new experiments aimed at getting a better understanding of the basic laws of matter. Many of the subtle changes occurring in atoms and molecules are difficult to measure at ordinary temperatures because of their rapid movement. But at low temperatures near absolute zero, atoms and molecules become quiet and can be more easily studied.

Ivan Simon, research physicist at Arthur D. Little Inc., operates the magnetic refrigerator. The temperature of the refrigerated space, the slender tube at the lower left, comes within a few tenths of a degree of absolute zero.

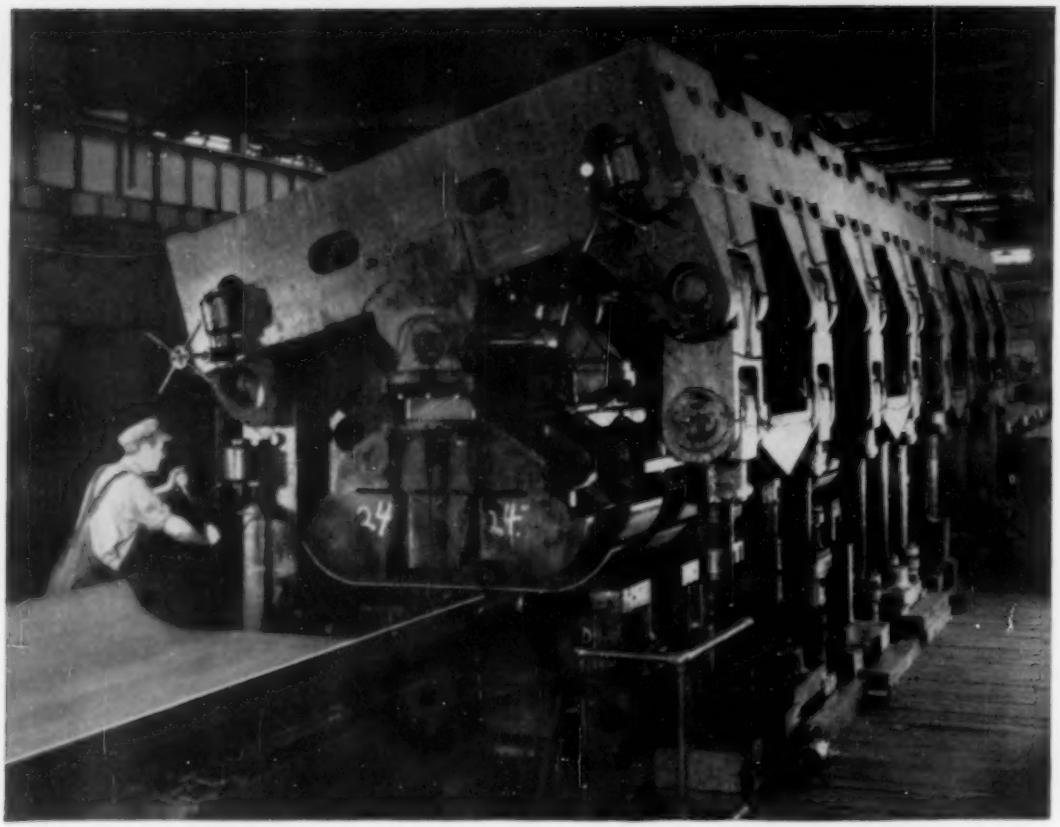

**30,000 lbs. of Nickel Iron** in eight "U-ing" dies start the bending of carbon steel sheet into tubular shape for large diameter line pipe. Closing dies require about 50,000 lbs. The Milwaukee plant of A. O. Smith Corp. has produced 400 miles of pipe per month. A plant in Houston, Texas, owned jointly with Armco Steel, can push out 200 miles per month. Both plants make sizes from 8⅝" to 34". Sets of dies contain 8 to 32 nickel iron castings supplied by Lindgren Foundry Co., Batavia, Ill.

# Nickel cast iron shapes oil line pipe ...outlasts unalloyed iron dies 5 to 1

400,000 CARBON STEEL SHEETS shaped by a single set of dies in use more than two years . . .

That's how nickel cast iron helps to save money in the production of oil and gas line pipe at A. O. Smith Corporation, Milwaukee, Wisc.

The sheets get their initial lengthwise bend . . . also their press into final cylindrical form . . . from heat treated 1.50% nickel-chromium-molybdenum cast iron dies.

Wear resistance of these dies contributes two basic advantages: *dimensional accuracy, plus uniformity of finished pipe.*

These advantages cannot be overemphasized . . . even slight variations in size would cause rejections, because line pipe is welded in 40-foot sections at the plant and later the lengths are joined together in the field.

Unalloyed gray iron dies, previously used for shaping pipe, wore rapidly and thus increased rejections.

In contrast . . . the nickel cast iron dies not only reduce rejects, but also give more than five times the service life of the unalloyed type.

Whatever your industry, when you face questions about metal, let us give you the benefit of our wide practical experience. Write for List A of available publications. It includes a simple form that makes it easy for you to outline your problem.

INCO **THE INTERNATIONAL NICKEL COMPANY, INC.** 67 Wall Street New York 5, N. Y.

TV is used to inspect chrome plated blades on lithography machines at the American Can Co., Cincinnati. Twice as fast as inspection by microscope, the TV set magnifies the blades' thin edges 288X. At the same time two thin vertical lines on the TV screen check tolerance limits.

W. Lunsford Long, president of Tungsten Mining Corp., described a new powder metallurgy alloy made from tungsten and small amounts of copper and nickel. The alloy has almost the same tensile strength of cold draw steel, is non-magnetic, non-rusting, and highly resistant to atmospheric corrosion.

Aluminium Ltd. is planning to double production of alumina in Jamaica. Present capacity of the Jamaican works is 230,000 tons per year. The new expansion will increase the potential output to 543,000 tons a year.

Dominion Foundries & Steel Ltd., Hamilton, Ontario, is planning a $12,000,000 expansion in buildings and equipment. A part of the program is slated for the addition of a second continuous electrolytic tinning line. Dofasco's oxygen producing plant is also being enlarged.

U. S. production of primary magnesium during 1954 declined 26 pct from the 93,075 tons produced in 1953 according to the U. S. Bureau of Mines. Estimated world production was placed at 140,000 tons, a drop from the 1953 figure of 170,000 tons. The U. S. accounted for more than 49 pct of the world total.

The first section of the 12 section E. W. Davis taconite plant at Silver Bay, Minn., is now in operation. When completed the entire facility will have an annual capacity of 3,375,000 long tons of iron ore pellets.

The widest Sendzimir cold reducing mill is now in operation at Republic Steel Corp., Massillon, Ohio. The Sendzimir mill can roll sheets up to 48 in. wide at 713 ft per min. It is a major facility in Republic's expansion of stainless steel operations by 25,000 tons annually.

Armco Steel Corp. plans to spend $111,000,000 in a new expansion program. In addition to rounding out processing and finishing facilities, steel ingot capacity will be increased 1,176,000 tons from the present annual capacity of 4,950,000 tons.

Westinghouse Electric Corp. has developed a zirconium alloy, Zircaloy-2, for use in atomic reactors. Containing 1.5 pct Sn, 0.12 pct Fe, 10 pct Cr, and 0.05 pct Ni, the alloy is so resistant to deterioration under reactor conditions that corrosion in a year was measured in ten-thousandths of an inch.



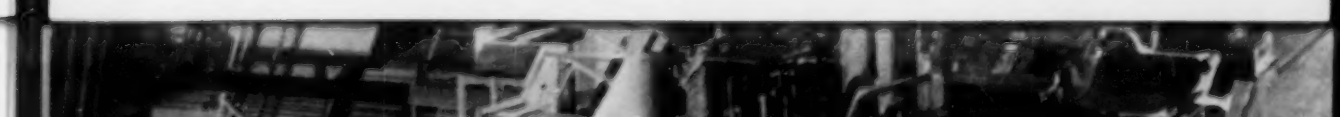

# Drift of Things

THIS past month all members of AIME were requested by the Board of Directors to vote on the resolution:

> BE IT RESOLVED, that the name of the organization be changed from "American Institute of Mining and Metallurgical Engineers, Inc.," to "American Institute of Mining, Metallurgical, and Petroleum Engineers, Inc."

The ballot sent to members also contained a note from the Secretary of the Institute. In it Mr. Kirkendall remarked that 1919 was the last time the name had been changed. The membership of the American Institute of Metals was added to AIME, and the word *metallurgical* included. With the rapid growth in petroleum members, he continued, it is now appropriate that the word *petroleum* be added.

With this continuing expansion of the Institute, it was intriguing to look up the circumstances of the first AIME meeting. A. B. Parsons' "History of the Institute" published in *Seventy-Five Years of Progress in the Mineral Industry* gives the background.

The industrial and technologic scene of 1871, the first year of AIME, was as follows:

A—The petroleum industry was still an infant, although the famous Drake well, near Titusville, Pa., had been discovered 12 years earlier. The chief market product was kerosene to burn in lamps, for Edison's first incandescent electric bulb was 8 years in the future. The light fraction from petroleum known as gasoline was something of a nuisance, and the refiners produced as little as possible.

B—Production of bituminous coal had passed that of anthracite a few years before 1871, but heating buildings was the principal use of both kinds of coal.

C—The production of pig iron in 1871 was a fairly well established industry. Most of the ores were magnetites from the eastern states, but iron ores had been found near Marquette and these were coming down to the furnaces in increasing quantity by lake transportation. Fuels used in the blast furnace included anthracite, coke, charcoal, and bituminous coal.

D—In 1871, 800,000 tons of steel were produced. A little steel had been made each year since the Civil War, but it was still a novelty. The country was just starting the tremendous extension of its railway system that was to be the backbone of steel consumption for many years. The same year, John A. Roebling successfully swung a suspension bridge over the Ohio River at Cincinnati and also drew plans for a much longer bridge to connect Manhattan and Brooklyn. For this bridge he decided to use steel (instead of iron) wire. This had never been done before.

E—The highest buildings in 1871 were eight and ten stories; the walls were massive structures of natural stone. Not until about 20 years later did the skyscraper era commence.

F—Copper came almost entirely from Michigan's upper peninsula, but not much was needed. The practical development of the electric dynamo and motor was not achieved until about 1880. Butte was still a silver camp, and although prospectors were roaming Arizona, the Apaches made much trouble and production of copper was negligible.

G—Portland cement was manufactured for the first time in the United States in 1871 at a small plant near Allentown, Pa.

H—Sulphur was obtained in small quantity from pyrites, but the chemical industry, to which sulphur is vital, was only of minor importance at that time.

I—Aluminum and magnesium were industrial and laboratory unknowns in 1871.

The original call for the establishment of the new professional organization was dated Wilkes-Barre, Pa., April 1871. The authors of the call explained their reasons for desiring this type of society.

"It must be evident to all practical men that the interchange of the varied experience of those engaged in such occupations in this country, could not fail to advance very materially the desired objects; it is therefore proposed to establish an American Institute of Mining Engineers, which will hold its meetings periodically in the great mining and metallurgical centres, where works of interest, such as mines, machine shops, furnaces and other metallurgical works, can be inspected, and the members exchange their views, and consult for mutual advantages upon the difficulties encountered by each; these 'Transactions' or 'Proceedings,' when published, would form a most valuable and greatly needed addition to our professional literature."

What were the thoughts of the men who gathered in Wilkes-Barre for that first meeting? The following excerpts from a paper presented in 1872 by E. C. Pechin, steelmaster of Dunbar, Pa., give a clue.

"The time has come when scientific research is to assume its true position—the day of 'sheer force and blind stupidity' . . . has gone forever . . . the physicist, the geologist and mineralogist; the chemist, the engineer, are as essential to success as the blast furnace itself. . . . There is no merely practical man, no matter how varied may have been his experience, or how long his practice, that will not benefit from the results of scientific investigation. That there is a growing sense of the importance of having thoroughly prepared scientific men in every department of business is evidenced by the institutions of higher learning that are springing up in different quarters, provided with able teachers. . . . We summon to our aid all that science can afford, mechanical ingenuity devise, money purchase, and energy and ability achieve, and when this is done, we fain must confess how little we have accomplished and how little we know compared with the vast possibilities that lie before us."

These are remarkable and prophetic words! The members of AIME in the mining, metallurgical, and petroleum fields have been the workers, the researchers, the engineering and scientific shock troops that have made the ideal of the founders a reality in 1955. In addition to giving recognition to a dynamic section of our profession, the proposed change in name of the Institute will, we hope, constitute another distinguished landmark in the history of AIME.

*Ed Weiss*

MORGAN
WORCESTER
Three Strand Continuous Rod Mill
COLORADO FUEL AND IRON CORP.
Pueblo, Colorado
MORGAN CONSTRUCTION COMPANY WORCESTER, MASS.
ROLLING MILLS • MORGOIL BEARINGS • WIRE MILLS • REGENERATIVE FURNACE CONTROL • EJECTORS • GAS PRODUCERS
H. H. Wood, Rep., Koppers Bldg., Pittsburgh, Pa. English Rep., International Construction Co., 56 Kingsway, London W. C. 2, Eng.

# NEW 75 KV
# *Electron Microscope*

**HIGH POWER, MEDIUM PRICED INSTRUMENT FOR EDUCATION, MEDICAL, BIOLOGICAL AND INDUSTRIAL INVESTIGATIONS**

The new EM-75 Console Electron Microscope offers unusual utility by providing most of the outstanding features for which the Philips EM-100 has become popularly accepted. It provides continuously variable magnification on the viewing screen — *1200 to 12000 diameters* as well as accelerating potentials continuously variable between *10 and 75 kilovolts*.

Resolution is better than 75 *Angstroms*. Servicing is practically eliminated — there are no electron tubes in the circuitry. An *air-lock* facilitates and speeds specimen interchange. Fluorescent *viewing screen* is 9 x 9 centimeters — a *beam wobbler* assures ultra-sharp focusing. Roll film carrier holds film for from 5 to 40 exposures from which a useful maximum magnification of 100,000x can be obtained. 15° angle *stereo device* permits preparation of three-dimensional micrographs.

Many additional features, particularly simplicity of operation make this microscope indispensable in studying the finite structures in the numerous problems of analysis, development, investigation, research and control. Our microscope application laboratory offers a unique service in supplying data on the applicability of electron microscopy to specific and general problems in addition to operator training. Let us tell you more about the advantages of higher magnification microscopy.

A *Norelco* PRODUCT

NORTH AMERICAN

*Serving Science and Industry*

PHILIPS

COMPANY, INC.

750 South Fulton Avenue, Mount Vernon, N. Y.

In Canada: Rogers Majestic Electronics Ltd., 11-19 Brentcliffe Road, Leaside, Toronto 17, Ontario

# Uniform Density and Structure Possible With Simultaneous High Pressure and Temperature

by R. Humphrey, M. Vilella and L. W. Tomarkin

THE Vitron process subjects substances, especially powders, to the simultaneous action of high temperatures and pressures. Under these extreme conditions, phenomena occur which result in the formation of compounds possessing many new properties. In a similar manner, chemical processes can be carried out by the Vitron process at high pressures and temperatures, that differ in theory and scope from the present use of autoclaves or bombs as reaction chambers. In reality, the scope of the work being carried out is extensive, and only an attempt will be made to summarize interesting aspects.

In the production of metals or alloys from powders, the Vitron process differs from powder metallurgical methods in that the simultaneous action of extremely high pressures and temperatures can be employed. Work has been done with the simultaneous application of pressures on the order of 40,000 atm with temperatures exceeding 5000°F. Even higher pressures may be obtained by modifying present die design. In addition, the process is not limited to powders for basic raw materials, as good quality ingots have been made from chips, turnings, sponge, scrap, etc., as can be seen from Fig. 1.

The Vitron process in action approaches a true hydraulic system. By utilizing the proper metallic lubrication and spacing between the die holder and dies and pressings, shrinkage of compacted powder during consolidation is radial as well as longitudinal. Thus, the forces acting on the powder being compacted and fused are equal in all directions. This condition is analogous to that of a solid immersed in a liquid system while being subjected to pressure. For example, all surfaces of a base metal have been completely clad with tungsten, tantalum, and carbides as shown in Fig. 2. In addition, metal-clad diamonds, ceramics, and other friable substances have been produced.

The use of this hydraulic principle in a metallurgical process has two advantages. First, powder pressings of greater length can be made without substantial differences in physical structure and density from one end of a bar to the other. Rods having a 10:1 ratio of length to diameter have been made. Second, the inconvenience of squeeze-out, bleeding, or segregation of any liquid phase or light constituent is eliminated. Other advantages are that long fusion periods are not required to make solid bars or ingots. Tungsten powder (65 mesh) was converted into a solid tungsten bar in less than 1 sec.

Certain alloys, such as stainless steels, when made by powder metallurgical procedures approach equilibrium conditions only after long soakings at sintering temperatures under appropriate conditions. The Vitron process can make such compositions under pressure in seconds and obtain homogeneous solid bars. This phenomenon occurs because of the simultaneous action of high temperature and pressure in a variable volume chamber. The high heat energy applied coupled with the simultaneous action of high hydraulic-like pressure forces fuses the minute powder particles into a forged bar.

Initially, small pellets $\frac{1}{8}$ in. diam and 1 in. long were made, Fig. 3. Now, with experience and increased knowledge of this process, bars of 1 in. diam and 4 in. long are common. Fig. 4 shows bar sizes currently being made. Commercial size wire bars of various metals have been produced. It should also be possible to produce large size ingots on the order of 100 to 500 lb by this process.

An important feature of the process is that it minimizes wear and tear and the need for replacing dies. Dies can be used for over 50,000 cycles before repair or replacement become necessary. The reason is that the die chamber itself is expendable and is inserted into a die holder. A crushable metallic casing acts in two ways: A—to lubricate the die surfaces, and B—to isolate the green refractory shell containing the charge. This feature is accompanied by a unique method of isolating hard powders or abrasives from all the wearing surfaces of the dies.

Fig. 1—Vitron process permits the making of good quality ingots from scrap. A titanium stud is shown machined from ingot of reclaimed scrap.

R. HUMPHREY, M. VILELLA and L. W. TOMARKIN are Chief Metallurgical Consultant, Vice President in Charge of Research, and President, respectively, Vitron Research Corp., Pearl River, N. Y.

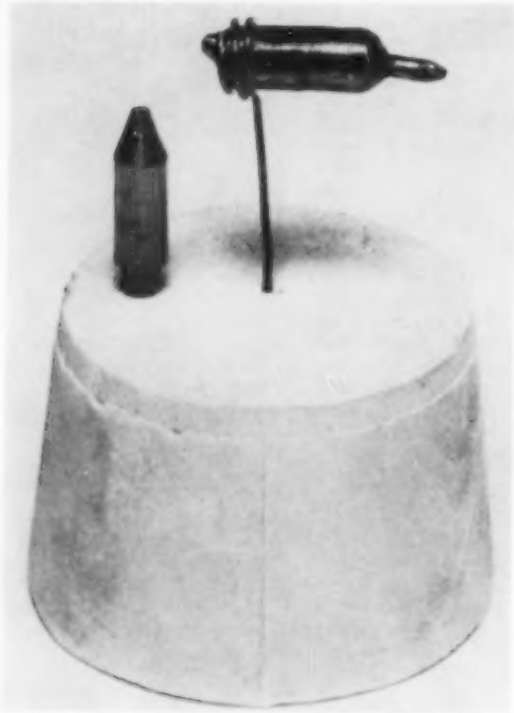

Fig. 2—Surfaces of a base metal can be clad with rarer metals. At left is a tantalum clad carboloy blank and at right a tantalum clad common nail.

In the Vitron process, substances are compacted, sintered, or subjected to chemical reactions or changes in a sealed chamber. In certain experiments, more than 15 pct water has been incorporated into molten silicate magma. This synthetic hydrated mineral, which decomposes when subjected to a moderate temperature, requires intense pressures and optimum sealing conditions to create.

Experience indicates that this process is adaptable to automation. Feeding, pressing, firing, and ejecting of metallic compacts can be performed in minutes rather than in hours.

### Chemical Reduction Processes

The utilization of autoclaves or bombs for performing chemical reduction processes involving high pressures and temperatures causes the reaction to occur in a constant volume chamber at variable pressures. In the Vitron process, the reaction occurs exactly in the reverse. Here the specific high pressure is kept constant while the volume of the reaction chamber is a variable. This is an example of the principle of Le Chatelier-Braun, which states that: "Whenever stress is placed on any system in a state of equilibrium, the system will always react in a direction which will tend to counteract the applied stress." This principle governs the phenomena occurring when alterations in equilibria result from changes in both temperature and pressure. Thus when a system in equilibrium is subjected to an increase in pressure, a reaction will take place which will favor the smaller volume; if the pressure on the system is decreased, a reaction will take place which will be favored by an increase in volume.

Fig. 3—Tantalum and tungsten molded to their theoretical densities. Consolidation of powders is shown when compared to their original container.

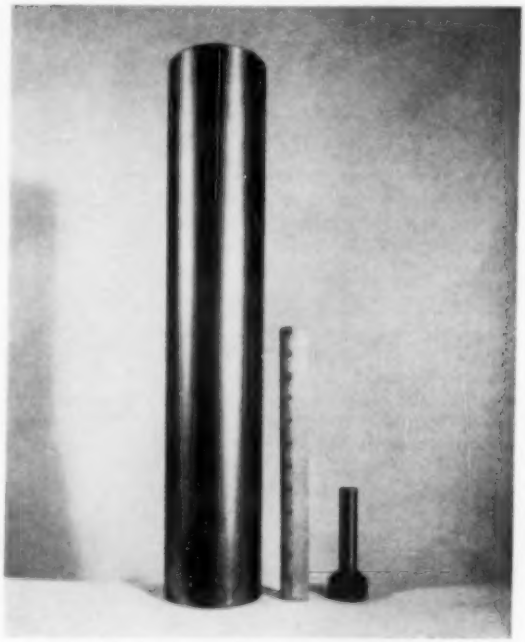

Fig. 4—Bar sizes currently being made are shown. Large size ingots on the order of 100 to 500 lb are possible.

Again, when a reaction absorbs heat, addition of heat would favor it, and the reaction would proceed to a greater extent at higher temperatures. Conversely, when a reaction liberates heat, addition of heat would tend to inhibit the reaction, and at higher temperatures the reaction would tend to reverse itself.

Theoretically, reduction reactions involve a change in energy level with a corresponding reduction in absolute volume. When aluminum, calcium, lithium, magnesium, sodium, potassium, etc., are used as reducing agents, the resulting oxides or halides are heavier than the free metal itself. When the halides or oxides of most heavier metals are reduced, the free metal is denser than the original compound. Thus an increase in pressure favors most reduction processes. Furthermore, a constant pressure system eliminates the undesirable vapor stage in reduction.

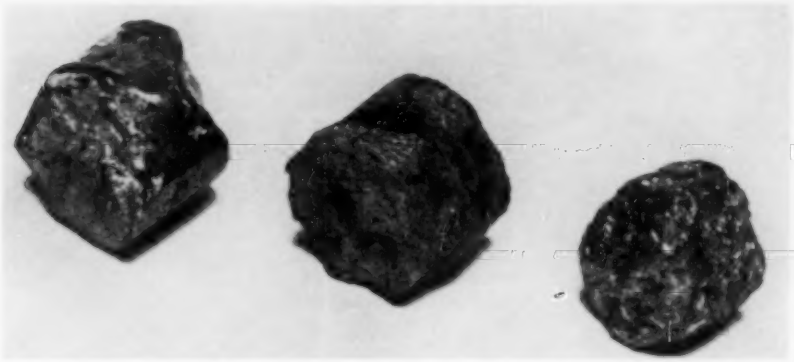

Fig. 5—Nickel, zirconium, and titanium phosphors have been produced. Industrial production is possible on any scale.

Such a system would also eliminate the need for flushings or the use of protective gases to counteract deleterious side effects, and prevent the segregation of the reactants.

Another important law of equilibrium applied in metallurgical processes is the phase rule of Willard Gibbs. The phase rule establishes definite numerical relationships between the number of components in a system, the number of co-existing phases in equilibrium, and the number of degrees of freedom. The degree of freedom depends on the number of components, the temperature, and the pressure. In most studies of today, pressure is ordinarily omitted as a variable and is assumed to be substantially constant at atmospheric pressure. Thus, the number of states, and reactions possible, have been limited. In the Vitron process, pressure may be varied, and the number of possible reactions increase manifoldly.

The general scope and magnitude of the Vitron process can be seen to be quite large. Thousands of different substances, alloys, and metals can be obtained, all of which can be expected to possess diversified desirable electrical, mechanical, or physical properties.

## Specific Projects

Various techniques for the preparation of free titanium from its oxides by direct reduction are being investigated by Vitron Research Corp. The reactions are exothermic and go to completion almost immediately when initiated. The reaction for practical purposes is nearly 100 pct efficient. The resulting complex secondary by-products and oxides are easily and efficiently eliminated. It is to be anticipated that with the advent of the Vitron process, many new materials, complex alloys, etc., can be produced under economical conditions.

For example, when applying the principle of the Vitron process to the simultaneous reduction of titanium in the presence of various other oxides such as chromium, cobalt, nickel, etc., metal alloys of high purity are obtained in one cycle with optimum conversion, and the resulting slag is easily eliminated by known and accepted standard procedures. Equated, it would be somewhat as follows: $TiO_2$ (rutile) + Cr, Co, or Ni oxide + Mg or Al (reducer) → Ti and Cr, Co, or Ni + Slag.

Another example of the versatility of the Vitron process is the preparation of nickel-phosphor alloys in various percentages of phosphorus to a maximum of 25 pct or more. Most metallic phosphorus alloys have unique physical properties. Nickel-phosphor is an outstanding example. It is made by the direct reaction of metallic nickel and phosphorus under heat and pressure. Practically no phosphorus is lost in the reaction. The technology of industrial production of nickel phosphors can be instituted on any desirable scale.

It forms an eutectic at 10 pct P, and can be melted by ordinary practices under standard conditions with little or no decomposition. When in the molten state, it coats or binds on contact with most ferrous alloys, carbides, and some ceramics. Its self fluxing characteristics reduce or eliminate preliminary pickling, descaling, or sand blasting of surfaces to be treated. Since the bond is of a chemical nature, the presence of pores or *non-wetted* areas is absent. It can be applied by methods such as hot dipping and spraying. It wets carbides, and properly applied will outperform many of the standard brazing compositions. Some nickel phosphor coatings have a hardness of Rc 60 to 65, and can be polished to a lustrous surface which is highly resistant to wear and corrosion. The addition of one of several metals to the initial constituents produces a series of nickel-phosphor alloys of high hardness. Its inherent hardness, wear and corrosion resistance, and nonsparking characteristics will probably make nickel-phosphor alloys desirable in many industrial operations. Fig. 5 shows some of the phosphors obtained.

The Vitron process has the following unique features:

A—The bodies treated are subjected to forces approaching true hydraulic pressures, thus permitting uniformity in density and structure throughout.

B—The die chamber which acts as an electric furnace is expendable.

C—The cost of this expendable chamber is negligible in relation to a pound of product produced.

D—This process permits prolonged exposures to controlled high temperatures and pressures without harm to the apparatus or dies.

E—The life of the apparatus, and die holders is long. It is not unreasonable to expect a die holder to last over 50,000 cycles.

F—The cost of manufacturing alloys is low due to the short individual cycles of operation.

G—This process lends itself practically to the production of many bodies by means of electrochemical reactions involving the application of high pressure-high temperature variable volume conditions.


## Acknowledgment

The research and development of this process has been made possible through the support of Paul Casavina.

# Iodide Process Produces Ductile Hafnium for Fabrication

by J. G. Goodwin and W. J. Hurford

HAFNIUM has become prominent in the atomic energy field as a material for control devices in nuclear reactors. Because of its very high captive cross-section hafnium control rods are used to adjust the reactivity of the reactor core. With the control rods completely inserted in the core, the high thermal-neutron-absorption of the hafnium will prevent the chain reaction from starting.

The earth's crust contains approximately 0.0004 pct Hf which makes it about as plentiful as arsenic, beryllium, germanium, and uranium, and more plentiful than mercury, tantalum, niobium, and silver. Associated with zirconium minerals in concentrations of between 0.5 to 2.0 pct, hafnium is usually recovered as a by-product of zirconium production.

To obtain soft ductile hafnium an iodide process similar to that used for zirconium is employed. The major difference between the two processes is the higher decomposition temperature of hafnium tetraiodide. Zirconium tetraiodide decomposes at about 2190°F and hafnium tetraiodide decomposes at about 2820°F.

The present high cost of the metal ($75 per lb of crystal bar hafnium) makes the yield in the processing of the metal a matter of utmost importance. If hafnium were not a by-product of zirconium production, the cost would probably be $275 to $300 per lb of hafnium.

### Melting Techniques

A double arc melting process had proved to be a practicable method for the consolidation of iodide hafnium crystal bars into a fabricable form. The method is to nonconsumably arc melt chopped crystal bars into a 2½ in. diam ingot using a tungsten tipped electrode and then to consumably arc melt the 2½ in. diam ingot into a 4 in. diam ingot. Fig. 1 shows the arc furnace.

A single melted 2½ in. diam ingot is shown in Fig. 2, and conditions for the double arc melted process and ingot hardness are given in Table I.

A process that permits the direct production of sound ingots from iodide hafnium crystal bar has recently been developed. It consists of tack welding the iodide hafnium crystal bars into a consumable electrode shown in Fig. 3. Fig. 4 shows how the bars are attached to the copper electrode and Fig. 5 the electrode stub. Melting conditions for consumable arc melting are adhered to with the exception of slightly higher currents (2800 to 2900 amp).

Melting is stopped when the calculated weight has been melted. The crucible with the consumable ingot is transferred to a tungsten tipped electrode arc furnace where the splatter ring is melted down and the bottom remelted. By constructing the electrode so that the crystal bars are joined as in Fig. 6, the ingot weight can be controlled to ±0.1 lb.

### Ingot Quality

Ingots produced by consumable techniques are quite sound. The average hardness of the ingots (171 Bhn per 3000 kg) is less than that for ingots produced by nonconsumable methods (184 Bhn per 3000 kg). The double melting method has the advantage of eliminating any chemical inhomogeneities which may exist in the crystal bars. It also permits the blending of solid scrap during melting. The single

J. G. GOODWIN and W. J. HURFORD are Associate Engineer, PWR Metallic Fuel Element Development Section and Manager, PWR Fuel Laboratories Section, respectively, with the Atomic Power Div., Westinghouse Electric Corp., Pittsburgh, Pa.

melting process provides a method for the rapid production of sound ingots.

In ingot conditioning, surface fusion is accomplished by rotating an ingot on a lathe fixture shown in Fig. 7 and running a weld bead over the periphery. The ingot on the left hand side of Fig. 8 has been conditioned by surface fusion. Fusion is done in a chamber shown in Fig. 9 under a helium atmosphere at a pressure slightly greater than one atmosphere, using a thoriated tungsten welding electrode. Power requirements are 250 to 300 amp at 17 to 24 v. The yield from crystal bar to conditioned ingot is 99.8 pct.

Surface fusion has a distinct advantage over other types of conditioning because it removes the majority of porosity usually found beneath the surface of arc melted ingots. Prior to the advent of surface fusion, the porosity beneath the surface was not removed and would appear on hot rolled plates as surface defects. To obtain a defect-free surface on a machined plate, extra stock had to be allowed for removal of the defects. Because surface fusion eliminates sub-surface porosity (and thus fabricated surface defects), plates can be hot rolled to thinner sizes with yield increases of up to 15 pct. A considerable saving of material is entailed by the use of this method of conditioning, as less metal is required per plate and less metal is converted to machine scrap. Table II gives the chemical analysis of hafnium plates.

Although originally developed for short, small diameter ingots, the surface fusion process has been adapted for the conditioning of 10-in. diam, ¼-ton zirconium alloy ingots and 12-in. diam, ½-ton zirconium alloy ingots.

## Fabrication

Nitrogen and oxygen dissolve in iodide hafnium and decrease the room temperature ductility and increase the hardness. As in the case of iodide zirconium, elevated temperatures reduce the effects of these dissolved gases, and the metal can be hot worked without difficulty.

Heating of iodide hafnium for pressing in the laboratory is done in an electric Glo-bar furnace; heating for rolling is done in an electric resistance furnace. A constant flow of argon is maintained in the resistance furnace to minimize the oxidation of the hafnium. Commercial gas and oil fired furnaces are satisfactory, providing the precautions recommended for zirconium such as the removal of scale from the furnace, cleaning of the hearth, and protection from direct impingement of the flames, are adhered to.

The rapid and uniform heating of lead baths and commercial salt baths provides a satisfactory method for heating iodide hafnium. Usually chloride salt baths are used with the concentration depending upon the temperature range desired. In addition to the high rates and uniformity of heating offered by salt baths, the molten salt adheres to the surface, reducing oxidation and providing a lubricant for certain types of fabrication such as extrusion.

## Forging

Forging of 50-lb, 4 in. diam iodide hafnium ingots has been successfully accomplished on a 300-ton forge press and on a 5-ton steam forge hammer. Before taking heavy reductions during forging, it is necessary to break up the cast structure which often contains extremely large grains. This is accomplished by pressing a 4 in. diam ingot at 2000°F into a 3½ in. square with reductions of approximately 12 pct. When properly heated and the cast structure broken up, iodide hafnium ingots have been given a maximum single reduction of 45 pct. A pressed slab 1½x5½ in.x length for the production of strip is produced by heating a conditioned ingot for 1 hr at 2000°F and forging to a 3½ in. square. The billet is reheated for 20 min, after which it is placed lengthwise on the anvil and pressed to 2 in. thick. Another 20 min preheat precedes the final forging to a 1½x5 in.x length slab. After cooling in air, the slabs are abrasive blasted to remove the oxide and conditioned by spot grinding.

Table I. Conditions for Double Arc Melting Process and Ingot Hardness

| Data | First Melt (Nonconsumable) | Second Melt (Consumable) |
|---|---|---|
| Melting rate | 1 lb per min | Approx 3 lb per min |
| Atmosphere | 2 argon: 1 helium | 1 argon: 1 helium |
| Pressure | 1 atm | 1/6 atm |
| Current | 1200 to 1800 amp | 2300 to 2500 amp |
| Voltage | 38 to 42 v | 30 to 35 v |
| Crucible waterflow | 10 gpm | 4 to 5 gpm |
| Ingot hardness (Bhn per 3000) | — | Avg—171<br>Range—160 to 180 |

## Strip Fabrication

Iodide hafnium strip is produced by heating a 1½ in. thick conditioned slab for 1 hr at 1700°F prior to hot rolling. An electric resistance furnace with a constant flow of inert gas is used for heating.

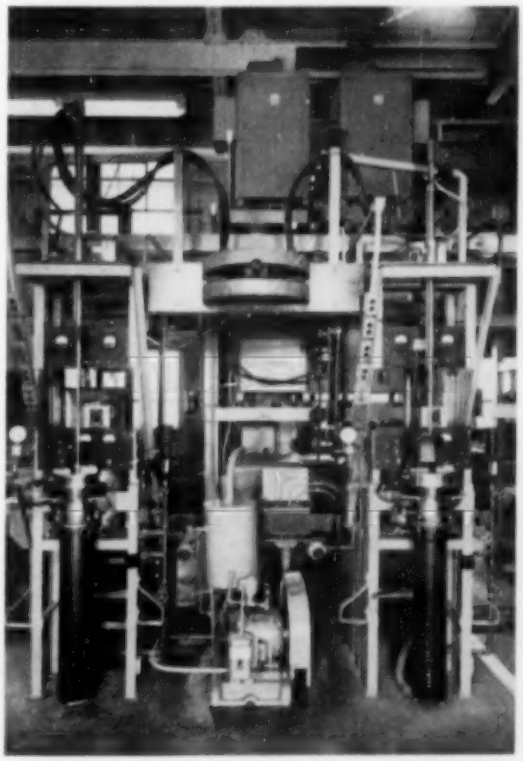

Fig. 1—A tungsten tipped electrode arc furnace is used to nonconsumably arc melt chopped crystal hafnium bars into a 2½ in. diam ingot.

Fig. 2—Chopped crystal bar hafnium feed stock and 2½ in. diam nonconsumable single melted iodide hafnium ingot are shown.

Reductions of 15 to 20 pct per pass are taken, and each pass is followed by a 15 min reheat. Strip has been rolled on a two-high hot mill with a roll speed of 165 ft per min. After hot rolling, the metal has a cold worked structure and should be annealed. Present practice is to anneal ¼ in. strip for 30 min at 1700°F after the final pass.

The oxide is removed from the strip by abrasive blasting because it cannot be removed with commercial caustic or sodium hydride baths and ordinary acids will not attack it. Hardness values for annealed iodide hafnium strip may be found in Table III.

### Rod and Wire Fabrication

The similarity between iodide zirconium and iodide hafnium is quite evident when fabricating rod and wire. Rods have been hot rolled commercially for use as wire drawing stock. Wire drawing stock is made by forging a 4 in. diam ingot into 1½ in. square with broken corners followed by hot groove rolling at 1800°F to a 5/16 in. round. Each pass on the groove rolls is an oval except for the final one. The 5/16 in. diam rod is sandblasted and pickled in preparation for a copper electroplate. After the rods are copper plated, they are given three baked lime coatings. The copper and lime are the wire drawing lubricants. Drawing is accomplished by taking individual drafts of 10 to 20 pct and annealing at 1400°F for 10 min after each 35 pct total reduction. The phosphate coating develcped for drawing zirconium and zirconium alloy wire has also been found suitable for drawing iodide hafnium wire.

Hot rolled rods can be made into cold drawn or swaged rods by following the same procedure as is

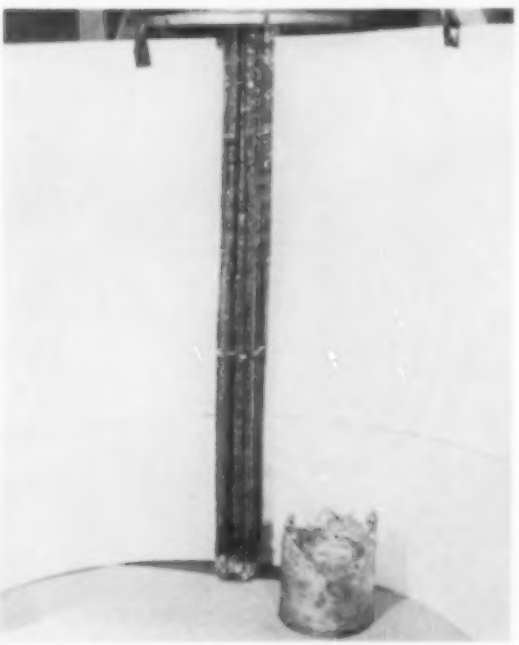

Fig. 3—Iodide hafnium crystal bars are joined for consumable arc melting.

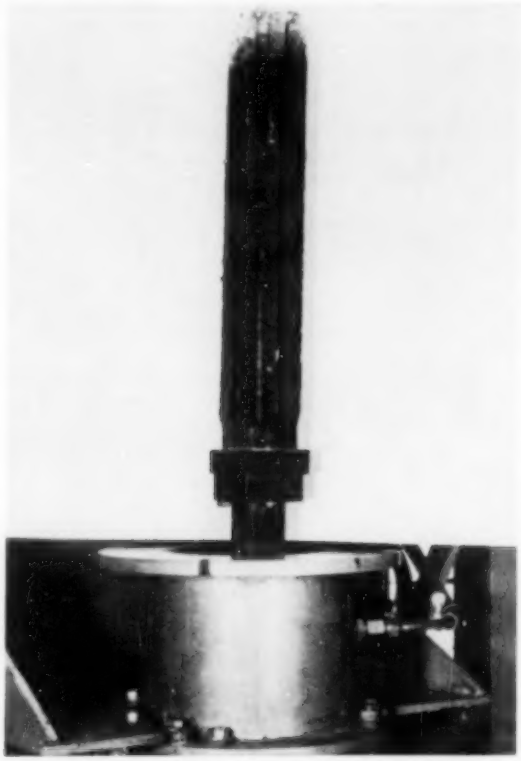

Fig. 4—Tack welded hafnium crystal bar stub at finish of consumable arc melt is shown with attachment of crystal bars at the copper electrode.

Fig. 5—Iodide hafnium consumable electrode stub with threaded hole for screwing onto the copper electrode is shown here.

used for wire drawing, that is, 10 to 20 pct individual reductions with intermediate anneals at 1400°F for 10 min after each 35 pct total reduction. The lubricants for cold drawing are similar to those used for wire drawing. Swaging does not require lubrication.

### Extrusion

The extrusion of hafnium shapes has met with the same problem as was encountered in the early extrusion of zirconium, namely, finding a lubricant that prevents galling. To date, extruded hafnium shapes have been limited to rods or simple shapes. Successful extrusions have been obtained by extruding bare after heating in a salt bath. The salt adhering to the billet surface appears to be a good lubricant. A lubricant of metallic lead dispersed in a carrier of heavy oil has also been found to be satisfactory. It has been found that temperatures in excess of 1800°F are necessary. Standard hot work tool steel, 9 pct W, 0.35 pct C, is used for tooling.

Table II. Chemical Analysis of Plates from Nonconsumably Arc Melted Iodide Hafnium Crystal Bar*

| Element | Pct | |
|---|---|---|
| | Range | Average |
| Hf | — | Major |
| Zr | 1.95 to 3.80 | 2.85 |
| Si | 0.003 to 0.010 | 0.006 |
| Fe | 0.015 to 0.050 | 0.025 |
| Al | >0.002 to 0.010 | 0.005 |
| Cu | >0.001 to 0.014 | 0.002 |
| Ti | 0.001 to 0.030 | 0.009 |
| Ca | >0.005 | >0.005 |
| Mn | >0.001 | >0.001 |
| Mg | >0.001 | >0.001 |
| Pb | >0.001 to 0.006 | 0.003 |
| Mo | >0.001 | >0.001 |
| Ni | 0.001 to 0.008 | >0.005 |
| Cr | >0.001 to 0.003 | 0.001 |
| Sn | >0.001 to 0.003 | >0.003 |
| V | >0.001 | >0.001 |
| W | >0.01 | >0.01 |
| O | 0.026 to 0.142 | 0.056 |
| N | 0.0010 to 0.0040 | 0.0017 |
| Cl | 0.02 to 0.03 | 0.02 |
| C | 0.01 to 0.05 | 0.032 |

* W. J. Hurford and R. J. McClintick. WAPD-RM-181, May 31, 1953.

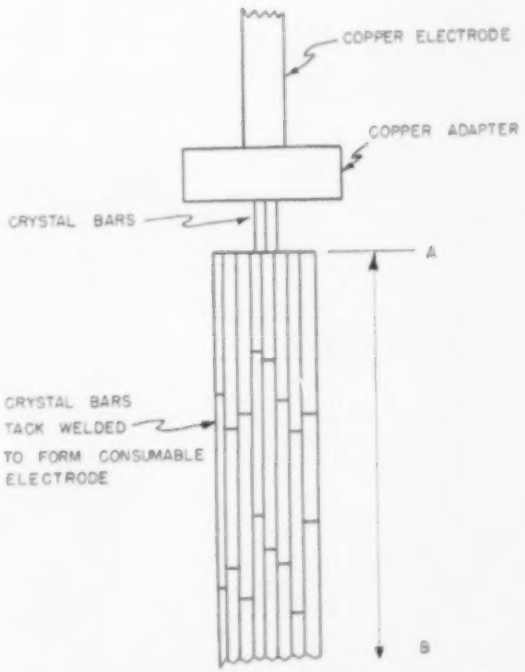


Fig. 6—Diagram shows how iodide hafnium bars are joined into a consumable electrode.

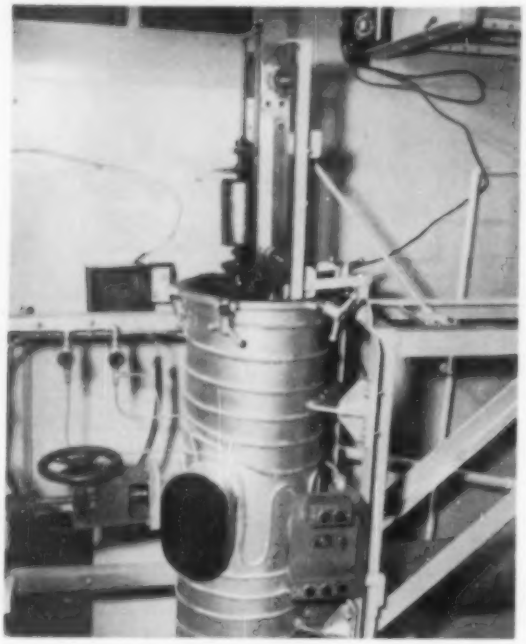

Fig. 7—The lathe fixture for rotating an ingot is shown inside the surface fusion unit.

Dies with a 45° approach angle, a blending radius of ¾ in., and a bearing length of 3/16 in. have been used with success. A 500-ton extrusion press has been used for this work with unit loading pressures as high as 200,000 psi and pressing speeds of 1 in. per sec. The extrusion constant calculated from the data of an extrusion of a 2.6 in. diam billet at 1800°F with a reduction ratio of 24:1 was found to be approximately 70,000 psi. Reduction ratios as high as 24:1 have been used.

Table III. Hardness of Hot Rolled Iodide Hafnium Strip*

| Data | Strip from Consumable Electrode Arc Melted Ingots |
|---|---|
| Range | 83 to 94 $R_B$ |
| Average | 88 $R_B$ |

* Annealed at 1700°F for ½ hr and air cooled.

## Cold Rolling

Cold rolled hafnium strip and foil have been made. Cold rolled strip can be easily produced by using hot rolled strip which has been blasted and pickled, and has had the hot rolled edges removed. For best results, individual reductions in thickness should not exceed 7 pct, and the total reduction should not exceed 30 pct without annealing. Total reductions of up to 50 pct can be made, but cracking becomes very severe. The material is extremely sensitive to the 30 pct reduction. Edge cracking usually begins at just about the 30 pct reduction and the cracks propagate rapidly with each succeeding reduction. The edge cracks initiated at the 30 pct reduction extend approximately ¼ in. into the metal. Fig. 10 presents hardness vs percent reduction for iodide hafnium.

Hafnium foil as thin as 0.013 in. has been rolled on a four high cold mill. By pack rolling at room temperature in hafnium, thicknesses to 0.005 in. have been obtained; by rolling on a Sendzimir mill, thicknesses to 0.004 in. have been obtained. Pack rolling at room temperature in steel has been attempted, but it has not been successful for thicknesses less than 0.007 in. It appears that the steel jacket elongates more rapidly than the hafnium and

Fig. 8—At right is a consumable arc melted iodide hafnium ingot with splatter ring melted down and scrap additions made and at left a similar ingot conditioned by surface fusion.

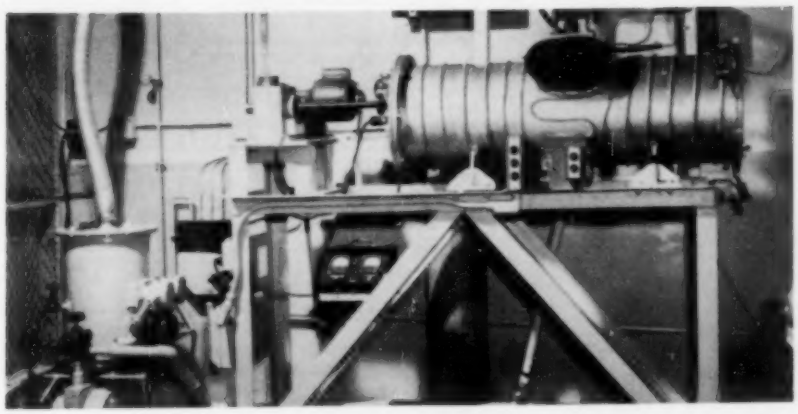

Fig. 9—Surface fusion unit used for conditioning ingots is shown.

consequently the hafnium is torn so that it resembles lace. Pack rolling at elevated temperatures would probably prove a good method for producing foil less than 0.005 in. thick.

### Machining

The similarity between iodide hafnium and zirconium with respect to fabrication also holds for machining. Hafnium is slightly more difficult than zirconium to machine and tends to shorten tool life. Like zirconium, hafnium tends to gall and build up on the tool unless proper machining techniques are used; the turnings produced are easily ignited by hot chips.

Best results in machining hafnium have been obtained by using cutters which have been sharpened to give a smooth curling chip of thickness little more than the depth of the cut. This necessitates high rake and clearance angles. Feeds and speeds must be adjusted so that the cutting tool enters the metal beneath the work hardened layer which generally is not more than 0.005 in. thick.

As in the case of zirconium, face milling is preferred to horizontal slab milling for the following reasons: A—face milling permits the use of inserted carbide teeth, B—the cutters are generally less expensive than those used for slab milling, and C—broken teeth are easily replaced. Carbide cutters with 6° to 10° negative radial rake and 10° to 15° positive axial rake give satisfactory results when the blades are ground to ⅛ in. x 45° chamfer. Clearance angles from 4° to 6° with approximately a ⅛ in. flat at the bottom of the cutter give a good finish. Water soluble oils are used as coolants.

The machining practice employed for aluminum is satisfactory for turning hafnium on a lathe. Satisfactory results can be obtained by using back and side rake angles up to 20°. Drilling of hafnium causes no difficulty, but when drilling thin sections improvement can be attained by sharpening the drills to angles more acute than normal. Sawing hafnium is more difficult than sawing zirconium primarily because of galling and the abrasive action on the saw blades.

Table IV. Hardness of Annealed Arc Melted Iodide Hafnium*

| Annealing Temperature | | Annealing Time | |
|---|---|---|---|
| °F | °C | 2 Hr | 20 Hr |
| 1382 | 750 | 215 Vhn | 200 Vhn |
| 1553 | 845 | 187 Vhn | 188 Vhn |
| 1652 | 900 | 185 Vhn | 180 Vhn |

* Data supplied by W. L. Mudge, Jr., WAPD.

Table V. Tensile Properties of Annealed Arc Melted Iodide Hafnium*

| Temperature | | Yield Strength, 0.2 Pct Offset, Psi | Ultimate Tensile Strength, Psi | Elong., Psi in 3 in., Pct | Reduction in Area, Pct |
|---|---|---|---|---|---|
| °F | °C | | | | |
| 75 | 24 | 22,400 | 59,400 | 35 | 38 |
| 300 | 149 | 17,500 | 46,100 | 43 | 48 |
| 500 | 260 | 12,100 | 37,700 | 51 | 50 |
| 700 | 371 | 10,100 | 29,700 | 56 | 62 |
| 900 | 482 | 9,500 | 26,100 | 63 | 70 |
| 1100 | 593 | 9,700 | 20,500 | 56 | 65 |

* The data listed were established on specimens tested in air. This resulted in some gaseous contamination at the higher test temperatures, e.g. the 1100°F specimen oxidized to the extent of being coated with a thin film of white powder after tests. Data supplied by W. L. Mudge, Jr., WAPD.

### Welding

With the exception of higher current requirements, the welding of hafnium is similar to that of zirconium. The currents used for ¼ in. thick plates vary between 160 and 200 amp at 16 v depending upon the penetration desired, and the current used for the complete penetration of a 0.1 sheet is about 90 amp at 18 v.

The surface tension of molten hafnium appears to be quite high, and when insufficient currents are used, the metal tends to agglomerate in balls. Because standard Heliarc equipment does not produce ductile welds, it is necessary to use a welding chamber with an inert atmosphere of helium or argon. In general, it has been found that hafnium welds (beta quenched) are stronger than the base metal. To date, all welding has been done using a tungsten electrode.

### Annealing

Hafnium thicker than 0.050 in. may be annealed in air without introducing more than surface contamination, providing the times and temperatures used are not excessive. Hafnium in thicknesses less than 0.050 in. should be annealed in vacuo or in an inert gas atmosphere. As usual, annealing times and temperatures are determined by the amount of prior cold work and the thickness of the section. Present

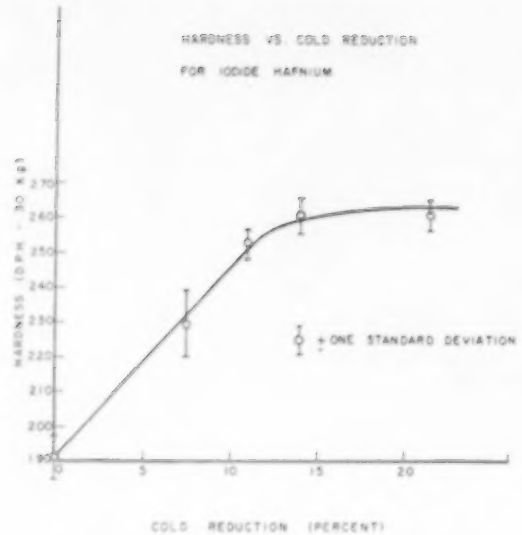


Fig. 10—Graph presents hardness vs percent reduction for arc melted iodide hafnium.

practice is to anneal ¼ in. thick hot rolled plates for ½ hr at 1700°F to obtain an ASTM grain size of 6 to 8. The oxidation resistance of hafnium in air is fairly good and somewhat better than that of zirconium. A penetration of 0.006 in. is obtained when iodide hafnium is heated at 1742°F for 2 hr in still air.

The recrystallization range for hafnium (1292° to 1382°F) is appreciably higher than that of zirconium (932° to 1022°F). Fig. 11 shows the temperature range over which recrystallization occurs and the effect of various cold rolling reductions. The

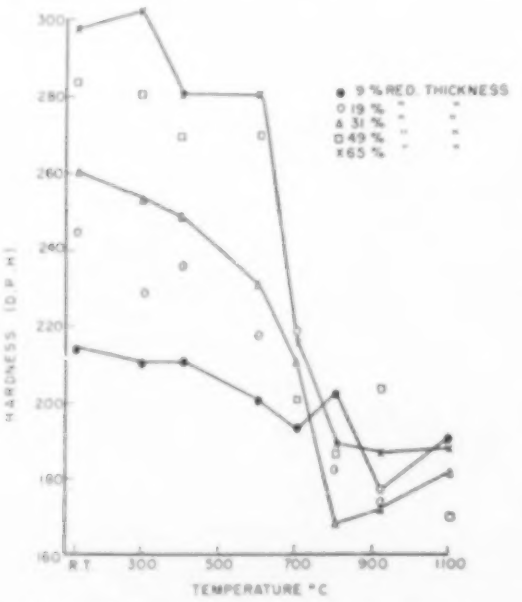


Fig. 11—Temperature range over which recrystallization occurs and the effect of various cold rolling reductions is illustrated.

Table VI. Creep of Arc Melted Iodide Hafnium Crystal Bar at 750°F (399°C)*

| Stress | Plastic Strain, Pct | Creep Rate Per Hr, in Per In. |
|---|---|---|
| 22,000 | 9.2 | $3.0 \times 10^{-4}$ |
| 24,000 | 17.9 | $7.2 \times 10^{-4}$ |
| 25,000 | 18.4 | $3.6 \times 10^{-4}$ |
| 27,000 | 22.2 | $8.6 \times 10^{-4}$ |
| 29,000** | — | 1 |

* W. L. Mudge, Jr., WAPD—102.
** Interpolated from tensile data.

preferred orientation of rolled hafnium has been found to be essentially the same as that of rolled zirconium. Table IV gives hardness data for various annealing times and temperatures.

Table V presents the tensile properties of annealed arc melted iodide hafnium. The specimens were annealed at 1650°F for 20 hr in vacuum prior to testing. Table VI gives the creep information available for arc melted iodide hafnium.


## Acknowledgment

Appreciation is due E. D. Baugh, J. Halapatz, F. R. Lorenz, H. R. Hoge, and F. G. Stengel, Bettis Plant, Westinghouse Electric Corp., for the information they supplied. The work was carried out under AEC Contract AT-11-1-GEN-14.


## References


S. M. Shelton and E. D. Dilling: The Manufacture of Zirconium Sponge (1953) *Zirconium and Zirconium Alloys*, ASM, pp. 82 to 120.

W. W. Stephens, H. L. Gilbert, and R. A. Beall: Consumable Electrode Arc Melting of Zirconium Metal (1953) *Zirconium and Zirconium Alloys*, ASM, pp. 121 to 130.

Z. M. Shapiro: USAEC, TID-5061, (1952) **1**, pp. 177 to 195.

Z. M. Shapiro: USAEC, TID-5084 (1952) **2**, pp. 95 to 111.

W. J. Hurford: Production Arc Melting of Crystal Bar Zirconium (Jan. 31, 1952) *Oak Ridge National Laboratory*, TID-5061, **1**, pp. 389 to 398.

R. B. Gordon and W. J. Hurford: Fabrication of Zirconium (1953) *Zirconium and Zirconium Alloys*, ASM, pp. 131 to 145.

J. L. Everhart: Titanium, Zirconium, Molybdenum, Tungsten, Tantalum, Columbium, Vanadium, and Hafnium as Engineering Materials (December 1951) *Materials and Methods*, **34**, pp. 89 to 104.

D. R. Kelker, P. J. Rieppel, and C. B. Voldrich: Cursory Attempts to Weld Hafnium to Stellite and Stainless Steel (May 13, 1952) Battelle Memorial Institute, BMI-744.

F. B. Litton: Preparation and Some Properties of Hafnium Metal (December 1951) *Journal of Electrochemical Society*, **98**, pp. 488 to 494.

R. K. McGreary and B. Lustman: Preferred Orientation in Zirconium (November 1951) JOURNAL OF METALS, pp. 994 to 1002.

F. M. Cain, Jr: A Simplified Procedure for the Metallography of Zirconium and Hafnium and Their Alloys (1953) *Zirconium and Zirconium Alloys* ASM, pp. 176 to 185.

J. D. Fast: The Allotropic Transformation of Hafnium and a Tentative Equilibrium Diagram of the System Zirconium-Hafnium (March 1952) *Journal of Applied Physics* **23**, pp. 350 to 351.

H. K. Adenstedt: Physical, Thermal and Electrical Properties of Hafnium and High Purity Zirconium (1952) *Trans.* ASM, **44**, pp. 949 to 967.

# Efficiencies of Electric Furnaces Can Be Increased by Using Higher Voltages

by E. L. French

EFFICIENCIES of carbide and ferroalloy electric furnaces can be increased by using higher voltages and higher power. This points the way toward the use of larger furnaces and the redesigning of existing equipment.

To obtain the benefits of higher efficiencies by the use of larger furnaces, it is necessary to operate at higher voltages. This is especially true when 60 cycle power is used.

The furnace operator, as a rule, prefers lower voltages because, when the voltage is raised for the same power input, the electrodes move higher in the charge and farther from the tap hole. The furnace may become hotter on top, operate less smoothly and tapping troubles may be increased. This could be corrected by using electrodes of smaller cross-section. Their higher resistance would cause them to seek a lower position in the charge in order to maintain the original furnace load.

Such a change is not always a simple matter so the natural tendency seems to be to take the line of least resistance and do nothing, even though higher voltages would lead to lower losses, higher power factor, higher load factor, higher production and lower costs.

## New Furnace Design

New furnaces can be properly designed for higher voltages so that they will operate as well as they now operate on lower voltages. Existing furnace equipment also can be redesigned to give better results. Usually, however, furnaces are kept operating as steadily as power conditions will permit and management prefers to avoid interference with continuity of operation. Certain changes, if required, may necessitate shutdowns of some duration, while in other cases all necessary preparations may be made in advance so that the actual shutdown time would be a minimum.

Proper design of the circuit between transformers and furnace is of vital importance in order to obtain both low reactance and low resistance. The former is necessary in order to get the desired power into the furnace and the latter in order that the electrical efficiency may be a maximum.

The electrical efficiency is the ratio of the resistance of the furnace itself to the resistance in the entire secondary circuit including the furnace. Hence the necessity of keeping the resistance of the outer circuit a minimum.

The power delivered by the transformer secondary to the furnace circuit multiplied by the electrical efficiency gives the power used in the furnace itself. This in turn multiplied by the thermal efficiency of the furnace gives the power remaining to produce the furnace product.

The thermal losses are relatively less in large furnaces because, when a furnace is so designed that it can form its own crucible in the charge, the volume of the crucible will vary with the power, whereas the losses from the crucible will vary as its area. If the crucible is considered as a sphere, the power will vary as the cube of its diameter, while the losses vary as the square of the diameter. Or stated in another way, in such a furnace the thermal losses will vary as the two-thirds power of the power used in the furnace.

This line of reasoning was first developed by W. S. Horry, the inventor of the Horry rotary carbide furnace. However, Horry applied this reasoning to the total power in the furnace circuit instead of to the power in the furnace itself and assumed a straight 3 pct loss in transformers and secondary copper. These electrical losses or the electrical efficiencies vary over a wide range in the same furnace at different loads and different voltages so that it is necessary to take them into account before comparing thermal losses in two cases.

### Advantages of Using Large Electric Furnaces With Higher Voltages

A. Lower first cost per unit of power utilized. One furnace is less expensive to build than two of half the rated power.

B. Lower labor costs per ton of product. Almost as much labor is required for a furnace of a given size as for one of twice that size providing proper mechanical feeding equipment is used.

C. Lower electrode costs per ton of product. Higher power per furnace required higher voltage to obtain a good power factor, which means that at a given current density in the electrodes, the size of electrodes required is relatively smaller for the larger furnace.

D. Lower power costs per ton of product. Larger furnaces have higher thermal efficiencies or relatively lower thermal losses from the furnace itself. The electrical losses in the secondary circuit outside of the furnace, at a given voltage increase with the load. At the same power factor at various loads the electrical efficiency remains the same. If at a given electrode setting furnace voltage is increased, the load will increase as the square of the voltage, but the electrical efficiency will remain the same. At higher electrode settings (i.e. higher arc or furnace resistances) electrical efficiency will increase.

E. L. FRENCH is a Consulting Engineer, New York City.

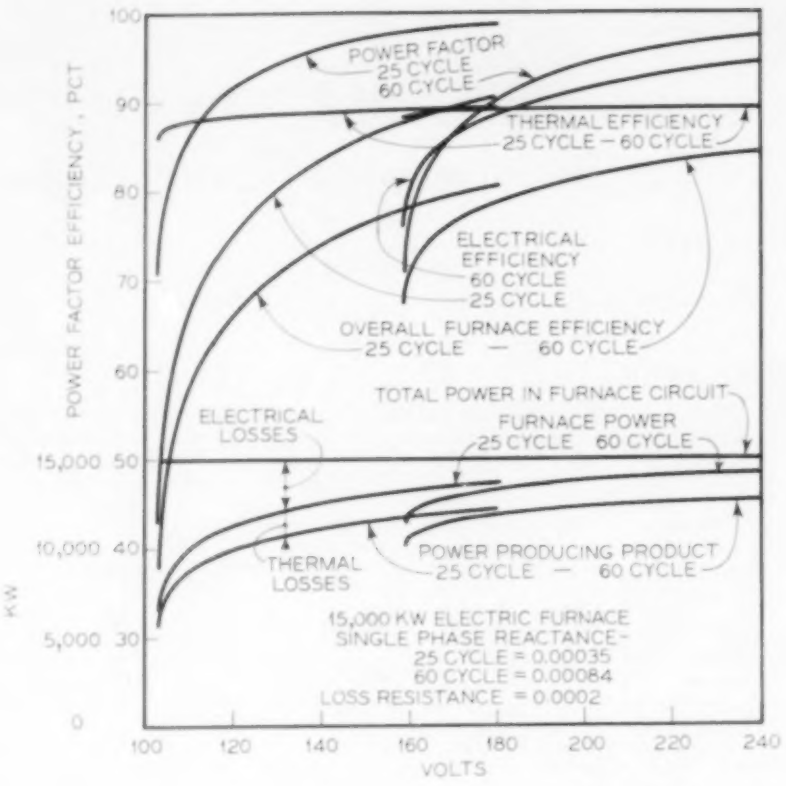


Fig. 1—With a fixed input of 15,000 kw, the effect of varying voltage on power factor, electrical, thermal, and overall furnace efficiencies is graphed. The remaining power to do useful work in the furnace is also shown.

### Thermal Losses

Thermal losses may be reduced by better insulation of the furnace though it is desirable not to carry this to the point where there will no longer be a crucible formed in the charge and molten material will be allowed to come in direct contact with the sidewall lining.

Sufficient insulation should be provided so that the walls of the furnace crucible will not form too closely to the electrode. Egress of the furnace gases will then take place with a minimum of interference and the tendency toward gas pocket formations and blows will be reduced.

Formerly it was common practice to design three phase furnaces with electrodes arranged in line rather than in triangle. While there may be, in

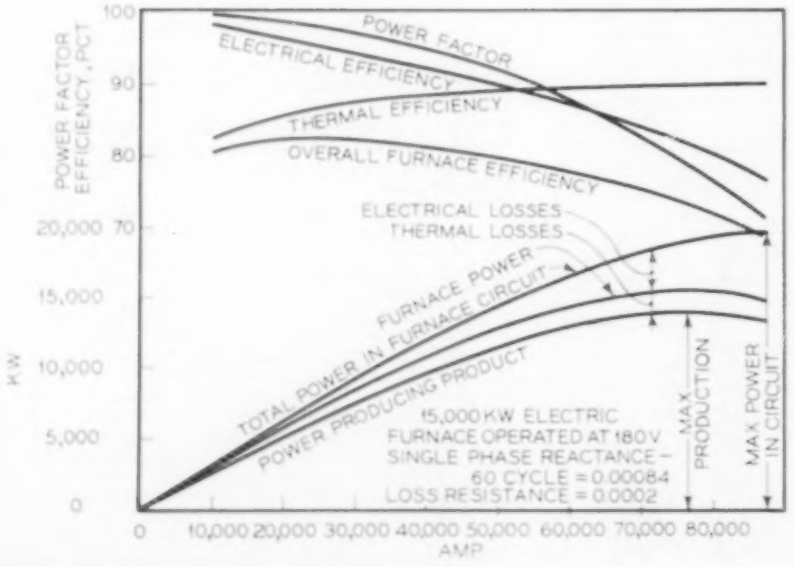


Fig. 2 — Characteristics of a 60 cycle furnace with the same reactance and loss resistance used in Fig. 1 is shown when operated at 180 v over a current range from 10,000 to 87,613 amp.

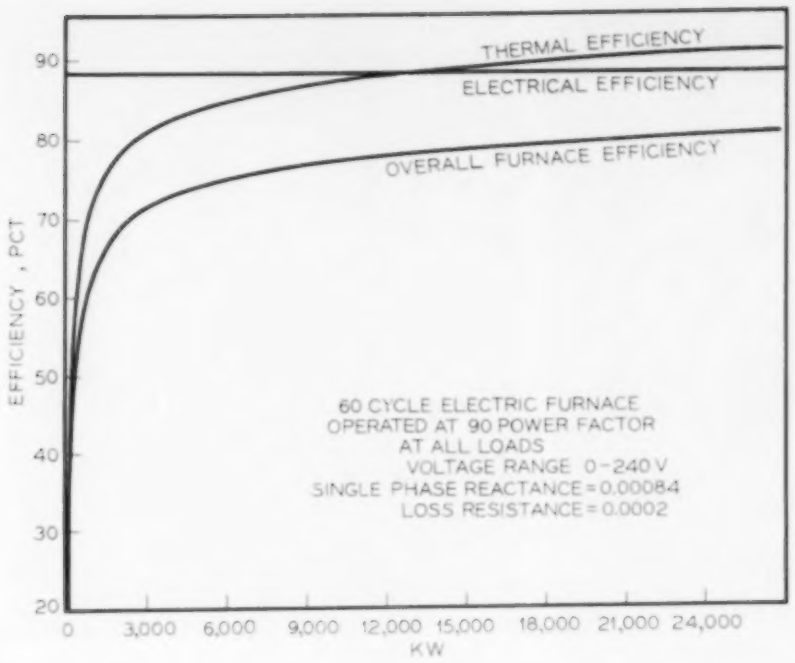


Fig. 3—Graph shows how efficiencies in a 60 cycle furnace vary with the load providing a 90 pct power factor is maintained at each load.

certain instances, some advantage with this arrangement, generally speaking the odds are in favor of the triangular arrangement since furnace reactance is lower, power factor higher, and the phases can be kept better balanced. This is impracticable with the *three in line arrangement*. One outside phase will always be less active, take less power, and produce less product.

### Electric Furnace Data

The conclusions reached are based on a 15,000 kw three phase furnace having a single phase reactance of 0.00084 ohm at 60 cycles or 0.00035 ohm at 25 cycles, and a resistance of the external furnace circuit (the so-called loss resistance) of 0.0002 ohm. The reactance chosen is lower than that of many existing furnaces but not beyond the range of good design.

From the original data electrical efficiencies can be calculated, but for the purpose of this article a thermal efficiency was assumed in a given case at a given power in the furnace itself which should be substantially correct, and then the thermal efficiency for any other power was calculated.

With a fixed input of 15,000 kw, Fig. 1 shows the effect of varying voltage on power factor, electrical, thermal, and overall furnace efficiencies; and the power remaining to do useful work in the furnace.

This data shows that:

A—Efficiencies improve as voltage is increased.

B—25 cycle furnaces are more efficient than 60 cycle furnaces at the same voltage.

C—60 cycle furnaces are more efficient than 25 cycle furnaces at the same power factor.

D—It is not desirable to operate any furnace at too low a voltage. This is relatively more true of 25 cycle than 60 cycle furnaces, because, although the required power at a good power factor can be obtained at a lower voltage with 25 cycles than with 60 cycles, the efficiency is lower at the lower voltages.

Fig. 2 shows the characteristics of a 60 cycle furnace with the same reactance and loss resistance used in Fig. 1, but operated at 180 v over a current range from 10,000 amp up to 87,613 amp.

This data shows that at a given voltage the:

A—Electrical efficiency decreases as the load increases.

B—Thermal efficiency increases as the load increases.

C—Overall furnace efficiency decreases as the load increases but it may be counterbalanced by going to higher voltages at the higher loads.

D—Maximum power in the furnace circuit is reached at 70.7 power factor.

E—Maximum power in the furnace itself in this instance is reached between 78.0 and 79.0 pct power factor.

Although maximum production can be obtained at a 78 or 79 pct power factor, it is not the optimum point of operation. For instance, in comparing operation at 79.6 pct power factor with operation at 91.5 pct power factor, overall furnace efficiency would be 73.3 pct as compared with 79.5 pct. Also while productive kilowatt would be increased 2300 kw, it would be necessary to pay for an additional 4340 kw in order to obtain it. This would mean approximately a 190 pct increase in cost of power per ton of product for the additional production. And the additional 25,000 amp per phase at the lower power factor would increase current density in the electrodes and increase in relatively greater proportion electrode consumption.

If production at the desired power factor is not sufficient, then a higher voltage should be used. Fig. 3 shows how efficiencies in a 60 cycle furnace vary with the load providing a 90 pct power factor is maintained at each load.

# Short Cycle Heat Treatment Improves Low Alloy Pipe Production

by James Kniveton

PRODUCTION of high strength oil well casing from plain carbon and low alloy steels has become commonplace since the introduction of short cycle heat treating less than a decade ago.

At that time, the strongest casing required by the oil industry was defined by API Grade N-80, designed for wells up to 10,000 ft deep. Basic requirement for this grade was a yield strength of 80,000 psi, for which a normalized and drawn, high manganese, molybdenum steel was considered necessary. Much of the steel contained chromium as well. Steelmen also faced the problem of upsetting or machining ends of this pipe to provide for joining sections in the field, generally a difficult problem with pipe of this strength.

Use of a short cycle heat treating process, however, now enables the steel industry to produce pipe of 80,000 psi minimum yield strength from plain carbon steel with a minimum of manganese, conserving important quantities of critical alloying elements. But this low alloy steel pipe is no mere substitute; it has proven better than the original product in several important respects. It is more easily machined than casing made by older methods, and the new heat treating method promises to make practical the production of casing for extremely deep wells with depths of 20,000 ft or more—110,000 psi and higher yield strengths, suitable for this use, have already been obtained with short cycle heat treatment.

A conventional heat and draw cycle—heat to 1650°F, quench, draw at 1250°F, and cool—takes at least 12 hr with high alloy steel. The short cycle quench and draw takes only 10 min to attain the same strength, comparable toughness, and superior machinability with plain carbon steel.

### Short Cycle Equipment

Key equipment in short cycle heat treating is a cylindrical gas fired furnace developed by Selas Corp. of America. A typical installation consists of a series of these furnaces—each of which is only 4 to 6 ft long and has a chamber diameter only slightly greater than the largest diameter to be processed. A predetermined, carefully controlled mixture of gas and air is fed under pressure to radiant cup burners set into the inner wall of the furnace. No flame comes in contact with the pipe because combustion is completed within the *duradiant* burner cup.

Uniform, high-speed heating is accomplished through *gradiation*, that is, a high gradient, or temperature difference, between burner cup and work, producing a very rapid transfer of heat by a combination of radiation and convection.

In operation, a number of barrel furnace units are lined up, with conveyor rollers between the units, to form a single, conveyorized furnace installation. Small, concave rollers, with their axes almost perpendicular to the line of pipe travel, were used originally. A slight offset in the direction of the axis provided a small, controllable amount of rotation.

While this type of roller is still used, more recent evidence of the value of high rates of rotation has led to the use of a pair of large diameter wheels turning on axes almost parallel to the line of pipe travel. Forward motion of the pipe is effected by offsetting the axis of rotation as much as 15°.

With either type of conveyor, each roller or pair of wheels is turned by an individual electric motor.

J. KNIVETON is Vice President, Selas Corp of America, Philadelphia.

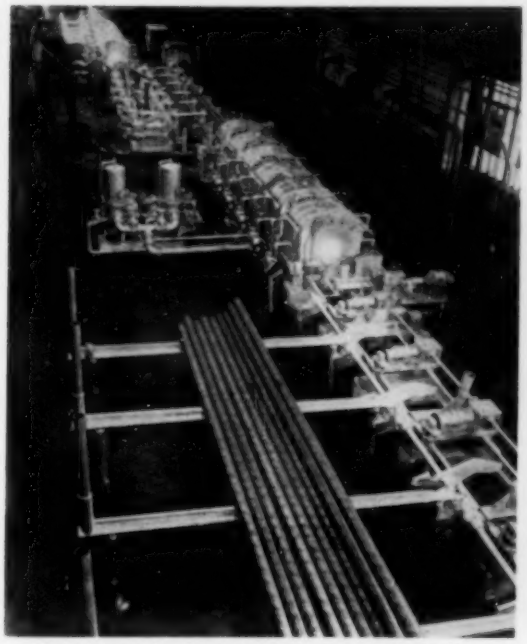

Fig. 1—Hardening and tempering oil well casing in Selas short cycle equipment is shown at the Spang-Chalfant div. of National Supply Co.

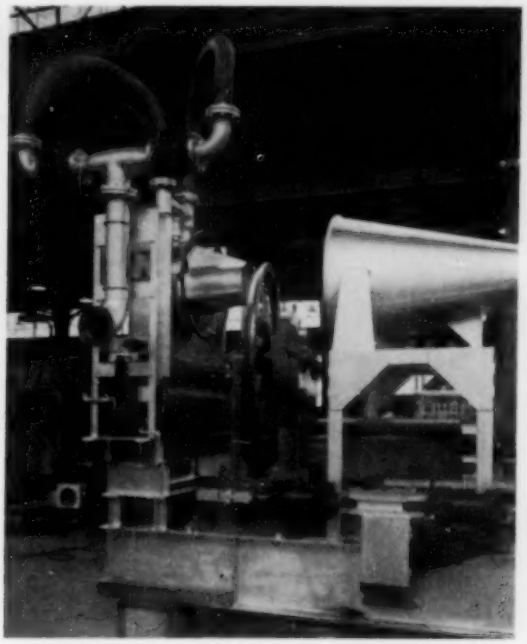

Fig. 3—Quench ring with spray guards was recently developed for short cycle quench and draw lines.

The entire conveying unit is mounted outside of the furnace away from the higher temperatures. Special temperature resistant alloys are needed only on those surfaces actually in contact with hot pipe. Wear is greatly reduced, and both maintenance and control are simplified.

Flexible control is an advantage of the use of individual barrel furnace units, also. Each barrel unit may be controlled individually, or several may be fired through a single control to form a heating zone.

The furnace control is generally arranged to provide high heat output only when the tubing is actually passing through. At all other times, the furnace is idled for fuel economy, longer refractory life, and more efficient temperature control.

The high heat level may be controlled according

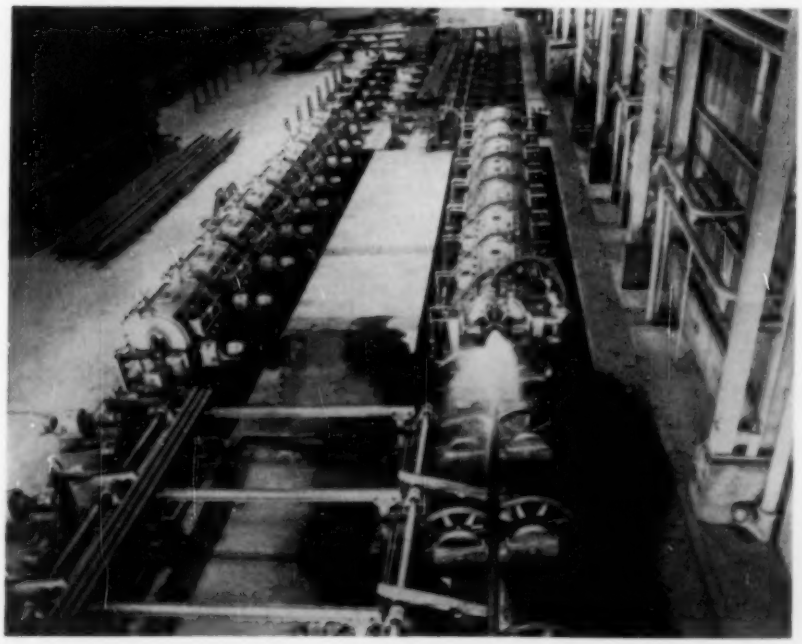

Fig. 2—Seamless tubing leaves the quench ring at Colorado Fuel & Iron Corp. mill. Disk-type conveyors are used in the quench line and roll type in the draw line.

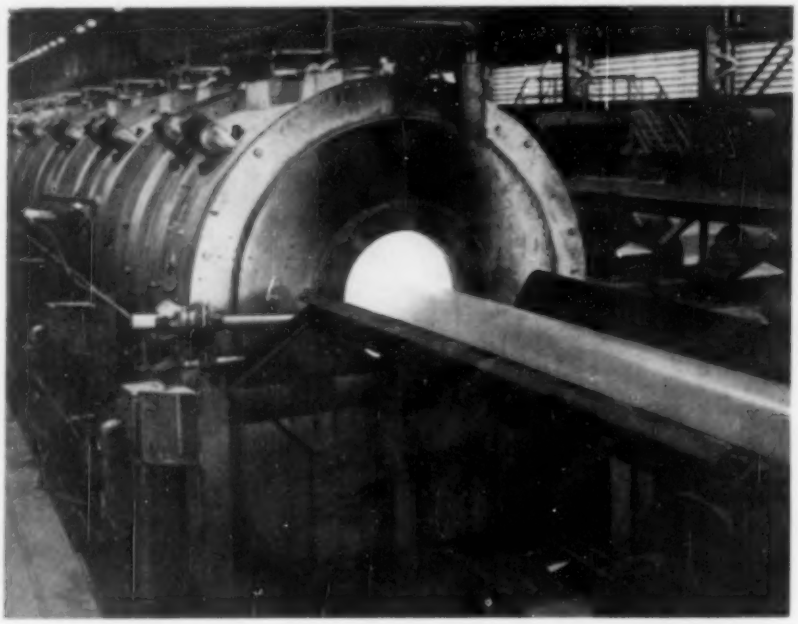

Fig. 4—Welded oil casing leaves the 33-barrel normalizing furnace at Lone Star. Tubing is shiny and scale free although no prepared atmosphere is used.

to a preset time-temperature cycle or by a sensing device measuring the temperature of the tubing passing through.

Combustion controllers accurately proportion gas and air, and feed the mixture under pressure to the burners. This pressure and proportioning remain constant even when individual burners or whole furnace units are turned down or completely shut off. This assures complete combustion, and a protective atmosphere of combustion products to prevent scale formation on the tubing. The protective atmosphere extends across the short interval between barrel units.

### Lines in Operation

Similar furnace lines had been used previously on many types of bar and tube stock, but the first continuous line for hardening and tempering oil well casing has been in operation since 1947 at the Ambridge, Pa., plant of Spang-Chalfant div. of the National Supply Co., shown in Fig. 1. Here 30 to 50-ft lengths of pipe are sent through a line of six barrel furnace units and a high pressure water spray, or

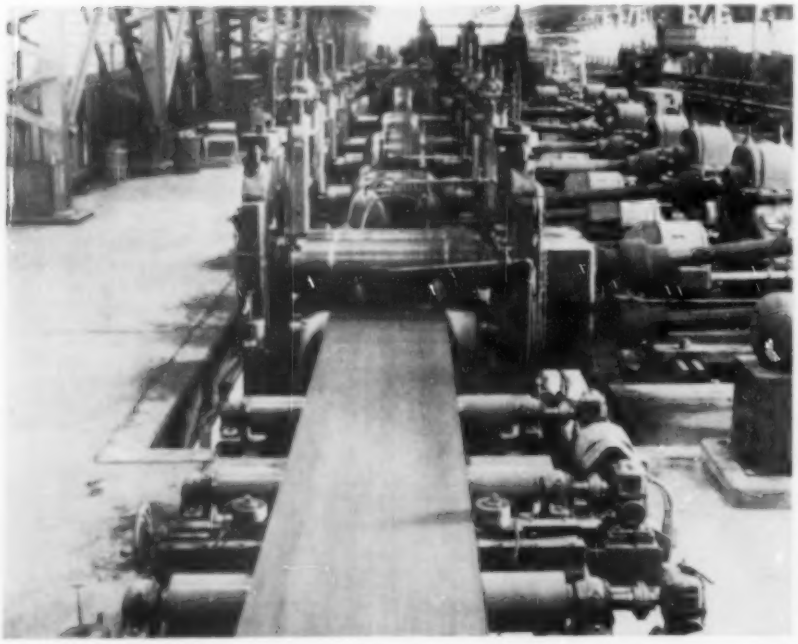

Fig. 5—Steel strip enters forming section of the Lone Star Steel Co.'s welded pipe production line. Short cycle, in-line normalizing permits completely automatic production.

Fig. 6—Cross-section of Duradiant burner used in short cycle heat treating is shown. Combustion is complete within the cup (flow of gases indicated by dotted line), and heat is transferred to workpiece by radiation (arrows) and by convection of nonoxidizing combustion products.

quench, at speeds that range from 3¼ to 6½ fpm. One end of a length of pipe will normally be entering the quench ring just as the other end enters the first furnace unit. The pipe reaches 1600°F before it enters the quench spray, which quickly brings the steel down to about 125°F.

A conveyor table moves the pipe laterally after it leaves the quench head, empties the pipe of any water that may be inside, and feeds the pipe into a draw furnace line running parallel to the quench line, at the same speed and in the same direction. In the draw line, the pipe is raised to about 1125°F in six barrel units, and then is discharged to cool slowly in the air.

This installation produces from 4.8 to 5.4 tons of quenched and drawn pipe per hr, ranging in size from 5½ in. OD × 0.304 in. wall of 9⅝ in. OD × 0.435 in. wall. The quench and draw line occupies 5850 sq ft, with combustion controllers and temperature control instruments occupying a separate room of 1400 sq ft. Two men operate the line, making all necessary changes for different sizes of pipe, checking the automatic functions, and loading pipe on the charging table and baling processed pipe on the discharge table.

In a similar installation at the Pueblo, Colo., mill of Colorado Fuel & Iron Corp., the draw line runs in the direction opposite to that of the quench line, in a U-shaped arrangement. This installation shown in Fig. 2, which has only recently begun production of high strength oil well casing, contains eight barrel units in each section.

One reason for having the quench line and the draw line separated laterally is to allow for mechanism to remove any water which may enter the tubing as it leaves the quench spray. In an automatic heat, quench and draw line recently constructed for another large steel mill, however, the hardening and tempering sections are placed in the same line. This offers simplified handling between quench and draw, and is made possible by successful control of water entering the pipe end. Another

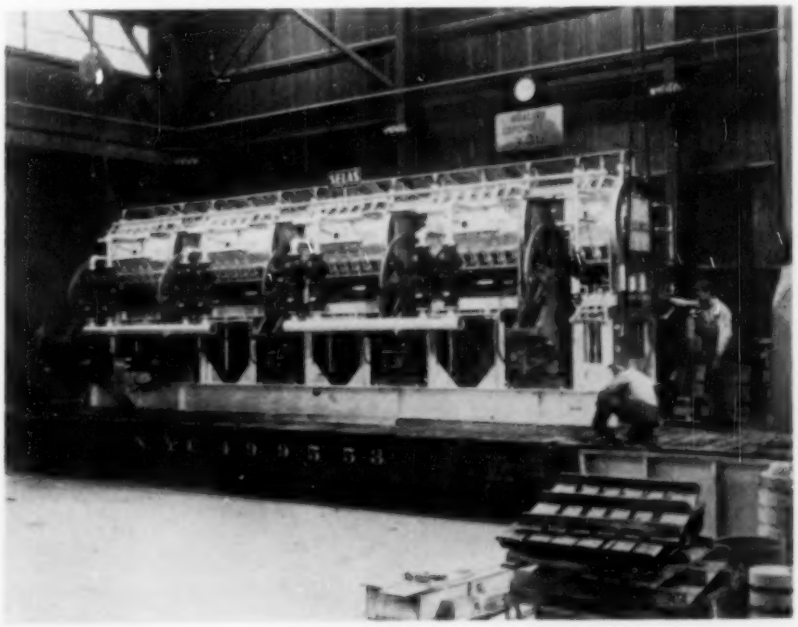

Fig. 7—A section of five barrel furnaces is loaded for delivery. The furnaces are complete, and require only connection to supply and control lines as the high heat section of a quench and draw line.

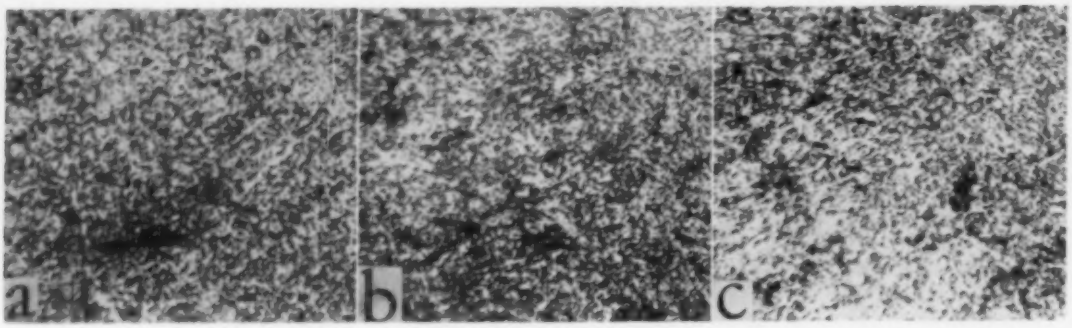


Fig. 8—Microstructure of seamless steel oil well casing after short cycle quench and draw are: a—section at outer surface, b—section at center of wall, and c—section at inner surface.

innovation in this latest installation is the use of a conical spray guard downstream from the quench head to hold the quench water close to the tubing for increased quenching efficiency as shown in Fig. 3.

Improvement in the quality of welded pipe has led to its increasing use in the oil industry, in competition with seamless tubing. Continuous, short cycle normalizing, a close counterpart to the short cycle quench and draw process, has played an important part in this development.

Current practice calls for heating the pipe to 1650°F, followed by cooling in air. While conventional normalizing processes call for the use of a relatively large furnace to bring the temperature up to 1600°F to 1700°F, in 6 min, and to hold it at temperature for 15 min, short cycle normalizing takes only 60 to 70 sec in a compact barrel furnace line.

At the Lone Star, Texas, mill of the Lone Star Steel Co. each of two Selas normalizing lines shown in Fig. 4 consists of a charge table, 33 barrel furnace units, and a discharge table. It occupies a ribbon of floor space 330 ft long and 8½ ft wide, an area of 2805 sq ft as compared to conventional normalizing equipment which requires 8400 sq ft. The furnaces are similar to those used in the quench and draw lines, except that gas and air are brought to each burner in separate lines and mixed in the specially designed nozzle.

The furnace units in each line are grouped in seven operating zones, independently controlled. One line handles large diameter pipe at up to 3000 lb per min, while the other handles smaller pipe at a maximum of 1500 lb per min. The speed of the pipe through the normalizing line is set to keep pace with production requirements, depending on the size and gage of the pipe.

### Mill Features

A unique feature of this mill is that there is no manual handling of the pipe from the initial coiled strip steel shown in Fig. 5, through cold forming, welding, cutting into lengths and normalizing. The entire cycle is completely automatic.

To accommodate variations in pipe diameter, wall thickness, and linear speed, the first four zones of each line are controlled to produce the desired tem-

Table I. Physical Properties of Short Cycle Treated Pipe

| | |
|---|---|
| Ultimate strength | 130,000 to 135,000 psi |
| Yield strength | 110,000 to 118,000 psi |
| Elongation in 2 in. | 25 to 28 pct |

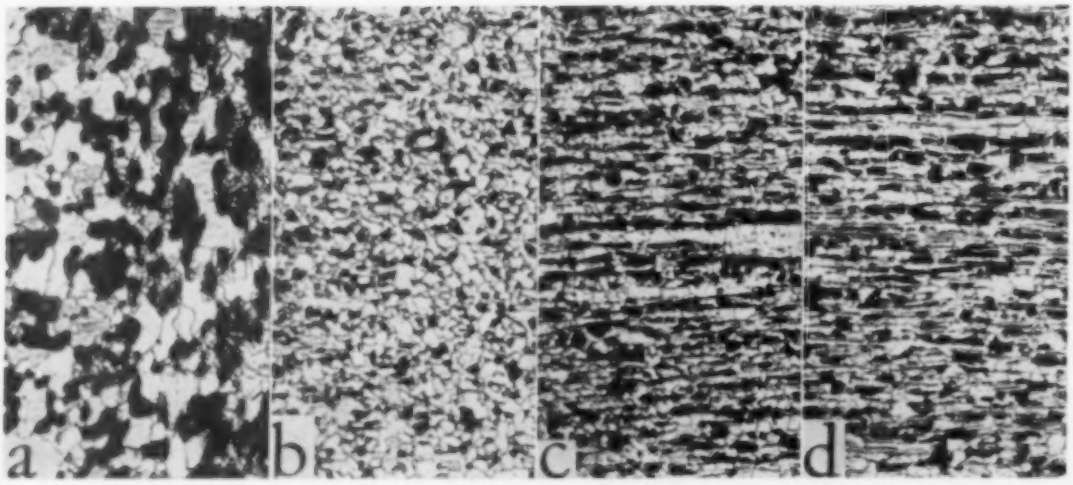


Fig. 9—As-welded microstructures of electrically-welded tubing 2 in. O.D. x 0.156 in. wall are: a—at weld line, b—⅛ in. from weld, c—¼ in. from weld, and d—180° from weld.

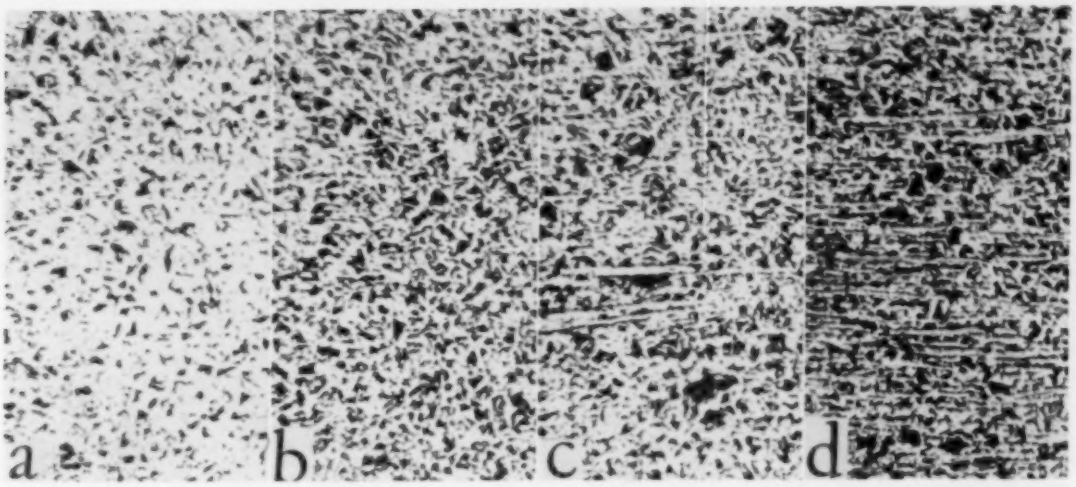


Fig. 10—Microstructures of electrically-welded tubing 2 in. O.D. x 0.156 in. wall after 1660°F short cycle normalizing are: a—at weld line, b—1/8 in. from weld, c—1/4 in. from weld, and d—180° from weld.

perature gradient while the remaining three zones are automatically regulated to complete the heating and to assure a uniform temperature from one end of each length of pipe to the other, and from pipe to pipe.

The barrel furnace design readily lends itself to a wide range of mechanical and thermal control. Conveying units are extremely flexible, since they operate in the cooler space between units, with controlled variation possible in forward speed of the tube. Burner groups can be turned down over a range of 15 to 1; and burners or whole units can be completely shut off while the line is in operation. Any increase or reduction in the flow of the fuel mixture results in an immediate corresponding change in radiation from the burner cup shown in Fig. 6.

Automation is an inherent feature. Barrel-furnace lines are controlled through automatic feedback circuits, providing for furnace operation according to the temperature of the stock leaving it. A novel form of feed forward circuit is also employed, where control of an individual unit depends on the temperature of stock entering it. In the latter case, the first units through which the tube passes may be operated at full capacity, while later units are adjusted to provide only the amount of heat required to reach and to hold the desired temperature.

Furnace temperature is usually measured by a radiation pyrometer sighting on the closed bottom of a tube extending into the furnace cavity, or by a suitable thermocouple. The segmented structure of the furnace permits unusually accurate determination of work temperature by mounting a radiation pyrometer outside of the barrel, where it will be least affected by radiation from furnace walls, gases, and other sources. Since short cycle heat treatment leaves the stock shiny and relatively scale free, this latter method is a fairly dependable technique.

Control of heat output is maintained through electrically operated valves in the fuel mixture supply line.

Another advantage stemming from the barrel furnace design is the simplicity of installation. All refractory materials are installed at the factory. Units consisting of several furnaces as in Fig. 7, permanently mounted with all conveying equipment on integral structural framework, are shipped to the steel mill ready for operation. At the mill, they need only be set in place, and control and feed lines attached. No furnace construction is necessary.

### Physical Properties

These features of short cycle heat treating equipment, however desirable, are important only to the degree that they enable the steel industry to produce pipe of superior physical quantities. The seamless tubing described as suitable casing for 20,000-ft wells can demonstrate such superior properties. The ranges given in Table I were obtained by short cycle treating seamless pipe with about 0.45 pct C, 1.50 pct Mn and 0.20 pct Si.

Conventionally treated pipe with the same yield strength shows higher values of ultimate strength and hardness and lower ductility with decreased toughness. The lower hardness resulting from short cycle treatment is particularly important wherever machining is involved.

The microstructure of this pipe is shown in Fig. 8. The microstructure is a fine, evenly grained, tempered martensite, with no free ferrite present.

Welded pipe shows similarly improved physical properties after short cycle normalizing. Microphotographs shown in Figs. 9 and 10 indicate that the short cycle treatment produces finer grain, with the complete elimination of banded or laminated appearance. The banding is undesirable since it imparts some directional properties to the steel, while the finer grain indicates higher hardness, strength, and yield-tensile ratio. While the ultimate strength is slightly higher after short cycle normalizing than after a conventional 15-min soak at 1650°F, the yield strength is much higher and more uniform around the pipe circumference.

Deeper wells and higher pipeline pressures have developed an increasing demand for high strength tubing for the oil industry, while defense and other requirements have made steelmen look to low alloy steels to meet this demand. High speed heat treatment has proved to be an important part of the answer to this dilemma.

# Box Car Roof Design for Open Hearths Evaluated at Inland Steel Co.

by P. W. Nutting

FOR many years, it has been the practice in Inland's No. 2 open hearth shop to install port roofs with a slope and hood arrangement similar to that installed in many other shops throughout the country. For example, on 200 ton furnaces, the port slope started at a point slightly in front of the bridgewall (12 ft 9 in. inside end buckstays) rising 3 ft in a longitudinal distance of 5 ft 9 in. The remainder of the port roof (7 ft 0 in.) was then installed as a level hood.

This design is common to many furnaces throughout the country and is probably a holdover from the old producer gas fired furnace. The hood section of the port roof gave very little difficulty, but the corbeled slope caused frequent trouble when it was necessary to do hot patching in this area. Because of this difficulty and also because of the widespread interest in port and port roof design, several roofs were installed with only a slope, omitting the level hood. It was a natural step from this design to the flat port roof or *box car roof* design.

### Box Car Roof

The first installation was made on one of the 200 ton furnaces in April 1952, despite the opinion of many of the operators that it would not perform satisfactorily. All subsequent roofs on this furnace have been of the same design. Average savings on the original installation and the repair necessary during the campaign are shown in Table I.

The saving may seem to be of a minor nature when considered for an individual furnace, but when applied to the 24 furnaces in the shop, it becomes a major saving in rebuilding and maintenance cost over a period of a year. It is recognized, however, that this savings would hardly be justified if the change in port roof design resulted in lowered production rates or increased fuel consumption. No. 34 furnace, on which the original box car roof was installed, has always been one of the slower furnaces and it was hoped that the change in port roof design might improve this condition.

Average production rates for the past three months for the furnaces with conventional port roofs was 17.9 tons per hr, tap to tap, while No. 34 furnace averaged 18.4 tons per hr. During the same period, fuel consumption on No. 34 furnace averaged 0.3 gal per ton less than the furnaces with conventional port roofs.

P. W. NUTTING is Assistant Superintendent, Inland Steel Co., East Chicago, Ind. This paper was presented at the AIME National Open Hearth Conference, Philadelphia, Apr. 18 to 20, 1955.

On the basis of these results, it was decided late in 1954 to extend the installation of box car roofs to all furnaces in the shop. Since then, as each furnace came down for rebuild, the necessary changes in the furnace iron work have been made and box car roofs installed. Production rates on the 200 ton furnaces so altered indicate a higher tons per hr figure on these furnaces than on those with the old type roof and no significant difference in fuel consumption. However, it is felt that sufficient data is not yet available to prove that the change in port roof design has resulted in increased production. The box car design, however, gives at least as good performance in respect to both production and fuel consumption.

### Roof Performance

Operators have frequently found that a practice or design which worked satisfactorily when applied experimentally to one furnace, does not prove equally satisfactory when applied to other furnaces. It was found on the original installation that the port section of the roof showed little wear during the full campaign, requiring virtually no patching. On subsequent installations, this has not been true, and on several occasions this section of the roof was replaced at less than 200 heats.

On No. 34 furnace, no excessive wear on the uptakes or end panels was indicated, but on similar installations on other furnaces, particularly in the case of the 175 ton furnaces, uptakes and neck arch supports have actually been washed out. Whether or not this is the result of the change in port roof design or some other operating factor has not yet been determined. There is little question, however, that the path of both the incoming and outgoing gases have been changed, both in the uptakes and under the port roof. This may be responsible for the difficulties being encountered. As a result of the above difficulties, the installation of box car roofs at No. 2 open hearth has been halted until a better evaluation of the program can be made.

Table I. Average Savings Using Flat Port Roof

| Cost Item | Savings as Compared to Conventional Roof, $ |
|---|---|
| Mason | 280 |
| Labor | 243 |
| Carpenters | 517 |
| Material | 0969 |
| Total | 8009 |

# Effect of Sinter Mix Composition and Additives on the Quality Of Blast Furnace Sinter

by E. C. Rudolphy, C. W. Boquist, and D. J. Carney

**Effect of variations in sinter feed composition on sinter strength, bulk density, reducibility, chemical composition, and microstructure were determined by sintering experimental samples on a production sintering machine. Increasing amounts of roll scale, ore fines, return fines, and blast furnace slag were most beneficial to feed permeability, sinter bulk density, and strength. Burnt lime additions improved feed permeability but were not beneficial to sinter strength or bulk density. Sinter reducibility was adversely affected by all additives.**

DEVELOPMENT of methods for evaluating sinter quality, which would in some way predict the behavior of the sinter during charging and smelting in the blast furnace, has been given considerable attention in recent years. In a previous investigation at South Works of the United States Steel Corp., standard sinter sampling and testing procedures were developed.[1,2] By modifying the sinter sampling device, a method of sintering *experimental mix* sinter samples upon a production Dwight-Lloyd sintering machine was also developed. This technique afforded a rapid and controlled method of investigating the effects of the various raw materials and additives on sinter quality and was used in this present investigation.

Since the beginning of the present study in 1953, the results of numerous sinter investigations have been published, most of which were concerned with production tests of iron ore sinter, both here and abroad. Three groups of investigators reported results of experimental sinter studies that were related to this investigation. Voice et al.[3] studied the effects of controlled variables on sinter quality by producing and testing experimental Northants iron ore sinter using an experimental sintering unit. Morrissey and Powers[4] determined the relationship between iron ore sinter quality and the moisture and coke content using a small laboratory sintering system. Burlingame et al.[5] studied the effects of "additives" upon iron ore sinter using a laboratory sintering apparatus and laboratory grade raw materials.

At South Works, it was considered desirable to study the effects of sinter mix composition and additives upon the quality of a flue dust-base sinter produced on a production sintering unit. Extrapolation of controlled laboratory test data to sintering plant operation lacking such precise control is not altogether satisfactory. Therefore, the present study was conducted in a manner which approximated production conditions as closely as possible. The raw materials used were those commonly encountered in the production of flue dust and flue dust ore-type sinters and these were varied within extremes encountered in this type of sinter production.

E. C. RUDOLPHY, Junior Member AIME, C. W. BOQUIST, and D. J. CARNEY, Member AIME, are Physical Metallurgist, Metallurgical Technologist, and Superintendent, No. 2 Electric Furnace Shop, respectively, South Works, United States Steel Corp., Chicago.

Discussion of this paper, TP 4051C, may be sent, 2 copies, to AIME by Jan. 1, 1956. Manuscript, Jan. 18, 1955. Blast Furnace, Coke Oven, and Raw Materials Conference, Philadelphia, April 1955.

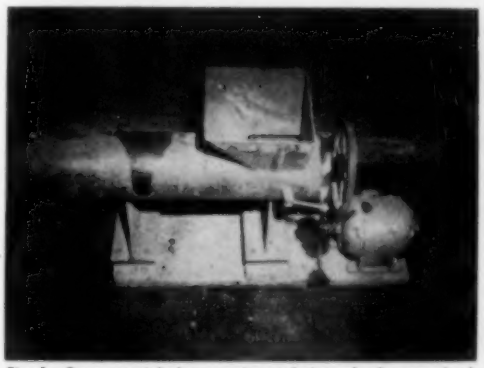

Fig. 1—Raw materials for experimental sinter feed were mixed by this miniature single shaft pug mill.

## Experimental Procedure

The experimental sinters were produced from 100 lb mixtures of sinter feed. The principal raw materials and additives used, their particle size, and approximate chemical composition are listed in Table I.

The mixing of the raw materials was accomplished by means of a miniature single shaft pug mill shown in Fig. 1. The use of the pug mill as a mixer was decided upon after encountering difficulty in reproducing the mixing and chopping effect of the sinter plant pug mill with other types of available small mixers. The miniature pug mill was constructed, consisting of 3½x2x¼ in. blades spaced 3 in. apart along a 3 ft shaft. Preliminary tests were run with this small mixer to establish the proper rotation speed and the required number of passes through the pug mill to thoroughly mix and distribute all the raw materials in a manner approximating the production pug mill.

Although the effects of varying the mosture content were determined in one particular series of tests, the amount of moisture added was changed as the composition of the experimental mix was varied. The aim in making water additions was to achieve a permeability as high as possible for each particular



*The Transactions papers appearing in the Journal of Metals during 1955 will subsequently appear in AIME Transactions Volume 203, and may be permanently referenced to that volume.*

Table I. Basic Raw Materials and Additives Used in Producing Experimental Sinters

| Material | Chemical Composition, Wt Pct | | | | | | Particle Size | Remarks |
|---|---|---|---|---|---|---|---|---|
| | Fe | $SiO_2$ | $Al_2O_3$ | CaO | MgO | C | | |
| Flue dust, current | 54.19 | 10.49 | 3.22 | 2.13 | 0.36 | 4.73 | 100 pct −20 mesh | Stock dust has been stored in open air for longer than 6 months |
| Flue dust, stock | 53.14 | 10.75 | 2.07 | 2.01 | 0.53 | 5.08 | | |
| Filter cake | 49.28 | 14.50 | 3.34 | 3.09 | 0.42 | 5.24 | 90 pct −180 mesh | |
| Oliver 3 ore fines | 59.59 | 5.29 | 1.53 | 0.10 | 0.06 | — | 100 pct −0.371 in. screen | |
| Roll scale | 70. | 0.5 to 4.0 | — | — | — | — | 100 pct −0.371 in. screen | Normal mill roll scale |
| Return fines | Analysis similar to that of sinter | | | | | | 100 pct −0.371 in. screen | |
| Burnt lime | — | 0.4 | — | 93. | 2.0 | — | −8 mesh | |
| Silica | — | 99.5 + | — | — | — | — | −200 mesh | Finely divided silica flour |
| Alumina | — | — | 98. + | — | — | — | −20 mesh | Alcoa alumina |
| Magnesia | 0.27 | 3.8 | 0.5 | 1.3 | 91.2 | — | −8 mesh | "Permanente 165" |
| Granulated blast furnace slag | 0.40 | 40. | 10. | 43. | 3.5 | — | −0.371 in. screen | From a basic iron furnace |
| Coke breeze | 15 to 10 pct volatiles; 10 to 12 pct ash | | | | | 80 to 85 | −8 mesh | Used as fuel |

group of raw materials within a given series of mixes.

An attempt was made to maintain a carbon content at 6 pct in all mixes by using coke breeze. Small variations in carbon content of the experimental mixes were caused by fluctuations and heterogeneity of the flue dust and filter cake used as raw materials. In one series of mixes, the carbon content was purposely varied to study its effects. This was accomplished by using a flue dust with a known low carbon content and adding coke breeze as required.

In the initial stages of this investigation, the experimental samples were sintered on the Dwight-Lloyd sintering machine in boxes as described in the previous investigation.[1] This method consisted of forming a box made of thin gage black iron sheet and fitting the box around a frame of the type used to obtain normal production sinter samples. The boxed sample frame was placed on an empty grate of the sintering machine ahead of the swinging spout and the experimental sinter feed placed within it. Care was taken to allow good distribution with some coarse material being placed as a hearth layer. Excess feed was piled on top to avoid contamination by the production sinter feed, this excess being removed as the bed was leveled. The sample was then allowed to sinter under normal production procedures. It was discovered that the sheet iron around the sample created a favorable passage for the air stream, and this condition caused top and edge sintering only, leaving a cone of unsintered material in the center. This condition was rectified by using a removable stainless steel box, Fig. 2, which allowed the use of the production feed as support for the experimental feed. Upon removing the frame, production sintering conditions were fully attained. The use of the sampling frames[1,2] for support and removal of the sintered sample was satisfactory.

Fig. 2—The removable stainless steel box shown in the center of the photograph was used for placement of the experimental sinter feed on the production Dwight-Lloyd sintering machine grates.

*Testing of Experimental Sinter Feed and Resultant Sinter:* The moisture content of the experimental sinter feeds was determined by loss in weight upon drying a representative sample at 150°C. The dried sample was submitted for chemical analysis.

The permeability of each experimental sinter feed was measured on a Dietert No. 320 permeability meter commonly used to test permeability of foundry sands. This instrument provided a rapid and simple permeability determination of acceptable accuracy for testing a material as heterogeneous as sinter feed. The index of permeability was simply the average reading obtained by testing five samples of the feed in the permeability meter. Increasing numerical permeability readings indicated increasing relative permeabilities. Each group of raw materials tested had inherent permeability characteristics, and the maximum permeability for any given series of experimental sinter feed was achieved by means of the water addition.

After sintering, the experimental mixes were allowed to air cool. All samples were tested for strength by using the 200 rpm tumbling and screen analysis test, the single index of strength being the "median particle size" in inches after tumbling and screening.[1,2] After the sinter strength had been determined, bulk density determinations were made on each sample, the results being reported in pounds per cubic foot.

Reducibility tests were run on all sintered samples in order to note the effect of raw materials or additives on reducibility. The loss in weight method of testing the reducibility of an aliquot 1 lb sample from the tumbling test was used. The time required for 90 pct weight loss in hydrogen at 800°C was used as the index of reducibility as described previously.[1]

Microscopic examination was made of representative particles from all sinter samples before and after reduction. The microstructure, oxide grain size, nonferrous oxide constituents present, and

extent of reduction were determined. Chemical analyses were made where variations in sinter feed constituents might change the chemical composition of the sinter considerably and thereby affect sinter strength, reducibility, or bonding characteristics.

## Results and Discussion

The raw materials used in this study were flue dust (current and stock), filter cake, return fines, ore fines, and roll scale. The additives used were burnt lime, coke, silica, alumina, magnesia, and blast furnace slag.

The composition of all experimental sinter feeds produced are summarized in Table II. The properties of these sinter feeds and of the resultant sinters produced are summarized in Table III, all pertinent chemical analyses being shown in Table IV. In addition, the properties of the various types of sinter are presented graphically in Figs. 3 through 7.

*Effect of Mixing Raw Materials:* In the initial studies with the small pug mill, it was discovered that raw material mixing is of great importance in the sintering process. Efficient mixing is especially important in the case of a flue dust sinter because the large globs of filter cake normally discharged onto the main sinter feed conveyer must be chopped into small pellets if the cake is to be sintered and also be efficient in promoting better feed permeability. The preliminary tests with the small experimental pug mill established that rotation speeds between 100 and 200 rpm were satisfactory. High speeds (500 rpm) broke the filter cake up into such small pieces that all benefits resulting from its addition were lost, and an actual loss in feed permeability took place. Prolonged repetitive mixing at slower speeds had a similar effect. Therefore, each mix was put through the pug mill six times at the 100 to 200 rpm speed. This was sufficient to reduce the filter cake to suitably sized pellets and to thoroughly mix and distribute all raw materials similar to production mixing. The pelletizing of materials such as filter cake and the distribution of these and other coarse materials homogeneously throughout the mix were found to be imperative for obtaining maximum permeability and sinter quality. This was shown very early in this study when a Simpson blade-type mixer was used for mixing the raw materials. Incomplete mixing and little pelletizing took place and the resultant experimental sinter was heterogeneously and incompletely sintered. This led to the experimentation with, and use of, the small pug mill as a mixer.

*Experimental Sinters:* From the previously mentioned list of raw materials, two *standard* experimental sinters were produced in order to obtain a series of standard property indices to which the remaining experimental feeds and sinters could be compared. The two standard compositions were typical of the two basic types of production sinter mixes encountered at South Works. These were, namely, a mixture containing approximately 20 pct ore fines and a mixture containing no ore fines. The properties of the two sinters were quite similar, and the averages were used in the subsequent comparisons (Table III). The permeability of the feed—165,

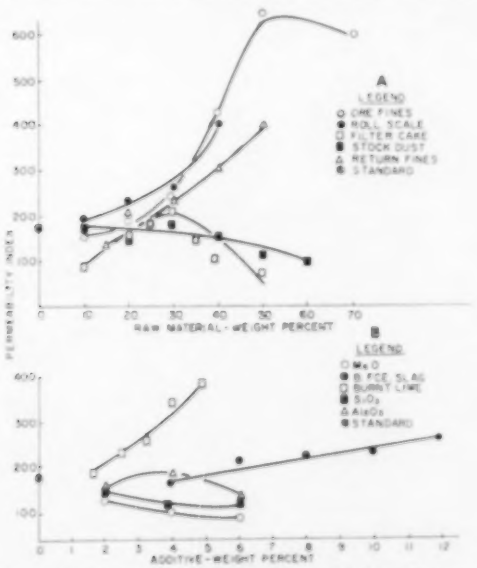


Fig. 3—The effects of increasing additions of the various raw materials and additives on sinter feed permeability are summarized. Graph *A* shows the effect of raw material additions and *B*, additive.

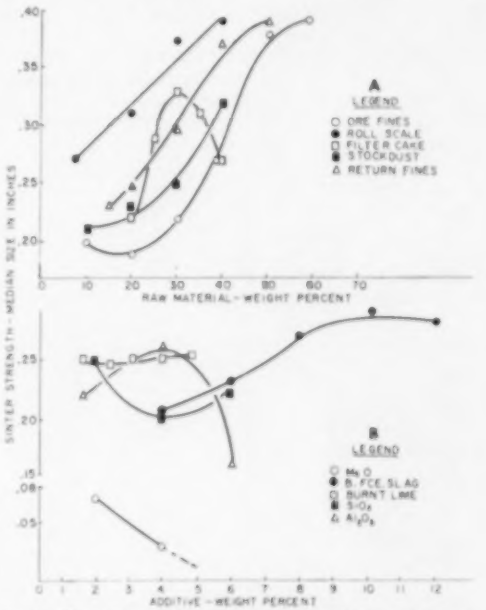


Fig. 4—The effects of increasing additions of the various raw materials and additives upon sinter strength are summarized. Graph *A* shows the effect of raw material additions and *B*, additive.

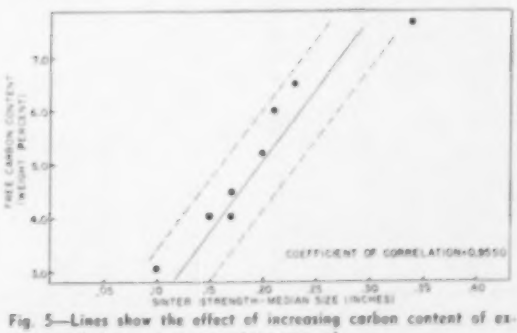


Fig. 5—Lines show the effect of increasing carbon content of experimental sinter mixes upon sinter strength.

the strength of the sinter—0.22 in. median size, the sinter reducibility index—170 min, the microstructure (Figs. 8a and 8b), and chemical analysis of the standard experimental sinter were similar to the normal flue dust sinter produced at South Works. The similarity in the properties of the two standard sinters and in the properties of subsequent samples whose composition approximated that of the standard was quite apparent and indicated the good reproducibility of the experimental technique used in the present study. Some of the reproducibility checks made are shown in Table III.

*Permeability of Experimental Sinter Mixes:* The effects of the various raw materials and additives on the permeability of sinter feed are summarized graphically in Fig. 3.

Of the various raw materials used, increasing additions of ore fines, roll scale, and return sinter fines had the most beneficial effects on sinter feed permeability. As shown in Fig. 3, additions of as little as 10 pct roll scale increased permeability above the standard. It was necessary to add 30 pct ore to achieve similar results. The use of a larger than normal (20 pct) amount of return fines achieved improved permeability, but the use of such large amounts of returns would not appear to be economical where supplies of roll scale or ore fines or other additives are available.

In the case of the foregoing raw materials, all three materials had particle sizes coarser than the other raw materials used in the respective sinter mixtures. The increase in the amount of coarse material added to the mix is the reason, therefore, for the increase in permeability. These three materials also had the same maximum particle size, −0.371 in. screen. This further emphasizes the beneficial effects of using small additions of roll scale (10 pct) compared to much larger additions of either ore fines or return fines.

It was noted that additions of filter cake, up to 30 pct, also increased permeability. In this case, the improved permeability was attained only when adequate mixing was exercised. Mixing broke the filter cake into small pieces and these pieces acted as nuclei for pellet formation. The high moisture content of mixes with more than 30 pct filter cake decreased the permeability of these mixes and thereby lowered the quality of the resultant sinters.

Of the various additives tested, only burnt lime and granulated blast furnace slag affected any im-

## Table II. Composition of Experimental Sinter Feeds

| Experimental Sinter No. | Constituents, Wt Pct* | | | | | | | | | |
|---|---|---|---|---|---|---|---|---|---|---|
| | Flue Dust | Filter Cake | Return Fines | Ore Fines | Roll Scale | Blast Furnace Slag | Stock Dust | $SiO_2$ (Added) | $Al_2O_3$ (Added) | MgO (Added) | Burnt Lime |
| Standard "A" | 47 | 20 | 20 | — | | | | | | | |
| Standard "B" | 27 | 20 | 20 | 20 | | | | | | | |
| 121 | 58 | 10 | 20 | | | | | | | | |
| 122 | 48 | 20 | 20 | | | | | | | | |
| 123 | 43 | 25 | 20 | | | | | | | | |
| 124 | 38 | 30 | 20 | | | | | | | | |
| 125 | 33 | 35 | 20 | | | | | | | | |
| 126 | 28 | 40 | 20 | | | | | | | | |
| 127 | 18 | 50 | 20 | | | | | | | | |
| 131 | 38 | 20 | 20 | 10 | | | | | | | |
| 132 | 28 | 20 | 20 | 20 | | | | | | | |
| 133 | 18 | 20 | 20 | 30 | | | | | | | |
| 134 | 8 | 20 | 20 | 40 | | | | | | | |
| 135 | — | 20 | 20 | 50 | | | | | | | |
| 136 | — | — | 20 | 70 | | | | | | | |
| 141 | 38 | 20 | 20 | — | 10 | | | | | | |
| 142 | 28 | 20 | 20 | — | 20 | | | | | | |
| 143 | 18 | 20 | 20 | — | 30 | | | | | | |
| 144 | 8 | 20 | 20 | — | 40 | | | | | | |
| 151 | 47 | 20 | 20 | — | — | 4 | | | | | |
| 152 | 45 | 20 | 20 | — | — | 6 | | | | | |
| 153 | 43 | 20 | 20 | — | — | 8 | | | | | |
| 154 | 41 | 20 | 20 | — | — | 10 | | | | | |
| 155 | 39 | 20 | 20 | — | — | 12 | | | | | |
| 161 | 38 | 20 | 20 | — | — | — | 10 | | | | |
| 162 | 28 | 20 | 20 | — | — | — | 20 | | | | |
| 163 | 18 | 20 | 20 | — | — | — | 30 | | | | |
| 164 | 8 | 20 | 20 | — | — | — | 40 | | | | |
| 165 | — | 20 | 20 | — | — | — | 50 | | | | |
| 166 | — | 10 | 20 | — | — | — | 60 | | | | |
| 171 | 45 | 20 | 20 | — | — | — | — | 2 | | | |
| 172 | 43 | 20 | 20 | — | — | — | — | 4 | | | |
| 173 | 41 | 20 | 20 | — | — | — | — | 6 | | | |
| 181 | 48 | 20 | 20 | — | — | — | — | — | 2 | | |
| 182 | 43 | 20 | 20 | — | — | — | — | — | 4 | | |
| 183 | 41 | 20 | 20 | — | — | — | — | — | 6 | | |
| 191 | 45 | 20 | 20 | — | — | — | — | — | — | 2 | |
| 192 | 43 | 20 | 20 | — | — | — | — | — | — | 4 | |
| 193 | 41 | 20 | 20 | — | — | — | — | — | — | 6 | |
| 201 | 52 | 20 | 13 | | | | | | | | |
| 202 | 47 | 20 | 20 | | | | | | | | |
| 203A | 37 | 20 | 30 | | | | | | | | |
| 203B | 37 | 20 | 30 | | | | | | | | |
| 204A | 27 | 20 | 40 | | | | | | | | |
| 204B | 27 | 20 | 40 | | | | | | | | |
| 205 | 17 | 20 | 50 | | | | | | | | |
| 211 | 16 | 20 | 20 | 30 | — | — | — | — | — | — | 1.6 |
| 212 | 16 | 20 | 20 | 30 | — | — | — | — | — | — | 2.4 |
| 213 | 15 | 20 | 20 | 30 | — | — | — | — | — | — | 3.2 |
| 214 | 14 | 20 | 20 | 30 | — | — | — | — | — | — | 4.0 |
| 215 | 13 | 20 | 20 | 30 | — | — | — | — | — | — | 4.8 |
| | | | | | Coke Breeze | | | | | | |
| 221 | 47 | 20 | 20 | 0 | | | | | | | |
| 222 | 47 | 20 | 20 | 1.0 | | | | | | | |
| 223 | 47 | 20 | 20 | 1.5 | | | | | | | |
| 224 | 47 | 20 | 20 | 2.0 | | | | | | | |
| 225 | 47 | 20 | 20 | 2.5 | | | | | | | |
| 226 | 47 | 20 | 20 | 3 | | | | | | | |
| 227 | 47 | 20 | 20 | 3 | | | | | | | |
| 228 | 45 | 20 | 20 | 3 | | | | | | | |

* Balance of composition was moisture and coke breeze. Sufficient coke breeze was added to each feed to attain a total carbon content of approximately 6 pct.

provement in feed permeability. Although the burnt lime increased permeability, it did not enter into complete solution upon sintering and had detrimental effects on other properties which made it unsuitable as an additive. However, granulated blast furnace slag allowed improved permeability and had other beneficial effects on sinter quality which would make this material beneficial as an additive in small quantities. Further discussion of these materials is made later in the text. As in the case of the raw materials discussed previously, it is believed that the particle size of these additives was the significant factor in increasing sinter permeability. Of the two materials, the slag was only slightly more coarse than the burnt lime, both being −0.371 in. in size.

Increasing additions of $SiO_2$, $Al_2O_3$, and MgO caused some decrease in sinter mix permeability but this was attributed primarily to the fine particle size. The bulk of these materials was of a sufficiently small particle size (−8 to −200 mesh) to cause a small reduction in permeability with increased additions. Additions of carbon did not materially effect permeability.

In each case where an addition of a raw material or additive has changed the sinter feed permeability, the effect of the particle size or the addition has been evident. The sinter properties, however, are affected principally by the composition of the addition and to only a minor extent by the particle size of the addition.

The moisture content of most of the mixtures studied in this investigation ranged from 10 to 13.5 pct. Variations within this range, however, were dependent upon the raw materials used in a given mixture. For example, sinter feeds containing larger amounts of roll scale, return fines, and ore fines required less moisture for increased permeability, primarily because of their coarse particle size. Since moisture additions were made to attain the highest permeability possible for a given mix, control of the moisture content could not be held constant throughout the investigation. The important effect of moisture content upon permeability was exemplified in the filter cake series; see Table III. There was an optimum moisture range above and below which permeability and sinter strength decreased. The effect of moisture, however, cannot be completely divorced from the effects of mixing, for in this case had the feed not been properly mixed the pellets would not have formed, the moisture would have been poorly distributed, and permeability decreased. On the other hand, with moisture contents above or below the optimum range, with or without proper mixing, the permeability was too low for thorough homogeneous sintering.

*Strength of Experimental Sinters:* The effects of the various raw materials and additives upon experimental sinter strength are summarized in Figs. 4A and 4B.

It is demonstrated in Fig. 4 that increasing additions of ore fines, roll scale, and return fines materially increased sinter strength. Additions of stock flue dust and up to 30 pct filter cake also were beneficial to sinter strength.

The use of 10 to 20 pct roll scale was more beneficial to strength than 30 to 40 pct of any other raw materials. Significant improvement in sinter strength from the use of ore fines was not attained until 40 pct of the mixtures consisted of ore fines. This suggests that adding small amounts of ore fines to a flue dust-base sinter mix might not be desirable in some cases.

The use of 30 to 40 pct return fines to increase permeability and strength might not be as economical as the use of lower amounts of other materials such as roll scale and ore fines when these latter materials are available. If such materials as these are not available or if fine concentrates or other materials are being sintered, the use of up to 50 pct returns could be highly beneficial, both from a quality and economic viewpoint. High percentages of returns will increase permeability and consequently the rate of sintering in such cases. This should more than compensate for the large recirculating load required.

Increasing additions of stock dust also yielded a small increase in strength. The reasons for this effect were not altogether clear. The explanation proposed

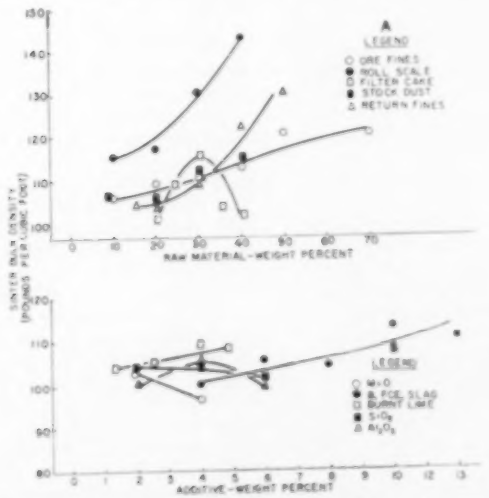


Fig. 6—The effects of increasing additions of the various raw materials and additives upon sinter bulk density are summarized. Graph *A* shows the effect of raw material additions and *B*, additive.

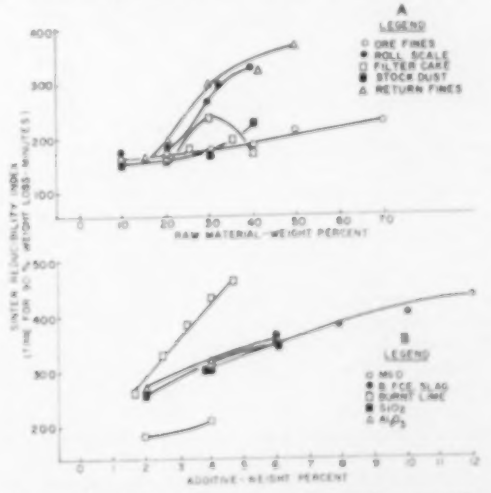


Fig. 7—Effect of increasing additions of the various raw materials and additives upon relative sinter reducibility are summarized. Graph *A* shows the effect of raw material additions and *B*, additive.

## Table III. Summary of the Properties of Experimental Sinter Feeds and Sinters

| Experimental Sinter No. | Experimental Feed Properties* | | Experimental Sinter Properties | | |
|---|---|---|---|---|---|
| | Moisture, Wt Pct | Permeability Index | Sinter Strength, Median Size, In. | Bulk Density, Lb Per Cu Ft | Reducibility Index, Time For 90 Pct, Min |
| Standard A | 11.3 | 161 | 0.23 | 101 | 180 |
| Standard B | 11.7 | 170 | 0.21 | 104 | 159 |
| 121 | 8.9 | 91 | NS† | — | — |
| 122 | 11.7 | 154 | 0.22 | 101 | 167 |
| 123 | 12.9 | 171 | 0.29 | 109 | 185 |
| 124 | 13.5 | 215 | 0.33 | 116 | 242 |
| 125 | 14.4 | 144 | 0.31 (0.30 Check) | 103 | 204 |
| 126 | 14.6 | 110 | 0.27 | 102 | 180 |
| 127 | 17.5 | 78 | NS† | — | — |
| 131 | 11.1 | 158 | 0.20 | 106 | 164 |
| 13E | 10.7 | 176 | 0.19 | 110 | 171 |
| 133 | 11.4 | 265 | 0.22 | 109 | 175 |
| 134 | 10.6 | 427 | 0.27 | 113 | 183 |
| 135 | 10.4 | 650 | 0.38 | 122 | 217 |
| 136 | 10.2 | 600 | 0.39 (0.38 Check) | 119 | 231 |
| 141 | 11.2 | 190 | 0.27 | 116 | 176 |
| 142 | 10.7 | 230 | 0.31 (0.30 Check) | 117 | 183 |
| 143 | 10.2 | 250 | 0.37 | 121 | 270 (89)‡ |
| 144 | 10.0 | 400 | 0.39 | 143 | 285 (83) |
| 151 | 11.3 | 165 | 0.20 | 100 | 270 (89) |
| 152 | 11.7 | 210 | 0.23 | 106 | 270 (79) |
| 153 | 11.9 | 217 | 0.27 | 104 | 285 (76) |
| 154 | 12.5 | 231 | 0.29 | 113 | 285 (73) |
| 155 | 13.1 | 255 | 0.28 | 110 | 285 (65) |
| 161 | 11.9 | 184 | 0.21 (0.20 Check) | 107 | 157 |
| 162 | 11.4 | 157 | 0.23 | 105 | 161 |
| 163 | 10.7 | 178 | 0.25 | 113 | 170 |
| 164 | 11.1 | 162 | 0.32 | 114 | 230 |
| 165 | 11.1 | 119 | 0.19 | 107 | 210 |
| 166 | 11.8 | 102 | NS† | — | — |
| 171 | 11.9 | 143 | 0.25 | 103 | 260 |
| 172 | 12.5 | 123 | 0.20 | 104 | 270 (89) |
| 173 | 11.5 | 119 | 0.22 | 101 | 285 (83) |
| 181 | 11.8 | 160 | 0.22 | 101 | 270 |
| 182 | 11.8 | 189 | 0.26 | 107 | 285 (89) |
| 183 | 10.9 | 136 | 0.16 | 99 | 285 (85) |
| 191 | 11.0 | 128 | 0.07 | 105 | 180 |
| 192 | 10.6 | 101 | 0.03 | 97 | 210 |
| 193 | 11.7 | 93 | NS† | — | — |
| 201 | 11.5 | 129 | 0.23 | 105 | 171 |
| 202 | 12.1 | 173 | 0.25 | 101 | 183 |
| 203A | 11.3 | | | | |
| 203B | 12.4 | 240 | 0.30 | 109 | 270 (89) |
| 204A | 10.7 | 305 | 0.37 | 123 | 270 (83) |
| 204B | 10.7 | | | | |
| 205 | 9.3 | 400 | 0.39 | 130 | 285 (76) |
| 211 | 12.1 | 190 | 0.25 | 104 | 260 |
| 212 | 11.7 | 226 | 0.24 | 107 | 330 |
| 213 | 12.3 | 260 | 0.25 | 108 | 330 (84) |
| 214 | 12.8 | 348 | 0.25 | 110 | 345 (84) |
| 215 | 12.5 | 370 | 0.26 | 109 | 345 (77) |
| 221 | 11.7 | 159 | 0.10 | 97 | 127 |
| 222 | 10.9 | 151 | 0.15 | 101 | 139 |
| 223 | 11.3 | 147 | 0.17 | 102 | 149 |
| 224 | 11.9 | 149 | 0.17 | 101 | 146 |
| 225 | 11.9 | 180 | 0.20 | 103 | 164 |
| 226 | 10.6 | 161 | 0.21 | 105 | 159 |
| 227 | 12.1 | 170 | 0.23 | 104 | 180 |
| 228 | 11.8 | 177 | 0.34 | 107 | 239 |

* The carbon content of all experimental sinter feeds was within the range of 5.5 to 6.8 pct, except for the carbon series.
† NS indicates that sample would not sinter.
‡ Numbers in parentheses indicate actual weight loss.

was that *stock* flue dust, as opposed to *current* flue dust, was more homogeneous especially in regard to carbon content. This effect was probably brought about through bedding of the stocked dust. This increased homogeneity allowed more uniform sintering, thus producing a slightly stronger sinter.

The reasons for the observed increases in sinter strength brought about by additions of the foregoing raw materials were noted when the microstructures were examined. In Fig. 8a, the structure of the standard sinter is shown. The iron oxide particles are bonded to some extent by fusion (iron oxide bonding) but to the greatest extent by siliceous glassy matrix (glass bonding). On the other hand, in Figs. 8c and 8d, the extensive iron oxide bonding of the sinters containing ore fines and roll scale is shown as well as the lack of the glassy matrix constituent. The role of iron oxide bonding in promoting sinter strength has been discussed in previous investigations.[1,4] It would be expected that sinters with structural features such as these would be stronger than sinters with a highly siliceous glass bond.

Of the various additives investigated, only blast furnace slag had any significant beneficial effects on sinter strength. The effects of additions of $SiO_2$, $Al_2O_3$, and burnt lime on sinter strength were negligible. Additions of MgO had deleterious effects on sinter strength.

The reason for the benefits or detriments derived from using the various additives were associated with the sinter bond. In the case of blast furnace slag, an extremely strong dense glass bond was formed, Fig. 8e, which accounted for the increase in strength. Although this dense glass bond was not as strong as the oxide bond of the roll scale and ore sinters, it was considerably stronger than the siliceous glassy bond of the standard sinter. The glass bond of the slag-containing sinter contained 75 to 85 pct fayalite and some $CaO \cdot Fe_2O_3$. The oxide grains were almost all rounded, indicating that considerable iron oxide had been dissolved in the glass. It is shown in Table IV that the slag-containing sinters have slightly higher lime and silica contents than the standard sinter. The fact that the lime from the slag addition is already fluxed with silica lowers the fusion point of the lime and allows the formation of the dense glassy phase on sintering,

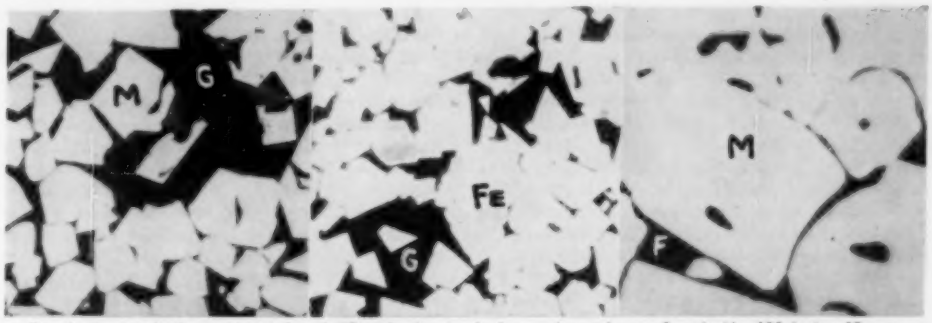


a—Sample is standard experimental sinter before reduction.

b—Sample is standard experimental sinter after reduction.

c—Sample No. 135 had a 50 pct ore fines addition.

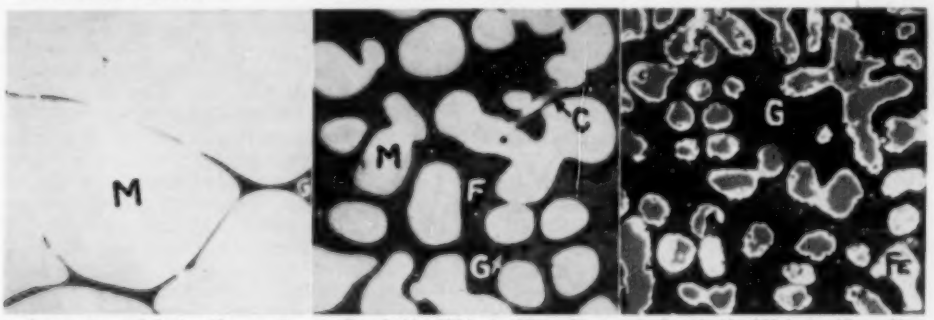


d—Sample No. 143 had a 30 pct roll scale addition.

e—Sample No. 155 had a 12 pct blast furnace slag addition before reduction.

f—Sample No. 155 had a 12 pct blast furnace slag addition after reduction.

Fig. 8—Micrographs show typical structures of some experimental flue dust sinters. The letters on various micrographs represent: *M*, magnetite ($Fe_3O_4$); *W*, wüstite (FeO); *Fe*, iron; *G*, glass; *F*, fayalite ($2FeO \cdot SiO_2$); and *C*, calcium-ferrite ($CaO \cdot Fe_2O_3$). Samples were unetched. X400.

which contributes to the higher strength of these sinters.

The use of burnt lime additions to sinter mixes has been discussed previously[1, 5] with conflicting results. The European practice of using lime additions in the production of ore sinter with great benefits has also been widely discussed.[7, 8] With the sintering practice and raw materials used in production of a flue dust-base sinter, burnt lime additions had no beneficial effects on sinter strength. The lime was not all taken into solution during sintering, as is shown in Fig. 9e. High lime additions by means of slag had improved sinter strength, and the reason for the different effects of the two additives may be associated with the difference in the ability of free lime to flux the impurities in the flue dust-type sinter when compared with granulated slag. Insufficient time and temperature were available during sintering for the burnt lime to completely react with the silica and iron oxide.

A similar series of observations were made in the case of the MgO-containing sinters. The poor strength of these sinters was attributed to the poor permeability of the mix and the fact that the MgO was not adequately taken into solution. Fig. 9d shows unreacted MgO and some of the matrix constituents formed when some of the MgO reacted with silica and iron oxide. Again, insufficient time and temperature were available for a sufficient chemical reaction to take place.

The additions of $SiO_2$ and $Al_2O_3$ altered the microstructure of the sinter without any significant effects on strength. Typical microstructures for sinters in this series are shown in Figs. 9a and 9c, which show principally an increase in the amount of the glassy matrix constituent. In both cases the glass was quite brittle.

The effects of increased carbon (fuel) content on sinter strength have been discussed by many authors. Fig. 5 graphically presents the results of the carbon addition series of this investigation. The correlation obtained was similar to that reported in previous investigations[1, 4, 6, 7] of both production and experimental sinters. As the carbon content of the mix increases, sinter strength increases. A micrograph of a typical high carbon (7.7 pct) sinter is presented in Fig. 9f, which shows the presence of coarse grains of iron oxide and a high percentage of fayalite in the matrix. Large amounts of $SiO_2$ in the sinter feed is not the only condition that is required for the formation of fayalite. Sinters in the low carbon range with high $SiO_2$ contents did not contain fayalite, while those in the high carbon range showed large amounts of fayalite, illustrating the important effect of temperature on fayalite formation.

*Bulk Density of Experimental Sinters:* The effects of the various raw materials and additives on sinter bulk density are summarized in Figs. 6A and 6B.

Very significant increases in experimental sinter bulk density were obtained as the amounts of ore fines, roll scale, and return fines used in the respective mixes were increased. Again, as in the cases of mix permeability and sinter strength, small additions of roll scale (10 to 20 pct) were more beneficial than a 30 to 40 pct addition of ore fines or return fines. Comparison of the microstructure typical of these sinters, Figs. 8c and 8d, and the standard, Fig. 8a, indicate the reason for the increase in bulk

density. The lack of pore space and glassy bond, the increase in iron oxide grain size and bonding, and the high iron content explain the higher densities. The structure, strength, and high bulk density of the roll scale-containing sinter indicate that this product might also be suitable for the open hearth as a charge oxide material.

No highly significant effects of any of the additives on sinter bulk density were noted, except in the cases of blast furnace slag and MgO. Blast furnace slag in contributing to the formation of a strong dense glassy bond also contributed to slightly increased sinter bulk density. The MgO additions were as detrimental to bulk density as they were to other sinter properties.

*Reducibility of Experimental Sinters:* The effects of the various raw materials and additives on relative sinter reducibility are summarized in Figs. 7A and 7B and in greater detail in Table III.

In general, it could be stated that, as the median size (strength) of the various sinters increased, the time required for 90 pct reduction (weight loss) also increased. The rate of gaseous diffusion, therefore, was affected by the median particle size. This relationship of sinter strength and reducibility has been noted in numerous investigations[1, 6, 9] and is well demonstrated in Fig. 10. However, in this entire study, no strong easily reduced sinters were produced. This was not in accord with another recent experimental sinter study.[1] The other factors which were noted to have affected sinter reducibility were: 1—the size of the iron oxide grains and 2—the type, composition, and nature of the sinter bond.

These factors were all evident throughout the reducibility studies of this investigation, and each is illustrated in Figs. 7A and 7B. In the case of increased additions of ore fines, roll scale, and return fines, the reducibility of the sinters became poorer as the addition of the particular raw material and the sinter strength increased. The high return fines sinter was bonded by the iron oxide and by the very dense glass, while the bonding of high ore fines and high roll scale sinters was by fusion of the oxide grains with only a minor amount of a glassy phase present, Figs. 8c and 8d.

It has been stated previously that iron oxide-bonded sinters reduced more rapidly than glass-bonded sinters of similar median particle size (strength).[1] The high ore fines sinters with iron oxide bonding did reduce more rapidly than a glass-bonded sinter of similar strength, for example, the return fines sinters. However, the iron oxide-bonded high roll scale sinters reduced considerably slower than the ore fines sinters. This difference was explained by the much higher bulk density and lower macro and microporosity of the roll scale sinters. Poor reducibility of very dense sinters was also noted in other investigations.[4, 10] These factors apparently reduce the benefits obtained from iron oxide bonding by inhibiting the diffusion of reducing gases and products of reduction. The poor reducibility of sinters containing high amounts of return fines was also caused by the high density as well as the presence of some dense glass bonding.

A typical production sample and the standard experimental sinter samples lost a total of 93 to 89 g

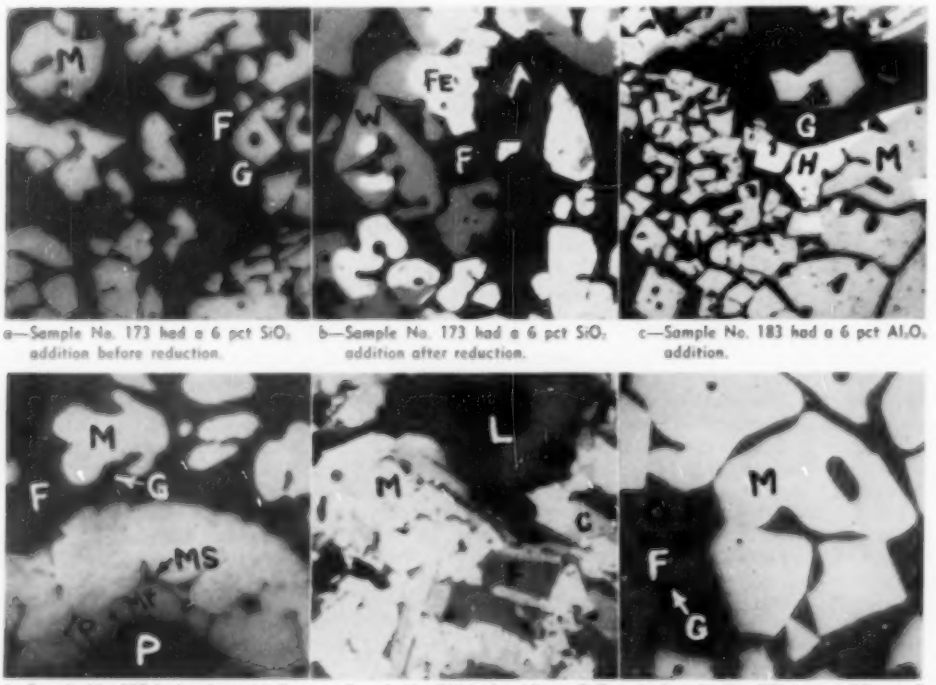


a—Sample No. 173 had a 6 pct $SiO_2$ addition before reduction.

b—Sample No. 173 had a 6 pct $SiO_2$ addition after reduction.

c—Sample No. 183 had a 6 pct $Al_2O_3$ addition.

d—Sample No. 192 had a 4 pct MgO addition.

e—Sample No. 215 had a 4.8 pct CaO addition. Sample was etched in water.

f—Sample No. 228 had a 7.7 pct C addition.

Fig. 9—Micrographs show typical structures of some experimental flue dust sinters. The letters on various micrographs represent: *H*, hematite ($Fe_2O_3$); *M*, magnetite ($Fe_3O_4$); *W*, wüstite (FeO); *Fe*, iron; *G*, glass; *F*, fayalite ($2FeO \cdot SiO_2$); *L*, lime; *C*, calcium-ferrite ($CaO \cdot Fe_2O_3$); *P*, periclase (MgO); *MS*, forsterite ($2MgO \cdot SiO_2$); and *MF*, magnesio-ferrite ($MgO \cdot Fe_2O_3$). Samples except e were unetched. X400.

(450 g original samples) on reducibility testing. However, a number of experimental samples had weight losses considerably below this range. A 70 g total weight loss at 800°C for a 450 g sample was not too uncommon. Some of the sinters in the roll scale and return fines series were in this category. The samples involved contained 30 pct or more of the respective constituents. Microscopic examination of these latter sinters showed that considerable oxide, in the form of wüstite (FeO), remained after reduction at 800°C. These results were associated with the nature of sinter bond, iron oxide characteristics, and densities of sinters. It was noted that reduction proceeded just so far, and further time at the standard test temperature induced no further weight losses in certain types of sinter. Additional reduction at 1000°C caused only a slight increase in sample weight loss. The foregoing behavior is not believed to detract from the reducibility test procedure, since the relative reducibility of sinters is all that is generally required. The reducibilities of sinters that fell in the foregoing category must be considered poorer as the total sample weight loss decreased. The time for 90 pct weight loss and the total sample weight loss were considered in rating reducibility. On this basis, sinters containing 30 and 40 pct roll scale and 30, 40, and 50 pct return fines had even poorer reducibility than the time for 90 pct weight loss indicated. For the purpose of illustrating this, the time for 90 pct reduction has been weighted by 30 min for each 5 g below the normal weight loss range. Figs. 7A and 7B have been plotted using the weighted figures.

Reducibility test results for sinters in the filter cake and stock dust series followed the pattern of poorer reducibility with increased strength. Sinters in this series had normal weight losses, which were similar to results obtained on testing similar production sinter samples. Micrographs of sinters in these series after reducibility testing are comparable to those of the standard experimental sinters after reduction, Fig. 8b. In the figure, iron as pseudomorphs after magnetite is shown embedded in the glassy matrix. These grains showed some internal cracking due to shrinkage and when etched in $SnCl_2$[11] would show very small amounts of iron oxide remaining.

Some of the additives had very deleterious effects on sinter reducibility. Additions of blast furnace slag, while improving other properties, caused markedly poorer sinter reducibility, Fig. 7B. This was explained by the nature of the sinter bond. The dense glassy bond had almost completely surrounded the iron oxide grains, as shown in Fig. 8e. The density of the bond inhibited the diffusion of reducing gases and products of reduction to cause poor reducibility. In Fig. 8f, the partially reduced oxide grains of the 12 pct slag sinter are shown surrounded by a zone of iron and the still dense matrix. The matrix constituents were not reduced in any of the sinters examined. Although considerable fayalite was found in these sinters, it was not the fayalite that was responsible for the poor reducibility.

Additions of 2, 4, and 6 pct silica and alumina, respectively, caused increasingly poor rates of reducibility. The reason for this poor reducibility was

**Table IV. Variation in the Chemical Composition of Experimental Sinters Containing Additives Which Altered the Normal Chemical Composition**

| Experimental Sinter No. | Additive, Wt Pct | Chemical Composition, Wt Pct | | | | | | Particle Size |
|---|---|---|---|---|---|---|---|---|
| | | Fe | $SiO_2$ | $Al_2O_3$ | CaO | MgO | C | |
| Standard experimental sinter mix | — | 53.98 | 10.81 | 2.36 | 2.16 | 0.38 | 6.03 | — |
| Standard experimental sinter | — | 55.08 | 11.17 | 2.59 | 1.93 | 0.38 | 0.22 | 0.22 in. median size |
| Average South Works production sinter mix* | — | — | 10.21 | 2.34 | 1.91 | — | 4.98 | — |
| Average South Works production sinter* | — | 60.04 | 10.73 | 2.62 | 1.96 | — | — | 0.233 in. median size |
| 141 | 10 Roll Scale | 55.30 | — | — | — | — | — | — |
| 142 | 20 Roll Scale | 60.34 | — | — | — | — | — | — |
| 143 | 30 Roll Scale | 62.45 | — | — | — | — | — | — |
| 144 | 40 Roll Scale | 63.28 | — | — | — | — | — | — |
| 151 | 4 Blast furnace slag | — | 11.36 | — | 2.10 | — | — | — |
| 152 | 6 Blast furnace slag | — | 13.07 | — | 3.68 | — | — | — |
| 153 | 8 Blast furnace slag | — | 13.56 | — | 4.80 | — | — | — |
| 154 | 10 Blast furnace slag | — | 13.84 | — | 5.53 | — | — | — |
| 155 | 12 Blast furnace slag | — | 14.22 | — | 5.73 | — | — | — |
| 171 | 2 $SiO_2$ | — | 14.21 | — | — | — | — | — |
| 172 | 4 $SiO_2$ | — | 14.70 | — | — | — | — | — |
| 173 | 6 $SiO_2$ | — | 15.50 | — | — | — | — | — |
| 181 | 2 $Al_2O_3$ | — | — | 3.78 | — | — | — | — |
| 182 | 4 $Al_2O_3$ | — | — | 5.64 | — | — | — | — |
| 183 | 6 $Al_2O_3$ | — | — | 6.60 | — | — | — | — |
| 191 | 2 MgO | — | — | — | — | 2.72 | — | — |
| 192 | 4 MgO | — | — | — | — | 3.98 | — | — |
| 193 | 6 MgO | — | — | — | — | NS† | — | — |
| 211 | 1.6 Burnt CaO | — | — | — | 3.10 | — | — | — |
| 212 | 2.4 Burnt CaO | — | — | — | 4.05 | — | — | — |
| 213 | 3.2 Burnt CaO | — | — | — | 4.75 | — | — | — |
| 214 | 4.0 Burnt CaO | — | — | — | 5.85 | — | — | — |
| 215 | 4.8 Burnt CaO | — | — | — | 6.28 | — | — | — |
| | | Experimental Sinter Mix Carbon Content, Wt Pct | | | | | | |
| 221 | 0 C (coke breeze) added | | | | 3.01 | | | |
| 222 | 1.0 C (coke breeze) added | | | | 4.05 | | | |
| 223 | 1.5 C (coke breeze) added | | | | 4.00 | | | |
| 224 | 2.0 C (coke breeze) added | | | | 4.49 | | | |
| 225 | 2.5 C (coke breeze) added | | | | 5.20 | | | |
| 226 | 3 C (coke breeze) added | | | | 6.09 | | | |
| 227 | 3 C (coke breeze) added | | | | 6.57 | | | |
| 228 | 3 C (coke breeze) added | | | | 7.70 | | | |

* The production data represents the average data obtained from 385 South Works sinter mix and sinter samples, October-November 1953.
† NS indicates that sample would not sinter.

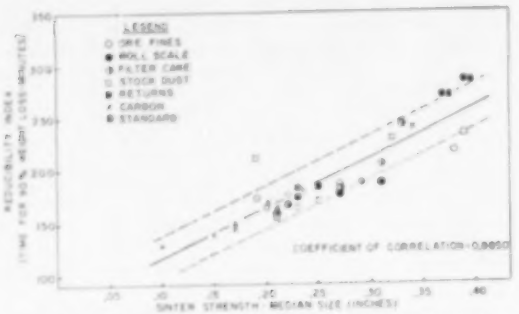


Fig. 10—Lines and data points show the relationship between the strength and reducibility of experimental sinters.

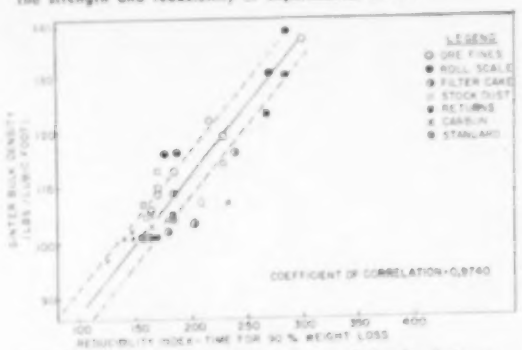


Fig. 11—Lines and data points show the relationship between the bulk density and reducibility of experimental sinters.

again the sinter bond. This is shown in Figs. 9a, 9b, and 9c. The microstructure of sinters containing 6 pct $SiO_2$ are shown before and after reduction and are similar to the slag-containing sinters discussed previously. The large amount of glassy matrix surrounds the iron oxide grains to a great extent. Fig. 9b shows the large amount of iron oxide remaining after reduction.

Magnesia additions had deleterious effects and burnt lime had no beneficial effects on sinter strength. The poor reducibility of the burnt lime-containing sinters was associated with the high lime glassy bond surrounding the iron oxide grains and the presence of significant amounts of $CaO \cdot Fe_2O_3$ which has been previously shown to be associated with poor reducibility.[3] The MgO-containing sinters had extremely slow rates of reduction for sinters of such low strength. The presence of forsterite[4] and uncombined MgO and the other matrix constituents shown in Fig. 9d contributed to poor reducibility. Another group of investigators noted similar effects of MgO.[5]

Increases in carbon content had no effect on sinter reducibility other than that resulting from increasing strength. The weight losses of these samples were normal and similar to high carbon production sinter test results. The presence of fayalite in the high carbon sinters did not, by itself, decrease sinter reducibility.

*Interrelation of Sinter Strength, Bulk Density, and Reducibility:* The interrelationship of these three sinter properties has been clearly demonstrated in this paper and is shown in Figs. 10 through 12. Fig. 10 shows the relationship between sinter strength and reducibility and has been discussed earlier in the text. Fig. 11 shows the relationship between sinter bulk density and reducibility. It should be noted that the "least squares" coefficient of correlation" is quite high in this relationship, indicating that these two properties are closely and directly related. This was well demonstrated in the roll scale-containing sinters where an appreciable increase in bulk density was attained as the raw material additions increased. By generalizing and using increased density as a measure of decreased porosity, it could be said that there was an inverse relationship between sinter porosity and reducibility. Similar results as these were found by Morrissey and Powers[1] in an ore sinter study.

In Fig. 12 the relationship between sinter bulk density and sinter strength is shown. Again, the correlation was quite good and it was felt that this relationship was due to the sinter bond. When the sinter was very densely bonded, whether by iron oxide or by the glassy phase, the sinters were stronger. This was illustrated by the roll scale and slag series of sinters. It was not particularly true in the case of the high $SiO_2$ sinters, but in these sinters the glassy bond was less dense and did not completely surround the iron oxide grains.

The interrelationship of these three properties was quite significant and to a great extent defined the limits of raw material mixtures and additives within which it is necessary to operate under production conditions in order to produce any given type of sinter. Although some of the findings of this investigation have been applied at South Works sintering plant, results are incomplete at this time. Preliminary data suggests, however, that these results are fully adaptable to actual production of blast furnace flue dust sinter.

## Conclusions

1—Those raw materials which significantly improved sinter quality were roll scale, ore fines, and return fines. Increasing additions of these materials were increasingly beneficial to all properties evaluated except reducibility. Additions of as little as 10 pct roll scale were as beneficial to sinter quality as 30 to 40 pct of the other raw materials.

2—Of the sinter feed additives studied, only small amounts of granulated blast furnace slag significantly improved sinter strength. The other additives, particularly magnesia, had deleterious effects on all sinter properties. Improved feed permeability was the only beneficial effect of burnt lime additions. All additives were deleterious to sinter reducibility.

3—Increasing additions of carbon significantly improved sinter strength. An increase of approximately 0.04 in. in median size was obtained with a 1 pct increase in carbon content.

4—Complete and thorough mixing of sinter feed

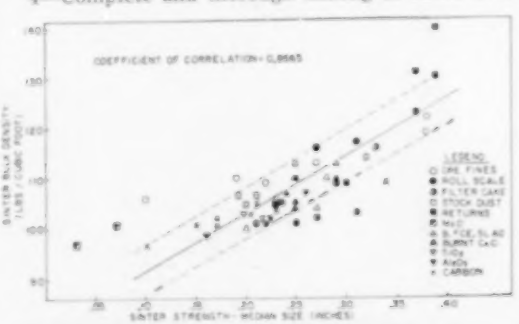


Fig. 12—Lines and data points show the relationship between the bulk density and strength of experimental sinters.

was found to be essential to good sinter quality. Poorly mixed experimental samples sintered heterogeneously and incompletely.

5—Control of the sinter feed moisture content was quite dependent on the type of sinter being produced. The optimum moisture content range for most of the mixtures studied in this investigation was from 10 to 13.5 pct. Significant increases or decreases below this range decreased sinter feed permeability.

6—The principal factors affecting sinter strength were: A—bulk density, B—size of the iron oxide grains, and C—the type and composition of the sinter bond. The dense coarse grained and iron oxide-bonded sinters were stronger than the porous and/or glass-bonded sinters.

7—The principal factors affecting sinter reducibility were: A—sinter strength, B—bulk density, C—size of the iron oxide grains, and D—the type and composition of the sinter bond. Iron oxide-bonded sinters reduced more rapidly than glass-bonded sinters of similar strength; but at very high bulk densities, reducibility was poor regardless of the type of bond.

### Acknowledgment

The authors wish to express their gratitude to the Blast Furnace and Sinter Plant personnel at South Works for their extensive aid in the preparation and sintering of the numerous mixes and for their valuable suggestions offered in the course of this investigation.

Discussion of this paper, if any, will appear in JOURNAL OF METALS, November 1956, and in AIME Metals Branch *Transactions*, Vol. **206**, 1956.

### References

[1] E. C. Rudolphy and D. J. Carney: Quality Control of Blast Furnace Sinter. *Proceedings* AIME Blast Furnace, Coke Oven, and Raw Materials Conference (1953) **12**, pp. 18-45.

[2] R. L. Stephenson and D. J. Carney: Sampling and Testing of Sinter. *Trans.* AIME (1953) **196**, pp. 309-311; MINING ENGINEERING (March 1953).

[3] E. W. Voice et al.: Investigation of the Effects of Controlled Variables on Sinter Quality, I—Development of Experimental Sinter Plant and Preliminary Results Using Northants Ore. *Journal* Iron and Steel Inst. (1951) **167**, pp. 393-399.

[4] H. A. Morrissey and R. E. Powers: Quality of Iron Ore Sinter as Related to Moisture and Coke Content. JOURNAL OF METALS (1954) **6**, No. 4, pp. 447-449.

[5] R. D. Burlingame, G. Bitsianes, and T. L. Joseph: Additives Produce Strong and Reducible Iron Ore Sinter. JOURNAL OF METALS (1954) **6**, No. 4, pp. 449-451.

[6] B. Hessle: New Metallurgical Experience with Sintering. *Jernkontorets Annaler* (1954) **129**, No. 8, pp. 383-446.

[7] P. K. Gledhill et al.: Effect of Mineral Additions and Moisture Control on the Sintering of Sierra Leone Concentrates. *Journal* Iron and Steel Inst. (1953) **175**, pp. 277-279.

[8] E. W. Voice et al.: Factors Controlling the Rate of Sinter Production. *Journal* Iron and Steel Inst. (1953) **175**, pp. 97-152.

[9] D. J. Carney and E. C. Rudolphy: Discussion of ref. 4. *Proceedings* AIME Blast Furnace, Coke Oven, and Raw Materials Conference (1954) **12**, pp. 58-63.

[10] R. J. Morton: Testing of Iron Ores and Agglomerates Related to Blast Furnace Use. *Proceedings* AIME Blast Furnace, Coke Oven, and Raw Materials Conference (1951) **10**, pp. 122-134.

[11] R. G. Welles: Microscopic Identification of Wüstite. *Analytical Chemistry* (1954) **26**, pp. 715-717.

[12] R. B. Snow: Identification of CaO-MgO Orthosilicate Crystals, Including Merwinite ($3CaO \cdot MgO \cdot 2SiO_2$), through the Use of Etched Polished Sections. *Trans.* AIME (1947) **172**, pp. 121-136; METALS TECHNOLOGY (June 1947).

[13] F. E. Croxton and D. J. Cowden: *Applied General Statistics*. (1945) New York. Prentice-Hall Corp.

[14] G. D. Elliot: *One Hundred Percent Sinter in the Blast Furnace*. Presented at the Blast Furnace and Coke Oven Assn. Meeting, Cleveland (October 1953).

# Production and Purification of $TiCl_4$

by L. W. Rowe and W. R. Opie

**A brief history of $TiCl_4$ production and purification is given. Chlorinator feed materials for the production of $TiCl_4$ are classified. The thermodynamics and kinetics of $TiCl_4$ production by chlorination of $TiO_2$ are discussed. Problems encountered in the chlorination and purification steps are outlined in detail.**

MOST of the current processes for the production of titanium metal require the use of $TiCl_4$ as a source of titanium values. This material can only be produced by a dry chlorination process, since it is immediately hydrolyzed in the presence of water. When pure, the tetrachloride is a colorless liquid boiling at 136°C. It fumes readily in moist air, reacting immediately with the moisture to form $TiO_2$ and HCl.

L. W. ROWE and W. R. OPIE, Member AIME, are Research Chemist and Supervisor of Geochemical and Metallurgical Dept., respectively, Research Laboratories, Titanium Div., National Lead Co., South Amboy, N. J.

Discussion of this paper, TP 4093D, may be sent, 2 copies, to AIME by Jan. 1, 1956. Manuscript, Mar. 30, 1954. New York Meeting, February 1954.

### History

The tetrachloride was prepared as early as 1826 by Dumas[1] who chlorinated a red hot mixture of carbon and $TiO_2$. Since then, numerous other mixtures have been used including rutile, ilmenite, beneficiated ilmenites, titanium pigment, slags, and the various titanium metalloids such as TiN, TiCN, TiOC, and $TiS_2$. $S_2Cl_2$, phosgene, and $CCl_4$ have been substituted for chlorine and CO has been used in place of carbon.

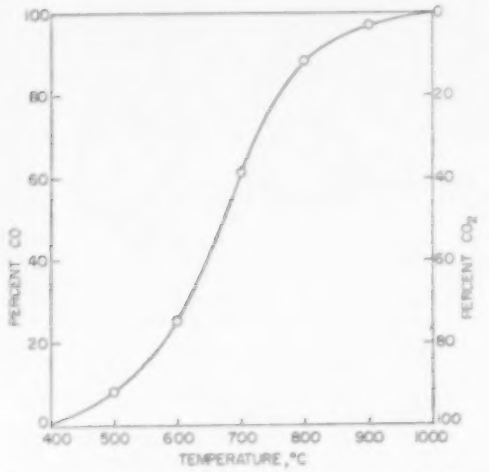


Fig. 1—Equilibrium of reaction 3 (Boudouard) of $CO_2$ with carbon to form CO is shown. The pressure is 1 atm.

The original patent for production of $TiCl_4$ was issued to Barton in 1916.[5] A mixture of $TiO_2$ and soft coal was carbonized to remove the volatile matter and form a hard porous cinder. This was chlorinated at 650°C.

A large number of patents, covering equipment modifications, charge preparation, chlorination procedure, and methods for condensation of the reaction mixtures, have been issued since the original application.

Extensive commercial production was not begun until 1935, with the tetrachloride used chiefly for the production of rutile pigment. Up to 1945, $TiCl_4$ was made using static beds. The chlorinators were constructed of acid-resistant brick, backed by one or more layers of insulating brick and enclosed in a metal shell.

The charge was fed at intervals through the top of the reactor and chlorine passed into the bottom of the bed. The reaction products were led out through a side delivery tube located near the top of the reactor. A dust collector or cyclone removed the solid reaction products; this unit was usually heated to above 150°C to prevent condensation of the tetrachloride at this point. The remaining gases were passed through a series of air or water-cooled condensers to remove the tetrachloride, and the final off gases led through a water scrubber to remove HCl and then into a caustic scrubber to remove chlorine.

The direct chlorination of ilmenite proved very difficult due to constant plugging of the condensing system with ferrous and ferric chlorides. The general practice was to use rutile ore, scrap pigment, or a low iron beneficiate such as can be obtained by leaching ilmenite with HCl. A feed mixture containing a 25 to 33 pct addition of coal or coke with tar or pitch as a binder was pressed into briquettes, carbonized to remove the volatiles, then charged hot to the chlorinator. The process was essentially batchwise, with a charge-upon-charge addition until the accumulation of gangue and unchlorinatable inerts caused a rapid decline in chlorination efficiency and necessitated discharging the reactor.

In the period from 1935 to 1945, numerous refinements were made in the chlorination technique. Suspensions of colloidal $TiO_2$, lignin, or clay were used as binders and alkali-metal hydroxides were added to improve briquette quality.[6] Chlorination units were operated adiabatically by controlling the bed level and chlorine rates or burning carbon in the bed at specified intervals. TiCN and silicon metal have also been added to the charge to furnish additional heat of reaction.[4] Attempts were made to process ilmenite by selective chlorination of iron values from the charge by controlling the carbon addition and reaction temperature. A number of equipment patents were also issued, which dealt with various methods for charging and discharging the reactors.

Many advances had been made in the development of fluidized solids processes during World War II. These techniques were applied to the manufacture of $TiCl_4$, since they offered a means of considerably reducing the processing cost by eliminating the briquetting and carbonization steps and by furnishing a way for maintaining continuous operation.

## Chlorinator Charge Material

The titanium content of various possible chlorinator feeds, both as received and as fabricated into a chlorination charge, may be approximated as given in Table I.

From a study of the heats and free energies of formation, Table II, of the various titanium sources for which data are available, it is apparent that the metalloids are less stable than the tetrachloride and will, therefore, chlorinate readily. The dioxide, on the other hand, is much more stable and can be chlorinated only in the presence of a reducing agent such as carbon or CO.

Table I. Titanium Content of Possible Chlorinator Feeds

| Titanium Source | Pct Ti As Received | Pct Ti* As Chlorination Charge |
|---|---|---|
| TiN | 77.4 | 77.4 |
| TiCN | 64.8 | 64.8 |
| Ti pigment | 59 to 60 | 47 to 48 |
| Rutile ore | 54 to 58 | 43.45 |
| Slag | 38 to 50 | 30 to 40 |
| Ilmenite ore | 27 to 36 | 22 to 29 |

* A 25 pct C addition was made where necessary.

From the standpoint of ease of chlorination and chlorinator throughput, it is obvious that the metalloids are by far the most efficient charge materials. A comparison of the cost per pound of contained titanium, however, shows that the use of ilmenite and slag has the greatest economic advantage; see Table III.

Because of the difficulties encountered in chlorinating ilmenite and titania-containing slags, rutile (about 98 pct $TiO_2$) has been accepted by the industry as an economical chlorinator feed material.

## Technology

Main reactions to consider in the chlorination of $TiO_2$ are as follows:

$$TiO_2(s) + 4Cl_2(g) + 2C(s) \rightleftharpoons TiCl_4(g) + 2COCl_2(g) \quad [1]$$

$$COCl_2(g) \rightleftharpoons CO(g) + Cl_2(g) \quad [2]$$

$$2CO(g) \rightleftharpoons CO_2(g) + C(s). \quad [3]$$

The equilibrium constants for each reaction can be calculated from available data, and the resulting constants mathematically related so that the partial pressures of all reactants and products can be determined, assuming equilibrium conditions and a total pressure of 1 atm.

As was shown by Godnov and Pamfilov,[9] the pressure of $COCl_2$ is negligible and, at equilibrium, only traces of chlorine are present. Therefore, the reactions of importance are

$$TiO_2(s) + 2Cl_2(g) + C(s) \rightleftharpoons TiCl_4(g) + CO_2(g) \quad [4]$$

$$TiO_2(s) + 2Cl_2(g) + 2C(s) \rightleftharpoons TiCl_4(g) + 2CO(g). \quad [5]$$

These reactions occur simultaneously and are strongly temperature dependent. As the chlorination temperature increases, the following effects occur: 1—The $CO/CO_2$ ratio in the product gases increases to satisfy the equilibrium of reaction No. 3; see Fig. 1. 2—The amount of carbon per mol of $TiCl_4$ produced increases because reaction No. 5 becomes the dominant reaction. 3—The total product gas volume increases. 4—The percentage of $TiCl_4$ in the product gas volume decreases. Effects 1 through 4 are illustrated in Fig. 2.

**Table II. Heat and Free Energy of Formation of Various Titanium Compounds**

| Compound | $\Delta H$, 298°K | $\Delta F$, 298°K |
|---|---|---|
| $TiO_2$ | −225.6 | −212.4[a] |
| $TiCl_4$ | −190.3 | −171.0[a] |
| TiO | −123.9 | −116.9[a] |
| TiN | − 80.5 | − 73.6[a] |
| TiC | − 43.8 | − 43.0[a] |

Another important factor to consider is the effect of temperature on reaction rate. The results of Pamfilov and Shikher,[10] as well as those obtained on a National Lead Co. laboratory unit which illustrate this temperature effect, are plotted in Fig. 3. Pamfilov used CO as a reducing agent, conducting the reaction at various temperatures for a period of 3.5 hr with a steady chlorine rate.

Results with solid carbon as a fuel were obtained during the chlorination of a briquetted mixture of ground $TiO_2$ and coal, using a 3.8 $TiO_2$/C ratio. Chlorine rate and time were held constant at 0.35 l per min and 4.0 hr, respectively.

Experimental runs have confirmed the thermodynamic and kinetic data presented herein. Sponge titanium metal will begin to chlorinate at a temperature as low as 120°C, the various metalloids will react vigorously in the 250° to 400°C range, and $TiO_2$+C chlorinated efficiently at 700°C. The reaction with the metalloids is highly exothermic and can be made to proceed adiabatically even in small scale equipment. Although the $TiO_2$+C reaction is considerably less exothermic, a fluidized solids chlorinator with a diameter greater than 20 in. can be operated under adiabatic conditions. Commercial scale static bed units require only a small heat input.

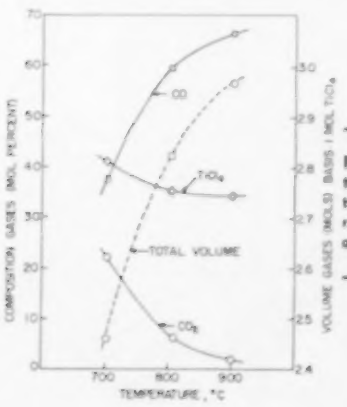


Fig. 2—Graph illustrates the effect of temperature on chlorinator gas volumes and composition.

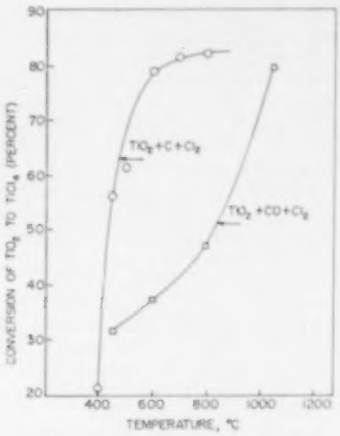


Fig. 3—Effect of temperature on chlorinator reaction rates is illustrated.

## Chlorinator Design

Two basic types of chlorinators are used: static bed and fluidized bed. Static bed units were briefly discussed in a previous section. The units used at Henderson, Nevada, in the Titanium Metals Corp. of America plant have been described by P. J. Maddex.[11]

The fluidized solids reactor is similar in construction to the static bed unit, although the ratio of height to cross-section is usually greater. The bed is supported on a perforated brick or ceramic plate and maintained in a fluidized state by the pressure of the gas stream. The feed may enter into the top of the reactor through a sealed hopper or be carried in above the plate by a portion of the gas stream. An overflow pipe located near the top of the bed discharges the inerts which are lighter than the feed mixture and tend to segregate to the top of the bed. On large scale units, the overflow level is usually adjusted so that portions of the bed can be recycled to permit strict temperature controls. The layers of insulating brick are dispensed with and cooling of the shell may even be necessary.

**Table III. Comparison of the Cost per Pound of Contained Titanium**

| Titanium Source | Dollars per Lb of Contained Titanium |
|---|---|
| Ilmenite | 0.02 to 0.03 |
| Slag (Quebec Iron & Titanium Corp. type) | 0.05 to 0.08 |
| Rutile | 0.10 to 0.15 |
| Ti pigment | 0.40 to 0.50 |
| TiCN | 0.75 to 1.00 |

Several advantages can be realized by use of the fluidized solids process. The excellent heat transfer and lack of channeling permits a three to fourfold production rate per unit area. Feed and discharge can be made continuous, thus eliminating the frequent shutdowns required for discharging of the static bed units. A carbon source of very low hydrogen content is used to reduce the possibility of fixed chloride formation.

The main problems encountered in $TiCl_4$ manufacture are found in the condensing and collecting of the reaction products rather than in the formation of the chloride. These difficulties spring from three major sources: 1—carry-over of very fine dust and

solid reaction products which can be only partially removed by cyclones; 2—plugging of condenser lines with mixtures of dust, liquid tetrachloride, and titanium oxychlorides; and 3—clogging of the off gas lines by hydrolysis of uncondensible tetrachloride fogs and mists which pass through the condensers. Corrosion of the condensing system with chlorine and HCl also contributes to the overall problem.

Mechanical dust carry-over can be eliminated to a large extent by careful charge preparation, close regulation of gas flows, and adequate cyclone design. Leakage of air into the system, especially near the reaction zone, causes oxidation of $TiCl_4$ and $FeCl_3$ to produce very fine $TiO_2$ and $Fe_2O_3$ particles, while moisture leakage will produce solid titanium oxychlorides. These effects can be minimized by thorough drying of the charge and by maintaining the system under a slight positive pressure. Cooling of the exhaust gas mixture by refrigeration will reduce fog formation and minimize plugging in this section of the system.

One of the chief problems in $TiCl_4$ manufacture is the separation and condensation of the reaction products, chiefly $TiCl_4$-$FeCl_3$ mixtures. The most effective method has been to spray the gases with cold $TiCl_4$ in a packed tower,[12] the discharge going to a settling tank for removal of the sludge. The clear liquor may be pumped to crude storage or recycled to the scrubbing tower. Another method involves spraying the mixture in an unpacked tower and condensing the solid fraction on a surface heated above the boiling point of the $TiCl_4$.[13] Selective separation of the iron chloride $FeCl_3$ can also be achieved by passing the gas mixture through a low melting $FeCl_3$-NaCl salt bath, with periodic removal of the excess $FeCl_3$ in a separate stage.[14] Even with these developments, handling of the large amounts of $FeCl_3$ and $FeCl_2$ produced during the chlorination of ilmenite has been very difficult. Complete selective chlorination of either titanium or iron values is probably impossible, although $FeCl_2$ production can be minimized by proper control of the reaction conditions. The large difference between the boiling points of $FeCl_3$ (315°C) and $TiCl_4$ (136°C) should permit ready separation of the two phases. In actual practice, however, the separation is only partially effective, and considerable amounts of very fine $FeCl_3$ are carried along with the gas stream. When the two components condense together, a heavy mud is produced which is very difficult to handle. In a continuous operation, the process is a slow cumulative one, with gradual build-up of $FeCl_3$ at points in the system where wall friction causes a lowering of gas velocity. Air leaks can aggravate the problems by causing a deposition of $Fe_2O_3$ along with $FeCl_3$.

A further complication with ilmenite ore is the necessity of recovering chlorine values tied up as iron chlorides. Direct oxidation of $FeCl_3$ is not too efficient, owing to its tendency to dissociate into the difficultly oxidizable $FeCl_2$.

Because of the inherent difficulties in handling ilmenite, the main charge materials employed to date have been rutile or low iron beneficiate. Present supplies of rutile appear to be inadequate for any greatly expanded titanium metal program, while supplies of ilmenite are almost inexhaustible. The only long term solutions to the raw materials program appear to be in the production of a low cost, high titanium beneficiate from ilmenite or in solving the technical problems associated with ilmenite chlorination and recovery of chlorine values from $FeCl_3$.

## Purification

The crude $TiCl_4$ is unsuitable for direct use in metal production owing to the presence of dust and sludge, dissolved gases, organic compounds, and various soluble metal chlorides such as $SiCl_4$, $SnCl_4$, $VOCl_3$, and $TiOCl_2$.

The dust and sludge, consisting of $FeCl_3$, $TiO_2$, fine carbon, and traces of heavy metal chlorides, can be removed by settling and decantation. The dissolved gas (mostly chlorine and phosgene), the low boiling impurities (chiefly $SiCl_4$ and $SnCl_4$), and the high boiling impurities (titanium oxychlorides) can be removed by a distillation step. A few chlorides, however, such as $VOCl_3$ and $MoCl_5$, tend to codistill along with $TiCl_4$ and require a chemical means of removal. A large number of purification agents have been used for this purpose. These include powdered metals,[15] metal hydrides,[16,17] amalgams, alkali-chlorides, and iodides,[18] $H_2S$,[19] and organic compounds such as soaps,[20,21] oils,[22] fats and waxes.[23] Most of these are added prior to, or during, the distillation step, the mechanism usually being to selectively reduce the interfering chloride to an insoluble higher boiling salt or to form a complex salt. If the purification agent is effective, a water white product can be obtained with impurities near the lower limit of spectrographic analysis methods.

About 4 lb of $TiCl_4$ are required for production of 1 lb of metal, even at 100 pct reaction efficiency. Because of this, the cost of tetrachloride will continue to be a major factor in the ultimate cost of the metal. A relatively cheap process for the production of pure $TiCl_4$ is essential if producers are to markedly decrease the cost of the metal. Production of a low cost, high titanium beneficiate for the chlorination charge and high recovery of chlorine values from the metal formation stage are means of achieving this goal.

Discussion of this paper, if any, will appear in JOURNAL OF METALS, November 1956, and in AIME Metals Branch *Transactions*, Vol. **206**, 1956.

## References

[1] J. B. A. Dumas: *Journal Pharm. Chim.* (1826) **12**, p. 300.
[2] L. E. Barton: *Titanium Tetrachloride*. U.S. Patent 1,179,394 (Apr. 18, 1916).
[3] C. De Rohden: *Titanium Tetrachloride*. U.S. Patent 1,707,257 (Apr. 2, 1929).
[4] P. S. Brallier: *Titanium Tetrachloride and Silicon Tetrachloride*. U.S. Patent 2,401,544 (June 4, 1946).
[5] L. Brewer: *Chemical Review* (1953) **52**, pp. 1-75.
[6] P. Gross, C. Hayman, and D. L. Levi: *Trans.* Faraday Soc. (1955) **51**, pp. 626-629.
[7] G. L. Humphrey: Heat of Formation of TiO, $Ti_2O_3$, $Ti_3O_5$, and $TiO_2$. *Journal* Amer. Chemical Soc. (1951) **73**, p. 1587.
[8] G. L. Humphrey: Heat of Combustion and Formation of TiN and TiC. *Journal* Amer. Chemical Soc. (1951) **73**, p. 2261.
[9] I. N. Godnov and A. V. Pamfilov: Chemistry of Titanium, VII, Thermodynamics of Chlorination Reaction. *Journal of Gen. Chem.* USSR (1937) **7**, pp. 1264-1267.
[10] A. V. Pamfilov and M. G. Shikher: Chemistry of Titanium, VIII, Chlorination of Titanium Compounds with a Mixture of Cl, and CO. *Journal of Gen. Chem.* USSR (1937) **7**, pp. 2760-2766.
[11] P. J. Maddex: Titanium Metal Production, Expanded at Henderson Plant. JOURNAL OF METALS (1954) **6**, No. 6, pp. 734-736.
[12] A. Pechukas: *Separation of FeCl, and TiCl*. U.S.

Patent 2,245,358 (June 10, 1940).
[14] I. J. Krchma: *Purification of Titanium Tetrachloride*. U.S. Patent 2,463,396 (Mar. 1, 1949).
[15] I. J. Krchma: *Separating Metal Halide Vapors*. U.S. Patent 2,533,021 (Dec. 5, 1950).
[16] W. F. Meister: *Purification of Titanium Tetrachloride*. U.S. Patent 2,416,191 (Feb. 18, 1947).
[17] D. G. Nicholson: *Purification of Titanium Halides by Treatment with Metal Hydrides and Distillation*. U.S. Patent 2,460,344 (Feb. 1, 1949).
[18] H. H. Schaumann: *Titanium Halides*. U.S. Patent 2,508,775 (May 23, 1950).
[19] H. Espenschied: *Purification of $TiCl_4$ with Iodides*. U.S. Patent 2,598,898 (June 3, 1952).
[20] A. Pechukas: *Decoloring Titanium Halides*. U.S. Patent 2,289,327 (July 7, 1942).
[21] Pittsburgh Plate Glass Co.: *Purification of Metal Halides*. British Patent 588,657 (May 30, 1947).
[22] Pittsburgh Plate Glass Co.: *Purification of Anhydrous Halides of Group IV Metals*. British Patent 600,003 (Mar. 30, 1948).
[23] L. G. Jenness and R. L. Annis: *Separation of Vanadium from $TiCl_4$*. U.S. Patent 2,230,538 (Feb. 4, 1941).
[24] W. Frey et al.: *Purifying Normally Liquid Chlorides of Metals of Group IV*. U.S. Patent 2,592,021 (Apr. 8, 1952).

---

Technical Note

# Residual Lattice Strains in Sectioned Bars of Plastically Deformed Iron

by C. J. Newton and H. C. Vacher

EXTENSIVE investigations in the field of residual strain measurement by X-ray diffraction have been made by Bollenrath, Hauk, and Osswald,[1] by Smith and Wood,[2,3] by Greenough,[4] by Rosenthal and Norton,[5] and many others. Since X-ray strain measurements apply only to those crystals of the test body which are of the proper condition and orientation to diffract and since the residual strains revealed may be accompanied by either body or textural stresses, there has been considerable disagreement among investigators with respect to the validity of conclusions in this field. Although the experimentors have employed a variety of loading schemes, surface preparations, and X-ray wave lengths, the observations almost invariably have been made only on the outer surfaces of the specimens. The present note is not to be construed as an exposition of a new method of stress analysis by X-ray strain measurements on sections but as a presentation of some results which point to interesting possibilities for further experiments with sections.

The two test rods used in this study were of ingot iron annealed at 910°C. The initial length of the gage section was 2 in. and the diameter was 0.415 in. Cross-sections were cut from the ends of the annealed rods to provide strain-free material. The tensile rod was axially loaded the desired amount in a commercial testing machine. A 1 in. portion of the gage length was cut from the other rod and was subjected to compression in the same machine. Details of this plastic straining of each rod are given in the upper half of Table I.

A half-cylinder piece about ¼ in. long was obtained by making a short longitudinal plane cut containing the axis of the rod near the center of the gage length. From adjacent material a disk about ⅛ in. thick was cut to provide the cross-section specimen. Later another section was cut from this same region with an angle of 30° between the normal to its surface and the axis of the test rod. A cross-section and a longitudinal section were cut from the compression rod in a similar manner. All of these as well as the strain-free cross-sections were mounted in Bakelite and used as specimens for the following X-ray strain measurements.

Table I. Plastic Deformation and X-Ray Measured Strains in Ingot Iron

| | Tensile Test Body | | Compressive Test Body | |
|---|---|---|---|---|
| Maximum axial stress | + 54,600 psi | | — 59,200 psi | |
| Measured radial strain | — 0.096 | | + 0.096 | |
| Calculated axial strain | + 0.192 | | — 0.192 | |
| Radiation | $K\alpha$ Co | $K\alpha$ Cr | $K\alpha$ Co | $K\alpha$ Cr |
| Crystallographic plane | (310) | (211) | (310) | (211) |
| | Residual Strain, Multiply by $10^{-4}$ | | | |
| Angle between normal to section surface and axis of test body | | | | |
| 0° (axial strain) | — 4.1 | — 3.4 | — 0.5 | — 0.4 |
| 30° | — 3.4 | — 2.1 | | |
| 90° (radial strain) | + 1.7 | — 0.4 | — 8.5 | — 4.0 |

During the course of the study, it became apparent that the condition of the surface of a specimen was a highly critical factor. One of the annealed strain-free specimens as a control was subjected to about 24 hr of polishing with fine alumina, interrupted about every 2 hr for etching with 1 pct nital. Its lattice parameter was determined at intervals from measurements on back-reflection X-ray diffraction patterns, which were calibrated with diffraction from tungsten powder. The parameter gradually approached the value found in the literature for strain-free iron and remained there, within the limits of the experimental error. This determined a long polishing and etching procedure which was adopted for all the specimens and which gave X-ray results from the surfaces believed to be representative of each specimen as a whole.

A large number of back-reflection patterns were made with cobalt and chromium radiation, all at normal incidence. Except for some preliminary stationary exposures made to monitor the removal of cold work from the surfaces, each exposure was made with the specimen slowly translating and the film slowly rotating. In appropriate cases a thin layer of a standard metal powder, tungsten with cobalt radiation and silver with chromium, was dusted over a film of vaseline on the surface of the specimen to serve to calibrate the X-ray patterns. After the preliminary work, four films were made,

C. J. NEWTON and H. C. VACHER, Member AIME, are associated with National Bureau of Standards, U. S. Dept. of Commerce, Washington.
TN 281E. Manuscript, Feb. 4, 1955.

Table II. Surface Stresses Calculated From Normal Strains, Multiply by $10^4$ Psi

| Tensile Case | Cobalt | | Chromium | |
|---|---|---|---|---|
| Cross-section | $\sigma_3 + \sigma_3 = 4$ | $\sigma_3 = \sigma_3 = 2$ | $\sigma_3 + \sigma_3 = 4$ | $\sigma_3 = \sigma_3 = 2$ |
| Longitudinal section | $\sigma_1 + \sigma_2 = -2$ | $\sigma_3 = -4$ | $\sigma_1 + \sigma_2 = 0.4$ | $\sigma_1 = -2$ |
| 30° section | $\sigma_2 + \sigma'_3 = 4$ | | $\sigma_2 + \sigma'_3 = 2$ | |
| Theoretical value | $\sigma_2 + \sigma'_3 = 3$ | | $\sigma_2 + \sigma'_3 = 3$ | |
| **Compression Case** | | | | |
| Cross-section | $\sigma_3 + \sigma_3 = 0.5$ | $\sigma_3 = \sigma_3 = 0.3$ | $\sigma_3 + \sigma_3 = 0.5$ | $\sigma_3 = \sigma_3 = 0.3$ |
| Longitudinal | $\sigma_1 + \sigma_2 = 6$ | $\sigma_1 = 6$ | $\sigma_1 + \sigma_3 = 4$ | $\sigma_1 = 4$ |

each with several sectors, each sector bearing the exposure from a particular specimen. Measurements (some of which were checked by two other persons in addition to an author) of these films provided the final data for this study, from which the residual strains given in the lower half of Table I were calculated.

An analysis of the precision of measurement indicates that the probable error in each value of the lattice strain is $\pm 1 \times 10^{-4}$. This rather large probable error arises principally from the considerable breadth of the diffraction maxima given by the very severely plastically deformed specimens. It follows, therefore, that the values of the strains presented in the table have a rather limited quantitative significance; however, they possess a high degree of qualitative reliability, since even in the earlier less carefully controlled experiments they lay in the same order.

Although the lattice strains are the directly measured quantities, the accompanying residual stress system is of more general interest. In order to calculate such a system by the method at hand, the following assumptions had to be made: 1—the stress in the interior of the gage length of the test bar before sectioning can be represented by three principal stress vectors $\sigma_1$, $\sigma_2$ and $\sigma_3$ the first of which is parallel to the axis of the bar and the latter two equal to each other and radial in the bar; and 2—the sectioning process reduces to zero all components of stress normal to the new surface, whereas the effect on those components lying in the plane of the cut is negligible.

Using these assumptions and the accepted values of Young's modulus and Poisson's ratio, $\sigma_2$ and $\sigma_3$ are obtained from the measured lattice strains normal to the surface of the cross-section, since $\sigma_1$ is zero in this specimen. In the surface of the longitudinal section, $\sigma_2$ is zero, $\sigma_3$ is known from the preceding, and $\sigma_1$ may be calculated. Similarly, the strain measured normal to the 30° section will give the sum of $\sigma_2$ and a $\sigma'_3$; the latter is a stress lying in the $\sigma_1$-$\sigma_3$ plane, 30° from $\sigma_3$ and 60° from $\sigma_1$. This sum may be compared with its theoretical value calculated from $\sigma_1$, $\sigma_2$ and $\sigma_3$ using the stress quadric[6] for homogeneous media. The reasonable agreement obtained indicates that the assumptions upon which the stress calculations are based are approximately correct. All of these stresses derived from the measured strains are presented in Table II. The probable error is about $1 \times 10^4$ psi.

The tensile rod seems to show residual axial compression of about 4 and $2 \times 10^4$ psi with cobalt and chromium radiation, respectively, and the compression rod seems to show a residual axial tension of about 6 and $4 \times 10^4$ psi with the two radiations, respectively. It may be of interest to compare the foregoing value from the tensile rod with the longitudinal principal compressive stress of $2 \times 10^4$ psi on the surface of a flat iron tensile specimen extended 26.4 pct and examined with cobalt radiation by Wood and Dewsnap.[7] Hence the two investigations indicate that the longitudinal residual stresses on the surface and in the interior of a tensile specimen are of the same sign and of the same order of magnitude. From this it follows that such stresses are not body stresses in the usual sense, but are more properly considered to be textural stresses.[8,9]

The limited amount of data presented in this note does not warrant the drawing of very positive conclusions, particularly with regard to the disputed identity of the harder and softer parts of the well known two-part system which is generally accepted in the explanation of residual strains in metals after plastic deformation.[10] The results do appear, however, to be more in line with the suggestions that the highly distorted material at or near crystal boundaries is the harder part,[2,10] rather than the suggestion that the harder part is an adjacent crystal of different orientation.[10] This is indicated by the observation that values of strain in Table I obtained from differently oriented groups (with cobalt and chromium radiation) were similar. The differences, although real, are small and may be due to differences in penetrating power of the radiations revealing disturbances, which can be minimized but not completely eliminated, brought about by the sectioning and surface preparation of the specimen.

## References


[1] F. Bollenrath, V. Hauk, and E. Osswald: Residual Stresses in Pure Tension Revealed by X-ray Diffraction Method. *Ztsch. Verein deutscher Ingenieure* (1939) **83**, p. 1239; abstracted in *The Welding Journal Research Supplement* (1942) **21**, p. 285-s.

[2] S. L. Smith and W. A. Wood: Internal Stress Created by Plastic Flow in Mild Steel and Stress-Strain Curves for the Atomic Lattice in High Carbon Steels. *Proceedings* Royal Soc. A (1944) **182**, p. 404.

[3] S. L. Smith and W. A. Wood: Stress-Strain Curve for the Atomic Lattice of Mild Steel in Compression. *Proceedings* Royal Soc. A (1942) **181**, p. 72.

[4] G. B. Greenough: Macroscopic Surface Stresses Produced by Plastic Deformation. *Journal* Iron and Steel Inst. (1951) **169**, p. 235.

[5] D. Rosenthal and J. T. Norton: A Method of Measuring Triaxial Residual Stress in Plates. *The Welding Journal Research Supplement* (1945) **24**, p. 295.

[6] I. S. Sokolnikoff: *Mathematical Theory of Elasticity*. (1946) p. 11. New York. McGraw-Hill Book Co. Inc.

[7] W. A. Wood and N. Dewsnap: Atomic Displacements Associated with Elasticity in Plastically Deformed Metals. *Journal* Inst. of Metals (1950) **77**, Pt. 1, p. 65.

[8] E. Orowan: Classification and Nomenclature of Internal Stresses. *Symposium on Internal Stresses in Metals and Alloys*. Inst. of Metals Monograph and Report Series (1948) No. 5, p. 47.

[9] C. W. MacGregor: The Significance of Residual Stresses. *Residual Stresses in Metals and Metal Construction*. (1954) W. R. Osgood, Ed., p. 103. New York. Reinhold Publishing Corp.

[10] G. B. Greenough: Quantitative X-ray Diffraction Observations. *Progress in Metal Physics*. (1952) B. Chalmers, Ed., **3**, p. 191. London. Pergamon Press.

**AIME OFFICERS:**
**President**—H. DeWitt Smith
**Vice-Presidents**—T. B. Counselman, W. A. Dean, Harold Decker, L. E. Elkins, A. B. Kinzel, W. W. Mein, Jr.
**President-Elect**—C. E. Reistle, Jr.
**Treasurer**—G. F. Moulton
**AIME STAFF:**
**Secretary**—Ernest Kirkendall
**Secretary Emeritus**—E. H. Robie
**Ass't. Secretaries**—J. B. Alford, H. N. Appleton, E. J. Kennedy, Jr.
**Field Secretary & Ass't. Secy**—R. E. O'Brien
**Ass't. Treasurer**—P. J. Apol

aime NEWS

# Electric Furnace Steel Conference Will Meet in Pittsburgh

WITH a plant trip to Allegheny Ludlum Steel Corp., Brackenridge, featured on the first day of the conference, the AIME is holding its 13th Annual Electric Furnace Steel meeting.

Headquarters for the conferees will be the William Penn Hotel on December 7, 8, and 9. Reservations should be made directly through this hotel or others in the Pittsburgh area.

The $7.00 registration fee includes a copy of the bound Proceedings when published. There is no registration fee for students at any of the sessions unless they wish a copy of the Proceedings. AIME members are entitled to a $2.00 reduction in the registration fee. The 1954 Proceedings are now available; $10.00 to nonmembers ($10.50 foreign), less 30 pct to AIME members and past registrants.

## *Preliminary Program for Electric Furnace Steel Conference*

### WEDNESDAY, DECEMBER 7

9 am to 9 pm
**Registration**

11 am
**Plant Trip**

Leave and return by chartered buses from William Penn Hotel for the Allegheny Ludlum Steel Corp. plant at Brackenridge, Pa. Box lunches will be provided on arrival at Brackenridge. Return by 5 pm.

### THURSDAY, DECEMBER 8

8:30 am
**Registration**

9:30 am
**Opening Session**

Welcoming remarks; announcements and report.

9:45 am
**Joint Session on Electrodes**

Better utilization of electric furnace electrodes through shop training programs. Papers covering handling, maintenance, and storage.

2:00 pm
**Joint Session on Degasification**

Discussion of present practices of degasification of liquid steel as used in various plants; new approach to degasification by vacuum treatment in the ladle as practiced in Europe at Bochumer Verein.

6:30 pm
**Reception and Cocktail Party**

7:00 pm
**Annual Fellowship Dinner**

Speaker: E. J. Hanley, president, Allegheny Ludlum Steel Corp.

### FRIDAY, DECEMBER 9

8:30 am
**Registration**

9:30 am
**Ingot Session on Cleanliness**

Factors affecting the cleanliness of alloy steels with (a) practices prior to slag off; (b) deoxidation and finishing practices. Use of motion pictures in the study of steel pouring.

9:30 am
**Castings Session**

Monolithic vs shaped refractories; effect of soluble and insoluble nitrogen on porosity; chromium reactions in acid and basic furnaces; quality control of melting practices.

2:00 pm
**Ingot Session on Stainless Steel**

Summary and appraisal of full melting cycle charge through tap; expert discussion on charge through oxygen blow, end of oxygen blow through skim or alloy control prelim, from skim covering deoxidizers, tap temperatures, and ladle additions.

2:00 pm
**Castings Session**

Appraisal of electric furnace arc operation and practice. Bull session on other phases not covered.

# NOHC Southern Ohio Section Meets in Columbus

THE AIME 19th annual conference of the Southern Ohio Section, NOHC was held at the Deshler-Hilton Hotel, Columbus, Ohio, Sept. 23, 1955, with 202 registrants.

The morning session on operating and combustion was chairmened by James Kirkpatrick, Youngstown Sheet & Tube Co., and Harold Frecka, Detroit Steel Corp. Papers included: *Atomization of Fuel Oil with High Pressure Gas* by Albert Meihack, Empire Steel Corp.; *What Can Be Done to Extend Life of Bottle Type Ladles* by E. R. Kercsmar, Armco Steel Corp.; *Application of High Alumina or Super Duty Suspended Fantail Nose Brick* by J. F. Pollack, Jones & Laughlin Steel Corp.; and *Report—European Trip* by C. R. Taylor, Armco Steel Corp.

The afternoon sessions had as Co-Chairmen A. P. Woods, Jr., and W. O. Richmond both of Armco Steel Corp. Papers presented were: *Statistical Study of Factors Affecting Basic Quality of Medium Carbon Killed Steel* by Frank Williams, Armco Steel Corp.; *Ladle Nozzle Setting Cage* by F. R. Smith, Jr., U. S. Steel Corp., with a discussion by J. T. McGlincy, Armco Steel Corp.; and *Comparison Chimney Type Checkers* by W. O. Richmond, Armco Steel Corp. A symposium of *Method Used to Control Scrapping Molds and Stools* closed the meeting.

The Southern Ohio Section's Annual Dinner was held that evening. H. G. Grim, Heppenstall Co., was toastmaster and Leo Wolman of Columbia University and Director of the National Bureau of Economic Research was principal speaker.

R. W. Shearman, Secretary of NOHC, R. W. Lewry, Chairman of the Section, and W. W. Bergman, Secretary of the Section, are shown.

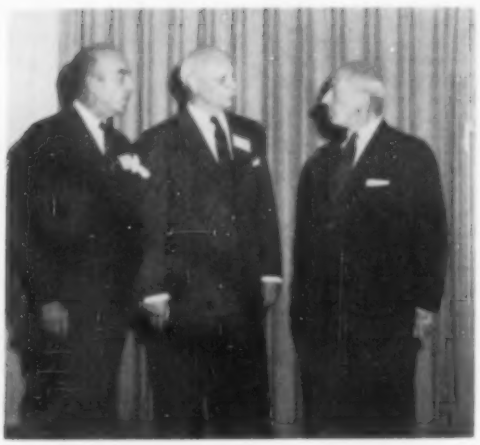

H. G. Grim, Chairman of NOHC, and Leo Reinartz, Past President of AIME, talk with Dr. Leo Wolman the speaker at the dinner.

## Connecticut Section Opens 1955-56 Season

The initial technical meeting of the 1955-56 season of the Connecticut Local Section was held on September 14 at the Hotel Elton, Waterbury, with about 30 members and guests present.

A. I. Blank, Vice Chairman of the section, was technical chairman of the meeting. Walter R. Meyer, president of Enthone, Inc., New Haven, was speaker for the evening. Subject of his talk was *Metallurgy of Electroplated Metals*. Five different types of electrolytic cells were shown and illustrated the actual plating process, effect of controlling pH of solutions, hydrogen evolution, and control and allied problems. Dr. Meyer illustrated his talk with lantern slides and through a means of optical projection showed plating solutions in action.

The effect of base metal in realizing a satisfactory plate was discussed along with the effects of a highly stressed electroplate on soft base metals. Distortion of the base metal by shear, machining, and buffing affects the adhesion bound of the plate as well ar the crystal size of the base metal. Other factors such as banding of bright plates, effect of organic compounds in the plating baths and effect on plates, brittleness of plates, throwing power of solutions, and porosity problems were discussed.

As is customary at these meetings, a technical volume was presented. L. E. Raymond was the recipient.

## Ballots on Name Change Sent Members

Changing the name of the Institute to "American Institute of Mining, Metallurgical, and Petroleum Engineers, Incorporated," was unanimously voted by the Board of Directors at the Annual Meeting. As this involves a change in the Constitution and in the Certificate of Incorporation, various lengthy formalities are involved. Among these is the sending of a ballot to all members asking for their approval of the change. These ballots were mailed late in September and must be returned to the Secretary of the Institute by the second Tuesday in November. If the vote supports the change, the matter will presumably be brought up at the annual business meeting of the AIME Feb. 21, 1956, after which, if all necessary actions are favorable, the new name will become established. Many changes will be necessary, such as in letterheads, seal, medals, and certificates, but it is intended that the abbreviation will continue "AIME" as before.

# Personals

A. P. MILLER

J. P. BANKSON

C. J. PARKINSON

**Alfred P. Miller** has been elected executive vice president, steel div., Merritt-Chapman & Scott Corp., New York, and executive vice president and general manager of Newport Steel Corp.

**Joseph J. Oravec** has been appointed chief development metallurgist, Duquesne Works, U. S. Steel Corp. He transferred from South Works of the firm, where he was general supervisor of metals research.

**H. A. Halupka** has joined the Brunswick Mining & Smelting Corp., Ltd., Bathurst, New Brunswick, Canada, as metallurgist. He had been mill superintendent for the Southwest Africa Co. Ltd., Grootfontein, Southwest Africa.

**William H. C. Webster,** Weirton Steel Co., has been transferred to Weirton, W. Va., as assistant general manager of sales, coated sheet products div. He had been located at Rochester, N. Y., as district sales manager.

**Victor A. Phillips** has been appointed lecturer in the metallurgy dept., University of Sheffield, England. Mr. Phillips had been associated with the English Electric Co.

**Douglas H. Polonis,** recently completed graduate studies in physical metallurgy at the University of British Columbia. He has been named assistant professor of metallurgical engineering at the University of Washington, Seattle.

**Harries A. Mumma, Jr.,** joined the Burroughs Corp., at the research center, Paoli, Pa. Mr. Mumma was formerly with the Brush Development Co., Cleveland.

**Wade W. Winner, Jr.,** turn supervisor, process control, U. S. Steel Corp., Kearny, N. J., is now located at the Edgar Thomson Works, Braddock, Pa.

**John P. Bankson** was appointed manager of sales for the Shenango-Penn Mold Co., Pittsburgh. Mr. Bankson has been employed in the sales div., Harbison-Walker Refractories Co., recently as assistant to the vice president.

**Julian M. Avery** has been named director of the product development div., Ethyl Corp., New York. Mr. Avery had previously been a consultant. He joined the company as a technical adviser in September 1952. He will retain these duties.

**Gerald A. Munson,** chief mineral engineer, Lithium Corp. of America, Inc., Minneapolis, has been transferred from Hill City, S. D., to Minneapolis. He will supervise the firm's mining interests in the United States and Canada.

**Ed T. Hewitt,** Electric Steel Foundry Co., is directing the newly established ESCO International div., handling the firm's export business. Mr. Hewitt is located in New York City.

E. T. HEWITT

**C. Jay Parkinson** was elected vice president and director of Anaconda Aluminum Co. Mr. Parkinson has been a counsel for the Anaconda Co. and some of its subsidiaries since 1941.

**Lawrence A. Roe** has been appointed minerals beneficiation engineer by the engineering div., International Minerals & Chemical Corp. Mr. Roe had been associated with the Bjorksten Research Laboratories, Madison, Wis.

**Karl Thomas Aust** has been named research associate in the metallurgy and ceramics dept., General Electric Research Laboratory, Schenectady. Dr. Aust has been a research associate at Johns Hopkins University, Baltimore.

**Eugene J. Kalil** is now associated with Kolisch & Kolisch, New York.

**Robert H. Jacoby,** formerly chief metallurgist and manager of quality control of Key Co., E. St. Louis, Ill., is now an associate of the St. Louis Coke & Foundry Supply Co.

**William S. Webb** has joined the Central Iron & Steel Co., Harrisburg, Pa. He had been associated with Arthur G. McKee & Co., Cleveland.

**R. V. Fostini, Jr.,** has accepted a position with the Westinghouse Atomic Power div., as an engineer. He had been on the staff of the Frankford Arsenal, Philadelphia.

**S. C. Huang,** Illinois Institute of Technology, dept. of metallurgical engineering, has joined the research div., Allis-Chalmers Mfg. Co., Milwaukee.

**Thomas P. Stanton,** Basic Refractories, Inc., Cleveland, has been transferred to Gary, Ind., as district sales manager.

**Enoch R. Needles**, senior partner, Howard, Needles, Tammen & Bergendoff, has been elected president of the American Society of Civil Engineers.

**Richard C. Campbell** has joined the Metal & Thermit Corp., New York, as metallurgical sales engineer.

**Alvin M. Weinberg** has been appointed director of Oak Ridge National Laboratory. Dr. Weinberg was formerly research director.

**Gordon Dean**, **Joseph H. Hirshhorn**, and **Philip D. Wilson** have been elected members of the board of directors, Callahan Zinc-Lead Co. Mr. Wilson is a Director of AIME.

**William H. Lang** has been appointed assistant vice president, U. S. Steel Corp., New York.

# Proposed for Membership
## — Metals Branch AIME —

*Total AIME membership on Sept. 30, 1955 was 23,282; in addition 1839 Student Associates were enrolled.*

*ADMISSIONS COMMITTEE*

*P. D. Wilson, Chairman; F. A. Ayer, Vice-Chairman; A. C. Bricker, R. H. Dickson, T. D. Jones, F. T. Hanson, Sidney Rolle, O. B. J. Fraser, F. T. Sisco, Frank T. Weems, R. L. Zinsfield, R. B. Caples, F. W. McQuiston, Jr., A. R. Lytle, H. R. Wheeler, L. P. Warriner, J. H. Senff*

*The Institute desires to extend its privileges to every person to whom it can be of service, but does not desire as members persons who are unqualified. Institute members are urged to review this list as soon as possible and immediately to inform the Secretary's office if names of people are found who are known to be unqualified for AIME membership.*

*In the following list C/S means change of status; R, reinstatement; M, member; J, Junior Member; A, Associate Member; S, Student Associate.*

**Arizona**
*Hayden*—Sharp, Melvin A., Jr. (J)
*Prescott*—Records, Robert B. (M)

**California**
*South San Francisco*—Chenkovich, Robert F. (J)
*Walnut Creek*—Szteinbaum, Victor D. (J)

**Colorado**
*Grand Junction*—Brown, M. O. (A)

**Connecticut**
*Woodbury*—Sebring, Frank R. (J)

**Illinois**
*Chicago*—Sanowskis, Albert C. (M) (C/S—A-M)
*Chicago*—Witchey, Robert H. (J)
*Lansing*—Penny, Emerson M. (J)

**Indiana**
*Chesterton*—Schrader, Carlton F. (M)
*Gary*—Peer, George J. (A)
*Gary*—Roloff, Don V. (J)
*Munster*—Baker, James T. (M) (R. C/S—S-M)

**Kentucky**
*Calvert City*—Dettmer, Philip B. (M) (C/S—A-M)

**Michigan**
*East Lansing*—Smith, Austen J. (M) (C/S—A-M)
*Flint*—King, Thomas C. (M)
*Ishpeming*—Urich, Daniel M. (J)

**Montana**
*Butte*—Sullivan, Robert E. (M) (R. C/S—S-M)

**Nevada**
*Boulder City*—Lang, Robert S. (M)
*Henderson*—Smith, Albert B. (J)

**New Jersey**
*Montclair*—Driver, Frank L. (J)
*Summit*—Walsh, William L. (M)

**New York**
*Jamaica*—Goodman, Herbert H. (M)
*New York*—Buck, C. Austin (J)

**Ohio**
*Columbus*—Cuddy, Lee J. (J)
*Columbus*—King, Clarence E. (A)
*Glendale*—Haught, Robert S. (A)
*Toledo*—Bringman, William A. (J)
*University Heights*—Brown, Jack T. (J)

**Pennsylvania**
*Beaver*—Schwab, Charles C. (J)
*Belle Vernon*—Fustich, Andy (M)
*State College*—Hoyt, Frank D. (J) (R. C/S—S-J)

**Tennessee**
*Chattanooga*—McClanhan, John J. (M)
*Knoxville*—Scott, James L. (A)

**Texas**
*El Paso*—Arguelles, Joaquin (J) (R. C/S—S-J)
*El Paso*—Harcus, Robert W. (M)

**Washington**
*Spokane*—Barnard, Lyle M. (J)

**Brazil**
*Sao-Paulo*—Chiaverini, Vincente (M)

**Canada**
*Quebec, Montreal*—Wade, Harry C. (M)

**England**
*New South Wales, Kotara*—Anderton, Jack (M) (R. M)

**France**
*St. Germain-en-laye*—Leroy, Pierre J. (M)

**Peru**
*La Oroya*—Ricketts, William F., Jr. (M)
*La Oroya*—Scott, Derek H. (J)
*Lima*—Burke, Michael A. (M)

**Sweden**
*Eskede*—Edstrum, John O. (J)

# Obituaries

**Karl Landgrebe** (Member 1912), retired steel executive, died at the age of 78. He had been vice president in charge of administration for U. S. Steel Corp.'s Tennessee Coal & Iron div. Prior to joining TCI in 1910, Mr. Landgrebe had worked with steel companies in Chicago, Toledo, and Bethlehem.

**Quincy Bent** (Member 1912) died on May 5. Mr. Bent had retired in 1947 as vice president of the Bethlehem Steel Co. He graduated from Williams College in 1901 and entered the employ of the Pennsylvania Steel Co. In 1903 he was transferred to its Lebanon plant. He became assistant to president of the Maryland Steel Co. in 1909 and general manager of its Steelton plant in 1916. Bethlehem Steel Co. acquired the Pennsylvania Steel properties in that year. Mr. Bent was made vice president in charge of operations at the height of war production activities during World War I. He became a vice president of Bethlehem in 1918 and held the post until his retirement.

## Necrology

| Date Elected | Name | Date of Death |
|---|---|---|
| 1934 | Charles F. Allen | Unknown |
| 1929 | Henry A. Doerner | Unknown |
| 1932 | J. R. Gill | June 1955 |
| 1903 | Arthur L. Hamilton | Mar. 20, 1955 |
| 1900 | L. Hanchett | Sept. 11, 1955 |
| 1948 | J. J. Harroy | Aug. 5, 1955 |
| 1945 | C. E. Higgins | Unknown |
| 1925 | James A. Hogle | Sept. 14, 1955 |
| 1931 | R. B. Lane | Sept. 1955 |
| 1948 | William C. Lenhardt | Unknown |
| 1946 | John V. Mangold | |
| 1940 | Sydney Nashner | Aug. 15, 1955 |
| 1949 | Earl J. Robishaw | Unknown |
| 1911 | Henry P. Smith | Sept. 4, 1955 |
| 1919 | Haakon Styri | Sept. 13, 1955 |
| 1897 | W. W. Taylor | May 25, 1955 |
| 1947 | Henry E. Warren, Jr. | Sept. 16, 1955 |
| 1951 | H. S. West | Sept. 2, 1955 |
| 1947 | Joseph G. Wilson | August 1955 |
| 1952 | H. C. Young | 1953 |

# Advertisers' Index


| | |
|---|---|
| **Ajax Engineering Corp.** *Eldridge, Inc.* | * |
| **American Bridge Div., U. S. Steel Corp.** *Batten, Barton, Durstine & Osborn, Inc.* | * |
| **American Machine & Metals Inc.** *The L. W. Ramsey Adv. Agency* | * |
| **Bailey Co., Wm. M.** *Walker & Downing* | Second Cover |
| **Basic Refractories Inc.** *The Griswold-Eshleman Co.* | * |
| **Bell Telephone Labs.** *N. W. Ayer & Son, Inc.* | * |
| **Braun & Co., C. F.** *The McCarty Co.* | * |
| **Buehler Ltd.** *Kreicker & Meloan, Inc.* | 1144 |
| **Consolidated Vacuum Corp.** *Charles L. Rumrill & Co., Inc.* | * |
| **Dow Chemical Co.** *MacManus, John & Adams, Inc.* | * |
| **Electro Met. Div., Union Carbide & Carbon Corp.** *J. M. Mathes, Inc.* | 1151 |
| **General Aniline & Film Corp.** *R. T. O'Connell Co.* | 1145 |
| **General Electric Co., X-Ray Dept.** *Klau, Van Pietersom-Dunlap Assoc.* | 1142 |
| **Great Lakes Carbon Corp.** *Davis, Parsons & Strohmeier, Inc.* | * |
| **Harbison-Walker Refractories Co.** *Walker & Downing* | * |
| **Hevi Duty Electric Co.** *Camm, Costigan, Inc.* | 1148 |
| **International Nickel Co.** *Marschalk & Pratt* | 1154 |
| **Jet Propulsion Laboratory, Caltech** *The Perrett Co.* | 1146 |
| **Leitz, Inc., E.** *L. W. Frohlich & Co., Inc.* | * |
| **Molybdenum Corp. of America** *Smith, Taylor & Jenkins, Inc.* | 1149 |
| **Morgan Construction Co.** *Davis Press, Inc., The* | 1157 |
| **North American Philips Co.** *Anders Assoc. Adv.* | 1158 |
| **Pittsburgh Lectromelt Furnace Corp.** *The Griswold-Eshleman Co.* | Third Cover |
| **Ramtite Co., The** *Marsteller, Rickard, Gebhardt and Reed Inc.* | * |
| **Shieldalloy Corp.** *Harold Schor Assoc.* | 1150 |
| **Smooth-Harwood Co.** *Allbright Associates Adv.* | * |
| **Steel City Testing Machines, Inc.** *Whipple & Black Adv. Co.* | 1143 |
| **Stokes Machine Co., F. J.** *John Mather Lupton Co., Inc.* | * |
| **Swindell-Dressler Corp.** *Walker & Downing* | * |
| **Titanium Alloy Mfg. Div.** *Comstock & Co.* | 1147 |
| **United States Graphite Co., The** *Price, Tanner & Willox, Inc.* | Fourth Cover |
| **U. S. Steel Corp.** **Columbia-Geneva Steel Div.** **Tennessee Coal & Iron Div.** **U. S. Steel Supply Div.** **U. S. Steel Export Co.** *Batten, Barton, Durstine & Osborn, Inc.* | * |
| **Utica Drop Forge and Tool Corp.** *Wilson, Haight, Welch & Grover, Inc.* | * |
| **Wyman-Gordon Co.** *John W. Odlin Co., Inc.* | * |


* Previous issue.

## Your electrode clamps are the key to

# LOWER OPERATING COSTS

*Lectromelt* offers you dependability, resistance to corrosion and high temperatures*

START a smelting furnace to work and there's no shutting down for making replacements. Every piece of equipment has to stay on the job until you make a complete shut-down. This is especially tough on electrode holders, since they're located where temperatures are highest and corrosive conditions worst.

You can make the electrode holders the strongest point in your furnace set-up by choosing Lectromelt equipment. Special care has been given to their design and plenty of metal goes into each unit. Clamps, supports and operating mechanisms are built generously to assure long life and low upkeep.

So many improvements have been made in clamps in recent years that many obsolete clamps are now being replaced with Lectromelt equipment.

Lectromelt engineers are expert on electrothermic problems. Our men have been dealing in problems of smelting and refining with electric-arc furnaces for many years. For this help, and for a free copy of Catalog No. 105 describing Lectromelt Furnaces, write Pittsburgh Lectromelt Furnace Corporation, 326 32nd Street, Pittsburgh 30, Pennsylvania.

Manufactured in... GERMANY: Friedrich Kocks GMBH, Dusseldorf... ENGLAND: Birlec, Ltd., Birmingham ... FRANCE: Stein et Roubaix, Paris... BELGIUM: S. A. Belge Stein et Roubaix, Bressoux-Liege ... SPAIN: General Electrica Espanola, Bilbao ... ITALY: Forni Stein, Genoa. JAPAN: Daido Steel Co., Ltd., Nagoya

*REG. T. M. U. S. PAT. OFF.

WHEN YOU MELT... MOORE RAPID *Lectromelt*

# PRODUCTS that are improving the efficiency and speeding production in American industry

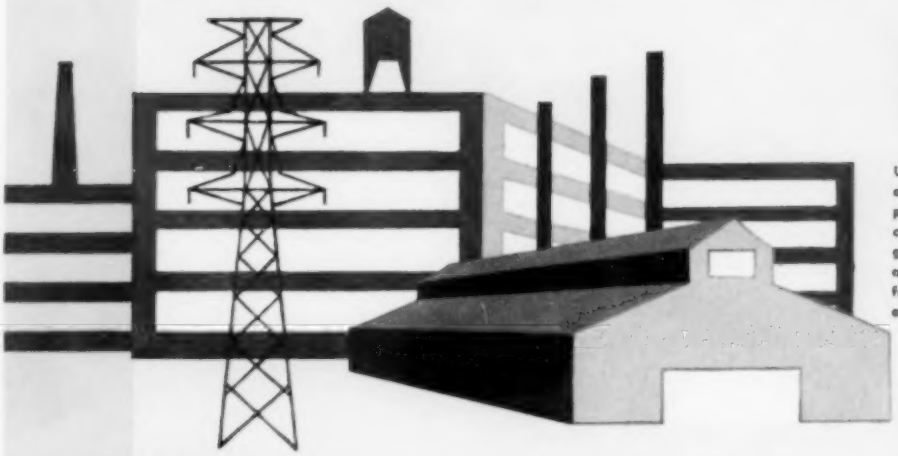

USG® Brushes are available in production or replacement lots in carbon, carbon-graphite, electrographitic, pure graphite and metalgraphite grades for all types of rotating electrical equipment.

GRAPHITAR® (carbon-graphite) is a versatile engineering material of carbon-graphite composition offered in many grades for bearings, seals, piston rings, pump vanes, thrust washers, valve seats, pistons, bushings.

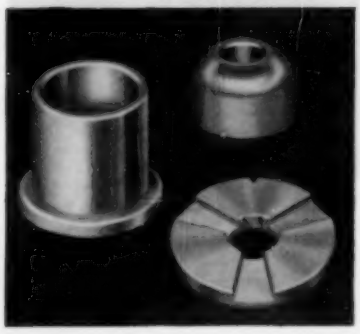

Metallurgical graphite grades for carbon control in iron and steel melting, mold coatings, hot topping compounds, Cordip®, Mexaloy® for refractory mixtures and other MEXICAN® products.

GRAMIX®: Sintered-metal bearings, gears, cams, slides, rollers, bushings and machine parts available in ferrous and non-ferrous alloys. The metal with the built-in lubrication.

206

OUR 101ST YEAR

## THE UNITED STATES GRAPHITE COMPANY

DIVISION OF THE WICKES CORPORATION • SAGINAW, MICHIGAN

# Journal of METALS

NOVEMBER 1955

## TRANSACTIONS SECTION

VOL. 7, NO. 11, IN TWO SECTIONS — SECTION TWO

| | | |
|---|---|---|
| **Melting of High Purity Uranium** | B. Blumenthal | 1199 |
| **Deformation Mechanisms of Alpha-Uranium Single Crystals** | L. T. Lloyd, H. H. Chiswik | 1206 |
| **Deformation and Recrystallization Textures of Rolled Uranium Sheet** | M. H. Mueller, H. W. Knott, P. A. Beck | 1214 |
| **Uranium-Chromium System** | A. H. Daane, A. S. Wilson | 1219 |
| **Transformation Kinetics in Uranium-Chromium Alloys** | D. W. White, Jr. | 1221 |
| **Compositional Changes of the Alpha Phase in a Eutectoid Cu-Al Alloy During Isothermal Transformation** | D. F. Toner, P. E. Gage, D. J. Mack | 1228 |
| **Creep of Polycrystalline Tin** | J. E. Breen, J. Weertman | 1230 |
| **Aging Effects in Commercially Pure Beryllium** | D. R. Mash | 1235 |
| **Preliminary Examination of the Quenching of Titanium Alloys** | L. D. Jaffe | 1241 |
| **Hardenability of Titanium Alloys Calculated from Composition: A Preliminary Examination** | L. D. Jaffe | 1245 |
| **Recrystallization Textures of a Cold-Rolled Aluminum Single Crystal** | Y. C. Liu, W. R. Hibbard, Jr. | 1249 |
| **Cleavage Steps on Zinc Monocrystals: Their Origins and Patterns** | J. J. Gilman | 1252 |
| **Discussion—Iron and Steel Div.** | | 1255 |
| **Discussion—Extractive Metallurgy Div.** | | 1260 |
| **Discussion—Institute of Metals Div.** | | 1262 |

Copyright 1955 by American Institute of Mining and Metallurgical Engineers, Inc.
Printed in U. S. A.

# Melting of High Purity Uranium

by Bernhard Blumenthal

**A melting process was developed by which high purity electrolytic uranium crystals can be converted into sound ingots without serious contamination. Careful preparation of the crystals, melting in a high vacuum, and directional solidification led to a metal of better than 99.993 wt pct purity. The metallographic examination showed a substantially clean metal with only residual amounts of a second phase which responded to heat treatment. The density of high purity uranium is 19.05 g per cu cm.**

FOR the study of the fundamental properties of uranium and its alloys, a base metal of high purity is needed, and an investigation was started at Argonne several years ago to examine various methods of preparing high purity uranium. Early success was achieved by the fused salt electrolysis process in preparing high purity metal in crystal form,[1] and the problem became that of melting the crystals into ingots without contamination. The electrolytic crystals contained a few ppm of heavy metals, less than 15 ppm C, and large quantities of potassium and lithium in the form of trapped fused salt electrolyte. On melting in vacuo in magnesia or urania crucibles, the metal picked up considerable quantities of carbon and some iron, copper, and silicon but lost most of the potassium and lithium. It was not metallographically clean, and much research work was necessary to determine the optimum melting conditions for minimum contamination. This work has resulted in the development of a melting procedure by which sound ingots can be prepared with only a limited contamination by carbon.

In the section entitled "Melting of the Electrolytic Metal," the equipment and processes that have been developed for melting the electrolytic crystals are described in detail. The "Metallography" section is devoted to the metallography of high purity uranium, and the section "Density of High Purity Uranium" contains the first property measurement on high purity uranium—a density determination.

## Melting of the Electrolytic Metal

**Apparatus**—*Melting and Vacuum Equipment:* Uranium may be melted in either resistance or induction-type electric furnaces. Resistance heating was found to be preferable to induction heating for melting down the electrolytic crystals, for several reasons: Although induction heating permits fast heating, this advantage cannot be utilized when crucibles with limited thermal shock resistance are used. Temperature control of induction-heated melts is poor, and the stirring effect increases the rate of contamination of the melt from the crucible, slag, or the furnace atmosphere; liquation and controlled solidification are difficult to carry out. Because of these objections, resistance heating was chosen.

A 10 kw Globar resistance furnace of low heat capacity permitted uniform heating of a uranium charge to its melting point in 45 min. The furnace was insulated with a removable aluminum shield so that, after melting and removal of the shield, the furnace could be quickly cooled to room temperature. The furnace was equipped with an apparatus for directional solidification; see Fig. 1a. The crucible was suspended in the center of the furnace; and when the melting was complete, the crucible was slowly lowered into the cold end of the furnace tube. Solidification took place upward from the bottom; and when the rate of lowering was small, a sound ingot free from sink holes and shrinkage cavities was produced.

To remove the large quantities of gas contained in the electrolytic crystals, melting in a high vacuum is mandatory. While, from the standpoint of contamination, melting in a highly purified argon atmosphere appeared feasible, lithium and potassium removal proved less efficient under such conditions. Also, a vacuum-melted ingot has a cleaner surface than one melted in an inert atmosphere. The vacuum system must be of very high pumping speed and leak tight so that a vacuum of less than $2 \times 10^{-3}$ mm Hg is attainable when the system is pumped down cold. The system must have a high pumping speed, so that the pressure maximum which may rise to $1 \times 10^{-1}$ mm during heating can be quickly reduced

B. BLUMENTHAL, Member AIME, is Associate Metallurgist, Argonne National Laboratory, Lemont, Ill.

Discussion of this paper, TP 4125E, may be sent, 2 copies, to AIME by Jan. 1, 1956. Manuscript, Feb. 7, 1955. Chicago Meeting, February 1955.



*The Transactions papers appearing in the Journal of Metals during 1955 will subsequently appear in AIME Transactions Volume 203, and may be permanently referenced to that volume.*

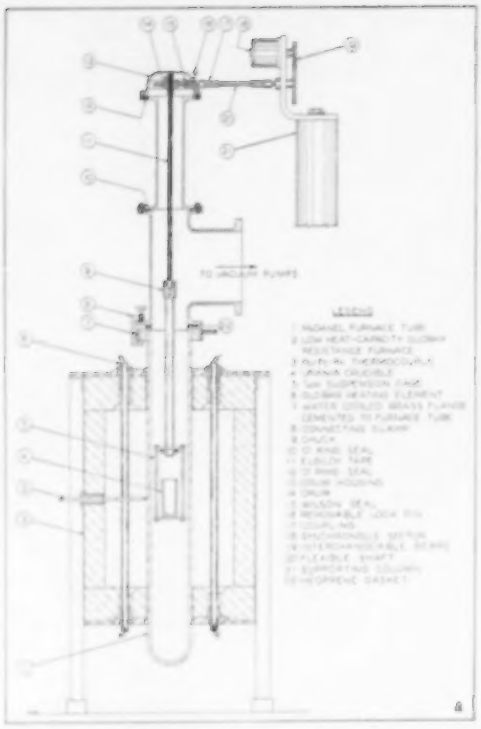

Fig. 1a—The 10 kw Globar resistance furnace of low heat capacity was used for heating the uranium charges. Diagram shows the apparatus for directional solidification used with the furnace.

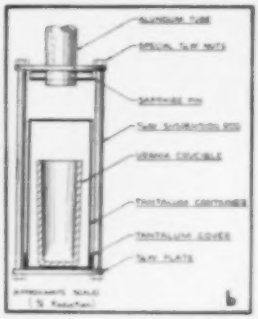

Fig. 1b—An enlargement of portions designated 4 and 5 in Fig. 1a shows the suspension, within the furnace tube, of the urania crucible and tantalum container in a TaW cage.

into the $10^{-6}$ range. A satisfactory vacuum system was built from a CVD 556 Kinney mechanical forepump, a MB 200 Distillation Products booster pump, and a MCF 700 Distillation Products oil diffusion pump. A water-cooled baffle and a liquid nitrogen cold trap completed the system; see Fig. 2. Since molten uranium is very sensitive to the smallest amount of oil vapor in the system, it is most important that no oil diffuse back into the furnace chamber; the conventional pot-type liquid nitrogen cold trap is unsatisfactory. A Chevron-type cold trap, Fig. 3, through which no oil molecule could pass without hitting a cold surface, was developed and used. The total cross-section of the trap was large enough to keep losses of pumping speed relatively small.

The temperature was controlled by a Pt—Pt-Rh thermocouple touching the outside center of the furnace tube and a Wheelco instrument in a conventional control circuit. For measuring the true temperature of the melt, the lowering apparatus was temporarily replaced by a head with an optical window and the temperature of a stationary melt measured with a Leeds and Northrup optical pyrometer. The true temperature of a melt approaching thermal equilibrium was always found to be 10° to 12°C lower than the temperature indicated by the Pt—Pt-Rh thermocouple. This correction was applied to the temperature measured by the outside Pt—Pt-Rh thermocouple. It can safely be assumed that the temperatures thus measured are correct within ±10°C.

*Crucibles:* Graphite crucibles are not suitable for melting high purity uranium because they contaminate the metal with carbon. Experiments were made with lime, alundum, zirconia, magnesia, and titanium carbide crucibles. All of these materials reacted with molten uranium. Real progress was made only after pure urania crucibles became available.[18] Although urania reacts with uranium, the reaction is slow at moderate temperatures, since uranium does not wet the crucible, and an obvious penetration of $UO_2$ into the melt was observed only when the metal was heated in an induction furnace to about 1700°C. Improvements in the quality of urania crucibles, shortening the melting time, and reducing the holding time at the melting temperature reduced the oxygen contamination; metal with less than 10 ppm O was readily produced. The urania crucibles lasted for four to five melts and would have lasted longer were it not for a slight undercut that slowly developed near the top of the melt which made it difficult to remove an ingot after several melts.

*Getters:* During the development of the melting and vacuum equipment, it was noted that contamination of the electrolytic metal by carbon could be substantially reduced by placing the urania crucible inside a tantalum cup; see Fig. 1b. The tantalum cup prevented the furnace atmosphere from reaching the electrolytic crystals or the molten metal without first coming in contact with the tantalum getter. Tantalum will remove residual organic vapors from the system and will permit fusion of electrolytic crystals into an ingot in a vacuum system without a cold trap. The use of a tantalum cup was of great help at a time when a vacuum system of high pumping speed with an efficient cold trap was not yet available. The present system with the Chevron-type cold trap no longer requires the use of the tantalum cup. In some experiments, zirconium partially or totally replaced tantalum without noticeable improvement.

**Analyses**—*Sampling Procedure:* Because of the extreme sensitivity of uranium to oxidation and contamination by carbon, an elaborate sampling procedure was used for the preparation of samples for analysis. After removal of the outer ingot layer, small turnings were taken at a slow rate from the entire cross-section with a carbide tool, using distilled water as a coolant. The sample, in a glass bottle, was rinsed several times in acetone, then in dilute $HNO_3$, and finally 15 to 20 times in pure distilled water. The water was decanted and the sample dried in a vacuum desiccator using a liquid nitrogen cold trap in conjunction with a small mechanical oil pump. Care must be taken to prevent oil vapors from entering the vacuum desiccator. Because of its clean surface, the sample is pyrophoric. Once a slight oxide coating has formed, the

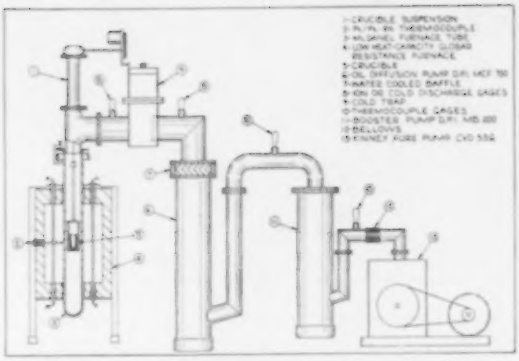

Fig. 2—The furnace and vacuum system used in melting the electrolytic uranium are shown schematically.

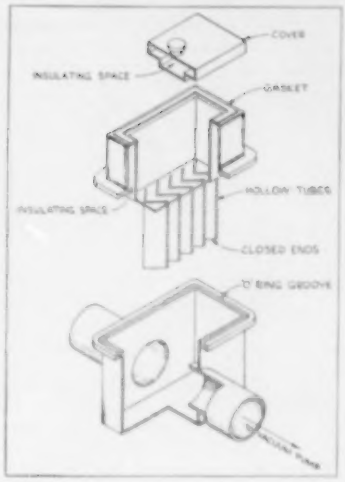


Fig. 3—Chevron-type cold trap shown in the diagram was developed by Robert E. Macherey at Argonne National Laboratory. The total cross-section is large enough to keep losses of pumping speed relatively small.

sample may be removed from the bottle for weighing in air and subsequent analysis.

This sampling method is used for carbon and nitrogen determinations only, since the glass itself may be a source of silicon contamination. Samples for spectrochemical analysis are cleaned with $HNO_3$ in a platinum dish, rinsed in distilled water, and dried with acetone.

*Analytical Methods:* The various analytical methods are adaptions of procedures previously described in the literature. The combustion method for carbon has been described by C. T. Rodden,[2] the Kjeldahl method for nitrogen by K. J. Jensen and R. J. Mundy,[3] the vacuum-fusion method for oxygen by D. H. Templeton and J. I. Watters,[4] the capillary trap method of oxygen analysis by W. G. Smiley,[5] the chlorine analytical method by R. G. Mansfield and D. H. Templeton,[6] and the carrier distillation method of spectrochemical analysis by S. F. Scribner and H. R. Mullin.[7]

**Electrolytic Metal and Its Preparation for Melting**—The electrolytic uranium is prepared by fused salt electrolysis, using a molybdenum cathode and a uranium anode in an electrolyte consisting of a eutectic mixture of LiCl and KCl and 30 pct UCl, at an initial current density of 100 amp per sq ft and at a temperature of 400° to 450°C in an argon atmosphere. The metal is low in carbon and spectrographically free from metallic impurities except for traces of aluminum, copper, iron, and silicon. It contains, however, lithium and potassium, probably in the form of trapped salt electrolyte. The electrolytic crystals are needlelike in shape and frequently exhibit a dendritic form, making it difficult to remove the trapped salt electrolyte and clean the metal thoroughly prior to melting. The cleaning procedure comprises: 1—treatment with $HNO_3$ for the removal of oxide films (concentration 1:3 ($HNO_3$:$H_2O$) which may be varied, depending on the rate of dissolution), 2—washing for 48 hr in running tap water, 3—a second $HNO_3$ rinse to remove the oxide film formed during washing, 4—rinsing five to ten times in distilled water, and 5—rinsing three times in 100 pct alcohol.

The crystals are placed in a fine wire mesh stainless steel basket and dipped first in a large beaker of $HNO_3$ and then in a beaker of water. For prolonged washing, the basket is rotated in an inclined position in a trough with running water, causing the crystals to tumble. The tumbling action should be very slight to prevent the crystals from breaking up into fine particles. Subsequent rinses are made by dipping the basket in beakers containing $HNO_3$, water, or alcohol. The clean grey crystals are collected on a fritted glass filter and most of the alcohol is quickly removed with an aspirator. The metal is placed in a porcelain dish, spread out, and placed in a vacuum desiccator connected to a mechanical oil pump equipped with a liquid nitrogen cold trap. After drying for 1½ to 2 hr, the metal has a very slight yellowish tinge, indicating the beginning of formation of an oxide film. If the surface of the metal looks decidedly yellow-green, the oxide film is heavy enough to interfere with the subsequent fusion. The desiccator is placed in a glove box, since the pure dry uranium crystals are pyrophoric and require handling in an inert argon atmosphere.

The metal is then pressed into compacts ¾ or 1 in. diam by ¾ in. in height under a pressure of 5000 psi. This pressure produces compacts of sufficient strength for handling, yet porous enough to permit gases to escape readily during heating. The crucible is charged inside the glove box with three to four compacts and quickly transferred to the furnace for immediate evacuation. The argon gas in the crucible protects the compact from ignition during transfer. The crystals and compacts are handled with clean grease-free tools.

**Melting Procedure**—After careful cleaning and drying, the electrolytic metal still contains residual electrolyte, water vapor, alcohol, and dissolved hydrogen. On first thought, it appeared advantageous to heat as slowly as possible to remove most of the gases at a low temperature.

Slow heating, however, did not produce satisfactory ingots. The individual particles did not fuse together, apparently because very stable films formed on their surfaces during heating. It appeared to be more important to heat fast and to reduce the time during which large surface areas were exposed to oxidation than to heat at the lowest possible total gas pressure. Such procedure makes imperative a vacuum system of high pumping speed.

The system is pumped down cold to an initial pressure of $5 \times 10^{-1}$ mm Hg. A pressure maximum of $10^{-4}$ mm Hg occurs during the early heating period and cannot be explained by the evolution of hydrogen or other gases and vapors from the electrolytic crystals alone, since it occurs both on heating of electrolytic compacts and on remelting of primary ingots.



analysis of these data shows that the use of a tan-

Table I. Composition of Some Primary High Purity Electrolytic Uranium Ingots

| Melt No. | Sample Location* | Ingot Weight, G | Chemical Analysis, Ppm† C | N | O | Spectrochemical Analysis,‡ Ppm† Al | Cr | Cu | Fe | Mg | Mn | Si |
|---|---|---|---|---|---|---|---|---|---|---|---|---|
| B-216 | *B* | 414 | 8 | <10 | — | <20 | <1 | <1 | 1 | <0.5 | <0.5 | 2 |
| | *BC* | | — | — | 7 | — | — | — | — | — | — | — |
| | *T* | | 14 | <10 | — | <20 | <1 | <1 | 1 | 1 | <0.5 | 1 |
| B-222 | *B* | 364 | 16 | <10 | — | <20 | <1 | 1 | 2 | <0.5 | <0.5 | 2 |
| | *T* | | 24 | — | — | — | — | — | — | — | — | — |
| B-260 | *B* | 430 | 10 | — | — | < 5 | 3 | 1 | 10 | <0.5 | <0.5 | 5 |
| | *T* | | 17 | — | — | < 5 | 2 | 1 | 3 | <0.5 | <0.5 | 5 |

* Letters for sample location represent: *B*, near the bottom end of the ingot; *C*, near the center of the ingot; *BC*, center of the bottom portion; and *T*, below the top of the ingot.
† Dashes indicate that values were not determined.
‡ All other elements including potassium and lithium were below the limits of spectrochemical detection. The limits of spectrochemical detection were similar to the ones listed in Table I, ref. 7.

It may be assumed that the gases released from the refractories contribute to the pressure rise. The present melting procedure attempts to complete the melting of 300 to 800 g of metal in 45 to 50 min. When the thermocouple indicates a temperature of 1200°C, the metal is kept at this nominal temperature for 3 min and the crucible is lowered into the cold portion of the furnace at a rate of 13 in. per hr. The ingot is probably solid after 10 to 15 min. If the metal is kept molten for an extended period of time, it will pick up both carbon and oxygen.

A satisfactory ingot obtained by this melting procedure is shown in Fig. 4. The electrolytic crystal compacts were prepared for this melt by the method described in the preceding section. If the metal is insufficiently washed, i.e., if the 48 hr washing and subsequent $HNO_3$ rinse are omitted, the metal will fuse poorly and the ingot will look like the one shown in Fig. 5. When primary ingots are combined by remelting to form a large ingot, a bright ingot will be obtained with only the top surface of the ingot discolored by oxidation. Ingots weighing 800 g have been produced by this method; see Fig. 6.

Fig. 4—A satisfactory standard primary high purity uranium ingot B-236 produced by the process described is shown in the macrograph.

Fig. 5 — Unsatisfactory primary high purity uranium ingot B-171 resulted when the metal was insufficiently washed. If the 48 hr washing and subsequent $HNO_3$ rinse are omitted, the metal will fuse poorly and the ingot will appear as shown in the macrograph. X2.

**Composition of High Purity Electrolytic Ingots**—The composition of some high purity primary ingots made by the procedure described in the foregoing sections is shown in Table I. High purity uranium contains an average of 15 ppm C, less than 10 ppm N, 8 ppm O, and an average of 6 ppm Al, 2 ppm Cu, 5 ppm Fe, 3 ppm Si, 0.5 ppm Mg, and occasionally 0.5 ppm Mn.

Table II shows the variation of the carbon content of top and bottom sections of four series of melts. Series *A* and *B* were made from crystals that were treated according to the procedure described in the preceding section. Series *C* and *D* were made from crystals that were not washed for 48 hr in running water according to step 2. The cleaning of these crystals began with step 3. The melts of series *B* and *D* were protected by tantalum cups. A statistical

Fig. 6—Standard consolidated high purity uranium ingot B-235 resulted when primary ingots were combined by remelting to form a large ingot. The surface is generally bright with the exception of the top surface which is discolored by oxidation. X1.

analysis of these data shows that the use of a tantalum cup does not significantly affect the carbon content of the metal. The carbon contents of the top sections are not consistently higher or lower than those of the bottom sections. The data of series *A* and *B*, on one hand, and of *C* and *D* on the other, may therefore be combined to yield an average carbon concentration. The data show that the carbon content of high purity metal made from washed crystals is 16±2.3 ppm at a confidence limit of 95 pct. The data also show that the accuracy of a single carbon determination is ±6 ppm and that the accuracy of duplicate determinations is ±4.5 ppm at 95 pct confidence limit.

The difference between 16 and 20 ppm C for metal made from crystals that were washed for a long period of time and others that were washed for only a few minutes may appear insignificant in view of the overlapping deviations and the spread of duplicate carbon determinations. While improvements in the appearance of the ingot and the better fusion of washed crystals may be sufficient to justify the prolonged washing, it is nevertheless felt that washing helps to control the carbon content of the metal in the following manner: The electrolytic crystals themselves probably have a very low carbon content. A substantial portion of the carbon content of the crystals is not in solution but is suspended in the salt electrolyte trapped in the crevices and corners of the dendritic crystals. Washing, therefore, should help to remove the salt and its carbon content. In any event, the carbon content of the primary ingots became consistently low only after prolonged washing was introduced into the process.

The oxygen content of high purity uranium was first determined at Sylvania Electric Products Inc. by vacuum-fusion analysis on 19 samples from four ingots giving an average of 8.4 ppm. When oxygen analyses could be made at Argonne, several more ingots were analyzed, and values of 5 to 8 ppm were obtained for primary melts. In view of the consistency of the results obtained at Argonne, it is felt that 8 ppm is a significant value for the oxygen content of primary high purity uranium. Chlorine analyses of a primary ingot (B-256) gave 4 to 6 ppm Cl. For analyses of large ingots consolidated from primary ingots, or portions thereof, see Table III.

By adding the average concentrations and allowing 15 ppm for the sum of all impurities not detected by the spectrographic method, high purity electrolytic uranium is estimated to be better than 99.993 wt pct pure.

**Table II. Carbon Content of High Purity Uranium Ingots**

| Number | Conditions | Carbon Content in Ppm: Top Section | Bottom Section | Average |
|---|---|---|---|---|
| B-216 | *A*—Crystals washed in running water. Melt protected by tantalum.* | 13, 14 | 3, 7 | 9.25 |
| B-222 | | 22, 26 | 15, 16 | 19.25 |
| B-225 | | 10 | 10 | 10.0 |
| B-236 | | 17, 18 | — | 17.5 |
| B-213 | *B*—Same as *A* but melt not protected by tantalum.* | 20, 14 | — | 17.0 |
| B-220 | | 9, 10 | 16, 24 | 14.8 |
| B-221 | | 18, 20 | 16, 19 | 18.3 |
| D-224 | | 12 | 11 | 11.5 |
| B-226 | | 15 | 19 | 17.0 |
| B-227 | | 12 | 16 | 14.0 |
| B-232 | | 20, 22 | 21, 21 | 21.0 |
| B-233 | | 16, 15 | — | 15.5 |
| B-234 | | 21 | — | 21 |
| B-178 | *C*—Crystals washed for short time only. Melt protected by tantalum.† | 15, 25 | 19, 23 | 21.0 |
| B-179 | | 25, 26 | 27, 30 | 27.0 |
| B-181 | | 15, 23 | 19, 21 | 19.5 |
| B-182 | | 24, 33 | 13, 19 | 22.3 |
| B-196 | | — | 11, 20 | 15.5 |
| B-188 | | 15, 16 | 13, 14 | 14.5 |
| B-183 | | 21, 22 | 15, 23 | 20.3 |
| B-194 | | — | 17, 17 | 17.0 |
| B-186 | | — | 24, 29 | 26.5 |
| B-201 | | 16, 18 | 15, 16 | 17.0 |
| B-202 | | 18, 24 | 23, 25 | 22.5 |
| B-190 | *D*—Same as *C* but melt not protected by tantalum.† | 14, 16 | 16, 20 | 16.5 |
| B-191 | | 19, 22 | 17, 23 | 20.3 |

* Average of conditions *A* and *B* was 15.9±2.3 ppm at 95 pct confidence limit.
† Average of conditions *C* and *D* was 20.0±2.3 ppm at 95 pct confidence limit.

## Metallography

**Preparation of Metallographic Specimens**—After mechanical preparation, the specimens were electropolished in an electrolyte containing 5 parts of 85 pct $H_3PO_4$, 8 parts of ethyl alcohol, and 5 parts of ethylene glycol at a current density of 30 milliamp per sq cm, using a stainless steel cathode and a platinum wire anode in contact with the surface of the specimen. They were etched electrolytically in a solution of 2 g citric acid, 0.5 cu cm $HNO_3$ (1.42), and 97.5 cu cm water at 15 milliamp per sq cm current density. In some cases, an electrolyte of 8.5 g $H_2C_2O_4$ in 100 cu cm water was used.

**Microstructure**—Electrolytic uranium that has been melted and directionally solidified has a microstructure as shown in Figs. 7 and 8. As-polished, the metal contains no large inclusions but numerous minute ones. As electrolytically etched, the metal shows $\alpha$ uranium and traces of a second phase which

Fig. 7—Micrograph of high purity uranium as-polished shows no large inclusions but numerous minute ones. X100. Area reduced approximately 30 pct for reproduction.

Fig. 8—When the high purity uranium was etched with $H_2C_2O_4$, $\alpha$ uranium became visible, and also seen were traces of a second phase which appears as an incomplete eutectoid network that does not follow the $\alpha$ grain boundaries. X100. Area reduced approximately 30 pct for reproduction.

Fig. 9—Numerous minute particles, believed to be particles of residual fused salt electrolyte, shown in uranium as-polished, were practically absent from high purity uranium that was liquated for 24 hr at 1200°C. X100. Area reduced approximately 30 pct for reproduction.

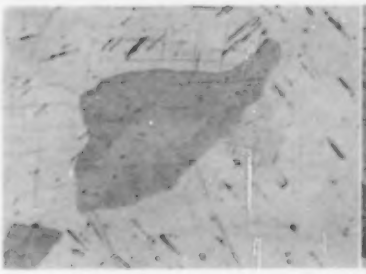

Fig. 10—When high purity uranium was etched with citric acid and $HNO_3$, comet trails which resemble channels, mostly empty, appeared. X100. Area reduced approximately 30 pct for reproduction.

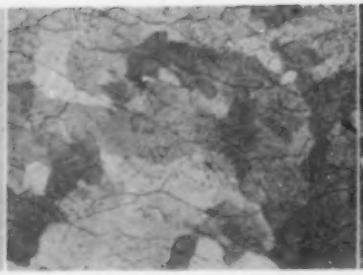

Fig. 11—Micrograph of directionally solidified uranium shows an increased amount of precipitate from an area adjacent to the periphery of the ingot. Sample was etched. X50. Area reduced approximately 30 pct for reproduction.

Fig. 12—After the uranium shown in Fig. 11 was annealed for 3 hr at 950°C and water quenched, all of the precipitate is in solution. Sample was etched. X50. Area reduced approximately 30 pct for reproduction.

appears as an incomplete eutectoid network that does not follow the boundaries of the $\alpha$ grains. This phase will be referred to as *precipitate* in the following discussion.

The many minute inclusions that are observed in high purity uranium (Fig. 7) appear as round or almost square holes at high magnification. Sometimes these inclusions are more numerous near the top of an ingot than near its bottom, and it is suspected that they are small particles of residual fused salt electrolyte. These particles are practically absent from metal that has been liquated for 24 hr at a temperature of 1200°C (Fig. 9).

The presence of the precipitate is minimized by rapid melting. Since the precipitate occurs in metal of both high and low carbon content, it was first thought to be associated with the oxygen content of the metal. However, the oxygen content of the metal turned out to be low. The precipitate is probably U(C, N, O) of which very small concentrations can be observed metallographically. Ten ppm of carbon by weight are the equivalent of 291 ppm UC by volume, a ratio that may partially explain the phenomenon. The ratios for the UN and UO are 239 and 213, respectively. Etching makes the individual particles which form the precipitate appear larger than they really are, and the volume of the total of all the impurities may account for the observed quantities of precipitate. Since the precipitate can be influenced by heat treatment, as discussed subsequently, its presence indicates a more or less contaminated metal.

*"Comet Tail" Phenomenon:* A peculiar phenomenon occurs on electrolytic etching of high purity metal (Fig. 10). Metal etched electrolytically in citric acid and $HNO_3$ shows *comet tails* that in shape resemble channels, in most cases, empty ones. The comet tails are parallel within one $\alpha$ grain. They do not occur when the metal is electrolytically etched with $H_2C_2O_4$ (Fig. 8). An $HNO_3$ etch subsequent to an $H_2C_2O_4$ etch also makes them appear. The comet tails are not caused by mechanical deformation inadvertently produced during the preparation of the specimens by cutting and grinding, since removal of metal from the surface of a specimen to the depth of 1/16 in. by electrolytic polishing does not eliminate their appearance on subsequent electrolytic etching. The comet tails are not affected by heat treatment and, therefore, are probably not caused by the presence of small uranium oxide, carbide, or nitride inclusions.

Sometimes the comet tails are more numerous near the top than near the bottom of a slowly directionally solidified ingot. They do not appear after liquation (8 hr at 1200°C). This might indicate that they are caused by a relatively light contaminant which is insoluble in uranium. Since the chlorine content of the metal is reduced from 4 to 6 ppm to less than 1 ppm during an 8 hr liquation at 1200°C, it may be that the comet tails are caused by the presence of residual fused salt electrolyte which is removed during the metallographic preparation. The removal of the contaminant may leave a channel-like cavity or a short hole which may become the starting point of a preferential dissolution of the base metal. On the other hand, it is quite possible that the comet tails are nothing but a preferential electrolytic etching effect.

**Effect of Heat Treatment on Microstructure**—If uranium is heat treated for 3 hr at 1000°C and water

Table III. Compositions of Some High Purity Consolidation Ingots Made from Standard Primary Uranium Ingots

| Melt No. | Sample Location* | Ingot Weight, G | Chemical Analysis, Ppm† | | | Spectrochemical Analysis, Ppm† | | | | | | |
|---|---|---|---|---|---|---|---|---|---|---|---|---|
| | | | C | N | O | Al | Cr | Cu | Fe | Mg | Mo | Si |
| B-235 | B | 802 | 18 | <13 | — | 10 | <1 | 3 | 15 | 0.5 | <0.5 | 5 |
| | T | | 28 | <10 | — | 10 | <1 | 2 | 10 | 0.5 | <0.5 | 8 |
| B-244 | B | 704 | 15 | <10 | 8 | 8 | <1 | 1 | 13 | 0.5 | 2 | <10 |
| B-272 | B | 806 | 10 | — | — | 5 | 1 | 1 | 7 | <0.5 | 0.5 | 5 |
| B-335 | B | | 19 | 7 | — | 5 | <1 | 1 | 2 | 0.5 | <0.5 | 10 |
| | C | 40 | — | — | 3 | — | — | — | — | — | — | — |
| | T | | 17 | 4 | — | 5 | <2 | 2 | 2 | <0.5 | <0.5 | 10 |

* Letters for sample location represent: *B*, near the bottom end of the ingot; *C*, near the center of the ingot; *BC*, center of the bottom portion; and *T*, below the top of the ingot.
† Dashes indicate that values were not determined.

Fig. 13 — Subsequent annealing for 3½ weeks at 635°C of the uranium shown in Figs. 11 and 12 produced well formed $\alpha$ grains with the precipitate reappearing both inside the grains and on the grain boundaries. Sample etched. X50. Area reduced approx. 30 pct for reproduction.

Fig. 14 — Subsequent annealing for 1 hr at 950°C and slow furnace cooling of the uranium shown in Fig. 13 produced a network pattern that was similar to, although coarser than, the pattern of the original precipitate, Fig. 11. Sample etched. X50. Area reduced approx. 30 pct for reproduction.

quenched, the precipitate will go into solution. If sufficient precipitate was originally present, it will reprecipitate on annealing in the high $\alpha$ range, e.g., for three weeks at 600°C. On reannealing in the $\gamma$ range and subsequent slow cooling, the precipitate will reappear in a dendritic pattern. Annealing in the $\beta$ range does not dissolve the precipitate as readily as annealing in the $\gamma$ range. A series of representative microstructures is shown in Figs. 11 to 14. Fig. 11 shows a high purity uranium with an increased amount of precipitate from an area adjacent to the periphery of the ingot. After 3 hr at 950°C and water quenching, all of the precipitate is in solution (Fig. 12). Quenching did not suppress the $\gamma$ to $\beta$ to $\alpha$ transformations; the $\alpha$ grain boundaries are rather ragged. Subsequent annealing for 3½ weeks at 635°C produced well formed $\alpha$ grains with the precipitate reappearing both inside the grains and on the grain boundaries (Fig. 13). Subsequent annealing for 1 hr at 950°C and slow furnace cooling reproduces a network pattern, coarser but otherwise similar to the original network precipitate (Fig. 14).

## Density of High Purity Uranium

Directionally solidified high purity uranium has a density of 19.050±0.002 g per cu cm at a confidence limit of 95 pct. This density value is an average of 24 determinations on two cylindrical specimens by the method of displacement of $CCl_4$.

This value is identical with the one reported by Katz and Rabinowitch to be the most reliable one.[8] The theoretical density calculated from X-ray data by Warren and Jacobs[9] with $a_o = 2.852$, $b_o = 5.865$, and $c_o = 4.945$ is 19.00 g per cu cm, considering that these parameters are almost certainly kX units,[10] and using an Avogadro number of $6.0235 \times 10^{23}$ and a conversion factor from kX to A units of 1.002034. The same calculation for data by Gordon[11] for $a_o = 2.8482$ kX, $b_o = 5.8565$ kX, and $c_o = 4.9476$ kX yields 19.042 g per cu cm. C. M. Schwartz and D. A. Vaughn[12] determined the lattice constants on uranium and found $a_o = 2.854$A, $b_o = 5.8670$A, and $c_o = 4.9555$A. These values give a theoretical density of 19.053 g per cu cm.

## Summary

A melting process has been developed for the consolidation of high purity electrolytic uranium crystals into sound ingots of high density without serious contamination. The metal is estimated to be better than 99.993 wt pct pure and is metallographically reasonably free from impurities.

## Acknowledgments

The present work would not have been possible without the close cooperation of many members of the staff of Argonne National Laboratory to whom grateful acknowledgment is expressed herewith. Thanks are due to Parker Deans, E. I. duPont de Nemours Co., for the statistical analyses and to Bernard Kopelman and Charles Gregg, Sylvania Electric Products Inc., for oxygen analyses. The author acknowledges with pleasure the help and advice of Richard J. Dunworth and the friendly discussions with H. H. Chiswik. He would like to express his indebtedness to Frank G. Foote, Director, Metallurgy Div., for his continuous interest and encouragement. Work was performed at Argonne National Laboratory under auspices of the AEC.

Discussion of this paper, if any, will appear in JOURNAL OF METALS, May 1956, and in AIME Metals Branch *Transactions*, Vol. **206**, 1956.

## References

[1] R. A. Noland and C. Marzano: *An Electrolytic Process for Refining of Commercial Uranium.* Paper presented at AIME Annual Meeting (February 1955).

[2] C. J. Rodden: Carbon, Hydrogen, Oxygen. *Analytical Chemistry of the Manhattan Project.* National Nuclear Energy Series. (1950) Ed. by C. J. Rodden, Div. VIII, **I**, Chap. 6, pp. 271-279. New York. McGraw-Hill Book Co. Inc.

[3] K. J. Jensen and R. J. Mundy: *Analytical Chemistry of the Manhattan Project.* National Nuclear Energy Series. (1950) Ed. by C. J. Rodden, Div. VIII, **I**, Chap. 3, Paragraph 2.1, pp. 210-211. New York. McGraw-Hill Book Co. Inc.

[4] D. H. Templeton and J. I. Watters: Low Pressure Methods. *Analytical Chemistry of the Manhattan Project.* National Nuclear Energy Series. (1950) Ed. by C. J. Rodden, Div. VIII, **I**, Chap. 27, pp. 644-661. New York. McGraw-Hill Book Co. Inc.

[5] W. G. Smiley: Determination of Oxygen in Metals Without High Vacuum by the Capillary Trap Method. *Analytical Chemistry* (1955) **27**, pp. 1098-1102.

[6] R. G. Mansfield and D. H. Templeton: Chlorine, Bromine, and Iodine. *Analytical Chemistry of the Manhattan Project.* National Nuclear Energy Series. (1950) Ed. by C. J. Rodden, Div. VIII, **I**, Chap. 7, Paragraph 2.3, p. 295. New York. McGraw-Hill Book Co. Inc.

[7] B. F. Scribner and H. R. Mullin: Carrier Distillation Method for Spectrographic Analysis and its Application to Analysis of Uranium Base Material. *Journal of Research* National Bureau of Standards (1946) **37**, pp. 379-389.

[8] J. Katz and E. Rabinowitch: *The Chemistry of Uranium, Part I.* National Nuclear Energy Series. (1951) Div. VIII, pp. 135-137. New York. McGraw-Hill Book Co. Inc.

[9] C. W. Jacob and B. E. Warren: *Journal* Amer. Chemical Soc. (1937) **59**, p. 2588.

[10] J. Thewlis: *Nature* (1951) **168**, pp. 198-199.

[11] J. Katz and E. Rabinowitch: *The Chemistry of Uranium, Part I.* National Nuclear Energy Series. (1951) Div. VIII, p. 134. New York. McGraw-Hill Book Co. Inc. Calculated from data given.

[12] C. M. Schwartz and D. A. Vaughn: Private communication, Battelle Memorial Institute.

[13] R. E. Corwin and G. B. Eyerly: Preparation of Refractories from Uranium Oxide. *Journal* Amer. Ceramic Soc. (1953) **36**, pp. 137-139.

# Deformation Mechanisms of Alpha-Uranium Single Crystals

by L. T. Lloyd and H. H. Chiswik

**The operative deformation elements in α-uranium single crystals under compression at room temperature have been determined as a function of the compression directions. The deformation mechanisms noted may be arranged with respect to their frequency of occurrence and ease of operation in the following order: 1—(010)-[100] slip, 2—{130} twinning, 3—{~172} twinning, and 4—under special conditions of stress application, kinking, cross-slip, {~176} twinning, and {011} slip. The composition planes of the {172} and {176} systems were found to be irrational. Cross-slip was shown to be associated with the major (010) slip system, coupled with localized interaction of slip on the (001) planes. The mechanism of kinking was found to be similar to that observed in other metals in that it occurred chiefly when the compression direction was nearly parallel to the principal slip direction [100] and was associated with a lattice rotation about an axis contained in the slip plane and normal to the slip direction: the [001] in the uranium lattice. The resolved critical shear stress for slip on the (010)-[100] system was found to be 0.34 kg per mm². In a single test it was shown that under compression in suitable directions twinning on the {130} also occurs at 600°C.**

DEFORMATION mechanisms of large grained polycrystalline orthorhombic α-uranium have been studied by Cahn.[1] A major slip system identified as the (010) with a probable [100] slip direction and a minor slip system on the {110} planes were reported; the slip direction of the minor system was not determined. The twinning systems that were identified experimentally included the {130} and the irrational {172} composition planes; observations of other traces which were not as frequent and which did not lend themselves to positive experimental identification led Cahn to postulate on the basis of indirect evidence that twinning also occurred on {112} and {121} planes. In addition to the foregoing slip and twinning mechanisms, Cahn also observed kinking and cross-slip in conjunction with the major (010) system; the cooperative cross-slip plane was not identified.

The availability of single crystals to the present authors has enabled them to check these results, particularly with reference to the doubtful mechanisms and the preference of operation of any one mechanism in relation to the direction of stress application. The tests were confined to compression only, primarily because of experimental limitations imposed by the size and shape of the available crystals. The tests were performed at room temperature except for one crystal compressed at 600°C. The compression directions were chosen to obtain a representative coverage of one quadrant of the stereographic projection. To test the existence of some of the deformation elements that were reported by Cahn, but were not found in the present study, several additional crystals were compressed in specifically chosen directions considered most ideal for their operation.

## Experimental Techniques

The single crystals were obtained by the grain coarsening technique described by Fisher.[2] They were prepared into suitable geometrical shapes by grinding and polishing on rotating laps, with final surface preparation performed in a $H_3PO_4$-$HNO_3$ electropolishing bath. A typical crystal readied for compression is shown in Fig. 1; their dimensions were rather small and depended upon the testing direction. Crystals isolated for compression in a direction close to the [010] axis, which lay roughly parallel to the longitudinal axis of the polycrystalline rod, were about 3 to 4 mm long and 5 mm² in cross-section, while those prepared for compression in other directions were smaller.

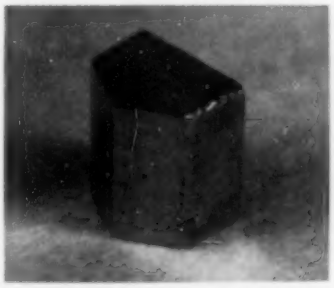

Fig. 1—Single crystal ready for compression illustrates the general shape of crystals that were compressed at room temperature. The two metallographic faces appear to the left.

Most of the crystals were free from twin markings and showed no evidence of Laue asterism. Several crystals, however, contained twin traces prior to compression; these were identified prior to compression so as to clearly distinguish them from those initiated during deformation. The origin of the twin markings prior to deformation may be ascribed to two sources: thermal stresses and specimen handling during isolation and preparation. Two other types of imperfections in the crystals should be mentioned: inclusions, which were probably oxides or carbides, and three of the crystals contained a small number of spherical included grains (<0.01 mm diam), which were remnants of unabsorbed grains from the coarsening treatment. The volume represented by these imperfections was small, and their presence presented no difficulties in the interpretation of the macrodeformation processes during subsequent compression.

Two compression fixtures were employed: crystals *A*, *B*, *C*, *E*, and *G* were compressed in a hand-operated screw-driven jig whose compression platens were designed to minimize axial rotation;

L. T. LLOYD, Junior Member AIME, and H. H. CHISWIK, Member AIME, are associated with Argonne National Laboratory, Lemont, Ill.

Discussion of this paper, TP 4106E, may be sent, 2 copies, to AIME by Jan. 1, 1956. Manuscript, Feb. 28, 1955. Chicago Meeting, February 1955.

the remaining crystals were compressed in a second fixture which was designed to further minimize the restraining forces at the compression faces by allowing their relative movement with respect to each other and to give a continuous record of the load-contraction curve. A schematic drawing of the latter fixture is shown in Fig. 2. The upper compression platen *A* had a spherical surface ground on its upper end; a matching spherical surface ground on plate *B* affixed to the cross-head of the machine insured axial loading. The lower compression platen *C* was supported by ball bearings, with the latter resting on base *D*. The platen surfaces in contact with the specimen and the surfaces in contact with the ball bearings were ground optically flat.

Load-contraction curves were recorded automatically by means of an extensometer attached to the upper and lower platens. The crystals were compressed in a screw-driven tensile machine at an average strain rate of $4 \times 10^{-4}$ in. per min. At the first indications of a sudden drop in load or a change in slope in the load-contraction curve, compression was interrupted and the crystal removed for metallographic and X-ray studies. This process was repeated on each crystal until it was evident that no further types of deformation markings would appear.

The orientations of the crystals were determined from back-reflection Laue photograms.[5] Trace identifications were made by either two-surface analysis or by the pole-locus[4] method. By means of a special micrometer specimen holder which permitted prechoosing of the area to be X-rayed, direct experimental verifications of the orientation relationships between parent and twinned portions were obtained from Laue photograms, containing both matrix and twin reflections.

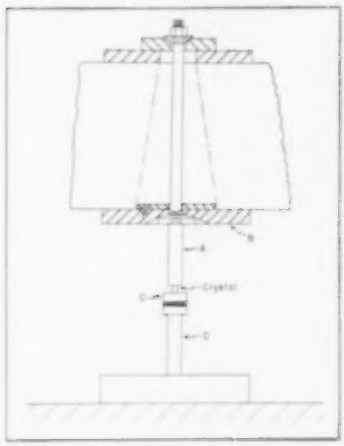


Fig. 2 — Schematic drawing shows the second compression fixture which was designed to further minimize the restraining forces at the compression faces. Letters represent: *A*, upper compression platen; *B*, platen affixed to the cross-head of the machine; *C*, lower compression platen; and *D*, the base on which platen *C*, supported by ball bearings, rested.

Table I. Compression Directions with Reference to Principal Axes in $\alpha$-Uranium

| Crystal | Displacement of Compression Direction From, In Degrees | | |
|---|---|---|---|
| | [100] | [010] | [001] |
| A | 68 | 16.5 | 74 |
| B | 71 | 80.5 | 22 |
| C | 56 | 34 | 89 |
| E | 87 | 89 | 3 |
| G | 2 | 89 | 88.5 |
| I | 74 | 16 | 89.5 |
| J | 73 | 24.5 | 73 |
| K | 32 | 77 | 61.5 |
| L | 89 | 1.5 | 89.5 |
| M | 64 | 78 | 29 |
| N | 19.5 | 71 | 89 |
| O | 27 | 84.5 | 64 |
| P | 89 | 61 | 29 |
| Q | 59 | 88.5 | 31 |
| R | 42 | 81.5 | 44 |
| S | 89.5 | 9.5 | 80.5 |
| T | 27.5 | 90 | 62.5 |
| U | 89.5 | 27 | 63 |
| V | 70 | 49.5 | 47.5 |
| W | 51.5 | 46 | 49 |
| X | 31.5 | 64.5 | 72.5 |
| Y | 46 | 89 | 44 |
| | 600°C Compression | | |
| F | 89 | 1 | 90 |

## Results

Twenty-two crystals were compressed at room temperature and one at 600°C. The compression directions are plotted in (001) standard projection in Fig. 3; their angular displacements with reference to the principal crystallographic directions are tabulated in Table I. The experimental data are discussed with reference to the modes of deformation that were observed.

**Slip Mechanisms**—*(010) Slip:* The most frequently observed deformation mechanism was slip on the (010) plane. All crystals except *A* and *E* contained traces which could be ascribed to (010) slip; see Fig. 4. It should not be inferred, however, that slip on the (010) plane was the predominant or preferred mode of deformation; in most instances, it was accompanied by twinning on one or more twin systems, by kinking, or by cross-slip. Only crystals *N* and *X* deformed exclusively by (010) slip; crystals *C* and *W* deformed mostly by (010) slip although some propagation of {130} twinning was noted. From Fig. 3 it is evident that these four crystals were favorably oriented for (010) slip.

The slip direction for this system may be deduced from several considerations. In nearly all metals, the slip direction is the most densely packed direction in the slip plane; this criterion would point to the [100]. Two experimental observations would seem to substantiate this. The asterism of Laue spots resulting from slip deformation has been shown in other metals to be due to an accompanying rotation about an axis lying in the slip plane and perpendicular to the slip direction.[6] Back-reflection photo-

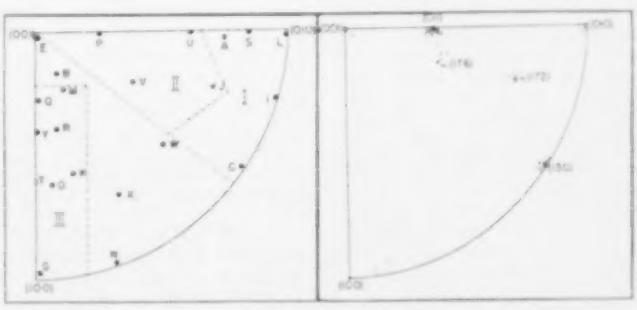


Fig. 3—Compression directions studied are plotted in (001) standard projection. Dotted lines delineate areas of operation of various mechanisms: (010) slip, all crystals except *A*, *E*; {130} twinning, areas I, II; {172} twinning, area II; {176} twinning and {011} slip, crystals *E*, *Y*; cross-slip, upper portion of area III; kinking, lower portion of area III.



Fig. 4—Two-surface analyses of deformation traces for all crystals are summarized. Also included is a summation of pole-loci of (011) slip traces on crystals *E* and *Y*.

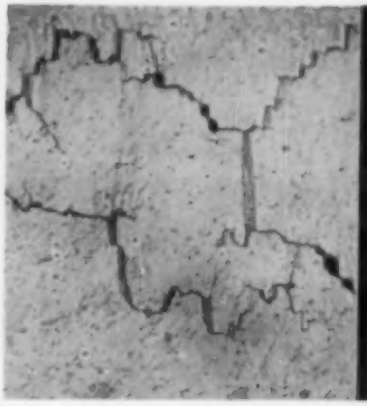

Fig. 5—Cross-slip in crystal *Y* is shown. The vertical (010) slip lines are joined by short (001) slip lines, resulting in the irregular traces. Bright field. X250. Area reduced approximately 30 pct for reproduction.

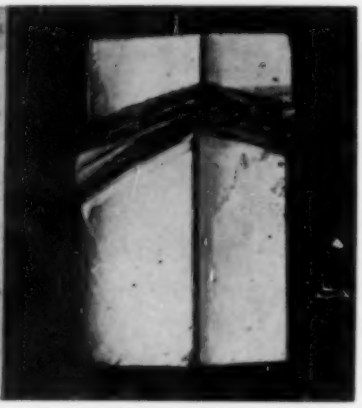

Fig. 6—Multiple kinking and irregular cross-slip traces in crystal *T* are shown. X22. Area reduced approximately 30 pct for reproduction.

grams taken from crystals that deformed by (010) slip invariably showed little or no distortion of the (001) pole, with considerable rotation of the other poles about it. In orthorhombic uranium the [001] direction lies in the (010) plane and is perpendicular to the [100] direction, indicating the latter to be the slip direction. A similar deduction may be derived from considerations of kinking which has been shown in all cases to occur when the direction of compression is nearly parallel to the slip direction.[10] As will be discussed, kinking was observed in crystals compressed in directions near the [100].

The critical resolved shear stress which is required for the initiation of substantial slip on the (010) plane was calculated from the data of crystals *I*, *J*, and *W*. These were the only crystals whose compression directions and length sizes were such that permitted slip to occur throughout the entire cross-section of the crystal, without interference from end restraints at the compression platens. The yield load was taken as that value at which the load-contraction curve deviated from linearity. The calculated values of shear stress for slip, resolved into the (010) plane and [160] direction, were 0.35, 0.36, and 0.32 kg per mm$^2$ for crystals *I*, *J*, and *W*, respectively.

*{011} Slip:* Eight sets of deformation traces on crystals *E* and *Y* were identified by the pole-locus method as being of the {011} family. These traces appeared on both metallographic faces of the crystals, but they were short and could not be matched across the common edge for two-surface analysis. A summation of the pole-loci of the eight trace directions, two from each metallographic face, is shown in Fig. 4. Metallographic evidence indicated these to have slip as their origin, in that subsequent electropolishing readily removed them. In most cases these slip traces emanated from the tips of {176} twins (e.g., trace *g*, Fig. 11), which indicates that they require rather complex stress systems for their initiation and that they probably represent a form of strain relief or accommodation for this twin system. Inasmuch as in crystal *E* there was an extremely small component of applied shear stress in the [100] direction, the investigator may speculate that the {011} slip must have been produced as an accommodation for the {176} twins, provided, however, that the [100] is assumed to be the slip direction—which is likely in that it is the most densely packed direction in that plane. It must be emphasized that this slip system was observed in only two crystals compressed in directions most unfavorable for slip on the major (010) system; hence, its role as a deformation mechanism in compression must be viewed as minor; furthermore, its identification by the pole-locus method is necessary but not sufficient.

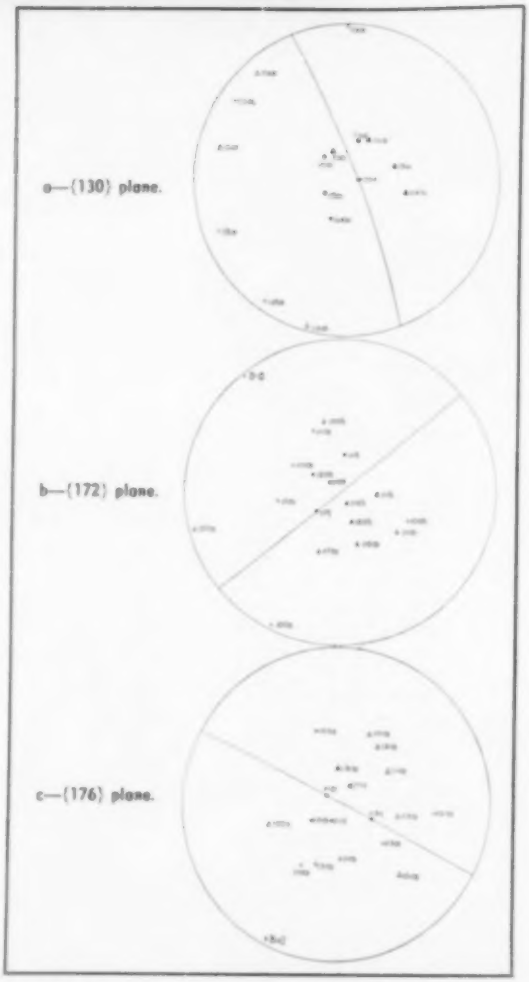


Fig. 7—Crystallographic orientation relationships of twins are shown in projections *a*, *b*, and *c*. Symbols represent: open circles, orientation of parent; triangles, orientation of twin; and solid circles are observed reflections on Laue photograms.

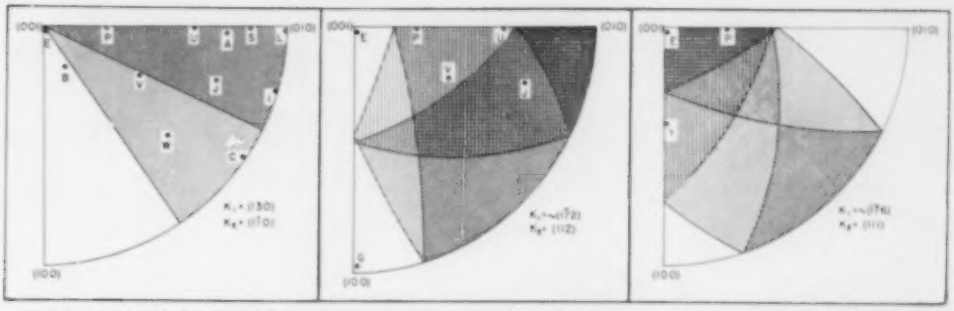

a—Standard projection for {130} plane. b—Standard projection for {172} plane. c—Standard projection for {176} plane.

**Fig. 8—Projections show areas of compression for twinning on the indicated systems. Letters indicate crystals yielding the respective twin systems. Single cross-hatching indicates that one twin plane will operate, double cross-hatching that two twin planes will operate, triple cross-hatching, three, and quadruple, four.**

**Cross-Slip**—Cross-slip deformation was obtained in crystals *M*, *Q*, *R*, *T*, and *Y* which were compressed in directions nearly parallel to the (010) plane. The early stages of deformation were characterized by a general surface roughening followed by the formation of distinct irregular traces. At high magnifications, the irregular traces were resolved into two distinct directions, e.g., Fig. 5. One of these traces, appearing almost parallel to the compression direction, was analyzed by pole-locus method to originate in (010) slip; the other trace directions appeared as short segments connecting the (010) slip traces. By extending the latter to the common reference edge and applying two-surface analysis, they were identified as (001) planes (Fig. 4).

In cross-slip, the slip direction is the same for the participating planes,[9-12] which would point to the [100] as the slip direction for the (001) plane. Some evidence for this may be derived from the fact that the gross displacement of one end of the crystal with respect to the other was in the [100] direction; also, the asterism of the Laue spots indicated a rotation about the [010] direction. This is the type of Laue spot distortion that would be expected from slip on the (001) plane in the [100] direction. It must be pointed out, however, that it was impossible to uniquely solve for rotation about the [010] direction because of the accompanying rotational asterism resulting from slip on the (010) planes.

**Kinking**—Kinking was observed in crystals *G*, *K*, *O*, and *T*. Two-surface analysis of the planes bisecting the slip planes in the parent metal and in the kink bands indicated their poles to lie near the [100] direction, Fig. 4. The formation of kink bands was characterized by sudden drops in load and audible *clicking* in much the same manner as during twinning. Crystals yielding this deformation exhibited considerable surface tilting in the form of bands ranging in width up to 0.1 mm, Fig. 6. In some cases the bands passed completely through the crystal with reasonably parallel boundaries; in others, the kink bands assumed lenticular shapes and ended within the bounding surfaces of the crystal. Twins that were present prior to compression were found to be bent at the kink band boundaries. In some instances {130} twins were formed within the kink bands; the compression directions were such that this twinning should not have occurred under conditions of simple axial loading, and it must be assumed that these were formed as a result of complex stresses.

Laue patterns from kinked areas exhibited extensive rotational asterism about the [001] direction, which is consistent with the type of asterism observed for the (010)—[100] slip system. In this sense, the kinking mechanism would appear to be basically associated with the major slip process and to be consistent with observations on other metals,[5-8] where it has been shown that the process may be described crystallographically as a rotation about an axis which lies in the slip plane and is normal to the slip direction—in uranium the [001].

**Twinning**—Three operative twinning systems were identified in the present study. They may be described in terms of their composition planes as 1—{130}, 2—{172}, and 3—{176}. The latter two have irrational indices; the indicated indices are those of planes close to the composition planes.

*{130} Twinning:* The most frequently observed twinning was on the {130} plane. Seventeen two-surface analyses of the composition plane ($K_1$)*

* For a good summary of twinning element terminology, see ref. 13.

yielded solutions within a range of approximately 3° of the {130} poles, Fig. 4. Metallographically, these twins exhibited straight and parallel boundaries whenever they passed through the crystal; they assumed lenticular shapes when they terminated within the crystal.

Solutions of Laue photograms containing reflections from both parent and twinned portions indicated the parent and twin lattices to be mirror images in the {130} planes, with a common (001) plane, Fig. 7a. The other crystallographic elements of this twin system, the $\eta_1$, $K_2$, and $\eta_2$ have been identified by Cahn[1] and verified by the present study as <310>, {110}, and <110>, respectively.

From geometrical considerations, the crystallographic directions of compression which are compatible with twinning on this system must lie within the acute angle portion of the unit sphere bounded by the $K_1$ and $K_2$ planes. This region is shown in Fig. 8a as the cross-hatched area of the standard projection; single hatching indicates that only one {130} type twin will operate in that area and double hatching that the two {130} type twins will operate. Superimposed on this projection are the compression directions of the crystals that exhibited deformation by this system. Agreement between predicted and observed areas of operation is good. The {130} twins in crystals *B* and *E* formed after considerable deformation by other mechanisms had occurred and only to a limited extent. Possibly, the crystallographic orientations of the compression directions

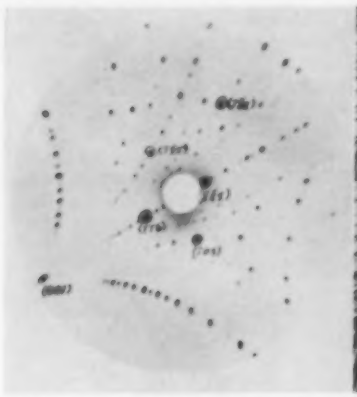

a—Photogram was taken before crystal *A* was compressed. Various planes are marked. X1½. Area reduced approximately 10 pct for reproduction.

b—Microstructure of crystal *A* is shown after compression. Polarized light. X250. Area reduced approximately 10 pct for reproduction.

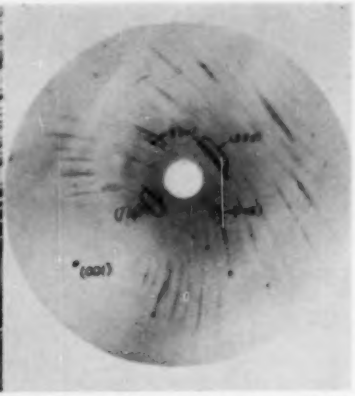


c—Photogram shows asterism after crystal *A* was compressed. Various planes are marked. X1½. Area reduced approximately 10 pct for reproduction.

Fig. 9—Asterism in crystal *A* that accompanies extensive {130} twinning, together with an illustration of microstructure and an analysis, is shown in two photograms, micrograph, and projection.

d—Projection shows an analysis of asterism rotation with the (001) plane pole rotated into the center of the projection.

had been sufficiently changed as a result of prior deformation to allow these twins to form.

Extensive {130} twinning was always accompanied by (010) slip; this was true even in crystal *L* which was compressed nearly perpendicular to the (010) plane, thus indicating that extensive {130} twinning is always accompanied by this accommodating mechanism. This is verified by Laue photograms from crystals deformed principally by {130} twinning which invariably showed rotational asterism of the spots about the [001] axis, as is well illustrated in Figs. 9a and 9c for crystal *A*. This type of lattice rotation is crystallographically similar to rotations that have been observed in other crystals under conditions of deformation that cause inhomogeneous shear or slip, such as kinking, in that the rotations are about an axis that lies in the slip plane and perpendicular to the slip direction. Ideally, when a crystal is twinned and the twin traverses the whole crystal, there should be no rotations but only a displacement of the planes corresponding to the total shear. In practice, however, this is not the case, as inhomogeneities of shear arise from several sources: either the twin does not go through the crystal, or perhaps it encounters another twin which prevents its shearing propagation. Judging from the microstructure (Fig. 9b), this is precisely the condition in crystal *A*, since both the (130) and ($1\bar{3}0$) twins were operative. The method of compression used for crystal *A* made no allowance for the relative motion of one end of the crystal with respect to the other and under such conditions a lattice rotation would be necessary to accommodate the twin. Such lattice distortions to accommodate twinning have been shown by Pratt and Pugh[4] to exist also in zinc.

The magnitude of this accommodation rotation was determined stereographically for the photogram of Fig. 9c. Fig. 9d shows the solution with the (001) plane pole rotated into the center of the projection. The discrepancy between the observed values of the magnitude of rotation is partially due to the inability to read the diffuse extremities of the arcs accurately and/or the possibility that the arcs of the ($\bar{1}\bar{1}6$) and ($\bar{2}\bar{2}5$) reflections might also include some intensity from the twinned material. This degree of rotation is approximately what might be expected on the basis of the magnitude of shear reported by Cahn for this twinning system ($s = 0.299$ and $2\phi = 81.5°$).

*{172} Twinning:* The second most frequently observed twinning system had an irrational composition plane with approximate indices of {172}. The identity of the composition plane ($K_1$) was obtained in six two-surface analyses; see Fig. 4. Stereographic solutions of Laue photograms from crystals *J* and *P* which contained both parent and twin reflections indicated the twinned material to be a mirror image

in a plane perpendicular to a <312> direction (Fig. 7b); in a twin of this kind, the latter is also the shear direction ($n_2$).

The metallographic appearance of these irrational twins was similar to the {130} type except that they were generally not as wide. These twins were found to grow progressively with gradual increases in load, as illustrated in Fig. 10; in the initial compression, twin *A* has progressed only a little more than halfway across the face; during the second compression the twin has extended and traversed the face entirely and twins *B* and *C* have been initiated; during the third compression, the latter grew sufficiently to cross the entire face.

Fig. 8b depicts the areas of crystallographic directions which would result in twinning on this system in compression, together with the compression directions that exhibited this deformation mechanism. The correspondence between the required and experimental directions is good, except for crystals *E* and *G*. The {172} twin traces in these crystals could be extraneous ones caused by handling or it is possible that they were formed by complex stress patterns resulting from prior deformation mechanisms.

*{176} Twinning:* A third twinning system was identified in crystals *E* and *Y*. The first compression of crystal *E* was accompanied by an audible click and the formation of several sets of twin traces; a composite micrograph of the metallographic faces is shown in Fig. 11. Two-surface analyses of traces *c-d* and *e-f* indicated the twin composition planes to have irrational indices close to {176}; this was substantiated independently by a pole-locus analysis of the single trace directions *h*, *o*, *s*, and *v*† on the same crystal plus four traces on crystal *Y*. From Laue patterns of both crystals containing diffraction spots from parent and twinned portions, the two lattices were found to be mirror images in a plane whose pole corresponded to a <512> direction (see Fig. 7c); by definition, the latter is also the twinning direction.

† Trace *v* is not shown in Fig. 11; it was developed on face *A* after a subsequent compression.

The $K_2$ plane, the magnitude of shear, and the shear direction were determined by goniometric measurements. The angles between the normals to the parent surfaces and the twin surfaces for traces *c-d* and *e-f* crystal *E* were measured on a bench microscope by a rotation about an axis parallel to the respective twin trace. The data were analyzed according to the stereographic method described by Greninger and Troiano,[10] and the results indicated shear directions within 2.5° and 6° of <512>, thus corroborating the X-ray determination. The values of the angle $2\phi$ were 85°30′ and 82°30′. The sense of shear agreed with that which would result from a twin system of $n_1 = [512]$ and $K_2$ equal to (111). These results are in agreement with the geometrical considerations of twinning, namely, that on a stereographic projection the great circle connecting the pole of the $K_1$ plane and the $n_1$ direction must contain the pole of the $K_2$ plane and that the indices of the $K_2$ plane must be rational and low, and its pole cannot be displaced from the $n_1$ direction by an angle greater than 20°, else the corresponding shear is impossibly great. The (111) pole indeed lies on such a circle and is displaced only 6° from the shear direction. The calculated $2\phi$ angle is 83°50′, in fair agreement with the experimental values. Thus, the complete identity of this twin system is: $K_1$ = irrational ~ $(\bar{1}7\bar{6})$; $K_2 = (111)$; $n_1 = [512]$; $n_2$ = irrational; $2\phi = 83°50'$; and $s = 0.216$.

The regions of operation of this twin system upon compression are depicted in Fig. 8c, along with the three compression directions that yielded this deformation mechanism. Evidence for {176} twinning in crystal *P* was rather sparse; however, one of the traces observed could best be explained by this mechanism.

*{112}, {121}, {011} Twinning and {110} Slip:* In addition to some of the experimentally observed deformation elements discussed previously, Cahn[1] has reported traces which he ascribed to {112} and {121} twinning and {110} slip; the latter he regarded as a minor slip system. Also, the identification of the {121} twins he regarded as indefinite, since it was based on only three traces analyzed by the pole-locus method; two of these were actually more compatible with a {110} plane.

In view of the uncertainty of the foregoing deformation mechanisms, several crystals were compressed in directions chosen so as to provide the most favorably oriented position for their operation. For slip, the choice was relatively simple; it is the direction inclined 45° to the slip plane and slip direction. The choice for a given twin system, however, is not as simple; geometrical considerations of twinning define the area of crystallographic

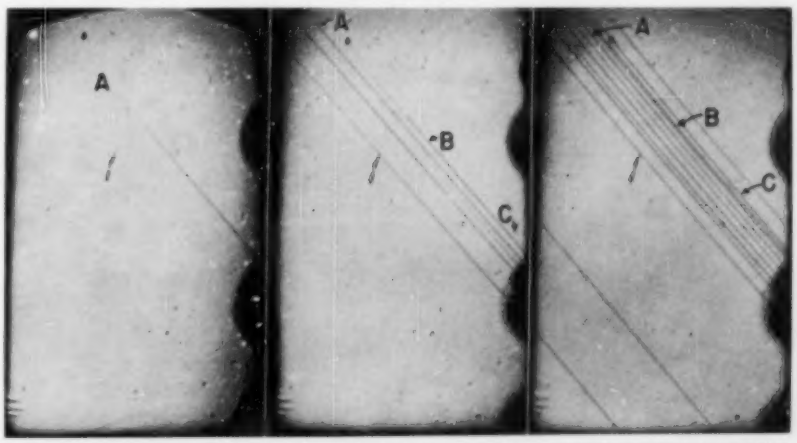


a—First compression, crystal *J*. b—Second compression, crystal *J*. c—Third compression, crystal *J*.

Fig. 10—Progressive growth of {172} twins in crystal *J* is illustrated in *a*, *b*, and *c* at three stages of compression. Polarized light. X30. Area reduced approximately 10 pct for reproduction.

directions of compression which would permit deformation on a given twin system to occur. The manner of choosing the most favorably oriented direction within this area, however, is rather uncertain; the problem is even more complicated when several twin systems are present and their areas of operation overlap each other, as is the case in uranium. Lacking a better criterion, it was postulated that the most suitably oriented direction might be that which would result in maximum contraction of the crystal.

In line with the foregoing, crystals *I* and *N* were oriented to test for {110} slip. Neither of these crystals exhibited deformation by this mechanism; crystal *N* deformed exclusively by (010) slip, and crystal *I* gave evidence of initial deformation by the same process followed by {130} twinning. From these results, it may be concluded that slip on the {110} is not operative at room temperature under compression.

Crystals *J* and *K*, which were oriented critically for {112} and {121} twinning, respectively, showed no evidences of twinning on these systems. The orientation of crystal *J* for the {112} twinning was the same as that necessary to result in maximum contraction of the crystal upon formation of {172} twins, since they are reciprocal to each other. The crystal deformed initially by (010) slip, followed by twinning on one of the {172} planes, and later by twinning on one of the {130} planes. Crystal *K*, oriented for {121} twinning, deformed initially by (010) slip and was followed by kinking. These results indicate that neither {112} nor {121} twinning can be regarded as operative in room temperature compression.

Frank,[28] from a theoretical analogy of the uranium lattice to that of zinc, postulated twinning on the {011} composition plane. This twinning system was not observed in any of the crystals studied; the traces that did correspond to the foregoing indices were identified as slip.

Notwithstanding the direct experimental efforts to obtain these questionable deformation systems, it should be pointed out that in several crystals a relatively small number of short traces were noted, either before or after compression, to which {112} or {121} indices could be assigned by the pole-locus method. The results suggested that the {112} traces are probably formed during cooling from the coarsening temperature, since they were generally present prior to compression. It may well be that the deformation mechanisms reported by Cahn[1] but not observed in the present study, are, indeed, operative at higher temperatures and under conditions of intergranular complex stresses present in polycrystalline materials. This view would be consistent with similar behavior in other metals,[4] where different slip mechanisms have been found to prevail at different temperatures. Similarly, Boas and Ogilvie[17] have identified slip systems in polycrystalline high purity aluminum and $\alpha$ brass which had not been observed in single crystals. In addition to the effects of temperature and stress complexity, such factors as differences in chemical purity and the effects of straining rates on twinning deformation[29-32] should also be considered.

**Compression at 600°C**—A single elevated temperature compressive test was performed on a crystal oriented so that its direction of compression was within 1° of the [016] direction. This test was performed to ascertain if {130} twinning was still operative at elevated temperatures, with no intention of investigating fully the effects of temperature on the choice of deformation mechanisms. The test was performed in a bell-jar container, filled with purified argon gas and equipped with a fixture which provided for axial loading of the crystal. The crystal was heated by a small platinum-wound furnace and the temperature measured with a chromel-alumel thermocouple. The compressive loading was applied after the specimen had reached the required temperature so as to allow its free expansion during heating. As the load was applied, several audible clicks occurred, and the resulting deformation traces were identified by two-surface analysis to be {130} twins. The twins were large and their bounding edges were somewhat irregular but, in general, they were lenticular in shape; at higher magnifications areas of entrapped untwinned material left within the twin bands could be noted. Even though this

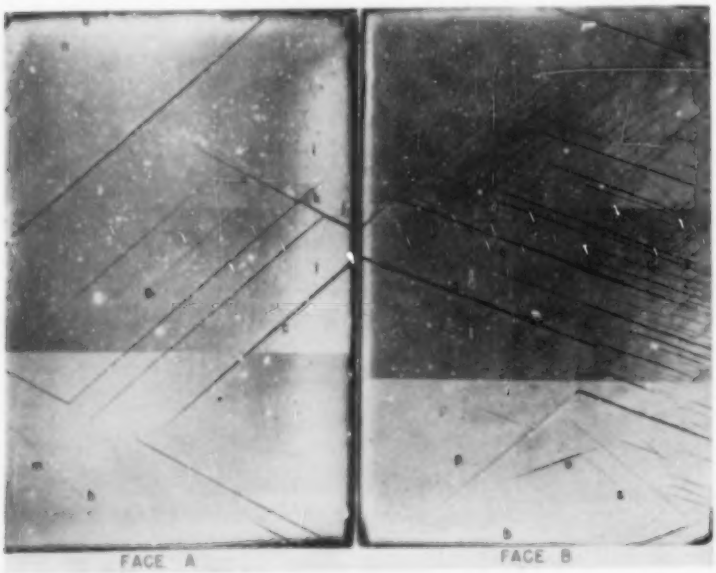


Fig. 11—Composite micrograph shows matching of {176} twin traces, in faces *A* and *B*, across the common edge on crystal *E*. Polarized light. X40. Area reduced approximately 20 pct for reproduction.

crystal was compressed at 600°C, the Laue spots obtained after cooling to room temperature indicated the same type of asterism, that is, rotation about the [001] axis, as that found for crystals compressed at room temperature in a similar direction.

## Discussion

The deformation mechanisms that have been identified as operative in the various crystals are summarized in Table II. Only those twinning systems are included which were unmistakably identified by two-surface analyses and/or Laue twin orientation relationship determinations. Similarly, the slip deformation mechanisms indicated are only those that resulted in microscopically visible traces. The major and most frequently occurring deformation mechanisms were: (010) slip, {130} twinning, and {172} twinning. Under special cases of stress application, deformation by kinking, cross-slip, {176} twinning, and {011} slip were noted. Their general areas of operation are indicated on a quadrant (001) standard projection in Fig. 3; the boundaries should not be considered exact but rather as outlines which include the crystals deformed by the various deformation mechanisms.

**Table II. Operative Deformation Mechanisms**

| | Operative Twin Systems* | | | Operative Slip and Associated Deformation Mechanisms† | | | |
|---|---|---|---|---|---|---|---|
| Crystal | {130} | {172} | {176} | (010) | Cross-Slip | Kinking | {011} |
| A | 2 | — | — | — | — | — | — |
| B | — | — | — | X | — | — | — |
| C | 1 | — | — | X | — | — | X |
| E | — | — | 4 | — | — | — | — |
| G | — | — | — | X | — | X | — |
| I | 2 | — | — | X | — | — | — |
| J | 1 | 1 | — | X | — | — | — |
| K | — | — | — | X | — | X | — |
| L | 2 | — | — | X | — | — | — |
| M | — | — | — | X | X | — | — |
| N | — | — | — | X | — | — | — |
| O | — | — | — | X | — | X | — |
| P | 2 | 2 | — | X | — | — | — |
| Q | — | — | — | X | X | — | — |
| R | — | — | — | X | X | — | — |
| S | 2 | — | — | X | — | — | — |
| T | — | — | — | X | X | X | — |
| U | 2 | 2 | — | X | — | — | — |
| V | 1 | 1 | — | X | — | — | — |
| W | — | — | — | X | — | — | — |
| X | — | — | — | X | — | — | X |
| Y | — | — | 2 | X | X | — | — |

* The number refers to the number of operative twin planes.
† X indicates that deformation of the indicated type was observed microscopically.

The present work has verified the existence of {130} and {172} twins and (010)-[100] slip, which were reported by Cahn,[1] and has determined the conditions of preferential operation of these systems in single crystals under compression at room temperature. {130} twinning was also found to be operative at higher temperatures. Kinking and cross-slip were found operative under certain conditions, with the latter being a cooperative deformation of the (010) and (001) planes. {112} and {121} twins and {110} slip which were reported by Cahn were not found to be operative in single crystals under compression at room temperature. The discrepancy may lie in the fact that in Cahn's work the deformation traces were obtained at varying temperatures and under conditions of complex stresses.

Deformation by irrational {176} twinning and by {011} slip had not been observed by Cahn. These deformations were found to be operative under limited conditions of stress application, particularly in the vicinity of the [001] direction and nearly parallel to the (010) plane, when deformation by the more prevalent mechanisms was effectively excluded. There is one inconsistency in the experimental results with regard to these deformation mechanisms: crystal *Q*, which was compressed in a direction suitable for their operation, nevertheless did not contain either {176} or {011} traces; it deformed extensively by (010)-(001) cross-slip. The reason for the inconsistency is not clear. In view of the restricted conditions of operation of these elements, it is not surprising that Cahn did not find them in his studies; on the other hand, the six traces which Cahn did observe and could not identify, but preferred to believe that they were extraneous surface markings, might well have been traces belonging to these deformation mechanisms.

From a consideration of the relative prevalence and ease of twin formation in compression directions permitting two or more twin planes to operate, some indirect evidence may be cited supporting the view of Bell and Cahn[11] that the twinning process is subject to a critical shear-stress law. These authors suggest that it is reasonable to expect a critical shear-stress law to apply to the spread of a twin across a crystal after a nucleus has formed. Some experimental observations in the present study would seem to substantiate this view. For example, crystals oriented for compression in directions near an element of twofold symmetry but slightly displaced from it (such as crystals *P*, *U*, *A*, *S*, and *L*), always resulted in the initiation of twinning on the plane of a given family which had the higher shear-stress resolved into the twinning plane and the twinning direction, only to be followed later by twinning on some other plane of the same family. A similar observation, with regard to the choice between two different systems, may be made for crystal *J*: both {130} and {172} twins were observed in this crystal, but the {130} twinning did not occur until after considerable deformation by {172} twinning had taken place. Apparently, even though {130} twins generally formed more readily, the crystal was so oriented that its direction of compression from a critical shear-stress viewpoint was more favorably oriented for initial deformation by {172} twinning.

Cahn[1] and Frank[10] made two generalizations, with regard to twinning, to which they attached special significance: the rationality, or near rationality, of the plane of shear and the fact that the observed composition plane is always the one of the higher indices in the case of reciprocal twins. In uranium it is the {130} and {172} twin planes which are operative rather than their respective reciprocals, the {110} and {112}. The same was found to be true for the {176} twin system; in no case were there traces found of its reciprocal, the {111}. The nearest plane of relatively low indices to the plane of shear for the {176} system is the {121} inclined 5°57′ to it, and the nearest direction is the <211> inclined at an angle of 6°28′. The deviations from rationality are substantial and suggest doubt as to the significance of this generalization. For this reason, no attempts were made to speculate as to the atom movements in this twin system, since a projection on the plane of shear would necessitate the consideration of a large number of planes; and if an analysis were made by considering the shear plane to be the nearest plane of low indices, considerable error would be introduced, yielding results of questionable value.



then multiplying each background corrected inten-

### Acknowledgments

The authors wish to acknowledge with gratitude the assistance of Maurice Odie in the metallographic preparation and isolation of the crystals. His careful and painstaking efforts in the manipulation of the rather small crystals in the preparation of specific directions of compression were invaluable. Thanks are due F. G. Foote and P. A. Beck for their advice and encouragement throughout the investigation. This paper is based upon work performed under the auspices of the AEC.

Discussion of this paper, if any, will appear in JOURNAL OF METALS, May 1956, and in AIME Metals Branch *Transactions*, Vol. **206**, 1956.


### References


[1] R. W. Cahn: Plastic Deformation of Alpha-Uranium; Twinning and Slip. *Acta Metallurgica* (1953) **1**, pp. 49-70.

[2] E. S. Fisher: Preparation of Alpha-Uranium Single Crystals. AIME Annual Meeting, (February 1955).

[3] A. Greninger: Determination of Orientations in Metallic Crystals. *Trans.* AIME (1935) **117**, p. 61.

[4] C. S. Barrett: *Structure of Metals*. (1952) 2nd Ed. New York. McGraw-Hill Book Co. Inc.

[5] E. Orowan: A Type of Plastic Deformation New in Metals. *Nature* (1942) **149**, p. 643.

[6] J. B. Hess and C. S. Barrett: Structure and Nature of Kink Bands in Zinc. *Trans.* AIME (1949) **185**, p. 599; JOURNAL OF METALS (February 1949).

[7] D. C. Jillson: An Experimental Survey of Deformation and Annealing Processes in Zinc. *Trans.* AIME (1950) **188**, p. 1009; JOURNAL OF METALS (September 1949).

[8] J. J. Gilman: Mechanism of Ortho Kink Band Formation in Compressed Zinc Monocrystals. *Trans.* AIME (1954) **200**, p. 621; JOURNAL OF METALS (May 1955).

[9] R. Maddin, C. H. Mathewson, and W. R. Hibbard, Jr.: Unpredicted Cross-Slip in Single Crystals of Alpha Brass. *Trans.* AIME (1948) **175**, p. 86; METALS TECHNOLOGY (February 1948).

[10] G. J. Ogilvie and W. Boas: Discussion of ref. 9. *Trans.* AIME (1948) **175**, p. 102; METALS TECHNOLOGY (August 1948).

[11] R. Maddin, C. H. Mathewson, and W. R. Hibbard, Jr.: The Active Slip Systems in the Simple Axial Extension of Single Crystalline Alpha Brass. *Trans.* AIME (1949) **185**, p. 527; JOURNAL OF METALS (August 1949).

[12] R. W. Cahn: Slip and Polygonization in Aluminum. *Journal* Inst. of Metals (1951) **79**, p. 129.

[13] E. O. Hall: *Twinning*. (1954) p. 42. London. Butterworths Scientific Publications.

[14] P. L. Pratt and S. F. Pugh: Twin Accommodation in Zinc. *Journal* Inst. of Metals (1951-1952) **80**, p. 653.

[15] A. B. Greninger and A. R. Troiano: The Mechanism of Martensite Formation. *Trans.* AIME (1949) **185**, p. 590; JOURNAL OF METALS (September 1949).

[16] F. C. Frank: A Note on Twinning in Alpha-Uranium. *Acta Metallurgica* (1953) **1**, pp. 70-74.

[17] W. Boas and G. J. Ogilvie: The Plastic Deformation of a Crystal in a Polycrystalline Aggregate. *Acta Metallurgica* (1954) **2**, p. 655.

[18] C. S. Barrett, G. Ansel, and R. F. Mehl: Slip Twinning and Cleavage in Fe and Si Ferrite. *Trans.* ASM (1937) **25**, p. 702.

[19] C. H. Mathewson and A. J. Phillips: Plastic Deformation of Coarse-grained Zinc. *Proceedings* Inst. of Metals Div., AIME (1927) p. 143.

[20] C. Benedicks: Discussion of ref. 19. *Proceedings* Inst. of Metals Div., AIME (1927) p. 192.

[21] R. L. Bell and R. W. Cahn: The Nucleation Problem in Deformation Twinning. Letters to the Editor. *Acta Metallurgica* (1953) **1**, p. 752.


---

# Deformation and Recrystallization Textures of Rolled Uranium Sheet


by Melvin H. Mueller, Harold W. Knott, and Paul A. Beck



**The rolling and recrystallization textures in 300°C rolled uranium sheet were investigated using a Geiger counter diffractometer with the modified Schulz reflection technique. Seven sections of sheet material were used in order to obtain sufficient data for quantitative pole figures by the reflection technique. A special integrating specimen table was used for obtaining and recording the data automatically. The rolling texture was described in terms of several "ideal orientations" in which the stronger orientations have either the (110) or (010) poles in the vicinity of the rolling direction. The recrystallization texture of the sheet uranium was also described by several "ideal orientations" which are somewhat different, except in one case, than the as-rolled "ideal orientations."**


RESULTS of an X-ray study of the deformation texture in rolled uranium rods were reported by Harris[1] in which a concentration of (010) and (110) poles was found in the rolling direction. More recently Seymour,[2] Mitchell and Rowland,[3] and Adam and Stephenson[4] reported results obtained on uranium sheet rolled under various conditions of temperature and amount of reduction. Since the results of Seymour as opposed to those of the two other groups of investigators are not in full agreement, it seemed justifiable to publish the present data, obtained concurrently with the previously mentioned investigations.[1-4] The results with rolled and recrystallized uranium sheet were also included in the paper, since they appear to be more complete than the only previously published texture data on recrystallized sheet.[5]

In the present investigation great care was taken to maintain complete separation of the reflections from different crystal planes, even in cases where the $2\theta$ angles differed from each other by less than


M. H. MUELLER, Member AIME, H. W. KNOTT, are associated with Argonne National Laboratory, Lemont, Ill., and P. A. BECK, Member AIME, is Research Professor of Physical Metallurgy, University of Illinois, Urbana, Ill.



Discussion of this paper, TP 4105E, may be sent, 2 copies, to AIME by Jan. 1, 1956. Manuscript, Feb. 7, 1955. Chicago Meeting, February 1955.

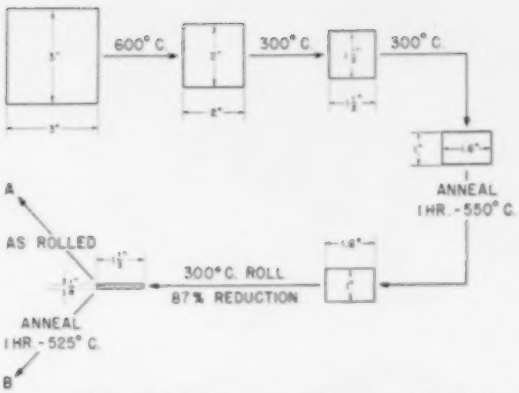


**Fig. 1—Uranium sheet used in the investigation was obtained from a casting of 3 in. sq section, according to this rolling schedule.**

a degree. A precaution important in determining recrystallization textures is integration, i.e., the scanning by the incident X-ray beam of a large number of crystals, so that representative sampling of the texture as a whole is achieved. The technique used in the present investigation[6] was designed with this end in view.

By using seven different sections through the sheet material and by assembling the data obtained with all into a single pole figure,[6] it was possible to avoid specimen tilting angles larger than 30° and, thereby, to minimize the errors commonly arising from defocusing[7] when the Schulz method is used at higher tilting angles.

## Experimental Method

*Specimen Preparation:* The uranium sheet used for the present orientation study was obtained from a casting of 3 in. sq section, as shown in Fig. 1. As indicated, the 1x1.6 in. strip was given an 87 pct reduction at 300°C to produce an $\frac{1}{8}$x1$\frac{1}{2}$ in. strip. During the rolling operation, the leading end was reversed for each pass. A part of this material, designated *A*, was used for the determination of the "as-rolled" texture and another part, designated *B*, was annealed 1 hr at 525°C and then used for the determination of the recrystallized texture.

The preferred orientation in this sheet material was investigated using the Schulz reflection method with the automatic instrument previously described.[5, 6] By using seven well chosen sections cut in different directions through the sheet, the quadrant of the pole figure can be adequately covered, with sufficient overlapping of the data from the various sections to afford a good check on the accuracy. Six of these sections consisted of a number of pieces similarly cut and held together by means of a jig. Since the reflecting surface on the seventh section was parallel to the rolled surface, it was prepared from a single piece of the sheet.

*Plotting of Data:* The intensity data for the construction of various pole figures were obtained with the automatic instrument previously described.[6] The uncorrected intensity for each $\phi$ and $\alpha$ position was plotted according to the sequence shown for section 7, Fig. 5 of ref. 6. A similar plot was prepared for each section and each reflection. A second plotting was then made on a master net which contained all data for a certain reflection from each of the seven sections. The corrected intensity, used for the final plot on the pole figure, was obtained by first subtracting background from the observed intensity and then multiplying each background corrected intensity by the correction factor appropriate for the tilting angle $\phi$ in question, as shown in Table I. Contour lines of the pole figure were then drawn on a transparent sheet placed over the net in which a total of 745 intensity values were plotted. It has been assumed that each of the four quadrants of a pole figure of this material would be practically identical because of the symmetry produced in reverse rolling and the elimination by etching of the surface layers of the sheet.

**Table I. Factors Used to Correct for the Decrease in Intensity as a Function of $\phi$**

| $\phi$ Angle | Correction Factor |
|---|---|
| 0 | 1.00 |
| 5 | 1.01 |
| 10 | 1.02 |
| 15 | 1.05 |
| 20 | 1.10 |
| 25 | 1.15 |
| 30 | 1.25 |

The correction factors given in Table I were determined by measuring the drop off in intensity with increasing $\phi$ angle of a strong reflection from a random sample of PbS powder. One of the factors which has an effect on the magnitude of this correction is the size of the slit system near the Geiger-Muller tube.[7] Since it was necessary to use a rather narrow receiving slit in order to maintain the required resolution for certain uranium reflections, the correction required at the higher $\phi$ angles was considerable.

## Experimental Results

*Rolling Texture:* The quantitative pole figures, with intensity contours, for the 300°C rolled sheet described previously, are reproduced in Fig. 2. It is evident from the (010) and (110) pole figures that there is considerable concentration of these two poles parallel to the rolling direction. However, in addition there is a considerable spread of these poles away from the rolling direction, which is especially evident in the (110) pole figure. There is a sharp concentration of (001) poles tilted 30° to 35° from the rolling plane normal toward the transverse direction and another (001) pole concentration tilted 15° to 20° from the rolling plane toward the rolling direction.

A separate symbol has been used in each pole figure to mark "ideal orientations" corresponding to maxima or high pole concentrations. These symbols, without the contour lines, have been transferred to the pole figures shown in Fig. 3 in order to show the compatibility of several "ideal orientations" with the high intensity areas which appear in the (010), (110), (001), and (100) pole figures.

The lines which form the quadrangles shown in Fig. 3 connect one maximum intensity area or one high intensity area from each of the pole figures mentioned previously. The four symbols which form the corners of these quadrangles have the correct angular relationship appropriate to the corresponding poles, namely, 90° between the (001) and the (010); (110) or (100); 90° between the (010) and (100), and 64° between the (010) and (110). The ideal orientation represented by quadrangle I is defined by definite intensity maxima in the (110), (001), and (100) pole figures; the ideal orientation corresponding to quadrangle II is defined by a definite intensity maximum in all four pole figures. It

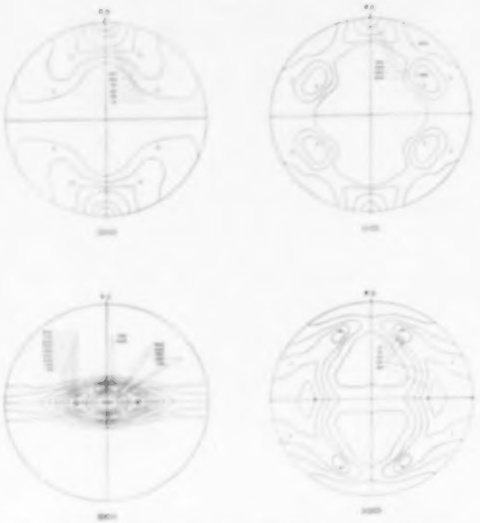

Fig. 2—Quantitative pole figures, with intensity contours, are given for uranium sheet rolled at 300°C to an 87 pct reduction.

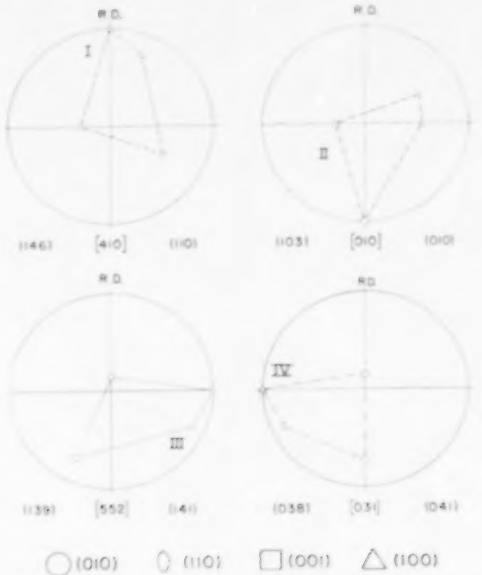


Fig. 3—Pole figures show the "ideal orientations" used to explain the relationship between the intensities found on the (010), (110), (001), and (100) pole figures of the as-rolled sheet.

represents a texture component probably more intense than that given by I. On the other hand, quadrangles III and IV are derived from a maximum in the (001) and a high intensity area of each of the other three pole figures. The ideal orientations III and IV are, accordingly, much less sharply defined than I and II, and they may be considered merely as representatives of an important orientation spread for which the (001) poles are concentrated near the maximum between the rolling plane normal and the rolling direction. Each ideal orientation shown in Fig. 3 is described under each pole figure in terms of 1—plane parallel to the rolling plane, 2—direction parallel to rolling direction, and 3—plane perpendicular to the rolling direction.

In addition to the pole intensity which may be accounted for by ideal orientations as shown in Fig. 3 and Table II, there is a considerable spread of the pole intensity around the highest intensity locations on the various pole figures which may be accounted for by orientations intermediate between the foregoing ideal orientations. These intermediate orientations may be generated, for instance, as follows: quadrangle I may be rotated 64° about the (001) to coincide with II, II may be gradually moved into III with all four poles shifting, and III may be rotated 26° about the (001) to coincide with IV. Orientation II is apparently more intense than I, IV, or III. The latter three seem to be of approximately equal intensity.

*Recrystallization Texture:* The pole figures for the 300°C rolled uranium sheet after recrystallization at 525°C are shown in Fig. 4. The (010) pole figure is very similar to that obtained for the as-rolled sheet; however, the distribution of the (110) and (100) pole intensity has changed considerably from the as-rolled material. The (001) pole figure shows a maximum pole concentration approximately 35° on each side of center toward the transverse direction, which is similar to the pole figure obtained before recrystallization. Although there are high intensity areas also 15° to 20° from the center of the (001) pole figure toward the rolling direction, the maxima observed in these locations, in the as-rolled sheet, disappear upon recrystallization.

In Fig. 4 symbols, similar to those used in Fig. 2, are used to designate high intensity areas in each pole figure. In Fig. 5 several different quadrangles are formed by connecting a symbol from each of the four pole figures. These quadrangles are used to represent ideal orientations which, as in the rolled condition, are described in terms of 1—plane parallel to the rolling plane, 2—direction parallel to rolling, and 3—plane perpendicular to rolling direction.

The location of quadrangle II is identical with quadrangle II shown for the as-rolled sheet. In the case of the recrystallization texture, this orientation is defined by definite intensity maxima in the (010) and (001) pole figures, with corresponding high intensity areas in the other two pole figures. The orientation represented by quadrangle VI has a common (001) location with II and it is defined by maxima in the (001), (110), and (100) pole figures and high intensity areas in the (010). The set of maximum intensity areas defining the orientation V are different from II and VI, except the (010) maximum which is common with II. Orientation V is reminiscent of the "cube" texture in face-centered-cubic metals. The location of the high intensity areas in pole figures which roughly define orientation VII are all different from those previously mentioned. The symbols used for this orientation, which probably represents only an important orientation spread, are formed from dashed lines. The strongest recrystallization texture component is VI, followed by II and V.

The preferred orientation in the recrystallized uranium sheet may be quite satisfactorily described by the four ideal orientations shown in Table III with considerable orientation spreads between 1—II and VI, 2—VII and II, and 3—II and V. The orientation spreads between the ideal orientations may be described in terms of a gradual movement or rotation of the various quadrangles. Thus, quadrangle II may be rotated 26° about the (001) pole

Table II. "Ideal Orientations" for Uranium Sheet 300°C Rolled

| "Ideal Orientation" | Plane Parallel to Rolling Plane | Direction Parallel to Rolling Direction | Plane Perpendicular to Rolling Direction | Multiplicity in Pole Figures |
|---|---|---|---|---|
| I | (4, $\bar{1}$7, 26) near (14$\bar{6}$) | Near [410] | (110) | 4 |
| II | (9, 0, 25) near (103) | [010] | (010) | 2 |
| III | (4, $\bar{1}$4, 45) near (13$\bar{9}$) | Near [$\bar{8}$82] | ($\bar{4}$, 17, 5) near ($\bar{1}$41) | 4 |
| IV | Near (038) | Near [031] | Near (041) | 2 |

Table III. "Ideal Orientations" for Uranium Sheet 300°C Rolled and Recrystallized at 525°C

| "Ideal Orientation" | Plane Parallel to Rolling Plane | Direction Parallel to Rolling Direction | Plane Perpendicular to Rolling Direction | Multiplicity in Pole Figures |
|---|---|---|---|---|
| II | (9, 0, 25) near (103) | [010] | (010) | 2 |
| V | (100) | [010] | (010) | 2 |
| VI | (7, 7, 19) near (113) | [$\bar{1}$10] | ($\bar{5}$, 13, 0) near ($\bar{1}$40) | 4 |
| VII | (2, 2, 15) near (116) | Near [41$\bar{1}$] | Near (883) | 4 |

to generate the spread connecting orientations II and VI. The spread between orientations VII and II may be similarly generated by a rotation and that between orientations II and V may be generated by a rotation around the (010) pole.

From a comparison of the intensities in various locations on the pole figures, it would seem that the relative amounts of the various ideal orientations in recrystallized sheet may be roughly expressed as

$$VI > II \cong VII > V.$$

## Discussion of Results

*Rolling Texture:* A comparison of the results reported for the as-rolled sheet in the present investigation with results recently reported by others is shown in Table IV. Although in some cases the ideal orientations for texture components reported by others do not coincide exactly with those reported here, the deviations are not very large and it is probable that essentially the same components are involved. Component II, or what is essentially equivalent to it, has been found in sheet uranium rolled under varying conditions in all three previous investigations.[2-4] Component I was previously found in two of the three investigations[3, 4] and it was reported[4] to increase in intensity with increasing rolling temperature. Seymour[5] did not find this component in room temperature rolled uranium sheet. On the other hand, Mitchell and Rowland[6] did not find component IV in sheet rolled at either high or low temperature, and Adam and Stephenson[4] did not find it in sheet rolled at 300° to 400°C or at 500° to 600°C, while Seymour[5] reported its presence in room temperature rolled sheet. Since in the present investigations this component, together with component III, accounts for a clearly defined intensity maximum in the (001) pole figure and for high intensity areas in the other pole figures for the 300°C rolled sheet, the deviating results of two of the preceding investigations[3, 4] cannot be ascribed to differences in the rolling temperature. Although admittedly it is probably best to consider "components" III and IV chiefly as representatives of an intense orientation spread hinging around the (001) intensity maximum 17° away from the rolling plane normal, rather than as well defined ideal orientations, the absence of a corresponding (001) maximum in the pole figures of the English and Canadian workers certainly represents a clear-cut and unexplained difference in experimental results.

On the basis of their theory of deformation textures, Calnan and Clews[4] predicted rolling textures for uranium sheet in which the rolling plane normal ranges approximately between (101) and (170) and the rolling direction between the normals of (010) and (110), depending on the relative importance in the deformation process of (130) and (172) twinning and of (010) slip. In comparing these predictions with the experimental results,[3, 4] it appears that

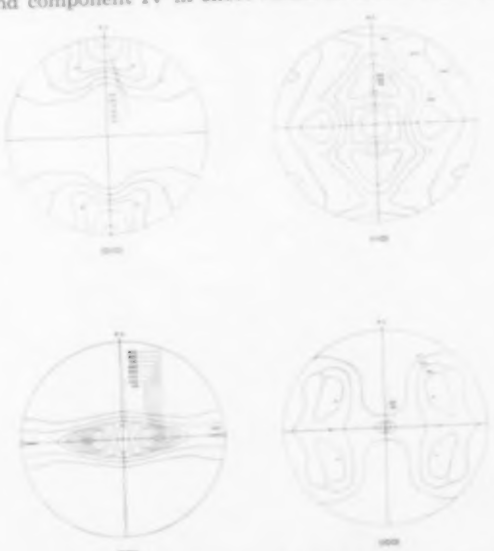

Fig. 4—Pole figures for 300°C rolled uranium sheet (see Fig. 2) are shown after recrystallization at 525°C.

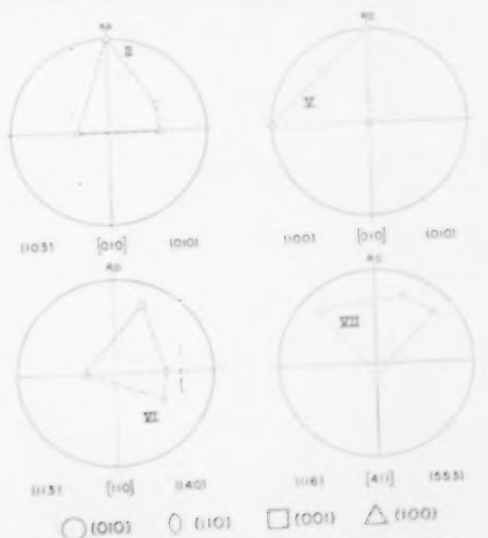


Fig. 5—Pole figures show the "ideal orientations" used to explain the relationship between the intensities found on the (010), (110), (001), and (100) pole figures of the recrystallized sheet.

component II, which has been found at all rolling temperatures, corresponds well to the prediction of Calnan and Clews for the case of deformation by twinning alone, or that of twinning with a small amount of slip. On the other hand, for the case of twinning with a large amount of slip, the prediction calls for an ideal orientation with approximately (170) in the rolling plane and (110) perpendicular to the rolling direction. Component I, which increases in intensity with increasing rolling temperature and which, therefore, might be thought of as connected with a relatively larger amount of slip, does, however, not even approximately correspond to (170) in the rolling plane. It corresponds, instead, to (146) in the rolling plane [58° away from (170)], in disagreement with the theoretical predictions based on the Calnan and Clews theory and known deformation mechanisms. Also, the theory does not account for the important orientation spread represented by III and IV.

In Table IV, the recrystallization texture components observed in the present investigation are compared with those reported by Mitchell and Rowland.[3] According to the latter workers, the single component (II) texture obtained by rolling at low temperature is retained on recrystallization. The Canadian workers reported that the high temperature rolled sheet, which showed a duplex texture (I and II) after rolling, developed essentially a single texture component upon recrystallization. In this recrystallization texture, (151) is approximately perpendicular to the rolling direction. Although this orientation is not exactly equivalent to component VI, as described in the present paper, it is reasonably close to it; for instance, the (140) pole which lies near the rolling direction for component VI is only 13° away from (151). Orientation V, which in the present investigation corresponds to a rather sharply defined component, was apparently not detected by Mitchell and Rowland in any of their specimens. That they did not report orientation VII is less significant, since this orientation merely represents an important spread in the recrystallization texture, and it does not correspond to a well defined maximum in any pole figure.

It is impossible at the present time to interpret the mechanism by which the recrystallization texture forms from the rolling texture. As mentioned, only one of the ideal orientations used to describe

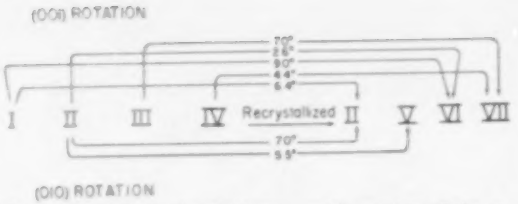


**Fig. 6—Schematic drawing illustrates possible rotations of the as-rolled "ideal orientations" which may produce the recrystallized "ideal orientations."**

the rolling texture is retained on recrystallization. Various rotations about the (001) and (010) poles may be used to describe the relationship between the components of the recrystallization texture and the rolling texture as shown in Fig. 6. The significance, if any, of these rotations in terms of a mechanism is not clear. The present paper is confined to the description of observed facts.

## Acknowledgments

The authors wish to express their appreciation to Robert Macherey and Howard J. Luetzow under whose supervision the material for this study was prepared. Thanks are also due Frank G. Foote and Surain S. Sidhu for their interest and encouragement. This work was performed at Argonne National Laboratory under the auspices of the AEC.

Discussion of this paper, if any, will appear in JOURNAL OF METALS, May 1956, and in AIME Metals Branch *Transactions*, Vol. **206**, 1956.

## References

[1] G. B. Harris: *Philosophical Magazine* (1952) Series 7, **43**, No. 336, p. 113.

[2] W. E. Seymour: *Trans.* AIME (1954) **200**, p. 999; JOURNAL OF METALS (September 1954).

[3] C. M. Mitchell and J. F. Rowland: *Acta Metallurgica* (1954) **2**, p. 559.

[4] J. Adam and J. Stephenson: *Journal* Inst. of Metals (1953-1954) **82**, p. 561.

[5] W. P. Chernock, M. H. Mueller, H. W. Fish, and P. A. Beck: *Review of Scientific Instruments* (1953) **24**, p. 925.

[6] M. H. Mueller and H. W. Knott: *Review of Scientific Instruments* (1954) **25**, p. 1115.

[7] W. P. Chernock and P. A. Beck: *Journal of Applied Physics* (1952) **23**, No. 3, pp. 341-345.

[8] E. A. Calnan and C. J. B. Clews: *Philosophical Magazine* (1952) **43**, p. 93.

**Table IV. Comparison of Results of Various Investigators**

| Components in 300°C Rolled Sheet, Present Investigation | Components Reported by Various Investigators, Under Conditions as Stated | | |
|---|---|---|---|
| | Seymour[2] | Mitchell and Rowland[3] | Adam and Stephenson[4] |
| I | — | High temperature rolled to 60 pct reduction | 1—500° to 600°C rolling to approx. 60 pct reduction<br>2—Greater intensity in material rolled to 80 pct reduction at 500° to 650°C than at 350° to 400°C |
| II | Room temperature rolled to 91 pct reduction | 1—High temperature rolled to 60 pct reduction | 1—Greater intensity in material rolled to 60 pct reduction at 300° to 400°C than at 500° to 600°C |
| | | 2—Low temperature rolled to 60 pct reduction | 2—Greater intensity in material rolled to 80 pct reduction at 350° to 400°C than 500° to 650°C |
| III | — | — | — |
| IV | Room temperature rolled to 91 pct reduction | — | — |
| **Components in Sheet Recrystallized at 525°C, Present Investigation** | | | |
| II | — | Low temperature rolled and recrystallized | — |
| V | — | — | — |
| VI | — | High temperature rolled and recrystallized | — |
| VII | — | — | — |

# Uranium-Chromium System

by A. H. Daane and A. S. Wilson

**The U-Cr system is of the simple eutectic type with some solid solubility of chromium in $\gamma$ and $\beta$ uranium. The eutectic occurs at 20 atomic pct Cr and melts at 859°C. The maximum solubility of chromium in $\gamma$ uranium is 4 atomic pct at the eutectic temperature, and in $\beta$ uranium the solubility is estimated to be 1 atomic pct. $\gamma$-$\beta$ and $\beta$-$\alpha$ transformations were found to occur at 737° and 612°C, respectively.**

DURING 1944 and 1945, the U-Cr constitution diagram was studied in this laboratory as a part of a research program on uranium metallurgy in the Manhattan Project, and the work was described in a Manhattan Project report issued in December 1945. This paper is based on that report, which has been declassified. Prior to this study, it had been shown by other Manhattan Project workers that the low Cr-U alloys could be quenched to retain the $\beta$ form of uranium.

## Experimental

The uranium used in this work was massive metal prepared in this laboratory and contained less than 0.1 pct of other elements. The chromium was 200 mesh powder obtained from the A. D. McKay Co. and was found on analysis to be 99.5 pct Cr with 0.3 pct Fe the major impurity.

Alloys, weighing 400 to 600 g, were prepared by induction heating the components to 1700°C in slip-cast $ZrO_2$ crucibles in a vacuum of $3 \times 10^{-3}$ mm Hg. To prevent too violent agitation of the melt by the induction field with subsequent crucible breakage and sample loss, the $ZrO_2$ crucible was placed in a graphite crucible, which was surrounded by a layer of powdered carbon insulation 2 to 3 cm thick. Polished vertical sections of the alloys were examined microscopically to confirm their homogeneity.

Heating and cooling curves were taken on the alloys by reheating them in $ZrO_2$ crucibles to 1200°C and inserting a mullite-protected chromel-alumel thermocouple into the melt by means of a slip seal in the vacuum head of the furnace. A recording potentiometer traced the curves which had a slope of from 3° to 6° per min.

Samples of the alloys were prepared for metallographic examination by conventional mechanical polishing techniques followed by an electrolytic polish in an ethylene glycol-phosphoric acid-ethyl alcohol bath. The structure of the alloys was brought out clearly by this procedure so that no further etching was required.

Samples for chemical analysis were taken from drillings from the top, center, and bottom sections of the alloys. The uranium was determined by titration with $Ce(SO_4)_2$ while the chromium was titrated with $FeSO_4$; the uranium and chromium totaled at least 99.6 pct in all of the alloys prepared.

A. H. DAANE is Associate Chemist, Ames Laboratory of the AEC, Ames, Iowa, and A. S. WILSON is presently associated with Engineering Dept., Hanford Works, Richland, Wash.

Discussion of this paper, TP 4065E, may be sent, 2 copies, to AIME by Jan. 1, 1956. Manuscript, Feb. 18, 1955.

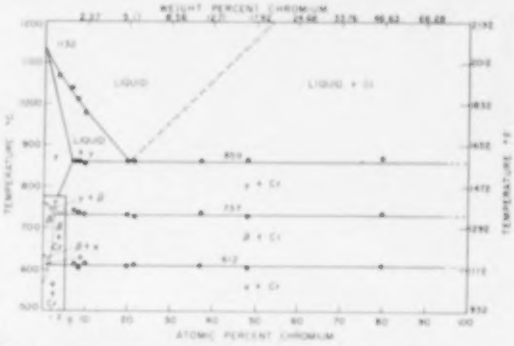

Fig. 1—Data obtained in the study of the U-Cr system was combined to construct the constitution diagram. The arrests observed in cooling curves are indicated by dots.

X-ray samples were prepared by filing bulk specimens in a helium-filled glove box and annealing the resulting powder in a zirconium-gettered helium atmosphere. A 114.6 mm diam Debye-Scherrer camera and a Weyland nonsymmetrical self-focusing camera were used with filtered copper radiation to obtain the powder X-ray diffraction data.

## Results

The data obtained in this study have been combined to construct the constitution diagram of the U-Cr system shown in Fig. 1 where the arrests observed in cooling curves are indicated by dots. The liquidus arrest was quite distinct in thermal data taken on alloys in the range 0 to 20 atomic pct Cr. The eutectic arrest was not observed in studies on the 2.5 and 4.5 pct Cr samples but appeared in the 7.5 pct samples, which suggested some solubility of chromium in $\gamma$ uranium. On quenching from 859°C, the 2.5 pct sample showed but one phase while the 4.5 pct sample contained a small amount of the eutectic along the grain boundaries; see Figs. 2 and 3. From this the maximum solubility of chromium in $\gamma$ uranium has been set at 4 pct. X-ray studies on these samples showed that the $\gamma$ phase was not retained at room temperature by quenching, but in each case a pattern was observed which has been identified with the $\beta$ phase of uranium. Thermal data show the $\gamma$-$\beta$ transformation of uranium lowered to 737°C as a consequence of this solubility. On quenching from the $\beta$ range (660°C), precipitation of chromium in the primary uranium is observed in the 2.5 and 4.5 pct Cr samples (see Figs. 4 and 5),

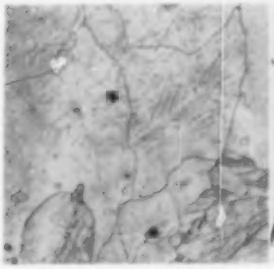

Fig. 2—2.5 atomic pct Cr alloy was quenched from 859°C. X250. Area reduced approximately 35 pct for reproduction.

Fig. 3—4.5 atomic pct Cr alloy was quenched from 859°C. X250. Area reduced approximately 35 pct for reproduction.

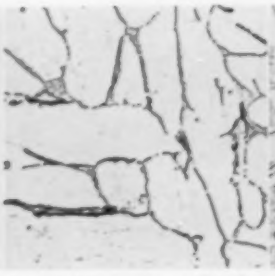

Fig. 4—2.5 atomic pct Cr alloy was quenched from 660°C. X250. Area reduced approximately 35 pct for reproduction.

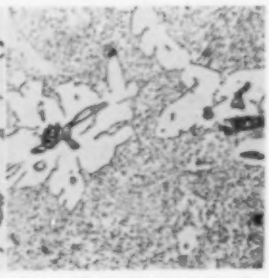

Fig. 5—4.5 atomic pct Cr alloy was quenched from 660°C. X250. Area reduced approximately 35 pct for reproduction.

Fig. 6—2.5 atomic pct Cr alloy was quenched from 500°C. X250. Area reduced approximately 35 pct for reproduction.

Fig. 7—4.5 atomic pct Cr alloy was quenched from 500°C. X250. Area reduced approximately 35 pct for reproduction.

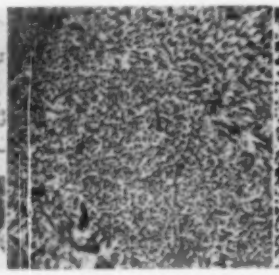

Fig. 8—19.9 atomic pct Cr alloy was furnace-cooled. X250. Area reduced approximately 35 pct for reproduction.

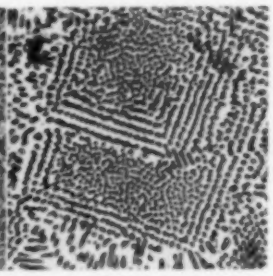

Fig. 9—22.2 atomic pct Cr alloy was furnace-cooled. X250. Area reduced approximately 35 pct for reproduction.

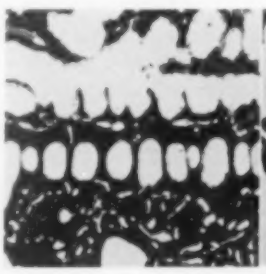

Fig. 10—37.7 atomic pct Cr alloy was furnace-cooled. X250. Area reduced approximately 35 pct for reproduction.

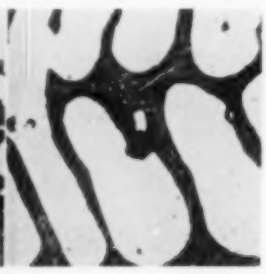

Fig. 11—80 atomic pct Cr alloy was furnace-cooled. X250. Area reduced approximately 35 pct for reproduction.

although the small amount of chromium remaining in solution, estimated to be 1 pct at 660°C, preserves the $\beta$ form of uranium and lowers the $\beta$-$\alpha$ transformation to 612°C. The increased amount of precipitated chromium in these samples on quenching from the high $\alpha$ range suggests that little chromium is soluble in $\alpha$ uranium; see Figs. 6 and 7.

The eutectic composition and temperature were established from thermal data and microstructures of 19.9 and 22.2 atomic pct Cr samples; see Figs. 8 and 9. The eutectic arrest was observed in the thermal data of all of the alloys except the 2.5 and 4.5 pct Cr samples. It is interesting to note that on slow cooling or annealing the typical eutectic structure is quite easily destroyed. In Fig. 5 the clear areas are eutectic uranium with the eutectic chromium agglomerated in the center. This is shown again in Fig. 10 where the large clear areas are the primary chromium with eutectic chromium collected into smaller areas in the uranium matrix. This same agglomeration of the eutectic components has been observed in the U-Th system.

The chromium liquidus was not observed in any of the thermal data taken on chromium-rich alloys and no evidence for a melting point or transformation arrest was found in thermal data taken on a sample of pure chromium heated to 1750°C. X-ray analyses on furnace-cooled 19.9, 50, and 60 atomic pct Cr samples show $\alpha$ uranium and chromium to be present, with the lattice spacing for the chromium being $2.878 \pm 0.02$A. This is the reported lattice spacing of chromium within the limits of error of the determination and suggests no solubility of uranium in chromium at room temperature; since the primary chromium in Fig. 11 shows no precipitation, it is assumed that there is little solubility at higher temperatures.

Since the main interest of this study was in the uranium-rich alloys, no time was spent in investigating the melting point and possible solid modifications of chromium.

## Acknowledgments

Contribution No. 399 from Inst. for Atomic Research and Dept. of Chemistry, Iowa State College. Work performed in the Ames Laboratory of the AEC.

Discussion of this paper, if any, will appear in JOURNAL OF METALS, May 1956, and in AIME Metals Branch Transactions, Vol. **206**, 1956.

# Transformation Kinetics in Uranium-Chromium Alloys

by D. W. White, Jr.

**The kinetics of isothermal transformation of $\beta$-to-$\alpha$ uranium have been studied over a broad temperature range in alloys containing from 0.3 to 4.0 atomic pct Cr. Two modes of transformation are indicated by the existence of two C-curves in the *TTT* diagram. The upper temperature mode is regarded as a nucleation and growth mechanism, whose rate is controlled by diffusion of chromium in the $\beta$ phase matrix. The lower temperature mode is martensitic in nature. The M. temperature increases with decreasing chromium content, suggesting that the two transformation processes become synonymous in unalloyed uranium.**

URANIUM metal undergoes two allotropic transformations in the solid state. The $\alpha$ phase, orthorhombic in crystal structure,[1] is stable from room temperature up to about 665°C. The $\beta$ phase, characterized by a complex tetragonal structure,[2] prevails from 665° to about 770°C. The $\gamma$ phase is body-centered-cubic[3] and is the stable modification from 770°C up to the melting point (about 1130°). In uranium of reasonable purity, neither of the two high temperature phases can be retained by quenching. However, the addition of certain alloying elements to uranium makes it possible to retain either the $\gamma$-uranium phase or the $\beta$-uranium phase at room temperature. Chromium alloyed in small amounts with uranium will permit retention of the $\beta$-uranium phase in a metastable state at room temperature upon quenching from a $\beta$-phase temperature.[4]

From available information[5] on the equilibrium phase diagram for the U-Cr alloy system (Fig. 1), it is to be expected that, however sluggish in its rate, the $\beta$ phase in such alloys should decompose eutectoidally to $\alpha$ phase and elemental chromium. It was the aim of this investigation to measure the rate and study the nature of this decomposition as a function of temperature and of chromium content. The investigation was reported in classified literature about five years ago and has recently been declassified for publication. In the meantime, there have appeared the papers of Holden,[3] Mott and Haines,[6, 7] and Butcher and Rowe[8] dealing with the metallography and the crystallography of the $\beta$-to-$\alpha$ transformation in U-Cr alloys. These investigators have confirmed several of the phenomenological observations that will be described in the present paper and have examined in considerable detail certain aspects of the transformation and its mechanism. Although all of these investigations have concerned themselves experimentally with U-Cr alloys for the most part, an important consequence has been a clearer understanding of the nature of the $\beta$-to-$\alpha$ transformation in uranium metal itself.

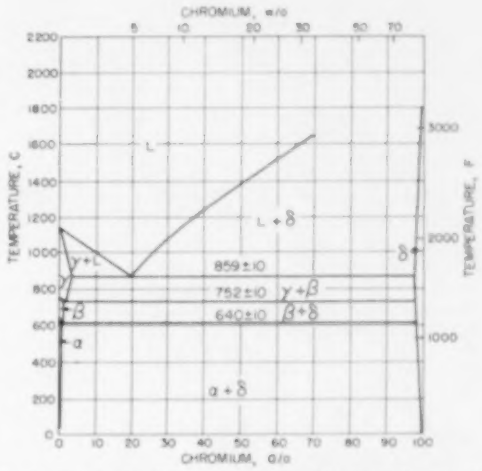


Fig. 1—Constitutional diagram is presented for the U-Cr system.[5]

## Experimental Procedure

This investigation dealt with a series of uranium alloys varying in chromium content from 0.3 to 4.0 atomic pct (0.066 to 0.90 weight pct). On five of the alloys, rates of isothermal transformation from the $\beta$ to the $\alpha$ phase were measured over a wide temperature range, leading to the development of *TTT* (time-temperature-transformation) diagrams. Transformation rates were measured over certain narrow temperature ranges on additional alloys.

The alloys were prepared by vacuum melting and casting, using zircon or magnesia crucibles and graphite molds. Electrolytic chromium was used as the alloying addition, and the uranium was Mallinckrodt biscuit metal that had been vacuum remelted and cropped to remove many of the nonmetallic impurities that had floated to the top of the ingot. The ingots, ¾ or 1 in. diam, were reduced in size by swaging. Alloys containing less than about 2 atomic pct Cr were swaged at 250° to 275°C, with initial and intermediate anneals at 550°C after every 75 pct reduction in area. Alloys with higher amounts of chromium were swaged at 550° to 600°C, although at the smaller sizes some of them were reduced by the procedure used on the more dilute alloys. Before use as test specimens, the swaged rods were annealed at 700° to 720°C for several hours, followed by slow furnace-cooling. The purpose of the anneal was to achieve the maximum amount of solution of the available chromium into the $\beta$ phase, as well as to remove extensive preferred orientation.

The isothermal transformation rates were measured dilatometrically, using a quenching dilatometer and an experimental technique similar to those employed by Davenport and Bain in their original work on the transformation kinetics of austenite in

D. W. WHITE, JR., Member AIME, is Supervisor, Materials & Processes, Knolls Atomic Power Laboratory, General Electric Co., Schenectady.

Discussion of this paper, TP 4107E, may be sent, 2 copies, to AIME by Jan. 1, 1956. Manuscript, Feb. 11, 1955. Chicago Meeting, February 1955.





tion. Actually, there was one exception to this pro-

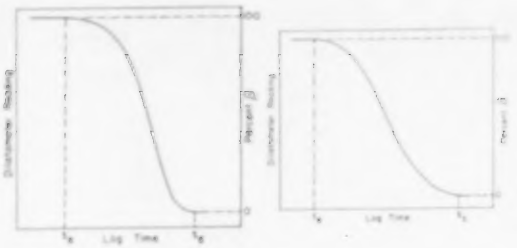

a—Type 1 rate curve is characterized by a large radius of curvature near the beginning of transformation and a smaller radius near the end of transformation.

b—Type 2 rate curve is characterized by more or less equal radii of curvature near the beginning and end of transformation.

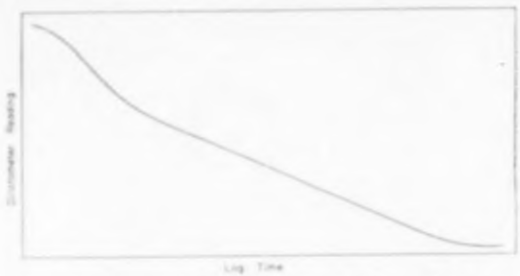

c—Type 3 rate curve shows the normal portion (type 2) followed by the linear portion, after which it flattens out when there is no further contraction.

Fig. 2—Three types of isothermal rate curves were found for U-Cr alloys.

ferrous alloys.[4] Since uranium undergoes a density increase of approximately 1 pct in transforming from the $\beta$ phase to the $\alpha$ phase, the corresponding linear contraction of about 0.3 pct for total transformation was a physical property convenient to measure in following the progress of transformation.

The procedure consisted of heating the specimen, a rod 4 in. in length by ¼ in. diam, in a bath maintained at a $\beta$-phase temperature of 700° to 725°C for 5 min (longer times were found to be unnecessary), then transferring quickly to the dilatometer in a bath maintained at some desired lower temperature and holding there until the specimen appeared to be fully transformed to $\alpha$ phase, i.e., until it ceased contracting. Dial readings were taken at suitable time intervals to permit plotting a smooth continuous curve. In general, molten Sn-Pb eutectic was used for the heating baths at temperatures down to 183°C, the freezing point of the bath, while water was used for isothermal transformation at 100°C and at room temperature. In a few cases salt baths, generally carbonates, were employed. A thin coating of silicone grease was applied to the surface of a specimen before each test to protect it against attack by the Sn-Pb solder. For any given alloy the same specimen was used over and over again for a large number of tests. It was observed that the specimen usually underwent a net increase in length of several hundredths of one percent with each test. After several runs had been made, a longitudinal void or crack tended to develop in the core of the specimen, starting at the ends, which simultaneously became mushroomed. The specimen was then usually replaced with a fresh one.

Metallographic methods were found to be rather

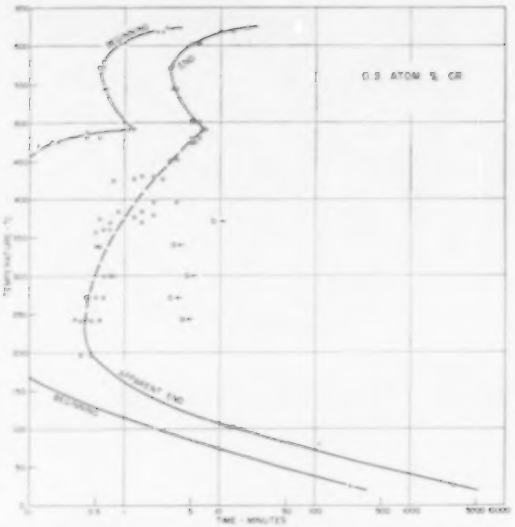


Fig. 3—*TTT* diagram for 0.3 atomic pct Cr-U alloy is shown.

unsuitable for quantitative measurement of the transformation rates in U-Cr alloys for several reasons: Firstly, it was found that mechanical polishing itself causes the surface of a specimen to transform. Therefore, the investigator would have to resort to the rather inconvenient procedure of preparing the polished surface prior to heat treatment of a specimen and then electrolytically polishing to clean up the surface after heat treatment. Secondly, the $\alpha$-uranium phase is not very easily distinguishable from polycrystalline $\beta$-uranium phase except when present in small amounts. Thirdly, the rate of transformation in alloys having very low chromium content may be so rapid at room temperature that there is not enough time to prepare and examine the specimen before further transformation occurs.

## Results

Isothermal transformation rate curves were obtained by plotting the series of dilatometer readings in each test against logarithm of time. By assuming that the ratio between the contraction at a given time and the total contraction equals the fraction transformed, the rate curves were more significantly plotted as percentage of $\beta$ phase (percentage untransformed) against logarithm of time.

Three types of rate curves were found. For convenience they are referred to as type 1, type 2, and type 3, and they are illustrated in Figs. 2a, 2b, and 2c, respectively. The times for beginning and end of transformation are designated respectively as $t_s$ and $t_e$. In a few cases transformation was not complete when the specimen ceased contracting, as will be discussed later; in such cases, $t_e$ refers to an *apparent end* rather than a true end of transformation. Attempts were made to determine empirical relationships for the type 1 and type 2 curves; the resulting relationships are presented in a following section of the paper.

*TTT* diagrams were obtained by plotting temperature of isothermal transformation against log $t_s$ and against log $t_e$.

*TTT Diagrams:* Figs. 3 through 7 give the *TTT* diagrams for five U-Cr alloys. The crosses on these curves represent beginning of transformation, $t_s$, while the open circles or squares represent the end

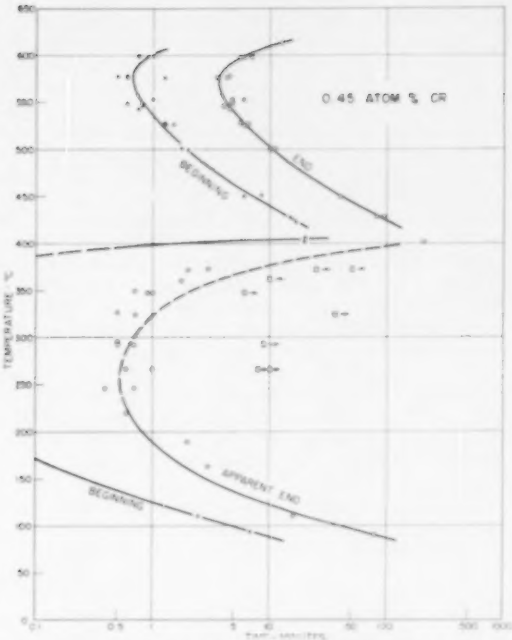


Fig. 4—*TTT* diagram for 0.45 atomic pct Cr-U alloy is shown.

or *apparent end* of transformation, $t_p$. (The distinction between the circles and squares will be described later.) The *TTT* diagrams for the 1.8 and 4.0 pct alloys are seen to be single C-shaped curves within the range of temperatures studied, while the diagrams for the 0.3, 0.45, and 0.6 pct alloys display double C's.

It was mentioned previously that the transformation tests were performed by quenching directly to the temperature selected for isothermal transformation. Actually, there was one exception to this procedure: The transformation of the 0.3 pct alloy at 100°C had to be performed by quenching in cold water and then reheating in boiling water. Apparently a quench directly into boiling water is not sufficiently drastic to prevent some transformation at the lower *nose* of the *TTT* curve. Similarly, this alloy could not be reheated to temperatures above the lower nose without transforming at the nose; and, therefore, direct quenching was the only procedure that could be used at such temperatures. However, both procedures, i.e., direct quenching and cold water quenching and reheating, were tried on the 0.6 pct alloy at 100° and at 200°C and found to give equivalent results.

*Rate Curve Types and Their Relation to the TTT Diagrams:* Different portions of the *TTT* diagrams are represented by each of the three types of rate curves. The primary purpose in fitting the type 1 and type 2 curves to mathematical equations or graphs was to facilitate identifying them, since the difference between these two curves as plotted in Figs. 2a and 2b is not immediately apparent. Knowing the distinction between them was helpful in deciding how to draw the *TTT* curves, especially in the region of transition between the two C's.

**Type 1**—Rate curves of type 1 were found for the transformations occurring in the upper C's of the *TTT* diagrams for the 0.3, 0.45, and 0.6 pct alloys and in the entire single-*C TTT* diagram for each of the 1.8 and 4.0 pct alloys. Type 1 curves were also observed for transformations at temperatures well below the nose of the lower C. In the temperature range in which the transformation rate was so rapid that only the end or apparent end of transformation was detectable, it was not possible to tell whether a rate curve was of type 1 or of type 2.

A type 1 rate curve as plotted in Fig. 2a is characterized by a large radius of curvature near the beginning of transformation and a smaller radius

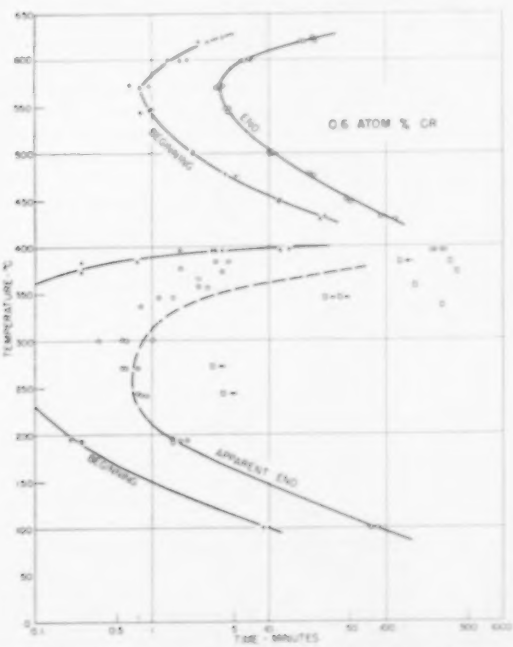


Fig. 5—*TTT* diagram for 0.6 atomic pct Cr-U alloy is shown.

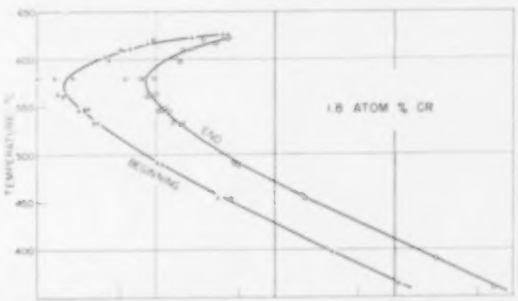


Fig. 6—*TTT* diagram for 1.8 atomic pct Cr-U alloy is shown.

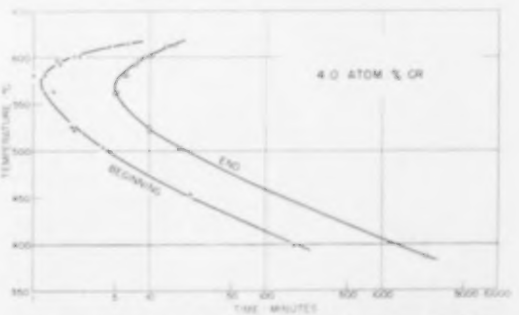


Fig. 7—*TTT* diagram for 4.0 atomic pct Cr-U alloy is shown.

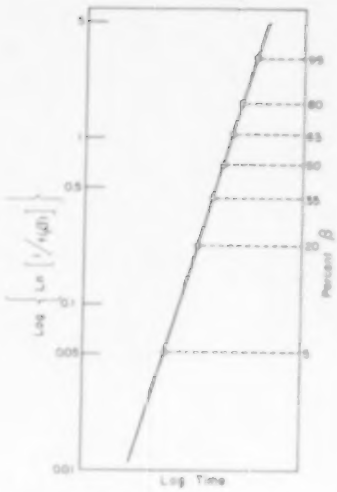


Fig. 8—Type 1 rate curve was replotted to give a straight line in accordance with Eq. 2.

near the end of transformation. It can be fitted by the exponential equation

$$f(\beta) = e^{-kt^m} \qquad [1]$$

where $f(\beta)$ refers to the fraction of $\beta$ phase (fraction untransformed) at time $t$, and $k$ and $m$ are constants at the given temperature of isothermal transformation. Taking logarithms twice, this relation becomes

$$\log \ln 1/f(\beta) = \log k + m \log t. \qquad [2]$$

Therefore, when the quantity on the left side of Eq. 2 is plotted against *log t*, a straight line is obtained, as shown in Fig. 8. These relations (Eqs. 1 and 2) allude to a similar expression by Johnson[9] for the rate of transformation of austenite to pearlite, based on the assumption that the rate of nucleation is proportional to $t^{(m-4)}$.

The type 1 rate curve can also be plotted in a way that is used to represent the velocity of an autocatalytic reaction. If the percentage either of transformed $\alpha$ or of untransformed $\beta$ phase is plotted on an autocatalytic scale, or on a probability scale, against time on an arithmetic scale, a reasonably good straight line is obtained. Fig. 9 is such a plot.

**Type 2**—Rate curves of type 2 were observed at the temperature of transition between the upper and lower C's for each of the 0.3, 0.45, and 0.6 pct alloys and down to temperatures as low as 396°C. The type 2 rate curve as plotted in Fig. 2b is characterized by more or less equal radii of curvature near the beginning and end of transformation. When replotted in either of the two fashions described previously for replotting a type 1 rate curve, a type 2 rate curve does not give a straight line. However, linearity is obtained when the percentage of $\beta$ phase is plotted on a probability scale against logarithm of time, as demonstrated in Fig. 10. Austin and Rickett found empirically that this method of plotting also applies to the rate of isothermal transformation of austenite to bainite.[11]

**Type 3**—As is seen in Fig. 2c, the first portion of a type 3 rate curve appears to be similar to type 2; but then, after a certain amount of transformation, it changes its course and proceeds linearly with log *t* until it finally flattens out when there is no further contraction. Type 3 rate curves vary in form, in that the type 2, or *normal*, portion may occupy a greater or lesser portion of the full curve and the linear portion may become flatter or steeper, respectively. Such variations depend upon composition and upon the temperature of isothermal transformation. There is no doubt that the linear portion is truly a part of the transformation rate curve because X-ray diffraction examination has shown that transformation is incomplete at the end of the normal portion and continues to proceed in the linear region.

Type 3 rate curves were most apparent in the 0.6 pct alloy, somewhat less apparent in the 0.45 pct alloy, and noticeable only to a slight extent in the 0.3 pct alloy. The highest temperature at which this type of curve was observed was 384°C. With decreasing temperature, the normal portion became increasingly more prominent and the linear portion correspondingly flatter and less prominent. For example, in the 0.6 pct alloy the linear portion of the rate curve accounted for 50 pct of the total contraction of the specimen during transformation at 373°C but only 20 pct of the total contraction during transformation at 358°C. Type 3 rate curves were still somewhat distinguishable down to about 325°C, but below this temperature the linear portion had such a small slope, if any, that it was debatable whether to regard the curve as type 3.

In the temperature range where type 3 rate curves or their semblance prevailed, the ends of the normal portions of the curves are denoted by open circles and the ends of the linear portions by open squares on the *TTT* diagrams. In several instances the test was stopped before the specimen had ceased contracting; in such cases, the last reading was plotted with an open square and an arrow pointing to the right. In the type 3 temperature range, the curves for apparent end of transformation are shown on the *TTT* diagrams as broken lines and correspond to at least 85 pct completion of total contraction.

## Observations and Discussion

The existence of two C's in the *TTT* diagrams for the lower chromium alloys and the difference in type of rate curves associated with each *C* indicate that there are two transformation modes, one at upper temperatures and another at lower temperatures. It is suggested that the upper temperature mechanism for the decomposition of the $\beta$ phase in U-Cr alloys is one that is controlled by the rate of diffusion of chromium in $\beta$-uranium, while the lower temperature mechanism is believed to be diffusionless. Competition between driving force and

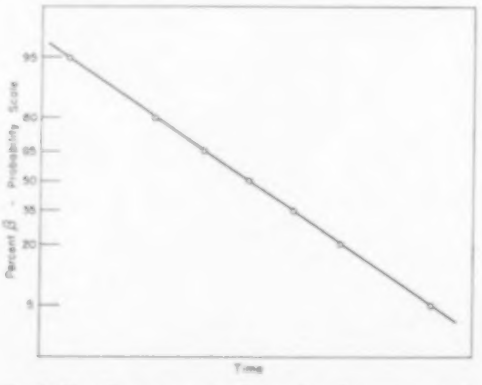


Fig. 9—Type 1 rate curve is shown after the percentage of transformation was replotted on a probability scale against time.

atomic mobility determines the rate of transformation in the upper C. As the temperature is lowered, a point is reached where the driving force, which is a function of the amount of undercooling, is sufficiently great to overcome the decreasing mobility of chromium atoms in the uranium lattice. The transformation can then proceed at the rapid rates characteristic of the lower C, except at very low temperatures, where the mobility of atoms even over very small distances may become sufficiently sluggish to influence the rate of transformation. The observations supporting the belief that the lower C process is diffusionless will be pointed out later.

The transformation product by either mechanism was shown by cursory X-ray diffraction examination to be $\alpha$ uranium. More detailed X-ray measurements would have to be made to determine if there are differences in orientation relationships or minor structural differences.

*Upper C as a Diffusion-Controlled Transformation:* By plotting the natural logarithm of the time for 50 pct transformation ($t_{50}$) against the reciprocal of the absolute temperature within the upper C for each of the five alloys, a straight line is obtained in the temperature range below about 530°C. Thus, in this range the following relation holds

$$\ln t_{50} = b/T + K' \qquad [3]$$

or

$$1/t_{50} = K\, e^{-b/T} \qquad [4]$$

where $b$, $K'$, and $K$ are constants and $T$ is temperature in °K. It may be speculated that above 530°C the driving force is changing rapidly with temperature so that this change seriously influences the rate of transformation. However, below 530°C the driving force changes relatively slowly with temperature so that the change in rate can be associated primarily with a change in atomic mobility. Thus, in the temperature range below 530°C, it can be assumed that the constant $b$ in Eq. 3 is approximately equal to $Q/R$, where $Q$ is an activation energy and $R$ is the gas constant. From the slope of the plot below 530°C, the value for $Q$ is computed to be about 34,000 cal per gram-atom.

Referring to Eq. 1, the exponent $m$ has a relatively constant value of about four below 530°C, implying from Johnson's assumption[9] that nucleation rate is essentially independent of time in this temperature range. Above 530°C, $m$ increases with temperature and at 580°C it has reached approximately five in value. The relative constancy of $m$ below 530°C means that Eqs. 3 and 4 hold for $t$ at any given amount of transformation and also that the rate curves for all temperatures in this range can be superimposed on a common curve by multiplying all time values in any one curve by a certain number. The multiplying factor is related to temperature as follows

$$\ln t_1/t_2 = Q/R\,(1/T_1 - 1/T_2) \qquad [5]$$

where $t_1$ and $t_2$ are the heating times at absolute temperatures $T_1$ and $T_2$ for a certain percentage of transformation. Thus, the value for $Q$ of 34,000 cal per gram-atom is constant for all percentages of transformation as well as for all compositions between 0.3 and 4.0 atomic pct Cr in the temperature range below 530°C in the upper C. To test the hypothesis that transformation in the upper C is indeed governed by the rate of diffusion of chromium in $\beta$ uranium, it would be of interest to make actual measurements of such diffusion rates at various temperatures and to compare the activation energy

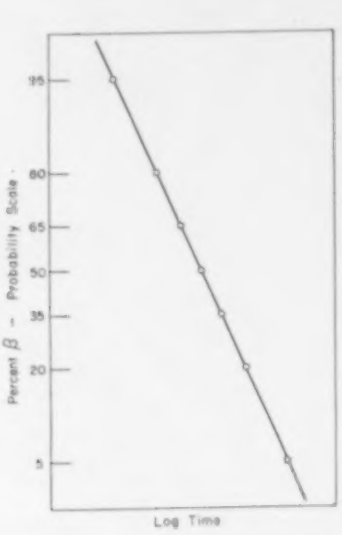


Fig. 10—Type 2 rate curve is linear when the percentage of $\beta$ phase is plotted on a probability scale against log $t$, according to the Austin-Rickett manner.[15]

obtained therefrom with the foregoing value for $Q$.

*Lower C as a Martensitic Transformation:* Several observations suggest that the lower temperature mode of $\beta$-to-$\alpha$ transformation in U-Cr alloys is martensitic. Although the transformation rate is much slower than that of most martensitic transformations, it is far too rapid to be controlled by the diffusion of the chromium at the prevailing temperatures; and therefore composition change does not appear to be involved. Another observation often characteristic of martensitic behavior is that the transformation can be nucleated by applied stresses, as evidenced by the immediate reversion of a surface layer of retained $\beta$ phase to $\alpha$ upon mechanical polishing. A third feature of the transformation is that it takes place athermally to a limited extent. Samples of the 0.3 and 0.6 pct alloys were quenched from about 715° to 300°C and held at the latter temperature until contraction had essentially ceased. They were then quenched into boiling water, wherein it was observed that further contraction took place isothermally. The amount of this contraction in comparison with that which normally occurs by transformation entirely at 100°C was 6 pct for the 0.3 pct alloy and 12 pct for the 0.6 pct alloy. The times for beginning and end of specimen contraction in the boiling water corresponded very closely with those that are observed when specimens are transformed entirely at 100°C. The evidence that transformation in the lower C is not actually complete when contraction ceases (at least at 300°C) led to the term *apparent end* of transformation, referred to earlier in the paper.

Further evidence that the lower C represents a martensitic reaction is derived from the work of Holden[5] and of Mott and Haines,[6,7] who studied metallographically the progress of $\beta$-to-$\alpha$ transformation in U-Cr alloys at temperatures corresponding to the lower C. They observed that the $\alpha$ phase formed and grew as plates, creating surface upheavals, and that these plates seemed to prefer only certain habit planes in the parent $\beta$-phase crystals. Scratches in the surface of a specimen were sheared by the transformation, indicating that the $\alpha$ plates were formed by the cooperative movement of atoms. These investigators also found some evidence for burstlike growth of the plates. The burst phenomenon may account for the steps in the

portion of the transformation rate curve illustrated in Fig. 11; this curve represents the transformation of the author's 0.45 pct Cr-U alloy at 361°C and was obtained by W. E. Seymour and J. F. Duffey, who used a sensitive, specially designed instrument employing electrical resistance as the means for measuring reaction kinetics.

Holden also studied the crystallography of the transformation and has identified the habit plane for the transformation with the {321} type $\beta$ plane, a rather unimportant plane in the tetragonal $\beta$-uranium crystal. As Holden pointed out, crystallographically unimportant habit planes are characteristic of martensite. Butcher and Rowe[5] have suggested that the {441} $\beta$ plane as well as {321} may be another habit plane for the transformation.

The association of type 3 rate curves with transformation in the lower *C* and principally at temperatures above 350°C suggests the simultaneous occurrence of transformation and of annealing of transformation stresses. It is plausible to speculate that transformation starts in a normal fashion (i.e., as in type 2 curve) and in accordance with a certain rate pattern. However, transformation stresses build up to a point where transformation would stop unless the stresses were relieved. This point is represented by the onset of the linear portion of the type 3 rate curve. In a temperature range that is favorable for stress relaxation, a steady state between transformation and annealing of transformation stresses then prevails until transformation is nearer completion. Above the temperature range in which a type 3 rate curve is observed, transformation stresses are relieved as rapidly as they are formed, and transformation can proceed without their opposition. At temperatures below the type 3 range, the driving force is so great that transformation can go essentially to completion before the transformation stresses offer effective back pressure.

The fact that the linear portion of the type 3 curve becomes flatter and less prominent with decreasing temperature is consistent with the suggestion of its association with stress relaxation. The relief of stresses[15] may occur by slip in the $\alpha$ phase[16] (and perhaps in the $\beta$ phase) and by grain boundary flow,[16] which occur readily above 350°C. At lower temperatures, the $\alpha$ phase can deform only by twinning[16] and the $\beta$ phase only by slip on {110} type planes in the <001> direction;[16] Holden[7] and Mott and Haines[8,9] attribute the slow transformation rates in U-Cr alloys at low temperatures to these deformation limitations.

*Effect of Chromium on Equilibrium Transformation Temperature for Uranium:* Chromium lowers the $\beta$-to-$\alpha$ equilibrium transformation temperature in uranium. From inspection of the *TTT* diagrams, this temperature appears to be about 630°C for all five alloys.

In measuring the rates of isothermal transformation it was observed that, at temperatures around 590°C and higher, the total contraction of the dilatometer specimen seemed increasingly too small to account for transformation from all $\beta$ to all $\alpha$. Therefore, it was wondered whether the eutectoid temperature might not be in the neighborhood of 590°C. However, the fact that the temperature assymptote of the upper *C* appears relatively constant for all compositions leads to the tentative conclusion that 630°C is the eutectoid temperature rather than a temperature above which an alloy is entirely in the $\beta$ phase. The peculiarity in specimen contraction above 590°C is unexplained; it may be associated with grain coarsening, which becomes very pronounced in this temperature range.

*Influence of Chromium Content on M, Temperature:* It is apparent from inspection of the *TTT* diagrams that the *M*, temperature, or temperature of transition between the upper and lower *C's*, is depressed with increasing chromium content. Since it was not possible to obtain a very good quantitative relationship solely from the data from the few *TTT* diagrams, special thermal analysis experiments were performed for a variety of alloy compositions. The specimen and attached thermocouple were quenched from 720° to 500°C, which is above the *M*, temperature for all compositions, and then cooled at a somewhat slower rate, during which time the temperature was continuously recorded. Two different ranges of cooling rates were employed: 56° to 120° and 209° to 292°C per min.

The thermal arrests, which were not particularly pronounced, are plotted in Fig. 12, and it is seen that,

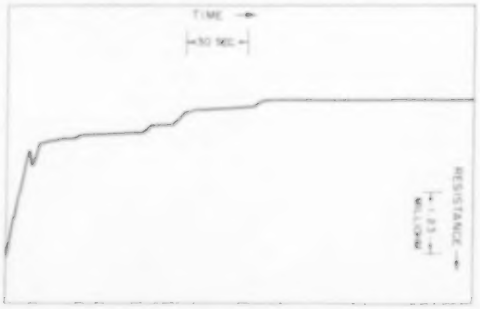


Fig. 11—Portion of a rate curve for isothermal transformation of 0.45 pct alloy at 361°C is shown. The curve plots the resistance of a 30 mil wire, 2 in. in length, as a function of time. The discontinuities may represent martensitic "bursts."

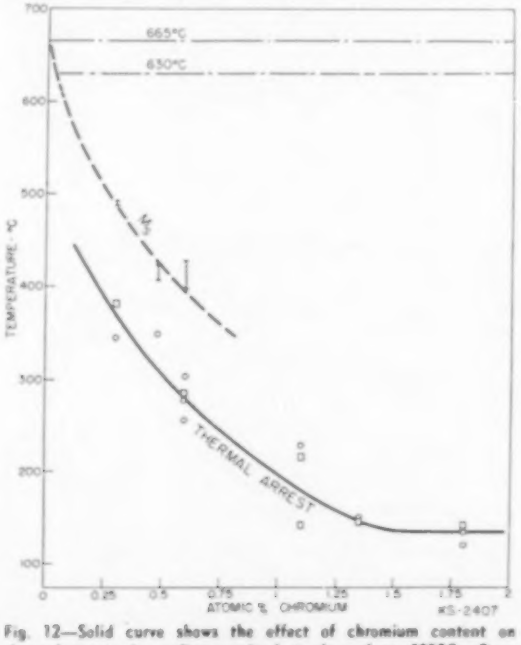


Fig. 12—Solid curve shows the effect of chromium content on thermal arrests in cooling retained $\beta$ phase from 500°C. Open squares represent cooling rate of 56° to 120°C per min and open circles represent 209° to 292°C per min. Probable variation of *M*, temperature with chromium content is shown with the dashed line.

for alloys containing less than about 1.5 atomic pct Cr, the temperature of thermal arrest decreases with increasing chromium content. It will be noted, however, that the thermal arrest temperature is not the $M_s$ temperature but rather some lower temperature at which transformation occurs at a relatively rapid rate. The variation of $M_s$ temperature itself with composition is shown in Fig. 12 by the dashed line drawn through $M_s$ temperature points obtained from the *TTT* diagrams and displaced from the curve for thermal arrest temperature by a constant temperature difference. This curve for $M_s$ temperature vs chromium content cannot be regarded as quantitatively accurate because it is not necessary that the displacement from the curve for thermal arrest temperature be constant. However, it is probably nearly constant, since the thermal arrest temperatures were similar for the different cooling rates.

An important consequence of the effect of composition on $M_s$ temperature is that qualitative extrapolation to 0 or nearly 0 pct Cr suggests that the upper *C* vanishes and that the two modes of transformation become synonymous in unalloyed uranium. Since chromium is absent, diffusion of chromium is, of course, no longer a rate-controlling factor as it is in the transformation of the alloys by the upper *C* process. Microstructural similarities would lead to the association of the $\beta$-to-$\alpha$ phase transformation process in uranium metal with that of the lower *C* in U-Cr alloys. Uranium that has been water quenched from a $\beta$-phase temperature and U-Cr alloys that have been transformed in the lower *C* both exhibit similar transformed $\alpha$ microstructures under polarized light. These structures have a serrated appearance, characterized by extremely irregular grain boundaries and grain sizes, fragmentation, twinning, and subgraining. Alloys transformed by the upper *C* process, on the other hand, are relatively devoid of these features and, rather, are feathery in appearance.

If a *TTT* diagram for pure uranium consisting entirely of a single *C* (lower *C* type) is imagined, the rates of isothermal transformation should be of measurable magnitude at very low temperatures and also at high temperatures approaching the equilibrium transformation temperature. The author's attempts to verify this prediction have been unsuccessful at low temperatures, probably because it is difficult to quench a specimen sufficiently rapidly to prevent transformation at the nose of the *C*-curve. However, retarded transformation was observed in commercial uranium metal at high temperatures; the uranium specimen was found to transform entirely to the $\alpha$ phase in 1 min at 650°C, in 2½ min at 653°C, and in 4 min at 654°C.

A further observation from Fig. 12 is that the solubility limit of chromium in $\beta$ uranium at around 720°C appears to be about 1.5 atomic pct, agreeing with the value cited by Mott and Haines.[5] By extrapolation of the dashed line, the $M_s$ temperature at this composition would appear to be about 250°C.

*Effect of Alloy Composition on Transformation Rate:* The rates of transformation to $\alpha$ uranium are lowered, both in the upper and lower *C*'s, with increasing amounts of chromium dissolved in the $\beta$ phase. In Fig. 13 are plotted the times for beginning and end of isothermal transformation at 550°C (in upper *C*) vs composition for a number of alloys in addition to those for which full *TTT* diagrams were obtained. The time required for transformation increases with chromium content up to about 1.7

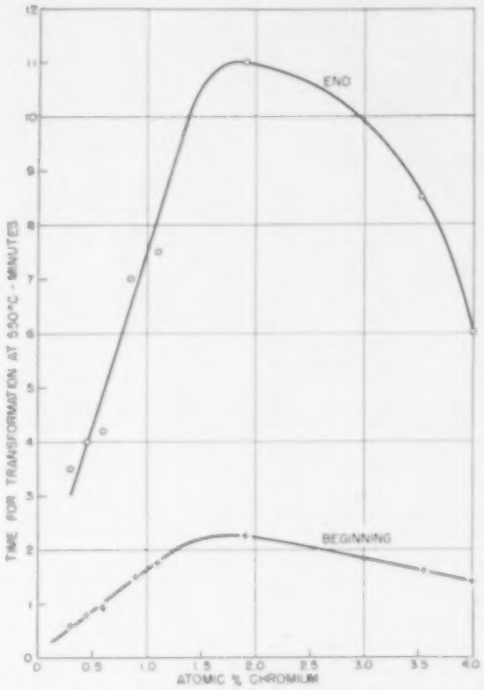


**Fig. 13—Curves show the effect of chromium content on the rate of isothermal transformation at 550°C.**

atomic pct, which is in general agreement with the value obtained in Fig. 12 for maximum solubility of chromium in $\beta$ uranium. With alloys of higher chromium content, however, transformation times actually become shorter. Presumably the second phase particles of undissolved chromium provide additional nucleation sites, thereby hastening the nucleation of $\alpha$ phase.

It is not known what effect excess chromium has upon the transformation rates in the lower *C* because rate measurements were not made in that region of the *TTT* diagram for the higher chromium alloys.

*Temperatures for Maximum Transformation Rates:* The nose, or temperature of maximum transformation rate, of the upper *C* is at about 575°C, irrespective of composition. The nose of the lower *C* appears to be in the general vicinity of 250°C. The maximum rate of transformation by the lower *C* mode is considerably greater than that by the upper *C* mode.

## Conclusions

1—U-Cr alloys can be transformed isothermally from the $\beta$-uranium phase to the $\alpha$-uranium phase by either of two modes. The higher temperature mode appears to be diffusion-controlled, while the lower temperature mode is martensitic and is the more rapid process.

2—Although the martensitic transformation occurs isothermally for the most part, there is evidence that it takes place athermally to a certain extent.

3—At temperatures above 325° to 350°C, transformation by the martensitic process appears to be aided by relief of transformation stresses.

4—The $M_s$ temperature decreases with increasing amounts of chromium in solution in the $\beta$ phase.

5—The two modes of transformation in U-Cr al-

loys become synonymous in the $\beta$-to-$\alpha$ transformation in unalloyed uranium. Microstructural observations suggest that the latter is associated with the lower $C$ martensitic process.

6—Transformation rate is decreased with increasing amounts of chromium in solution in the $\beta$ phase. Undissolved second phase chromium tends to hasten the transformation.

7—The maximum rate of transformation is at 575°C by the upper temperature mode and in the neighborhood of 250°C by the lower temperature mode, irrespective of alloy composition.

8—Applied stress induces transformation of the metastable $\beta$ phase to the $\alpha$ phase in U-Cr alloys.

9—Chromium dissolved in $\beta$-uranium lowers the $\beta$-to-$\alpha$ equilibrium transformation temperature from 665° to about 630°C.

10—The maximum solubility of chromium in $\beta$-uranium at temperatures of 700° to 725°C is 1.5 to 1.7 atomic pct.

11—The rates of transformation below 530°C by the upper temperature process fit an Arrhenius equation, giving a value for the energy term of 34,000 cal per gram-atom. It is suggested that this value may represent the activation energy for diffusion of chromium in $\beta$-uranium.


### Acknowledgments

Assistance in performing the experiments was provided by C. S. Barker, L. S. DeLuca, and J. F. Duffey. Discussions of the results with J. E. Burke and A. N. Holden were very helpful. The AEC is to be acknowledged for sponsoring this investigation under Contract No. W-31-109 Eng-52 and for permission to publish it.

Discussion of this paper, if any, will appear in JOURNAL OF METALS, May 1956, and in AIME Metals Branch *Transactions*, Vol. **206**, 1956.


### References


[1] C. W. Jacob and B. E. Warren: The Crystalline Structure of Uranium. *Journal* Amer. Chemical Soc. (1937) **59**, p. 2588.

[2] C. W. Tucker, Jr.; The Crystal Structure of the Beta Phase of Uranium. *Acta Crystallographica* (1951) **4**, p. 425.

[3] A. S. Wilson and R. E. Rundle: The Structures of Uranium Metals. *Acta Crystallographica* (1949) **2**, p. 126.

[4] H. A. Saller and F. A. Rough: Compilation of U. S. and U. K. Uranium and Thorium Constitutional Diagrams. *Unclassified AEC Report BMI-1000* (June 1, 1955) p. 22.

[5] A. N. Holden: The Isothermal Transformation of Metastable Beta-Uranium Single Crystals. *Acta Metallurgica* (1953) **1**, p. 617.

[6] B. W. Mott and H. R. Haines: A Metallographic Study of the Transformation of Beta to Alpha Uranium in Two Stabilized Alloys. *AERE Report M/R 1211* (1953).

[7] B. W. Mott and H. R. Haines: Étude métallographie de la transformation $\beta \rightarrow \alpha$ de l'uranium dans les alliages stabilises uranium-chrome. *Revue de Métallurgie* (1954) **60**, No. 9.

[8] B. R. Butcher and A. H. Rowe: Phase Transformation in Uranium. *Nature* (1953) **172**, p. 817.

[9] E. S. Davenport and E. C. Bain: Transformation of Austenite at Constant Subcritical Temperatures. *Trans.* AIME (1930) **90**, p. 117.

[10] W. A. Johnson: Discussion of paper by F. C. Hull, R. A. Colton, and R. F. Mehl: Rate of Nucleation and Rate of Growth of Pearlite. *Trans.* AIME (1942) **150**, p. 208; METALS TECHNOLOGY (August 1942).

[11] J. B. Austin and R. L. Rickett: Kinetics of the Decomposition of Austenite at Constant Temperature. *Trans.* AIME (1939) **135**, p. 396; METALS TECHNOLOGY (September 1938).

[12] C. W. Tucker, Jr.: Unpublished work at Knolls Atomic Power Laboratory, General Electric Co. X-ray diffraction lines of cold-worked uranium were found to sharpen with annealing temperatures of 350° to 400°C.

[13] R. W. Cahn: Plastic Deformation of Alpha-Uranium; Twinning and Slip. *Acta Metallurgica* (1953) **1**, p. 49.

[14] M. B. Reynolds: Unpublished work at Knolls Atomic Power Laboratory, General Electric Co. Damping measurements suggested grain boundary flow in uranium at a significant rate at 370°C.

[15] A. N. Holden: Growth and Crystallography of Deformation of $\beta$-Uranium Single Crystals. *Acta Crystallographica* (1952) **5**, p. 182.


---

Technical Note

# Compositional Changes of the Alpha Phase in a Eutectoid Cu-Al Alloy During Isothermal Transformation


by Daniel F. Toner, Paul E. Gage, and David J. Mack


MUCH work has been done on the decomposition of the $\beta$ phase at the eutectoid composition, 11.9 pct Al, in the Cu-Al system by Smith and Lindlief,[1] Mack,[2] Klier and Grymko,[3] Haynes,[4] and others. In all of the mechanisms proposed by these workers for the decomposition of the $\beta$ phase, it was stated that the $\alpha$ phase must precipitate rich in aluminum with respect to the equilibrium composition of 9.4 pct Al at 565°C.

To check this hypothesis, it was necessary to have a master curve relating equilibrium aluminum content of $\alpha$ to lattice parameters of $\alpha$. A number of binary Cu-Al alloys of increasing amounts of aluminum were prepared by Ampco Metal Inc. These alloys, received as-cast, were given a 30 pct reduction of area by hot-working and then annealed at 900°C for homogenization and slowly cooled in the


D. F. TONER, Student Member AIME, is Graduate Student, Dept. of Mining & Metallurgy, University of Wisconsin, P. E. GAGE, formerly Graduate Student, University of Wisconsin, is associated with Kaiser Aluminum Co., Chicago, and D. J. MACK, Member AIME, is Associate Professor of Metallurgical Engineering, Dept. of Mining & Metallurgy, University of Wisconsin, Madison, Wisc.



TN 297E. Manuscript, June 13, 1955.

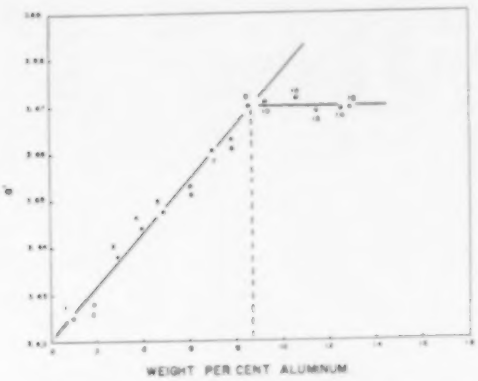


Fig. 1—$a'$ lattice parameters were plotted against the aluminum content to obtain the master curve.

furnace. Specimens cut from these alloys were used for determination of their $\alpha$ lattice parameters.

The lattice parameters were determined on a Norelco X-ray diffractometer. The (200) reflection occurring in the range of 49.6° to 50.3° $2\theta$ was used in all $\alpha$ lattice measurements to keep the absorption error approximately constant from one alloy to the next. The (200) reflection of the $\alpha$ was chosen because there are no interfering lines from the other phase patterns.[6]

The $a'$* lattice parameters were determined by the usual method. The data so determined are plotted in Fig. 1 to give the master curve. From Fig. 1 it may be seen that the maximum equilibrium content of the $\alpha$ in these furnace-cooled alloys is approximately 8.7 pct Al. This indicates that the solubility of aluminum at lower temperatures may be less than at 9.4 pct Al as the present equilibrium diagram indicates.[7] Also, specimen 9 (8.49 pct Al) had a small amount of the eutectoid present as determined from metallographic examination, thus confirming the X-ray evidence from Fig. 1.

* $a'$ is used to designate a value of the $\alpha$ lattice parameter which is uncorrected for adsorption errors and is not the true lattice parameter but one of a higher $d$-spacing by about 0.012A.

The $\alpha$ lattice parameters of the specimens originally used by Mack[2] were then measured. The specimens were picked at various isothermal temperatures and times close to the beginning and end of the $\alpha$ precipitation as shown on the *TTT* diagram, Fig. 2.

The $a'$ lattice parameters of the transformed specimens† were used to determine the aluminum composition of the $\alpha$ phase from the master curve of Fig. 1. These results are shown graphically in Fig. 3 and indicate that, at the higher temperatures and shorter isothermal times, the $\alpha$ phase precipitates poor in aluminum and grows richer in aluminum as time progresses. As the temperature drops, the initial and final compositions of $\alpha$ are richer in aluminum than at higher temperatures. At 400°C they approach the same composition.

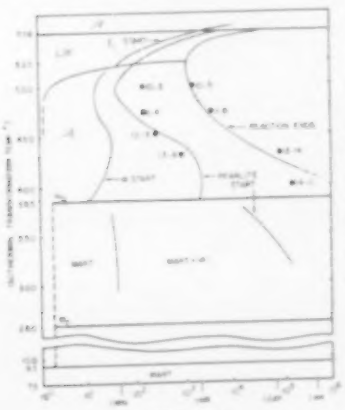

Fig. 2—Time-temperature-transformation data is given for a eutectoid aluminum bronze.

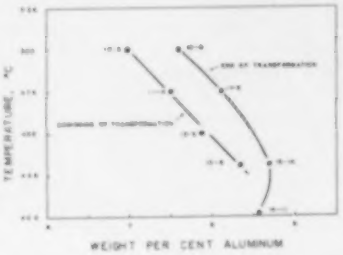


Fig. 3—Changes in aluminum composition during isothermal transformation are shown.

† These specimens contained: 88.07 pct Cu, 11.88 pct Al, 0.02 pct Fe, 0.01 pct Mn, and the balance others.

Since these results were contrary to what was expected and had been previously proposed,[1-4] it was decided to check the corresponding change in the (203) $d$-spacing of the $\beta'$ martensitic phase because, as aluminum diffuses into the $\alpha$ phase increasing its lattice parameter, the $\beta'$ phase lattice parameter should decrease. The (203) reflection of $\beta'$ phase was used because it was the closest reflection to the (200) $\alpha$ reflection.

Some of the original alloy was therefore homogenized for 1 hr at 810°C and isothermally transformed at 450°C. These specimens were quenched into water at 2, 10, 45, and 80 sec. The (203) $d$-spacing was calculated and plotted against the time of isothermal transformation. These results are shown in Fig. 4. It may be observed that this $d$-spacing decreases with increasing time indicating that the aluminum atoms are diffusing from the $\beta$ or $\beta_1$ phase into the $\alpha$ phase before the $\beta$ or $\beta_1$ is transformed into $\beta'$ martensite by the quench.

The transformed specimens used in this study were previously used by Mack,[2] as has been mentioned. Therefore, since they were eight years old, a specimen of the original alloy was transformed, duplicating the treatment given specimen 12-5 which was homogenized at 810°C for 1 hr and isothermally transformed for 8 min and water-quenched. By use of the master curve, Fig. 1, it was

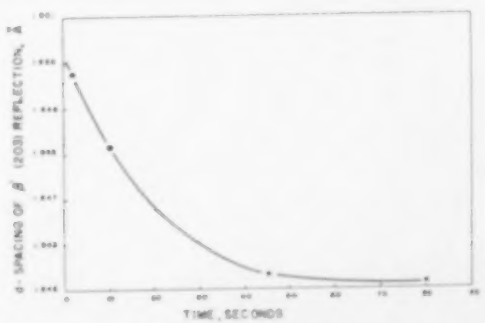


Fig. 4—Change in $d$-spacing of $\beta'$ (203) resulted when the (203) $d$-spacing was calculated and plotted against the time of isothermal transformation.

observed that the freshly prepared specimen had 9.1 pct Al as compared to 7.9 pct Al for the eight year old specimen, loss of 1.2 pct Al over the eight years.

The authors believe that, since the equilibrium solubility of aluminum in the $\alpha$ phase decreases with decreasing temperature, the aluminum composition in the $\alpha$ phase will, over a period of time (eight years), diffuse to lower equilibrium solubility of aluminum. However, the possibility exists that this apparent shift in composition may be due to other causes.

Presently, work is in progress using a high temperature powder camera on the Cu-Al $\beta$ phase decomposition which tends to support the observations mentioned previously with respect to the $\alpha$ phase compositions during isothermal transformations.

This work seems to indicate that, since the proeutectoid $\alpha$ in isothermally transformed aluminum bronzes is copper-rich rather than aluminum-rich as previously assumed, the proposed mechanism of the $\beta$ decomposition must be revised. In addition, the work indicates that the solid solubility of aluminum in copper to form $\alpha$ may be considerably less than heretofore believed.


### Acknowledgments

The authors gratefully acknowledge the assistance of S. W. Bailey, Dept. of Geology, University of Wisconsin, W. W. Edens, formerly associated with Ampco Metal Inc., and J. F. Klement, Technical Director at Ampco.


### References


[1] C. S. Smith and W. E. Lindlief: *Trans.* AIME (1933) **104**, p. 69.

[2] D. J. Mack: *Trans.* AIME (1948) **175**, p. 240; METALS TECHNOLOGY (September 1947).

[3] E. P. Klier and S. M. Grymko: *Trans.* AIME (1949) **185**, p. 611; JOURNAL OF METALS (September 1949).

[4] R. Haynes: PhD. Thesis, University of Sheffield (1952).

[5] A. J. Bradley and P. Jones: *Journal* Inst. of Metals (1953) **51**, No. 1, p. 131.

[6] I. Obinata: *Memoirs* Ryojun College of Eng. 3 (1931) pp. 285, 295.

[7] G. V. Raynor: *Annotated Cu-Al Equilibrium Diagram.* (1944) London. Inst. of Metals.


---

# Creep of Polycrystalline Tin


by J. E. Breen and J. Weertman



**The creep rate of polycrystalline tin was studied as a function of temperature and stress in constant stress experiments. The temperature was varied from room temperature to almost the melting point of tin. Activation energies were calculated from tests run at the same stress. It was found that on a log creep rate vs inverse temperature plot the experimental points did not fall on one straight line but on a line which changed its slope in the 90° to 160°C region. Two activation energies for the creep of tin can be calculated from the data: a value around 26,000 cal per mol at high temperatures and a value around 11,000 cal per mol at low temperatures. It is suggested that the discrepancies between the creep activation energies and those of self-diffusion can be accounted for if self-diffusion takes place predominately by Zener's ring mechanism rather than through vacancy or interstitial movement.**


SHERBY, Orr, and Dorn[1] and Dorn[2] have recently reviewed some of the data on high temperature creep of metals. The data show that the activation energy of high temperature creep is approximately equal to the activation energy of self-diffusion. This same correlation has also been successfully made between the activation energy of grain boundary relaxation and that of self-diffusion.[3, 4] The metal tin does not fit into this simple picture. Its activation energies of self-diffusion differ appreciably from that of grain boundary relaxation and of creep. Fensham,[5] from a precisely performed experiment, has determined that the activation energies of self-diffusion of tin are 10,500 and 5,900 cal per mol along the $C$ and $A$ axes, respectively. There are two energies because of the anisotropic nature of tin. Rotherham, Smith, and Greenough[6] have shown that the grain boundary relaxation activation energy is 19,000 cal per mol (measurements made from room temperature to 100°C). Puttick and King[7] found the same activation energy for grain boundary slip in bicrystals of tin (180° to 225°C region).

Until recently, there was no high temperature large strain creep data on tin suitable for activation energy calculations. At rather small strains (up to 0.01), Tyte[8] had made a series of measurements on tin from which activation energies can be calculated. In Fig. 1 are plotted some of his data on a log creep rate vs inverse temperature graph. It can be seen that Tyte's work indicates that at a relatively low temperature the activation energy is around 7,400 cal per mol but at higher temperatures the activation energy increases. Since Tyte measured the creep only for small strains, it is doubtful if a


J. E. BREEN and J. WEERTMAN, Junior Member AIME, are associated with Metallurgy Div., Naval Research Laboratory, Washington, D. C.



Discussion of this paper, TP 4015E, may be sent, 2 copies, to AIME by Jan. 1, 1956. Manuscript, Sept. 8, 1954. Philadelphia Meeting, October 1955.

This paper is based on a portion of a thesis by J. E. Breen submitted, in partial fulfillment of the requirements for the degree of Master of Science, to the University of Maryland.

correlation between activation energy of self-diffusion and creep should be observed.

Breen,[8] from constant stress and constant load creep tests for strains up to one, found an activation energy of around 11,000 cal per mol in the 20° to 130°C region. This value agrees with one of the activation energies of self-diffusion. However, Frankel, Sherby, and Dorn,[9] for strains up to 0.4, found an activation energy of 21,000 cal per mol in the 100° to 205°C region in constant load creep tests. The present experiment was undertaken to clarify the situation with regard to the activation energy of tin. The last section of this paper indicates how the various observed activation energies can perhaps be fitted into a consistent picture.

## Experimental Details

The method that was used for applying a constant stress to a specimen was that developed by Andrade.[10] The experimental set-up is shown in Fig. 2. It consists of a fixed grip attached to the upper end of the specimen and a lower grip connected to a hyperbolic weight. As the specimen elongates, the hyperbolic weight sinks into a constant level water tank. The stress increase, normally caused by the reduction in the specimen cross-sectional area, is eliminated by the reduction in load caused by the buoyancy of the water. Strain was measured by a traveling microscope focused on an index mark placed on the lower chain. For the very rapid creep tests, a motion picture camera was used. As a check on these last tests, it was ascertained that the speed of the weight through the water with no specimen attached was several orders of magnitude faster than the fastest creep rate used.

The specimens used were in the form of wires 0.234 cm diam and 10 cm in length. They were made of 99.9 pct pure Sn containing 0.01 pct Cu, 0.01 pct Pb, 0.01 pct Bi, and 0.01 wt pct Fe as the principal impurities. The specimens in the series labeled *A*, *B*, and *C* in this report were annealed at a temperature of approximately 205°C for 2 hr which resulted in a grain size of approximately 53.0 grains per sq mm. Those in series *D* were annealed at 100°C for 1 hr and developed a grain size of approximately 715 grains per sq mm. Metallographic examination showed no change in grain size after testing.

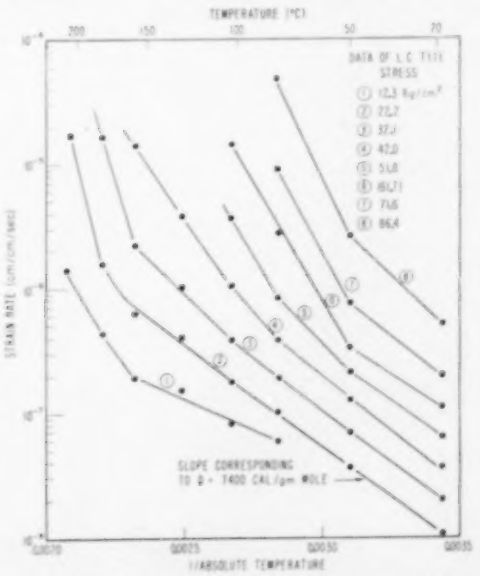


Fig. 1—Logarithm of creep rate is shown vs inverse absolute temperature for tests run under various loads. Data is that of L. C. Tyte[7] on polycrystalline tin.

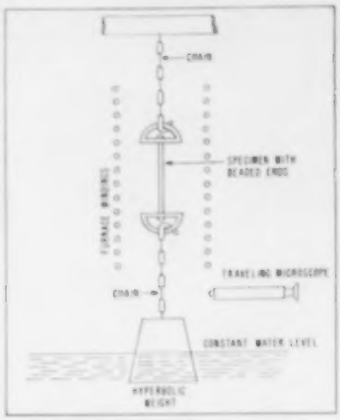


Fig. 2—Schematic diagram shows experimental set-up used for applying a constant stress to a specimen.

The temperature was measured with a thermocouple attached to the upper grip. The temperature was controlled to within ±1.5°C.

## Results

Typical creep curves for specimens of series *A*, *B*, and *C* (Fig. 3) show a transient, then steady state, followed by third stage creep. Fig. 4 shows curves obtained for the smallest grain size under both constant load and constant stress. Fig. 5 shows the initial portion of Fig. 4 and indicates that for these tests there was very little transient creep. The creep

Table I. Steady State Creep Rate Under Constant Stress

| Series | Temperature, °C | Creep Rate, Cm/Cm per Min | Stress, Psi |
|---|---|---|---|
| *A*, 629 psi | 220 | 0.115 | |
| | 214 | 0.046 | |
| | 209 | 0.047 | |
| | 194 | 0.013 | |
| | 187 | 0.00548 | |
| | 179 | 0.00553 | |
| | 170 | 0.00242 | |
| | 150 | 0.00099 | |
| | 133 | 0.00031 | |
| | 96 | $3.69 \times 10^{-5}$ | |
| | 77.5 | $9.0 \times 10^{-6}$ | |
| *B*, 828 psi | 234.5 | 0.56 | |
| | 204 | 0.173 | |
| | 191 | 0.053 | |
| | 172.5 | 0.0225 | |
| | 156.5 | 0.0074 | |
| | 133 | 0.0025 | |
| | 116 | 0.00091 | |
| | 101 | 0.000515 | |
| | 73 | 0.000118 | |
| | 55 | $3.8 \times 10^{-5}$ | |
| | 38.5 | $1.52 \times 10^{-5}$ | |
| *C*, 1394 psi | 204.5 | 1.7 | |
| | 184.5 | 0.538 | |
| | 161 | 0.153 | |
| | 136 | 0.0312 | |
| | 108.5 | 0.00754 | |
| | 90 | 0.00214 | |
| | 64 | 0.000314 | |
| | 52 | 0.000126 | |
| | 22 | 0.000036 | |
| *D*, fine grain size | 21.1 | $1.6 \times 10^{-4}$ | 728.4 |
| | 21.1 | $2.5 \times 10^{-5}$ | 827.8 |
| | 21.1 | $2.0 \times 10^{-4}$ | 827.8 |
| | 21.1 | $2.1 \times 10^{-4}$ | 827.8 |
| | 21.1 | $6.6 \times 10^{-5}$ | 1059.5 |
| | 21.1 | $6.0 \times 10^{-5}$ | 1059.5 |
| | 21.1 | $18.1 \times 10^{-5}$ | 1324.4 |
| | 21.1 | $16.7 \times 10^{-5}$ | 1324.4 |
| | 21.1 | $18.8 \times 10^{-5}$ | 1324.4 |
| | 21.1 | $21.5 \times 10^{-5}$ | 1324.4 |
| | 21.1 | $54 \times 10^{-6}$ | 1655.5 |
| | 21.1 | $64.8 \times 10^{-6}$ | 1655.5 |
| | 93 | $19 \times 10^{-4}$ | 629.1 |
| | 93 | $37 \times 10^{-4}$ | 728.4 |
| | 93 | $59 \times 10^{-4}$ | 728.4 |
| | 93 | $28 \times 10^{-4}$ | 827.8 |
| | 93 | $75 \times 10^{-4}$ | 827.8 |
| | 93 | $280 \times 10^{-4}$ | 1059.5 |
| | 133 | $237 \times 10^{-4}$ | 728.4 |

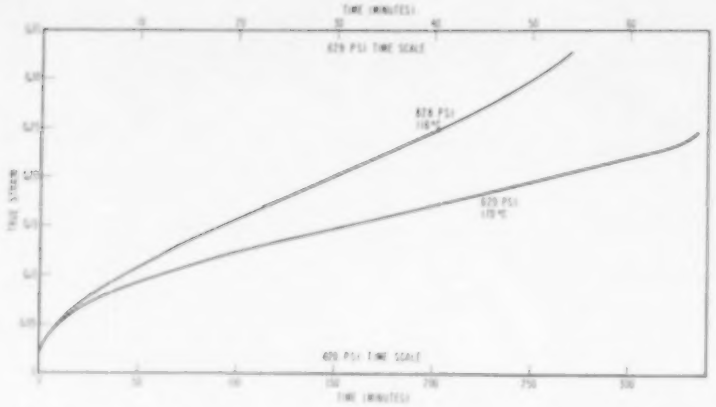

Fig. 3—Typical creep curves are given for specimens in series *A*, *B*, and *C*.

rate of the fine grain tin was much larger than that of the coarser grain specimens.

The point of interest in this experiment is the activation energy of creep which is obtained in the following manner: A plot is made of the natural logarithm of the steady state creep rate as a function of the inverse absolute temperature for specimens that have crept under the same stress. The slope of the line obtained is equal to the activation energy divided by the gas constant. In Table I are given the steady state creep rates of all the measured samples. In Fig. 6 are plotted all points in series *A*, *B*, and *C*. It is obvious that all the points for similar specimens which had crept under the same stress do not fall on one straight line. The points can be separated into a high temperature region having an activation energy of about 26,000 cal per mol and a low temperature region having a value of about 11,000 cal per mol. Values for the different series of tests are given in Table II.

Another way to obtain the activation energy of creep which is used in constant load tests[1, 2] is to plot the strain as a function of $\theta$ where $\theta$ is equal to $t \exp(-Q/RT)$; $t$ is the time, $Q$ the activation energy, $R$ the gas constant, and $T$ the absolute temperature. In Figs. 7 and 8 a plot of this type is made for the data of series *B*. In Fig. 7 an average activation energy of 17,600 cal per mol is used. The scatter in the points is reduced by using two activation energies of 14,100 and 20,700 cal per mol. However, these values differ quite appreciably from those determined by the steady state creep rates. The reason for this discrepancy is that calculations of activation energies from plots such as those shown in Figs. 7 and 8 give weight to the transient portion of the

Table II. Activation Energies Calculated from Steady State Creep Rates

| Specimen Series | Cal per Mol for Temperature Range | |
|---|---|---|
| | 130° to 224°C | 20° to 100°C |
| *A*, 629 psi | 27,800 | — |
| *B*, 828 psi | 26,200 | 12,500 |
| *C*, 1394 psi | 22,700 | 10,400 |
| *D*, fine grain | — | 11,000 |

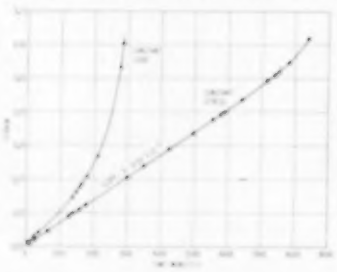

Fig. 4—Typical creep curves are given for specimens in series *D*. True strain is plotted as a function of time.

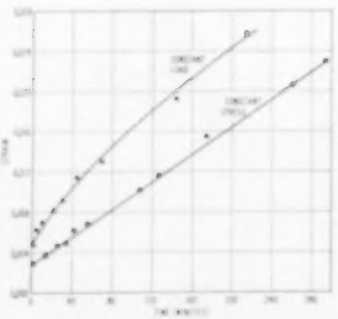

Fig. 5—Initial portion of creep curves of Fig. 4 are shown. True strain is plotted as a function of time.

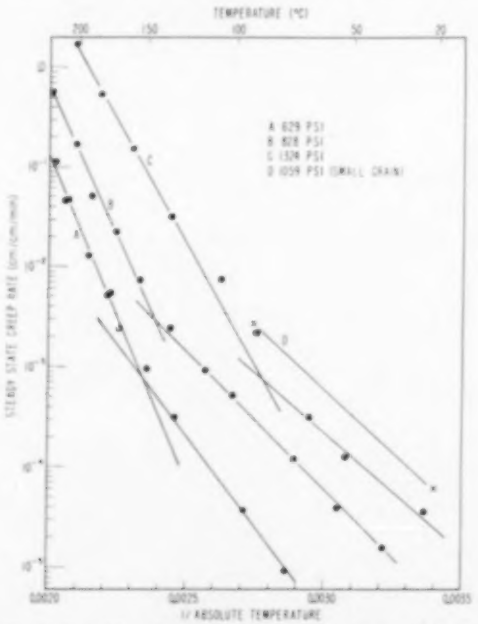


Fig. 6—Logarithm of creep rate is plotted vs inverse absolute temperature for all tests in series *A*, *B*, and *C* and two tests in series *D*.

Table III. Time, Min, to Reach a Fixed Strain

| Series | Temperature, °C | Strain 0.05 | 0.10 | 0.15 | 0.20 |
|---|---|---|---|---|---|
| *A*, 629 psi | 220 | 0.078 | 0.46 | — | — |
| | 214 | — | 0.72 | 1.78 | 3.87 |
| | 209 | — | 0.79 | 1.82 | — |
| | 194 | 0.26 | 2.55 | 6.42 | — |
| | 187 | 3.1 | 10 | 18.8 | — |
| | 179 | 0.995 | 5.5 | 13.2 | 23.3 |
| | 170 | 1.66 | 12.6 | 30.6 | 51.6 |
| | 150 | 5.0 | 35 | 88.5 | 138 |
| | 133 | 43 | 164 | 323 | — |
| | 96 | 280 | 1280 | 2650 | — |
| | 77.5 | 1080 | 4850 | 9700 | 15,500 |
| | 23.4 | 76,600 | — | — | — |
| *B*, 828 psi | 224.5 | 0.03 | 0.108 | 0.194 | 0.28 |
| | 204 | 0.0934 | 0.297 | 0.587 | 0.875 |
| | 191 | 0.16 | 0.57 | 1.44 | 2.40 |
| | 172.5 | — | 0.8 | 2.35 | 4.5 |
| | 156.5 | — | 2.9 | 7.4 | 13.4 |
| | 133 | 2.5 | 11 | 26 | 44 |
| | 116 | 9.5 | 43 | 94 | 149 |
| | 101 | 17 | 82 | 176 | 273 |
| | 73 | 90 | 435 | 835 | — |
| | 55 | 260 | 1370 | 2870 | 3830 |
| | 38.5 | 1030 | 4140 | — | — |
| *C*, 1394 psi | 204.5 | — | 0.021 | 0.041 | 0.0705 |
| | 184.5 | — | 0.034 | 0.062 | 0.158 |
| | 161 | — | 0.1 | 0.3 | 0.585 |
| | 136 | — | — | 0.9 | 2.0 |
| | 108.5 | — | 0.95 | 3.6 | 8.7 |
| | 90 | — | 4.6 | 14.6 | 32.2 |
| | 68 | — | 23 | 87 | 217 |
| | 52 | — | 76 | 264 | 624 |
| | 23 | — | 2120 | — | — |

creep curve. The transient portion may or may not have the same apparent activation energy as the steady state part. The fact that the activation energy of tin, determined by Frenkel, Sherby, and Dorn,[11] is just about equal to the high temperature portion of Fig. 8 shows that there is probably no inconsistency between the present work and theirs, since they plotted their data in the manner given in Figs. 7 and 8. Another way to calculate the activation energy of creep which is equivalent to that given in Figs. 7 and 8 is to plot the logarithm of the time to reach a fixed strain as a function of the inverse temperature. In Table III are given the times to reach various strains. In Table IV are given activation energies calculated from plots of these times. From this table, it can be seen that at higher strains the activation energies approach those calculated from the steady state creep rate.

In Fig. 9 the logarithm of the creep rate is plotted as a function of stress for the fine grain tin. A log-log plot of creep rate as a function of stress would show the data as parallel straight lines. In Fig. 10 the logarithm of the creep rate times exp $(Q/RT)$ is plotted as a function of the logarithm of the stress. This plot indicates that the creep rate can be equated to constant $\sigma^{n}$ exp $(-Q/RT)$, where $\sigma$ is the stress and $Q$ is the activation energy of self-diffusion. In this case, $Q$ is equal to 11,000 cal per mol.

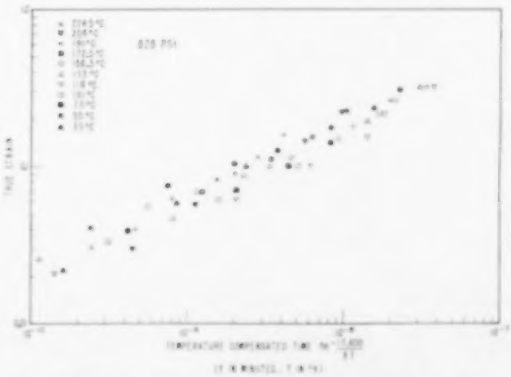

Fig. 7—Logarithm of true strain is plotted vs the logarithm of the temperature-compensated time for tests of series *B*.

## Discussion

The experimental work just described has shown that the apparent activation energy of creep in the neighborhood of the melting point of tin is around 26,000 cal per mol, while near room temperature it is much smaller and seems to be around 11,000 cal per mol. The fact that there are two activation energies of creep of tin is not surprising, since it is an anisotropic metal. For example, it also has two activation energies of self-diffusion.[5] What is troublesome about tin is that the activation energies of self-diffusion and creep do not agree. At high temperatures, self-diffusion is fastest in the direction having the activation energy of 10,500 cal per mol as contrasted with the observed creep activation energy of 26,000 cal per mol in this temperature range. At low temperatures, the fast direction of self-diffusion has an activation energy of 5,900 cal per mol as contrasted to the higher activation energy of 11,000 cal per mol for creep. As mentioned previously, the activation energies of creep in other metals that have been investigated do seem to agree with those of self-diffusion. This suggests that in tin the mechanism of self-diffusion is different from the rate controlling process in creep, while in other metals the same mechanism is operative in both

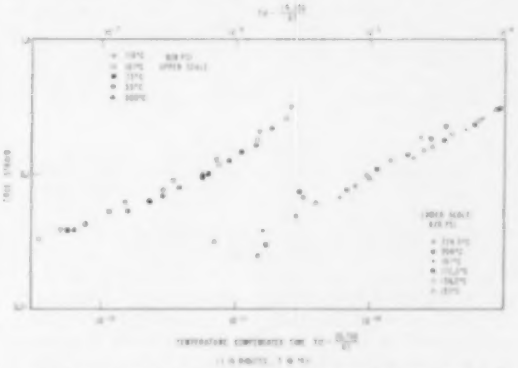

Fig. 8—Logarithm of true strain is plotted vs the logarithm of the temperature-compensated time for tests of series *B*.

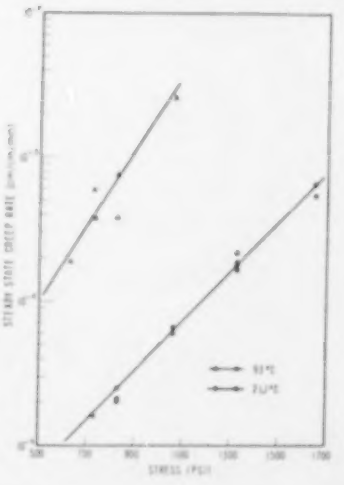

Fig. 9—Logarithm of creep rate is plotted vs stress for tests in series *D*.

Table IV. Activation Energies Calculated from Data in Table III

| Strain | A, 629 Psi | B, 828 Psi | C, 1394 Psi |
|---|---|---|---|
| | Cal per Mol for Temperature Range 130° to 226°C | | |
| 0.05 | 26,700 | 18,900 | — |
| 0.10 | 27,700 | 20,700 | 17,200 |
| 0.15 | 27,700 | 20,900 | 18,400 |
| 0.20 | — | 22,300 | 20,400 |
| | Cal per Mol for Temperature Range 20° to 100°C | | |
| 0.05 | 17,600 | 15,000 | — |
| 0.10 | 17,100 | 14,800 | — |
| 0.15 | 16,600 | 14,200 | 17,600 |
| 0.20 | — | 13,500 | 15,000 |

cases. Vacancy (or interstitial) movement is one mechanism of self-diffusion. This mechanism may also account for creep. For example, creep theories of Nabarro[12] and of Herring[13] use a mass transport of vacancies (or interstitials) to account for creep in wires at low stresses and high temperatures. If creep is controlled by the dislocation climb mechanism,[14] vacancies (or interstitials) are important, since they are created or destroyed during climb. Another mechanism of self-diffusion is Zener's ring mechanism.[15] This mechanism, however, cannot possibly account for creep because a crystal remains perfectly unchanged after rotation of a ring. In face-centered-cubic metals, the vacancy mechanism appears to be the most important one for self-diffusion.[16] It does not necessarily follow that in tin, with its more complex structure, the situation will remain the same. The disagreement between the activation energies of creep and self-diffusion thus might constitute indirect evidence that Zener's ring mechanism is the predominate mechanism of self-diffusion in tin. Perhaps a well thought out Kirkendall experiment may give more direct proof of this suggestion.

If it is assumed that the explanation of the discrepancies between the activation energies of creep and self-diffusion is due to the fact that Zener's mechanism is predominate in one case and the vacancy mechanism in the other, there still remains the difficulty of resolving the grain boundary relaxation activation energy with those of creep and self-diffusion. Rotherham, Smith, and Greenough[6] found an activation energy of 19,000 cal per mol in the region where the fast self-diffusion activation energy is equal to 5,900 cal per mol and that of creep is approximately 11,000 cal per mol. If grain boundary relaxation is controlled through the vacancy mechanism, it is to be expected that the activation energy of grain boundary relaxation would be that of steady state creep. However, the most successful model[17] to explain grain boundary relaxation does not depend on vacancy movement but on a *localized melting* of regions in the grain boundary. The activation energy of grain boundary relaxation on this model is not that of self-diffusion but is proportional to the heat of fusion. The apparent agreement between the activation energy of self-diffusion and grain boundary relaxation in other metals is strictly fortuitous on this model. Therefore, there is no reason to expect that in tin the activation energy of grain boundary relaxation should be equal to that of steady state creep or of self-diffusion.

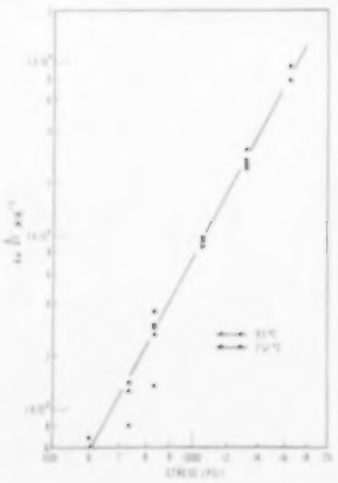

Fig. 10—Logarithm of $K \exp(Q/kT)$ is plotted vs logarithm of the stress for tests in series D. $Q$ = 11,000 cal per mol.


## Acknowledgments

The authors wish to thank Paul Shahinian and W. S. Pellini for their encouragement and suggestions during the course of this work and Wilbert J. Huff, University of Maryland, for permission to use the data in test series *D* which had previously been used as part of a Master's thesis at the University of Maryland.

Discussion of this paper, if any, will appear in JOURNAL OF METALS, May 1956, and in AIME Metals Branch *Transactions*, Vol. **206**, 1956.


## References


[1] O. D. Sherby, R. L. Orr, and J. E. Dorn: Creep Correlations of Metals at Elevated Temperatures. *Trans.* AIME (1954) **200**, p. 71; JOURNAL OF METALS (January 1954).

[2] J. E. Dorn: Some Fundamental Experiments on High Temperature Creep. *Inst. of Engineering Research Report* University of California (1954) series No-22, issue No-35.

[3] T. S. Ke: A Grain Boundary Model and the Mechanism of Viscous Intercrystalline Slip. *Journal of Applied Physics* (1949) **20**, p. 274.

[4] T. S. Ke: On the Structure of Grain Boundaries in Metals. *Physical Review* (1948) **73**, p. 267.

[5] P. J. Fensham: Self-Diffusion in Tin Crystals. *Australian Journal of Scientific Research* (1950) **3A**, p. 91.

[6] L. Rotherham, A. D. N. Smith, and G. B. Greenough: The Internal Friction and Grain Boundary Viscosity of Tin. *Journal* Inst. of Metals (1951) **79**, p. 439.

[7] K. E. Puttick and R. King: Boundary Slip in Bicrystals of Tin. *Journal* Inst. of Metals (1952) **80**, p. 537.

[8] L. C. Tyte: The Rate of Viscous Flow of Metals: Part I, Tin. *Proceedings* Physical Soc., London (1938) **50**, p. 11.

[9] J. E. Breen: *Creep Rupture Properties of Tin Tested at Constant Stress.* Master's Thesis, University of Maryland (June 1954).

[10] R. E. Frenkel, O. D. Sherby, and J. E. Dorn: Activation Energies for Creep of Cadmium, Indium, and Tin. *Inst. of Engineering Research Report* University of California (1954) series No-22, issue No-36.

[11] E. N. da C. Andrade: On the Viscous Flow in Metals and Allied Phenomena. *Proceedings* Royal Soc. (1911) **84**, p. 1.

[12] F. R. N. Nabarro: Deformation of Crystals by the Motion of Single Ions. *Report of a Conference on the Strength of Solids.* (1948) p. 75. London. Physical Soc.

[13] C. Herring: Diffusional Viscosity of a Polycrystalline Solid. *Journal of Applied Physics.* (1950) **21**, p. 437.

[14] N. F. Mott: The Mechanical Properties of Metals. *Proceedings* Physical Soc., London (1951) **64B**, p. 729.

[15] C. Zener: Theory of Diffusion. *Imperfections in Nearly Perfect Crystals.* (1952) p. 289. New York. John Wiley and Sons.

[16] N. F. Mott: Slip at Grain Boundaries and Grain Growth in Metals. *Proceedings* Physical Soc., London (1948) **60**, p. 391.

# Aging Effects in Commercially Pure Beryllium

by D. R. Mash

**A strong yield point with attendant enhanced mechanical properties was found in commercially pure beryllium under certain conditions of heat treatment. Beryllium specimens also responded to both quench and strain aging treatments. Based on these results, a possible means of obtaining increased normal temperature mechanical properties is suggested.**

COMMERCIALLY pure beryllium has been found to exhibit the yield point phenomenon and several other aging manifestations under certain conditions of heat treatment. This behavior is not surprising in view of the present accumulation of experience regarding such effects in numerous metals; but in addition to extending this experience to include beryllium, the present study is of interest because aging effects are generally associated with the presence of small amounts of solute elements. The well known lack of tensile ductility in beryllium at normal temperatures is also considered to be due to impurities in some way.

In the present investigation, the view was taken that beryllium of commercial purity (greater than 98 pct) should be considered as a dilute alloy and that precipitation phenomena may well exist which could lead to enhanced mechanical properties. In connection with this possibility, published data on the variation of mechanical properties with temperature are of interest. For example, Fig. 1 illustrates the variation of ductility (percentage of elongation) and ultimate strength as a function of temperature for beryllium of various histories.[1] Although these curves are somewhat schematic in nature, they clearly indicate the possibility that precipitation of an unstable phase and/or aging effects occur during tests in the region 400° to 700°C. The existence of such behavior should be recognized as affecting the properties of the commercial material and perhaps can be employed advantageously.

## Experimental Method

All testing was done at room temperature using a Baldwin universal testing machine. A microformer extensometer was used in conjunction with a microformer-type stress-strain recorder. All tests were conducted at constant loading rate, the slowest rates being used. This corresponded to 120 lb per min in the 1200 lb full scale range and 300 lb per min in the 6000 lb full scale range.

After the rate of loading was set in the elastic range of the material during the early part of the test, no further adjustments were made, allowing the test to proceed at that setting. In the plastic region of the curve above the yield region, strain rates of from 0.002 to 0.006 in. per min were regularly obtained.

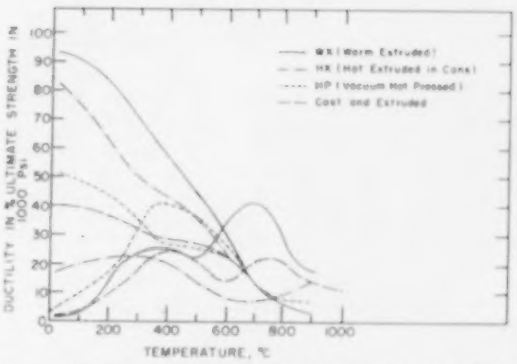
DUCTILITY IN % ULTIMATE STRENGTH IN 1000 Psi
TEMPERATURE, °C
WX (Warm Extruded)
HX (Hot Extruded in Cans)
HP (Vacuum Hot Pressed)
Cast and Extruded

**Fig. 1—Variation of beryllium ductility (lower curves) and ultimate strength (upper curves) is given as a function of temperature. Data is taken from ref. 1.**

All experimentation was carried out on specimens machined from the same lot of beryllium, lot No. Y5036BP. Table I shows the chemical analysis as furnished by the supplier, Brush Beryllium Co., as well as the standard specifications to which commercial beryllium is produced. Both ¼ in. thick hot pressed plate and ½ in. round hot pressed and warm extruded rods were obtained. The history of the material is reported to be as follows:

1—Beryllium metal plates, produced from a standard hot pressed QMV beryllium metal block 4x15x40 in., were cut off and finished machined to ¼x6x12 in. flat plates. The original hot pressed block was made by hot pressing −200 mesh vacuum cast attritioned powder at about 1050°C under vacuum.

2—Beryllium rod was hot pressed and warm extruded. Extrusion billets were machined from the regular hot pressed blocks followed by extrusion at 425°C. The extrusion was done without jacketing, and graphite was used as a lubricant. The rods were then straightened at 720°C, after which they were annealed at 800°C for 15 min.

Both flat tensile specimens and round tensile specimens were tested. The former were machined from the plate stock into standard specimens according to specifications shown in ASTM E8-52T. The nominal cross-section was 0.25x0.500 in. and the gage length was 2 in. The round specimens were

D. R. MASH, Junior Member AIME, formerly associated with California Research and Development Co., Livermore, Calif., is associated with Standard Oil Co. of California, San Francisco.

Discussion of this paper, TP 4069E, may be sent, 2 copies, to AIME by Jan. 1, 1956. Manuscript, June 28, 1954.

Table I. Chemical Analysis of QMV Beryllium Powder Sample from Lot Y5036BP

| Element* | Y5036BP, Wt Pct | QMV Specifications, Wt Pct |
|---|---|---|
| C, Be | 99.02 | >98.00 |
| S, Al | 0.0310 | <0.15 |
| C, B | 0.0006 | — |
| S, Fe | 0.1180 | <0.20 |
| S, Mn | 0.0190 | — |
| S, Ni | 0.0130 | — |
| S, Co | 0.0002 | — |
| S, Cr | <0.0003 | — |
| C, BeO | 0.92 | <1.50 |
| $Be_2C$ | — | <0.35 |
| Mg | — | <0.30 |

* C stands for chemical analysis and S for spectrographic analysis.

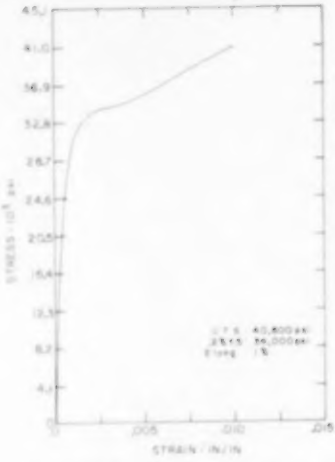

Fig. 2—Hot pressed beryllium plate tensile specimen No. 25 is shown in the as-received condition.

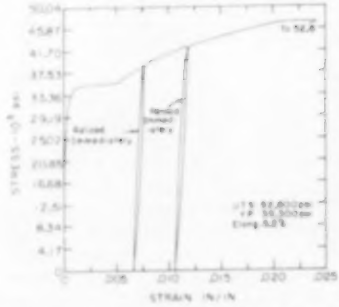

Fig. 3—Hot pressed beryllium plate tensile specimen No. 17 was annealed at 800°C for 6 hr and furnace cooled at approximately 2°C per min (800° to 500°C).

of approximately 0.185 in. diam, 2 in. gage length, and were threaded on the ends.

After machining, the specimens were given the recommended chemical etching treatment. This consisted of removing approximately 0.002 in. from the surface in a bath consisting of 213 g $CrO_3$, 1800 ml concentrated ortho phosphoric acid, and 106 ml concentrated sulphuric acid. Macroetching was carried out at about 100°C.

Metallographic examination of both round and plate stock revealed that a uniformly small grain size (approximately 0.020 mm average grain diameter) was obtained with numerous twins as well as a liberal number of inclusions in the material.

## Experimental Procedure

The general procedure involved annealing specimens at various temperatures followed by cooling at various rates in order to observe the effect on the room temperature mechanical properties of the test material. The effect of solution heat treating fol-

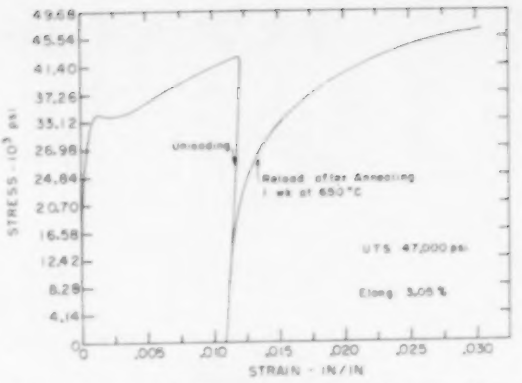


Fig. 4—Hot pressed beryllium plate tensile specimen No. 19 was fully annealed at 800°C for 6 hr prior to testing as shown. The upper yield point was 34,300 psi and the lower, 33,950 psi.

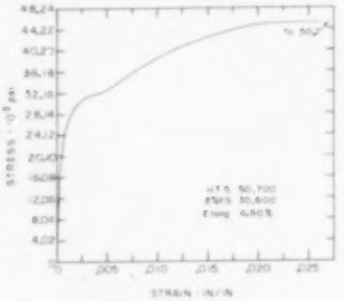

Fig. 5—Hot pressed beryllium plate tensile specimen No. 18 was fully annealed at 800°C for 6 hr and then fully annealed at 650°C for one week.

lowed by low temperature aging treatments (quench aging treatments) was also studied to some extent, as was the effect of prestrain and aging on mechanical properties (strain aging treatments). Annealing followed by varying cooling rates produced the most interesting results and will be dealt with primarily in this study.

The annealing treatments were carried out in several ways: A vacuum ($2x10^{-4}$ mm Hg) annealing furnace was employed for extended tests at the higher temperatures (600° to 900°C). Full annealing involved cooling the specimen down to room temperature with the furnace at a rate of about 2°C per min in the range 900° to 500°C and less than 1°C per min below this temperature. This is referred to as full annealing or as furnace cooling hereafter. Except for several bars tested in the *as-received* condition, all specimens were annealed initially at 800°C for 1 hr in a lead bath, the specimens being contained in a stainless steel can with zirconium turnings and sealed on both ends. Before removing the specimens, this unit was allowed to cool in air at a rate which is estimated as between 5° and 7°C per min. This is referred to as slow air cooling. Specimens heated for short times were treated in air. When heat treatment was followed by cooling in still air, it is referred to as air cooled. Water quenching from the annealing temperature and oil quenching were also done and are so designated.

Annealing temperatures were controlled to within 5°C of the desired temperature.

## Experimental Results

Typical results of this study are shown in Figs. 2 through 12 and are summarized in Tables II and IV. Due to differences in specimen history, it

difference. Fig. 9 is an example of the most subdued yield effect. Fig. 10, No. 29, is an example of the

Table II. Hot Pressed Beryllium ¼ In. Plate, Typical Tensile Data after Various Treatments

| Specimen No. | Treatment* | 0.2 Yield Strength, Psi | Upper Yield Point, Psi | Lower Yield Point, Psi | Strain at Yield Point, Pct | Ultimate Tensile Strength, Psi | Elongation,† Pct | Remarks |
|---|---|---|---|---|---|---|---|---|
| 23 | As received | 34,000 | — | — | — | 40,800 | 1.0 | Slight inflection at yielding. |
| 2 | As received | 34,100 | — | — | — | 51,800 | 3.6 | Slight inflection at yielding. |
| 17 | 800°C, 6 hr *FC* | — | — | 35,300 | 0.55 | 52,800 | 5.2 | |
| 19 | 800°C, 6 hr *FC* | — | 34,300 | 33,900 | 0.40 | — | — | Not taken to failure. |
| 6 | 750°C, 24 hr *FC* | — | — | 32,700 | 0.35 | 47,700 | 2.75 | Broke at defect. |
| 37 | 800°C, 1 hr *SAC* 900°C, 4 hr *FC* | 31,100 | — | — | — | 50,700 | 4.5 | Definite inflection at yielding. |
| 34 | 800°C, 1 hr *SAC* 900°C, 4 hr *FC* | — | — | 37,300 | 0.50 | 54,100 | 4.5 | |
| 18 | 800°C, 6 hr *FC* 650°C, 1 week *FC* | 30,600 | — | — | — | 50,700 | 4.5 | Definite inflection at yielding. |
| 19 | 800°C, 6 hr *FC* 1.1 pct strain, 650°C, 1 week *FC* | 30,500 | — | — | — | 47,000 | 3.05 | |
| 29 | 800°C, 1 hr *SAC* | 31,100 | — | — | — | 47,300 | 2.75 | |
| 38 | 800°C, 1 hr *SAC* | 32,100 | — | 32,100 | 0.25 | — | — | Mild yield point. |
| 33 | 800°C, 1 hr *SAC* | 28,200 | — | — | — | — | — | |
| 40 | 800°C, 1 hr *SAC* | 28,300 | — | — | — | — | — | |
| 39 | 800°C, 1 hr *SAC* | 32,100 | — | 32,100 | 0.25 | — | — | Mild yield point. |
| 36 | 800°C, 1 hr *AC* | 30,000 | — | — | — | 40,500 | 2.75 | |
| 35 | 800°C, 1 hr *AC* 600°C, 40 min *AC* | 30,200 | — | — | — | 48,000 | 5.25 | Slight inflection at yielding. |

* *FC* stands for furnace cool, *SAC* for slow air cool, and *AC* for air cool.
† Note: Reduction of area values were comparable to elongation values.

is convenient to separate the description into that dealing with hot pressed plate tensile specimens and that concerning the hot pressed, warm extruded round specimens.

*Hot Pressed Beryllium Plate Tensile Specimens:* A typical room temperature stress-strain curve of the as-received (as hot pressed) material, No. 25, is shown in Fig. 2. An inflection point can be observed in the region of yielding. For comparison, a fully annealed specimen, No. 17, is exhibited in Fig. 3. A strong yield point is seen which extends to 0.5 pct strain before strain hardening begins. Unloading, followed by immediate reloading, shows that the yield point has been completely removed. Comparison of mechanical properties of these two specimens shows that No. 17 is superior to No. 25 in all respects. A more extensive comparison of properties is summarized in Table II. This treatment was found in the present study to result in uniformly higher properties than are generally associated with hot pressed stock, Table III.[3,4] A temperature of 700°C was determined to be the approximate minimum temperature for the full annealing treatment to obtain the strong yield point and attendant enhanced mechanical properties.

Fig. 4 shows the effect of annealing for one week at 650°C after a prestrain of 1.1 pct, while Fig. 5 shows the results of the same treatment with no prestrain. In the former case, the reloading curve indicates complete recovery with no yield point indication; however, the relative importance of overaging, recovery, and possibly grain growth were not evaluated. Total elongation of the specimen was low by comparison to fully annealed specimens described previously. The specimen shown in Fig. 5 indicates that with no prestrain the strong yield point due to the initial full annealing at 800°C has been replaced by an inflection point. Apparently, the critical state of precipitation required to produce the marked yield point has been passed, although properties remained relatively high. Elongation did not suffer greatly from this treatment. Further tests were carried out using various cooling rates. Air cooling and faster rates of cooling from the *solution* range, 700° to 900°C, failed to produce any manifestation of the yield point phenomenon. However, slow air cooling of a series of specimens proved quite interesting. In no case was a strong yield point observed; however, the curves exhibited various degrees of the phenomenon: no yield point, a definite inflection point, or a mild (less extensive) yield point. Ths could be partly accounted for by slight differences in the actual cooling rates but it is felt that inhomogeneity of the material is the major factor. This was given further confirmation in other tests in this study where samples treated together exhibited variations in behavior with regard to yield. Fig. 6 is an example of a slowly air cooled specimen in which the yield point effect is very mild. It is noteworthy that mechanical properties are again lower than those of fully annealed specimens.

In general, with no prestrain, treating above the solution range, air cooling, or faster cooling followed

Table III. Typical Tensile Data for Production Beryllium

| Fabrication Method | No. of Samples | Tensile Strength, Psi | 0.2 Yield Strength, Psi | Pct Elongation | Pct *R/A* | Reference |
|---|---|---|---|---|---|---|
| Hot pressed | 10 | 45,800 | 31,600 | 2.7 | 2.6 | 3* |
| | 134 | 41,200 | 32,200 | 1.6 | 1.5 | 3* |
| | 16 | 41,000 to 53,000 | 30,000 to 37,000 | 2 to 3.5 | 1.2 to 2.9 | 4 |
| | — | 30,000 to 50,000 | 25,000 to 40,000 | 1.3 | — | 2 |
| Hot pressed and warm extruded | 14 | 79,400 | 44,500 | 6.3 | 6.9 | 3* |
| | 20 | 73,230 | 48,980 | 3.5 | 3.6 | 3* |
| | — | 73,000 to 98,500 | 42,000 to 67,400 | 9.5 to 12.8 | 5.5 to 10.9 | 2 |

* Average values.



Table IV. Hot Pressed, Warm Extruded ½ In. Beryllium Rod, Typical Tensile Data after Various Treatments

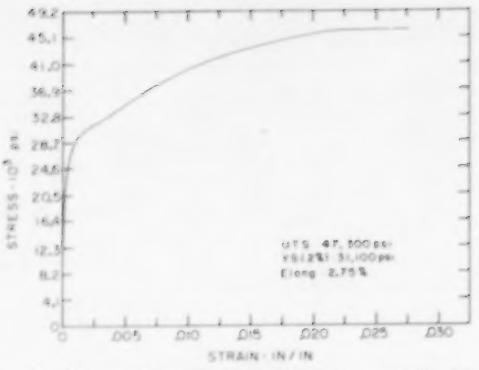


Fig. 6—Hot pressed beryllium plate tensile specimen No. 29 was annealed at 800°C for 1 hr and slowly air cooled.

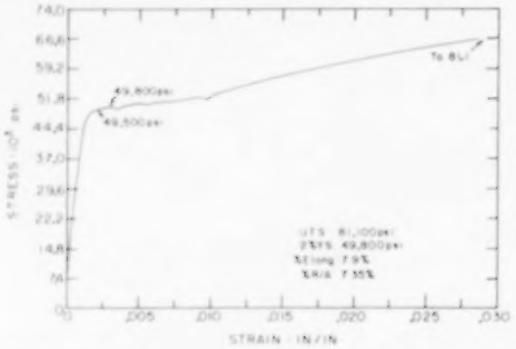


Fig. 7—Hot pressed, warm extruded beryllium rod round tensile specimen No. 27 is shown in the as-received condition.

by a low temperature aging treatment (quench aging) was ineffective in producing a strong yield point in this study. The best results obtained were after aging at 600°C for 40 min where an inflection point only was obtained.

The effect of prior strain in producing strain aging effects was studied to some extent. In this case, it was found that above 500°C, even for aging times of the order of minutes, recovery was the predominant effect. Aging at 370°C for 45 min after 0.5 pct strain produced a mild yield point. There is no doubt that more extensive studies of the variables would develop the optimum conditions for showing both the strain and quench aging phenomena in hot pressed material.

*Hot Pressed, Warm Extruded Rod:* Similar treatments to those already described were carried out on this material with additional effort spent in varying the conditions in order to observe the various aging effects more clearly. For this reason, only a few of the specimens were taken to failure.

Fig. 7 shows an as-received specimen, No. 27. Discontinuous yielding over a 1 pct strain range after the initial yield point of 49,500 psi can be observed. Mechanical properties are relatively high and compare favorably with those reported in the literature for this product, Table III.

Full annealing from above 800°C completely removed any manifestation of the yield point. An example of this is seen in Fig. 8 where mechanical properties are somewhat lower than No. 27.

Slow air cooling produced very strong yield points in a number of specimens and mild ones in others. It is believed that inhomogeneity accounts for this difference. Fig. 9 is an example of the most subdued yield effect. Fig. 10, No. 29, is an example of the strong yield point which can be produced by slow air cooling. Fig. 10 is a typical record of tests carried out varying strain, temperature, and time. After unloading at approximately 1.25 pct strain, annealing at 800°C for 40 min and air cooling completely removed any yield point effect, and complete recovery took place. After a small strain of 0.25 pct, annealing for ½ hr at 500°C brought out a mild yield point with some strengthening. After 0.3 pct strain, annealing at 700°C for ½ hr and air cooling caused recovery with no yield effect. However, aging at room temperature for 16 hr produced a very mild yield point effect. Faster quenching, such as oil quenching, from 700° or 800°C after small strains, produced no effect except complete recovery and loss of all yield point effect, as can be seen in Fig. 11.

The effect of several treatments on specimen No. 50 can be seen in Fig. 11. Strain of 1 pct followed by 300°C for 15 min, air cooled, brought out a definite yield point. After further straining, a similar treatment again produced the yield point phenomenon. Sample No. 49A, on the other hand, did not show a yield point after aging with no prestrain at 300°C for 15 or 30 min. Quench aging treatments provided an interesting result as shown in Fig. 12. Although no yield point was obtained, definite strengthening was observed by aging at 300°C, while aging above and below this temperature showed lower yield strengths.

As in the case of the hot pressed plate tests, optimum mechanical properties corresponded with the occurrence of the aging effect. Even though both quench and strain aging effects were observed in the case of extruded rod, it is felt that more extensive work would be required to uncover optimum conditions for producing the effects. Table IV compares a number of specimens given various treatments. It is interesting to note that these treatments greatly affect the mechanical properties. Yield strengths especially are compared, since most specimens were not taken to failure. It has been found that those beryllium specimens with the highest yield strength values will produce the optimum ultimate strengths and ductility values.

## Discussion

The present study of commercially pure beryllium should be considered as an addition to the growing list of metals exhibiting aging effects and it may serve as an indication for future work in improving the mechanical properties of beryllium. If increased

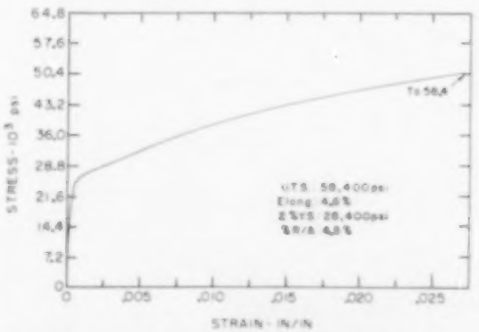


Fig. 8—Hot pressed, warm extruded beryllium rod round tensile specimen No. 55 was annealed at 800°C for 1 hr, slowly air cooled, and then fully annealed at 900°C for 4 hr.



ing information on low temperature solubility of

timum conditions as represented by presence of the

Table IV. Hot Pressed, Warm Extruded ½ In. Beryllium Rod, Typical Tensile Data after Various Treatments

| Specimen No. | Treatment | 0.2 Yield Strength, Psi | Upper Yield Point, Psi | Lower Yield Point, Psi | Strain at Yield Point, Psi | Ultimate Tensile Strength, Psi | Elongation,† Pct | Remarks |
|---|---|---|---|---|---|---|---|---|
| 27 | As received | 49,800 | — | 49,500 | — | 81,000 | 7.9 | Discontinuing yielding, mild yield point. |
| 55 | 800°C, 1 hr *SAC* 900°C, 4 hr *FC* | 28,400 | — | — | — | 58,400 | 4.6 | — |
| 50 | 800°C, 1 hr *SAC* | 34,900 | — | 34,900 | 0.25 | — | — | Mild yield point. |
| 52 | 800°C, 1 hr *SAC* | 34,500 | — | 34,500 | 0.25 | — | — | Mild yield point. |
| 51 | 800°C, 1 hr *SAC* | — | 53,800 | 52,000 | 1.0 | — | — | — |
| 31 | 800°C, 1 hr *SAC* | 34,600 | — | — | — | 67,600 | 5.6 | — |
| 53 | 800°C, 1 hr *SAC* | — | 56,100 | 51,400 | 1.0 | — | — | — |
| 49 | 800°C, 1 hr *SAC* | — | 54,000 | 51,900 | 1.0 | — | — | — |
| 54 | 800°C, 1 hr *SAC* | 34,100 | — | 34,100 | 0.25 | — | — | Mild yield point. |
| 52A | 850°C, 1 hr *OQ* 200°C, 1 hr *AC* | 33,200 | — | — | — | | | |
| 53A | 850°C, 1 hr *OQ* 300°C, 1 hr *AC* | 44,400 | — | — | — | | | |
| 54A | 850°C, 1 hr *OQ* 400°C, 1 hr *AC* | 32,000 | — | — | — | | | |

* *FC* stands for furnace cool, *SAC* for slow air cool, *AC* for air cool, and *OQ* for oil quench.
† Note: Reduction of area values were comparable to elongation values.

purity of the metal is difficult to attain on a commercial scale by present known production methods, it is possible that suitable alloying additions may effect the desired results by means of a precipitation phenomenon when accompanied by suitable heat treatment. The effect may be that of precipitation involving the added element itself or the addition may promote precipitation of the element or elements causing brittle behavior in the current material.

The effect of cooling rate from a *solution* heat treating temperature range in either producing or restraining the yield point phenomenon and the subsequent effect on the yield strength of the material can be interpreted on the basis of precipitation of an unstable phase arising from the presence of impurities in commercially pure beryllium. The presence of both quench and strain aging leads to the belief that more than one type of impurity may be responsible. However, the greater effectiveness of the former (including critical cooling rate treatments) tends to create interest in precipitation hardening possibilities on the basis of the present results. Reasoning in this way, it should be pointed out, does not in any way deny the possibility of a dislocation mechanism underlying the yield point phenomenon itself. Both substitutional and interstitial solute elements can presumably make up an atmosphere for dislocations giving rise to a yield point under the proper conditions. The formation of this atmosphere may be considered as the first stage in the precipitation process; a dislocation certainly would offer the most likely site for the nucleation of an unstable second phase just as it is for the presence of interstitial atoms. The former case would probably be more critical, however, for showing the yield point markedly, since as precipitation progressed the chances of dislocation escape decrease and normal hardening effects would greatly overshadow any such tendency. Finally, if overaging occurred, of course, no yield point could be expected.

From the analysis shown in Table I, it can be noted that the beryllium used in this study contained a number of residual elements including aluminum, boron, iron, manganese, and nickel. Exist-

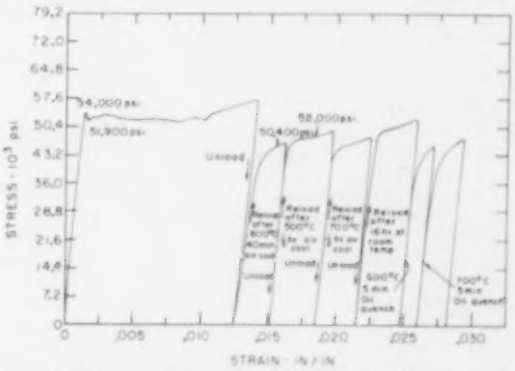


Fig. 10—Hot pressed, warm extruded beryllium rod round tensile specimen No. 49 was annealed at 800°C, slowly air cooled.

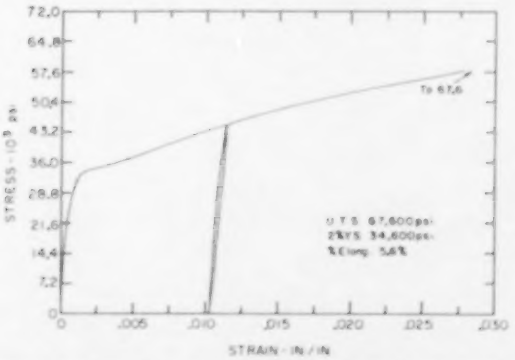


Fig. 9—Hot pressed, warm extruded beryllium rod round tensile specimen No. 31 was annealed at 800°C for 1 hr, slowly air cooled.

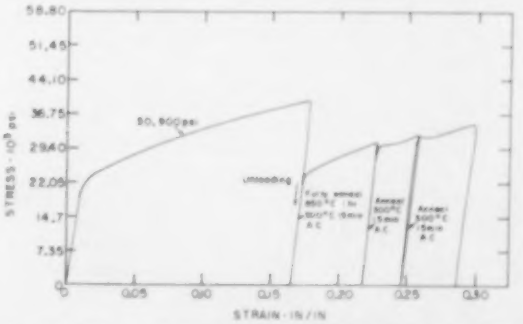


Fig. 11—Hot pressed, warm extruded beryllium round tensile specimen No. 50 was fully annealed at 850°C for 1 hr.



## Preliminary Examination of the Quenching of Titanium Alloys

ing information on low temperature solubility of these elements is scarce but it appears that the amounts in equilibrium are very small and one or more of the foregoing elements may contribute to the quench aging effects. In addition, copper is another possibility although not shown in the analysis of Table I. The elements oxygen, nitrogen, and carbon probably have a slight solubility in beryllium, and their presence may either directly or indirectly account for both quench and strain aging effects, since only very small solubility is necessary to promote aging effects.

A recognition of the yield point phenomenon and its apparent effect on mechanical properties in commercially pure beryllium is of importance in achieving a greater degree of uniformity of product as well as obtaining maximum properties. In both rod and plate specimens, it appears that production practices, fortuitously or not, have produced material closely approaching the best structural conditions as defined by this investigation. In this regard, it should be noted that the test material was on hand about one year before actual testing. The effect of this time interval on the characteristics of the *as-received* material is not known but may have had some bearing.

Another important fact to consider appears to be the apparent inhomogeneity of the material as shown by the variation in the resulting yield point effect in specimens treated alike. Furthermore, the difference in critical cooling rate between hot pressed plates and hot pressed, warm extruded rod point up the effect of specimen history on this study, but also could well indicate that difference in analysis exists between the two materials. It is known that each successive fabrication step in beryllium production results in some increase in impurity contents, especially in oxygen and iron.

The extensive strain associated with the sharp yield points in the specimens (in plate and in rods) is very interesting in the light of the present lack of knowledge of operative deformation processes in beryllium and presents a subject for further study.

A most striking fact to be gained from the tests on the rod specimens is that the high yield values are associated with the presence of the yield point; where no yield point is found, the yield strength values are much closer to those found in hot pressed plate products. The greater ductility is also associated with the presence of the aging effects in every case. It should be pointed out, also, that properties reported here were obtained using an extremely slow strain rate. Faster rates would be expected to produce higher values. In all cases, greater uniformity of properties was found by obtaining optimum conditions as represented by presence of the yield point phenomenon.

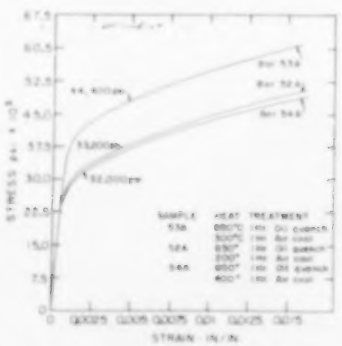


Fig. 12—Hot pressed, warm extruded beryllium rod shows the effect of several aging treatments on the yield strength.

## Summary and Conclusions

It has been found that marked differences in the mechanical properties and tensile stress-strain relationships of a number of beryllium tests specimens from the same lot of material could be effected by simple heat treatments. Furthermore, manifestations of both quench and strain aging phenomena have been found to exist.

A strong yield point was found to exist in the material with attendant enhanced mechanical properties under the following conditions:

1—*Hot Pressed Plate:* Full annealing was carried out from above 700°C (700° to 900°C range used in this study). Furnace cooling at approximately 2°C per min was employed.

2—*Hot Pressed, Warm Extruded Rods:* Rods were slowly air cooled at approximately 5° to 7°C per min from above 700°C (700° to 900°C range employed in this work).

Cooling in still air and faster rates of cooling from the *solution* treating range were found not to produce the yield point or any other aging effect in either type of specimen.

Furnace cooling of hot pressed, warm extruded bars from the solution range was found to show no yield point and exhibited lower tensile properties than material treated by other means.

Beryllium specimens were found to respond to both quench and strain aging treatments. Optimum conditions to show the maximum effect of such treatments probably have not been employed here, however.

It is felt that the foregoing information may possibly be employed to advantage in several ways:

1—Comprehensive investigation of alloying possibilities may uncover a means of increasing the mechanical properties of beryllium through a precipitation mechanism. Substitutionally soluble elements such as cobalt, aluminum, boron, iron, nickel, and copper may prove beneficial provided suitable heat treatment is employed.

2—Residual oxygen, carbon, or nitrogen may be responsible for the effects; in which case, a means of obtaining the optimum properties and product uniformity in the commercially pure material by suitable heat treatments after fabrication, such as already described, is indicated.

3—By an appreciation of these effects, close control of production variables such as cooling rates and chemical analyses will provide a commercially pure beryllium with the most uniform properties that are possible to obtain.

## Acknowledgment

This work was performed under the auspices of the U. S. Atomic Energy Commission.

Discussion of this paper, if any, will appear in JOURNAL OF METALS, May 1956, and in AIME Metals Branch *Transactions*, Vol. **206**, 1956.

## References

[1] W. W. Beaver: Fabrication of Beryllium by Powder Metallurgy. *Metal Progress* (1954) **65**, No. 4, p. 92.

[2] W. W. Beaver et al.: A Study of Factors Relating to the Consistency of Mechanical Properties in Extruded Beryllium. *NYO 1120* (Aug. 15, 1953).

[3] E. E. Baldwin and R. F. Koenig: Mechanical Properties of Beryllium. *KAPL 1049* (Feb. 15, 1954).

[4] W. W. Beaver and B. C. Raynes: Mechanical Properties of Beryllium Metal. I. Hot Pressed Powder. *BBC-48* (June 26, 1951).

# Preliminary Examination of the Quenching of Titanium Alloys

by Leonard D. Jaffe

**From the limited experimental data in the literature, preliminary values were derived for the thermal diffusivity of titanium alloys and for the quenching severity of various mediums used in heat treating them. The thermal diffusivity, under quenching conditions, was found to be approximately 0.006 sq in. per sec. The quenching severity *H* for brine is approximately 8, for water 4, for oil 0.9, for air 0.08, and for argon 0.02 in.$^{-1}$ The quenching severity of the Jominy-Boegehold end quench water jet against titanium alloys appeared effectively infinite. Using these results, graphs were prepared showing ideal round sizes and Jominy positions having cooled conditions equivalent to those at the center and surface of titanium alloy rounds, plates, and sheets quenched in various media.**

THE importance of proper quenching of steel parts has long been recognized, and much quantitative work has been done on the subject. Recently, it has become evident that for titanium alloys, too, the rate of cooling from high temperature is important in obtaining high strength and hardness. Maximum hardness and strength may not be attained in the as-quenched condition but rather after a subsequent tempering or aging treatment. Nevertheless, if cooling from temperatures near the $\beta$ transus is too slow, for the hardenability of the alloy used, a soft $\alpha$-$\beta$ structure will be produced which will not harden on subsequent aging.[1-4]

The quenching of parts of practical interest can usually be approximated by simple shapes, such as cylinders (*rounds*) and plates (or sheets) of various thickness and combinations of these. A standard that has been used extensively for comparison purposes is the center of an *ideal round:* a cylinder quenched in a medium that instantly cools its surface to room temperature.[5] For steel, considerable practical use has been made of the Jominy-Boegehold end quench hardenability specimen,[6,7] and its value for titanium alloys is becoming evident. It therefore appeared worthwhile to attempt comparison of cooling conditions in titanium alloy rounds and plates of various sizes quenched in various media with cooling conditions in ideal round and Jominy quenches. These comparisons are based upon measurements reported in the literature.

## Quenching Severity of Jominy Water Jet and of Brine

As one starting point, there were available the data of Phillips and Tobin[8] for positions on a Jominy specimen having the same hardness as the centers of round bars of various size quenched in 5 pct NaOH brine, shown in Table I. The Jominy specimen is a round bar, normally 1 in. diam and 4 in. long, quenched by a water jet at one end and air cooled on the other surfaces.[7] After quenching, hardness is measured vs distance from the quenched end on longitudinal flats ground 0.015 to 0.10 in. deep. The data of Table I were based on a subsized specimen of $\frac{3}{4}$ in. diam. Since the positions tested are close to the jet quenched end, cooling there may be taken as due solely to the jet, and air cooling can be neglected. These positions are then equivalent to various locations near one surface of an 8 in. plate jet quenched on both sides.

Table I. Equivalence of Jominy Distance to Center of Brine Quenched Round*

| | After Phillips and Tobin[8] | | | | |
|---|---|---|---|---|---|
| Round diam, in. | $\frac{1}{4}$ | $\frac{3}{8}$ | $\frac{1}{2}$ | $\frac{3}{4}$ | $\frac{1}{4}$ |
| Jominy distance, in. | $\frac{1.6}{16}$ | $\frac{2.0}{16}$ | $\frac{2.2}{16}$ | $\frac{2.4}{16}$ | $\frac{2.6}{16}$ |

* Commercial 3.5 pct Mn, 2.2 pct Al, and 0.11 pct C titanium alloy, quenched from 1635°F. Based on equal hardness as-quenched in 5 pct NaOH brine.

Assuming that the thermal diffusivity is constant and that Newton's law of cooling holds, temperature vs time curves at corresponding positions in Jominy specimen and round bar then may be calculated for various assumed quenching severities of the water jet and of the brine. Cooling curves are generally taken to be metallurgically equivalent when they show the same time to reach a temperature halfway between the initial (heat treating) temperature and the final (quenching medium) temperature.[9] On this basis, using Russell's tables,[9] supplemented by heat flow tables derived in similar fashion by the author for positions near the surface of severely quenched plates, it was found that the experimentally observed equivalence, Table I, was best matched if the quenching severity $H$ of the Jominy water jet was taken as infinite ($H = \infty$). This means that the jet quenched surface should be considered as instantly cooled to the temperature of the water

L. D. JAFFE, Member AIME, formerly associated with Ordnance Materials Research Office, Watertown Arsenal, Watertown, Mass., is Chief, Materials Section, Jet Propulsion Laboratory, California Institute of Technology, Pasadena, Calif.

Discussion of this paper, TP 4026E, may be sent, 2 copies, to AIME by Jan. 1, 1956. Manuscript, July 27, 1954. Philadelphia Meeting, October 1955.

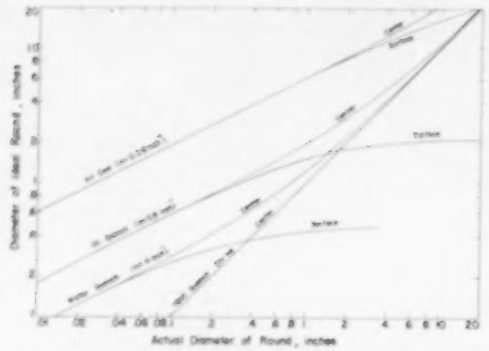


Fig. 1—Sizes of actual and ideal rounds having equivalent cooling conditions are compared.

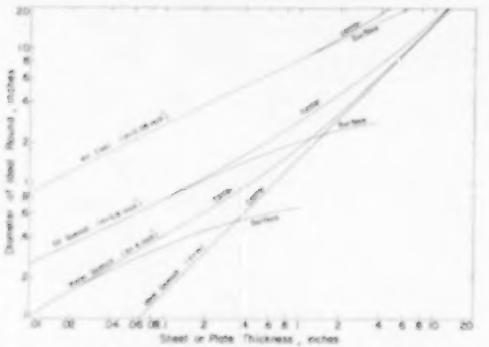


Fig. 2—Sizes of plate or sheet and ideal round having equivalent cooling conditions are compared.

(ideal quench). With this value for the jet, the ideal round size equivalent to a 2.2/16 in. Jominy distance was calculated, using the author's tables, to be 0.631 in. As the corresponding brine quenched round size was measured at ½ in. (Table I), this indicates, according to the curves of Hollomon and Zener,[10] that the quenching severity $H$ of the brine against titanium alloy was 8.0 in.$^{-1}$. The curves referred to are based on equal cooling coefficient, which is thought to be the best basis for comparison of cooling curves at center positions.[11]

## Diffusivity

The calculations described previously do not require a knowledge of the thermal diffusivity $a$. The later quantity may be obtained, on the same assumptions, from Phillips and Tobin's measurements

Table II. Cooling Rates at Center of ½ In. Sq Titanium Alloy Bars Quenched in 5 Pct NaOH Brine

| Composition | Quenched From °F | Rate At °F | Rate,* °F per Sec | Calculated Thermal Diffusivity, Sq In. per Sec |
|---|---|---|---|---|
| 3.5 pct Mn, 3.2 pct Al, 0.11 pct C | 1800 | 1600 | >500 | >0.0090 |
| | | 1400 | 340 | 0.0054 |
| | | 1800 to 1200 | 240 | 0.0064 |
| 7.9 pct Mn, 0.13 pct C | 1650 | 1600 | 450 | 0.0076 |
| | | 1200 | 230 | 0.0043 |
| | | 1650 to 1200 | 170 | 0.0054 |
| | | Mean | | 0.006 |

* Data of Phillips and Tobin.[5]

Table III. Cooling Rates at Center of Oil Quenched Titanium Alloy Bars and Sheet

| Composition | Quenched From °F | Size | Rate At °F | Rate,* °F per Sec | Calculated Quenching Severity, $H$, In.$^{-1}$ |
|---|---|---|---|---|---|
| 3.5 pct Mn, 3.2 pct Al, 0.11 pct C | 1800 | ½ in. sq bar | 1450 | 120 | 1.16 |
| | | | 1400 | 85 | 0.78 |
| | | | 1800 to 1200 | 40 | 0.34 |
| | | 0.1 in. sheet | 1200 | >500 | >1.8 |
| | | | 1400 | 330 | 1.04 |
| | | | 1800 to 1200 | 120 | 0.35 |
| 7.9 pct Mn, 0.13 pct C | 1650 | ½ in. sq bar | 1450 | 180 | 2.6 |
| | | | 1200 | 70 | 0.76 |
| | | | 1650 to 1200 | 55 | 0.62 |
| | | 0.1 in. sheet | 1200 | >500 | >1.9 |
| | | | 1650 to 1200 | 180 | 0.48 |
| | | Geometric Mean | | | 0.9 |

* Data of Phillips and Tobin.[5]

of cooling rates at the center of brine quenched ½ in. sq bars, Table II. A ½ in. sq bar may be considered, for heat flow calculations, as the volume common to two perpendicular intersecting ½ in. plates. Using Russell's tables for plates, the thermal diffusivity that would give the observed cooling rates was calculated for quenching severity $H = 8.0$ in.$^{-1}$, with the results shown in Table II. The average of the calculated values is 0.006 sq in. per sec. This may be taken as a preliminary value for the thermal diffusivity of $\beta$ titanium containing some alloying elements in the range 1800° to 1000°F.

## Quenching Severity of Other Mediums

Once the diffusivity is known, quenching severity for other mediums can be calculated from cooling curves. Table III shows the data for oil, leading (by means of Russell's tables) to a calculated quenching severity $H = 0.9$ in.$^{-1}$. For air and argon, severities were low enough so that the cooling could be considered exponential with time, simplifying the computations. Tables IV and V show the data, leading to the calculated severities of $H = 0.08$ in.$^{-1}$ for air and $H = 0.020$ in.$^{-1}$ for argon.

By comparing the calculated severities of brine, oil, air, and argon with measured cooling rates for a Ni-Cr alloy quenched in these and other media,[12-14] quenching severities for other media used in quenching titanium alloys were estimated. Table VI gives the results. The degree of circulation or agitation during quenching of the titanium alloys was not given but was probably moderate.

Having the quenching severities, it is possible to find the size of the round bar quenched in a medium of infinite $H$ (ideal round size) whose center cools at a rate equivalent to that anywhere within a simple shape quenched in any of the media listed. Methods for center positions[10] and for other positions[11, 15] are given in the literature. To simplify

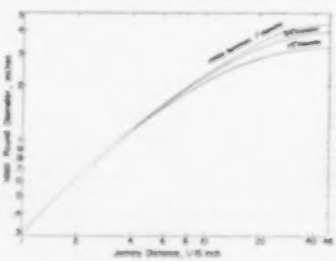

Fig. 3—Jominy distance and ideal round size having equivalent cooling conditions are compared.

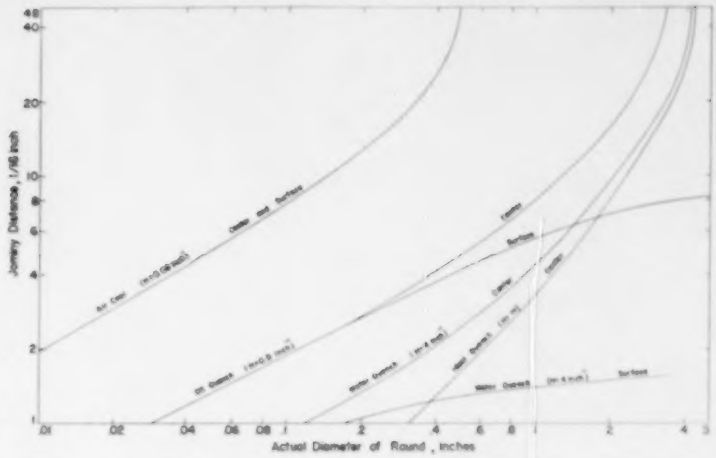


Fig. 4—Round size and Jominy distance having equivalent cooling conditions are compared. Jominy specimen has a 1 in. diam.

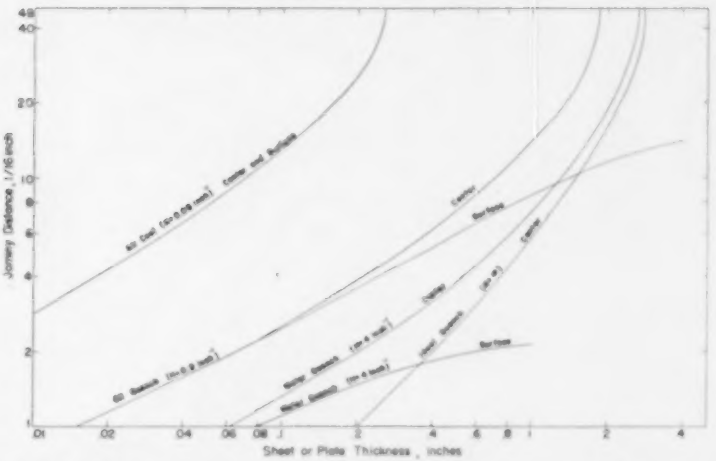


Fig. 5—Plate or sheet size and Jominy distance having equivalent cooling conditions are compared. Jominy specimen has a 1 in. diam.

application, Figs. 1 and 2 were calculated from the references cited and permit direct comparison of cooling conditions at center and surface of titanium alloy rounds, plates, and sheet, quenched in water ($H = 4$ in.$^{-1}$), oil ($H = 0.9$ in.$^{-1}$), and air ($H = 0.08$ in.$^{-1}$), with those at the center of an ideally quenched ($H = \infty$) round.

## Cooling Conditions in Jominy Specimens

Next, the positions on the end quench hardenability specimen having cooling conditions equivalent (half-temperature time) to those at the center of ideal rounds of various sizes were calculated, using Russell's tables. Water jet quenching of one end with $H = \infty$ and air cooling of the sides and opposite end with $H = 0.08$ in.$^{-1}$ were considered for specimens 4 in. long and 1, ¾, and ½ in. diam. Fig. 3 gives the results.

From Figs. 1 through 3, the positions on 1 in. diam Jominy specimens having cooling conditions equivalent to those at center and surface of rounds, plates, and sheets quenched in water, oil, and air were obtained and are plotted in Figs. 4 and 5.

## Discussion

The limitations of the Grossmann-Asimow[8,10,19] approach to equivalence of cooling conditions, as applied to steel, have been discussed by a number of authors.[11,17-18] Since the same limitations generally hold when the material considered is titanium alloy, they need not be reviewed here. The approach, despite its limitations, has proved to be of value for steel.

The scatter in the calculated quantities for brine and oil quenching, shown in Tables II and III, is certainly due primarily to the assumption that the quenching severity is independent of temperature. For these media which boil during the quench, it is well known that there are three stages of quenching—vapor blanket, vapor transport, and liquid

Table IV. Cooling Rates at Center of Air Cooled Titanium Alloy Bars and Sheet

| Composition | Cooled From °F | Size | Rate At °F | Rate,* °F per Sec | Calculated Quenching Severity, $H$, In.$^{-1}$ |
|---|---|---|---|---|---|
| 3.5 pct Mn, 3.2 pct Al, 0.11 pct C | 1800 | ½ in. sq bar | 1700 | 16 | 0.101 |
| | | | 1400 | 9 | 0.070 |
| | | | 1800 to 1200 | 8.5 | 0.062 |
| | | 0.1 in. sheet | 1600 | 40 | 0.108 |
| | | | 1400 | 27 | 0.084 |
| | | | 1800 to 1200 | 24 | 0.070 |
| | | | 1400 | 13.5 | 0.098 |
| 7.9 pct Mn, 0.13 pct C | 1650 | ½ in. sq bar | 1200 | 7 | 0.064 |
| | | | 1650 to 1200 | 10 | 0.078 |
| | | | 1400 | 23 | 0.087 |
| | | 0.1 in. sheet | 1200 | 18 | 0.066 |
| | | | 1650 to 1200 | 21 | 0.066 |
| | | | | Mean | 0.08 |

* Data of Phillips and Tobin.[4]

cooling—and the quenching severity differs from stage to stage.[15,16,22] For air and argon quenches where there is but one stage, the scatter is much less, Tables IV and V.

The thermal diffusivity found for titanium alloy (0.006 sq in. per sec) is somewhat lower than that accepted for steel (0.009 sq in. per sec).[16,23] The quenching severities, Table VI, are about three times as high as those accepted for steel, under conditions of moderate circulation or agitation.[16,23] While other factors are involved, the lower thermal conductivity of titanium, compared to that of iron, contributes to both of these differences.

It must be recognized that the values reported here are of a preliminary nature, not only because of the inherent limitations of the method but also because they are based upon experiments not designed primarily to obtain such data.

Table V. Cooling Times for Argon Cooled Titanium Alloy Bars*

| Time, Min | Temperature,† °C | Calculated Quenching Severity, $H$, In.$^{-1}$ |
|---|---|---|
| 1 | 590 | 0.020 |
| 2 | 450 | 0.021 |
| 3 | 375 | 0.019 |
| 5 | 270 | 0.018 |
| | Mean | 0.020 |

* 0.225 in. round bars, of several compositions, cooled from 750°C.
† Data of Holden, Ogden, and Jaffee.[12]

An experimental program aimed specifically at obtained diffusivity and quenching severity for titanium alloys is certainly desirable. In the interim, however, it is hoped that the results given here will be of practical value.

## Conclusions

On the basis of the limited experimental data in the literature, preliminary values have been derived for the thermal diffusivity of alloyed titanium under quenching conditions (approximately 0.006 sq in. per sec) and for severity of quench of this material in brine, water, oil, air, and argon ($H$ = 8, 4, 0.9, and 0.02 in.$^{-1}$, respectively). The quenching severity of the water jet used in the end quench hardenability test of titanium alloys was found to be effectively infinite.


## Acknowledgment

The author would like to thank C. W. Phillips, University of Michigan, for permission to use unpublished material.

Discussion of this paper, if any, will appear in JOURNAL OF METALS, May 1956, and in AIME Metals Branch *Transactions*, Vol. **206**, 1956.


## References


[1] W. M. Parris, P. D. Frost, and J. H. Jackson: Heat Treatment of High Strength Titanium Base Alloys. *Trans.* ASM (1954) **46**, pp. 568-586.

[2] H. D. Kessler and M. Hansen: Transformation Kinetics and Mechanical Properties of Titanium-Aluminum-Molybdenum Alloys. *Trans.* ASM (1954) **46**, pp. 587-608.

[3] L. D. Jaffe: Heat Treatment of Titanium Generalized in Terms of Beta Prime. *Trans.* AIME (1954) **200**, p. 210; JOURNAL OF METALS (February 1954).

[4] L. D. Jaffe: Heat Treatment of Titanium. *Metal Progress* (1955) **67**, No. 2, pp. 101-108. Choosing a Titanium Alloy. *Metal Progress* (1955) **67**, No. 3, pp. 104-108.

[5] M. A. Grossmann, M. Asimow, and S. F. Urban: Hardenability, Its Relation to Quenching, and Some Quantitative Data. *Hardenability of Alloy Steels.* (1939) pp. 124-196. Cleveland, ASM.

[6] W. E. Jominy and A. L. Boegehold: Hardenability Test for Carburizing Steel. *Trans.* ASM (1938) **26**, pp. 574-606.

[7] *Method of Determining Hardenability of Steels.* (1953) New York. SAE Handbook. Also, Amer. Soc. for Testing Materials Std. A255-487.

[8] C. W. Phillips and J. C. Tobin: *Phase Transformations and Heat-Treatability of Titanium-Base Alloys.* To be published. University of Michigan Final Report to Watertown Arsenal, WAL 401/81-18 (June 1953).

[9] T. F. Russell: Some Mathematical Considerations on the Heating and Cooling of Steel. *First Report* Alloy Steels Research Committee, Iron and Steel Inst. (1936) pp. 149-187.

[10] J. H. Hollomon and C. Zener: Quenching and Hardenability of Hollow Cylinders. *Trans.* ASM (1944) **33**, pp. 1-18.

[11] J. H. Hollomon and L. D. Jaffe: *Ferrous Metallurgical Design.* (1947) pp. 61-75, 175-195. New York. John Wiley and Sons.

[12] F. C. Holden, H. R. Ogden, and R. I. Jaffee: Heat Treatment, Structure, and Mechanical Properties of Ti-Mn Alloys. *Trans.* AIME (1954) **200**, pp. 169-184; JOURNAL OF METALS (February 1954).

[13] F. Wever: The Theory and Practice of Steel Hardening. *Archiv für Eisenhüttenwesen* (1936-1937) **5**, p. 367.

[14] H. Scott, G. T. Williams, and B. F. Shepherd: Quenching Mediums. *Metals Handbook.* (1948) pp. 615-620. Cleveland, ASM.

[15] M. A. Grossmann and M. Asimow: Hardenability and Quenching. *Iron Age* (1940) **145**, No. 17, pp. 25-29; No. 18, pp. 39-45.

[16] M. Asimow and M. A. Grossmann: Hardening Characteristics of Various Shapes. *Trans.* ASM (1940) **28**, pp. 949-985.

[17] Symposium on the Hardenability of Steel. *Special Report No. 36* Iron and Steel Inst. (1946).

[18] F. W. Jones and W. I. Pumphrey: Some Experiments on Quenching Media. *Journal* Iron and Steel Inst. (1947) **156**, pp. 37-54.

[19] D. J. Carney and A. D. Janulionis: Examination of the Quenching Constant, H. *Trans.* ASM (1951) **43**, pp. 480-496.

[20] A. R. Troiano and L. J. Klinger: Limitations of the End-Quench Hardenability Test. *Trans.* ASM (1952) **44**, pp. 775-802.

[21] E. W. Weinman, R. F. Thompson, and A. L. Boegehold: Correlation of End-Quenched Test Bars and Rounds in Terms of Hardness and Cooling Characteristics. *Trans.* ASM (1952) **44**, pp. 803-844.

[22] D. J. Carney: Another Look at Quenchants, Cooling Rate and Hardenability. *Trans.* ASM (1954) **46**, pp. 882-927.

[23] N. B. Pilling and T. D. Lynch: Cooling Properties of Technical Quenching Liquids. *Trans.* AIME (1920) **72**, pp. 665-668.

[24] T. F. Russell and J. C. Williamson: Surface Temperature Measurements During the Cooling of a Jominy Test-Piece. Symposium on the Hardenability of Steel. *Special Report No. 36* Iron and Steel Inst. (1946) pp. 34-46.

[25] M. A. Grossmann: Hardenability Calculated From Chemical Composition. *Trans.* AIME (1942) **150**, pp. 226-259; METALS TECHNOLOGY (June 1942).


Table VI. Quenching Severity for Various Media Against Titanium Alloys

| Medium | Quenching Severity, $H$, In.$^{-1}$ |
|---|---|
| 20 pct NaOH (−12°C) | 8.5 |
| Iced brine | 8.5 |
| 5 pct NaOH | 8.0 |
| Brine | 8.0 |
| Ice water | 4.2 |
| Water | 4.0 |
| Oil | 0.9 |
| Boiling water | 0.2 |
| Air | 0.08 |
| Argon | 0.02 |

# Hardenability of Titanium Alloys Calculated from Composition: A Preliminary Examination

by Leonard D. Jaffe

**From data found in the literature, a method has been derived for calculating hardenability of titanium alloys from their composition. A single graph gives the contributions of each alloying element. These are simply added to a base hardenability for unalloyed titanium. Results agree satisfactorily with measured hardenabilities.**

RECENTLY the importance of hardenability of titanium alloys in permitting attainment of high strength and hardness has become apparent. If a titanium-base alloy has adequate hardenability for the section size and quenching practice used, it can generally be heat treated to high strength and hardness either by simple quenching or cooling from temperatures near the $\beta$ transus, by quenching and tempering (aging), or perhaps by direct isothermal transformation of $\beta$.[1, 2] If the hardenability is inadequate, high strength cannot be attained. Preliminary charts translating hardenability requirements for shapes quenched in various media into terms of Jominy end quenched hardenability specimens or ideal round sizes are now available for titanium alloys.[3]

The method proposed in 1942 by M. A. Grossmann for calculating hardenability of steels from composition has proved to be of great practical value.[4] It appeared worthwhile to see whether, using information available in the literature, a corresponding method for calculating hardenability of titanium-base alloys could be derived.

## Data

No systematic experimental study of the hardenability of titanium-base alloys has yet been made. There is available, however, a considerable quantity of scattered data bearing on hardenability. Some investigators determined Jominy curves on one or several alloys. Others reported as-quenched hardness for specimens of a few alloys cooled at various rates or in various media. Still others gave the as-quenched hardness for systematically varied composition, using one or several cooling mediums.

The measurements utilized in this work were limited to hardness. Strength measurements were not used because a low strength may reflect high hardness combined with brittleness. Since, in general, the hardness of titanium alloys goes through a peak as the cooling rate is varied from extremely fast to extremely slow, the cooling conditions at which peak hardness was found were taken as the measure of hardenability.[1, 2]

When as-quenched hardness was found to drop as the content of an alloying element (believed to increase hardenability) was raised, this was taken as an indication that the cooling rate was faster than that giving peak hardness; otherwise, the hardness should go up because of solid solution hardening. Also, if the hardness increased on tempering at low temperatures, this was again taken to indicate that the cooling rate had been faster than that giving peak hardness. Many of the data did not indicate precisely the cooling conditions for peak hardness but merely set a maximum or a minimum bound, or a bracket. Since the sizes of specimens quenched and the location of the hardness readings were not always given, it was occasionally necessary to estimate reasonable limits for them. Only the nominal compositions were available in some cases. As quenching from below the $\beta$ transus is equivalent to starting with a mixture of $\alpha$ and $\beta$ phases, whose individual composition would differ from the overall composition of the alloy, only measurements after quenches from above the $\beta$ transus were used. Hardness measurements on samples heated during metallographic mounting were also discarded.

Because of their bulk, the data used will not be reproduced. They have been or will be published elsewhere.[5-10]

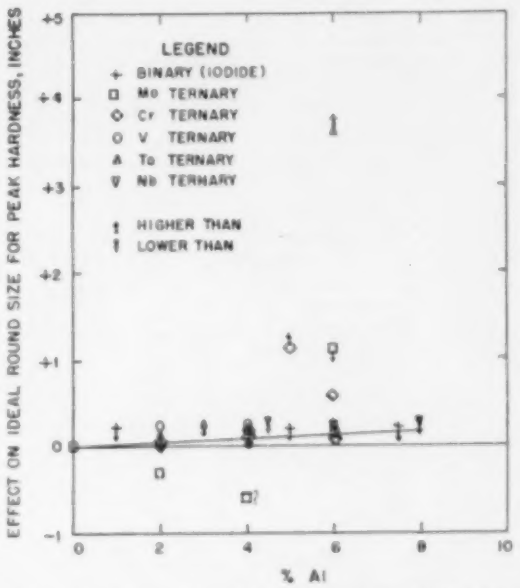


Fig. 1—Data are shown for the effect of aluminum on hardenability of titanium alloys. The curve drawn is based on tabulated numerical values.

## Approach

All data were first translated into terms of ideal round size. For conversion from Jominy or quenched round or sheet, the author's graphs were used.[3] For a few furnace cools or helium quenches where cooling rates were given, conversion was made on the basis of equal cooling coefficient.[11]

Plots of ideal round size for peak hardness against percentage of alloying element were next made for

L. D. JAFFE, Member AIME, formerly associated with Ordnance Materials Research Office, Watertown Arsenal, Watertown, Mass., is Chief, Materials Section, Jet Propulsion Laboratory, California Institute of Technology, Pasadena, Calif.

Discussion of this paper, TP 4025E, may be sent, 2 copies, to AIME by Jan. 1, 1956. Manuscript, July 27, 1954. Philadelphia Meeting, October 1955.

binary alloys of titanium with molybdenum, chromium, vanadium, iron, and manganese. Some measurements were also available for binary alloys with aluminum, copper, and tantalum, but since these set only maximum bounds for ideal round size of all compositions, no plots could be made. Experimental data were available on eleven ternary or more complex alloys containing, nominally, only titanium and elements covered by the plots. The effects of individual alloying elements, read from the plots, were combined both additively and multiplicatively and compared with the experimental ideal round sizes for the eleven complex alloys. In these comparisons, the ideal round size for peak hardness in unalloyed titanium was used as an undetermined parameter and adjusted to provide best overall fit. The best fit for the additive scheme was obtained with an assumed ideal round size of 0.12 in. for unalloyed titanium. For the multiplicative scheme, best fit was obtained with an assumed 0.50 in. for unalloyed titanium.

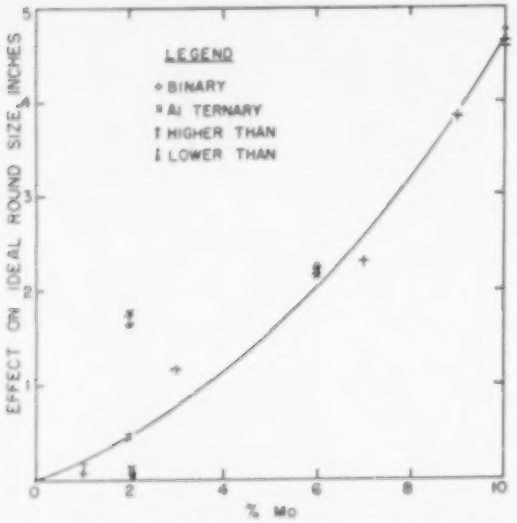


Fig. 2—Data are shown for the effect of molybdenum on the hardenability of titanium alloys.

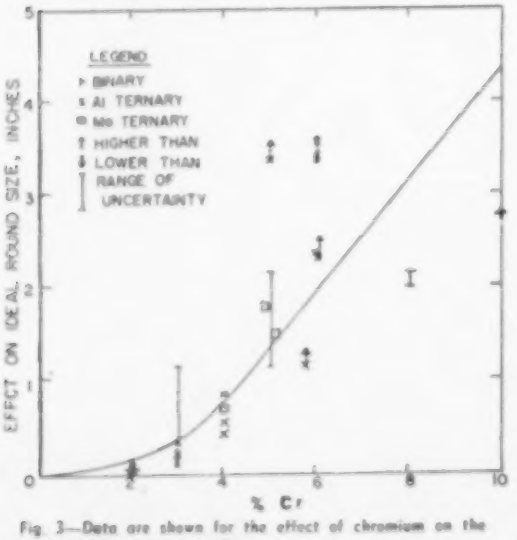


Fig. 3—Data are shown for the effect of chromium on the hardenability of titanium alloys.

At best fit, the average difference between calculated and experimental ideal round size for the complex alloys was 19 pct for additive combination and 25 pct for multiplicative. Also, the measured ideal round size for peak hardness of unalloyed titanium was under 0.16 in. Assuming such a value for the multiplicative scheme made the calculated values for the alloys differ from the measured by a factor of three or more in many cases. Finally, the additive scheme is simpler to use than the multiplicative. For these three reasons, attempts at deriving a multiplicative scheme were abandoned and attention concentrated on the additive method.

The hardenability of Ti-Al alloys was apparently too low to permit satisfactory measurement. The effect of aluminum on hardenability was therefore obtained from measurements on ternary alloys of titanium and aluminum with chromium, molybdenum, vanadium, iron, manganese, tantalum, and columbium, in which the content of the third element was held constant. The results are plotted in Fig. 1.

Measurements on both Ti-Mo binary alloys and Ti-Mo-Al ternaries were then used to obtain the effect of molybdenum, Fig. 2. Next, the effect of chromium was determined from data on alloys with titanium, aluminum, and molybdenum, Fig. 3. The effects of vanadium, iron, manganese, and carbon were successively found in similar fashion, Figs. 4 through 7. The few data available on nitrogen additions led to inconclusive results for nitrogen. For oxygen only a single datum was found: the measured hardenability of a chrome-iron alloy with nominally 0.30 pct O was 0.39 in. lower than that calculated for the normal sponge content of about 0.1 pct O; oxygen apparently lowered the hardenability about 0.2 in. per 0.1 pct O. On this basis, the hardenability of unalloyed iodide titanium would be 0.2 in. as compared to 0.1 in. for sponge of good quality, which was used in preparing most of the alloys discussed. No measurements pertaining to effect of hydrogen were found.

## Results

Fig. 8 summarizes the effects of the various ele-

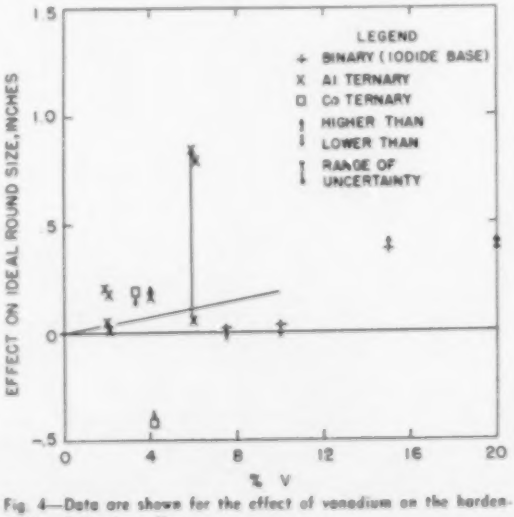


Fig. 4—Data are shown for the effect of vanadium on the hardenability of titanium alloys.

ments investigated. The hardenability of a titanium-base alloy of known composition may then be found by adding the effects of the separate elements, as given in Fig. 8, to the base value for unalloyed titanium: 0.1 in. for sponge or 0.2 in. for iodide. (These base values are so small that they can often be neglected.) The answer will be the ideal round size having peak as-quenched hardness. Conversion to the Jominy distance at which peak hardness will occur may be made by a chart presented in a companion paper.[4]

The validity of Fig. 8 was examined by comparing hardenability calculated for it with measured hardenability for all alloys for which precise hardenability measurements were available (essentially, for which position of peak hardness on a Jominy bar had been determined). Table I shows the compositions, Fig. 9 the results. The difference between calculated and measured hardenability averages 17 pct. Part of the difference is doubtless due to error in the hardenability measurement; the median difference is only 9 pct.

## Discussion

It is interesting to note that carbon and oxygen lower hardenability of titanium alloys, in accord with reports that they accelerate isothermal decomposition of $\beta$.[5-8] Nitrogen, for which results were not obtained, probably does likewise. Although under equilibrium conditions aluminum stabilizes $\alpha$ at the expense of $\beta$,[1] it nevertheless increases hardenability slightly. Vanadium also increases hardenability slightly, perhaps more so than indicated by the curves drawn. Manganese raises hardenability moderately. Chromium, molybdenum, and iron add greatly to hardenability.

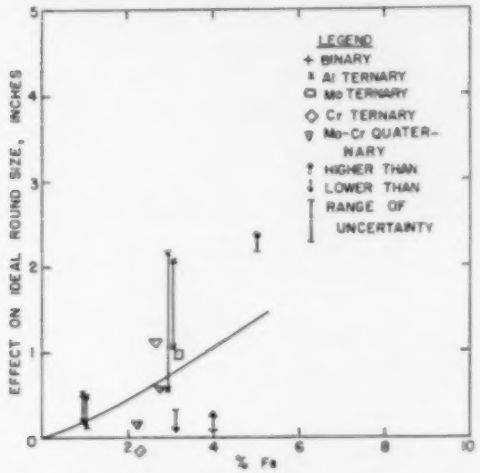


Fig. 5—Data are shown for the effect of iron on the hardenability of titanium alloys.

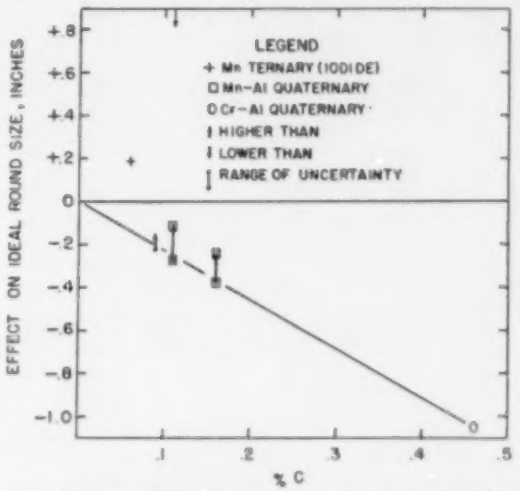


Fig. 7—Data are shown for the effect of carbon on the hardenability of titanium alloys.

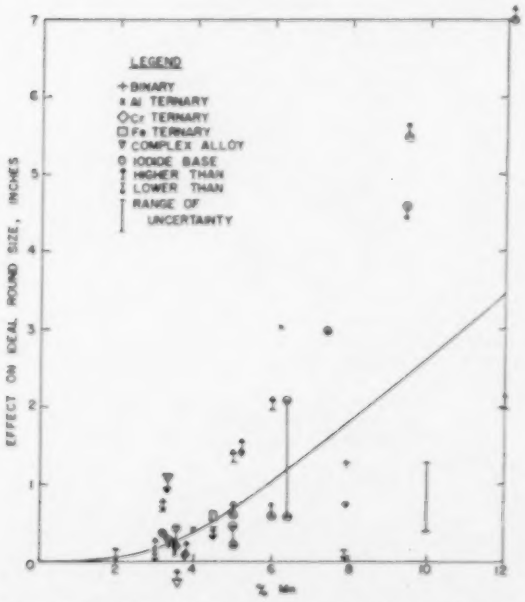


Fig. 6—Data are shown for the effect of manganese on the hardenability of titanium alloys.

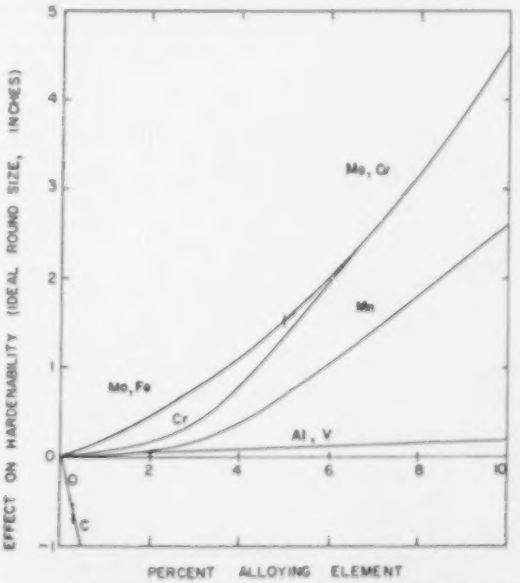


Fig. 8—The effect of alloying elements upon the hardenability of titanium alloys is summarized.

Table I. Comparison of Calculated and Measured Hardenabilities of Titanium-Base Alloys

| Composition, Pct | Hardenability, Ideal Round Size, In. | | Literature Reference |
|---|---|---|---|
| | Calculated | Measured | |
| 7 Mo | 2.6 | 2.4* | 21 |
| 9 Mo | 4.0 | 4.0* | 8 |
| 7.9 Mn | 1.9 | 1.4 | 16 |
| 5.0 Cr, 2.3 Fe | 2.0 | 1.4 | 8 |
| 4.3 Mn, 3.2 Fe | 2.2 | 2.4 | 8 |
| 4.5 Mn, 0.84 Fe | 0.8 | 0.9 | 8 |
| 4.0 Cr, 2.3 Mo | 1.4 | 1.4 | 8 |
| 4.9 Cr, 2.0 Mn | 1.8 | 2.4 | 8 |
| 5.1 Cr, 1.9 Mo | 2.0 | 2.0 | 8 |
| 2 Mn, 2 Al | 0.6 | 0.6 | 12 |
| 6 Mn, 2 Al | 2.2 | 2.4 | 12 |
| 6 Mo, 4 Al | 2.2 | 2.4 | 12 |
| 4 Cr, 2 Al | 0.9 | 0.6 | 13 |
| 4 Cr, 4 Al | 1.0 | 0.8 | 13 |
| 4 Cr, 6 Al | 1.0 | 1.1 | 13 |
| 6 Cr, 2 Al | 2.1 | 2.5 | 13 |

* Based on several measurements. Other values are single measurements.

The ideal round size calculated by the method described is that at which the particular composition will have peak hardness. Somewhat lower hardenability may be acceptable in practice, since peak hardness need not always be attained. It is advisable, however, to have enough hardenability so that hardness well above that required for service will be reached on quenching or on quenching and aging. This extra hardness is needed because overaging, slower cooling procedures, etc., will usually introduce some softening.[1, 2, 10] Hardenability corresponding to peak hardness should therefore be a good general guide.

Hardenability of titanium alloys can be increased somewhat by quenching from below rather than above the $\beta$ transus (from the $\alpha$-$\beta$ range rather than from the all-$\beta$ range), since this practice generally enriches the $\beta$ in alloying elements.[1, 10] The calculation scheme given here refers to alloys quenched from the $\beta$ transus; it might be possible to apply it to alloys quenched from below the transus by using, in calculation, the estimated composition of the $\beta$ phase prior to quenching.

It is obvious that somewhat different curves could be drawn through the points of Figs. 1 through 7 and that a scheme for hardenability could be better based upon a direct and systematic experimental program. Until such a program is complete and in view of the satisfactory agreement shown in Fig. 8, it is believed that the scheme outlined may be used as an interim tool. Since it is empirical, it should not be extrapolated very far.

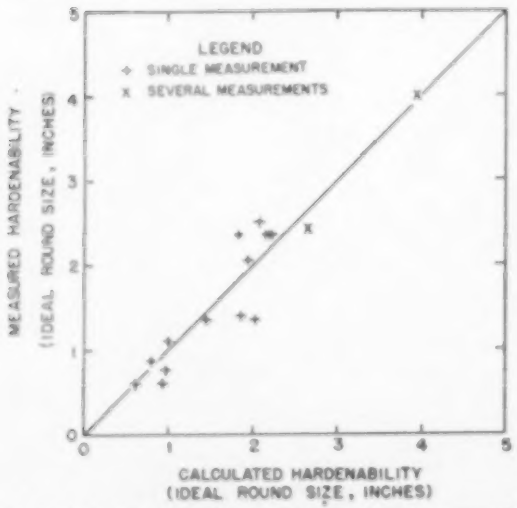


Fig. 9—Calculated hardenability of titanium alloys is compared with good hardenability measurements.

## Conclusions

A preliminary method has been derived for calculating the hardenability of titanium alloys from their composition. It consists of adding contributions for individual alloying elements to a base hardenability for unalloyed titanium. Results are in satisfactory agreement with the good hardenability measurements so far reported.

Discussion of this paper, if any, will appear in JOURNAL OF METALS, May 1956, and in AIME Metals Branch *Transactions*, Vol. **206**, 1956.

## References


[1] L. D. Jaffe: Heat Treatment of Titanium Generalized in Terms of Beta Prime. *Trans.* AIME (1954) **200**, p. 210; JOURNAL OF METALS (February 1954).

[2] L. D. Jaffe: Heat Treatment of Titanium. *Metal Progress* (1955) **67**, No. 3, pp. 101-108. Choosing a Titanium Alloy. *Metal Progress* (1955) **67**, No. 3, pp. 104-108.

[3] L. D. Jaffe: Preliminary Examination of the Quenching of Titanium Alloys. *Trans.* AIME (1955) **203**, pp. 1241-1244; JOURNAL OF METALS.

[4] M. A. Grossmann: Hardenability Calculated From Chemical Composition. *Trans.* AIME (1942) **150**, pp. 226-259; METALS TECHNOLOGY (June 1942).

[5] H. L. Adenstedt, J. R. Pequinot, and J. M. Raymer: Titanium-Vanadium System. *Trans.* ASM (1952) **44**, pp. 990-1003.

[6] F. R. Brotzen, E. L. Harmon, and A. R. Troiano: Decomposition of Beta Titanium. *Trans.* AIME (1955) **203**, pp. 413-419; JOURNAL OF METALS (February 1955).

[7] E. S. Bumps, H. D. Kessler, and M. Hansen: Titanium-Aluminum System. *Trans.* AIME (1952) **194**, pp. 609-614; JOURNAL OF METALS (June 1952).

[8] C. R. Cook, Jr.: Titanium Alloys. To be published; Alleghany-Ludlum Steel Corp. Final Report to Watertown Arsenal, WAL 401/26-34 (April 1953).

[9] D. J. DeLazaro and W. Rostoker: Correlation Between Microstructure and Mechanical Properties of Titanium-Molybdenum Alloys. *Trans.* ASM (1954) **46**, pp. 292-311.

[10] F. C. Holden, H. R. Ogden, and R. I. Jaffee: Heat Treatment, Structure, and Mechanical Properties of Ti-Mn Alloys. *Trans.* AIME (1954) **200**, pp. 169-184; JOURNAL OF METALS (February 1954).

[11] H. R. Ogden, F. C. Holden, and R. I. Jaffee: Effect of Alpha Solutes on the Heat-Treatment Response of Ti-Mn Alloys. *Trans.* AIME (1955) **203**, pp. 105-112; JOURNAL OF METALS (January 1955). Also, F. C. Holden, A. A. Watts, H. R. Ogden, and R. I. Jaffee: Heat Treatment and Mechanical Properties of Ti-Cu Alloys. *Trans.* AIME (1955) **203**, pp. 117-125; JOURNAL OF METALS (January 1955).

[12] H. D. Kessler and M. Hansen: Transformation Kinetics and Mechanical Properties of Titanium-Aluminum-Molybdenum Alloys. *Trans.* ASM (1954) **46**, pp. 587-608.

[13] H. D. Kessler and M. Hansen: Transformation Kinetics and Mechanical Properties of Titanium-Aluminum-Chromium Alloys. *Trans.* ASM (1954) **46**, pp. 609-639.

[14] H. D. Kessler: Improving Titanium-Aluminum Binary Alloys by Addition of a Third Component. To be published; Armour Research Foundation Interim Reports to Watertown Arsenal, WAL 401/103 series.

[15] L. Luini and E. Lee: Investigation of the Heat Treatment of Commercial Titanium-Base Alloys. *Trans.* AIME (1954) **200**, pp. 581-592; JOURNAL OF METALS (May 1954).

[16] H. Martens: Effect of Cooling Rate on Hardness of

Commercial Titanium Alloys. To be published. *Trans.* AIME (1956) **206**.

[17] H. R. Ogden, D. S. Mayku'h, W. L. Finlay, and R. I. Jaffee: Mechanical Properties of High Purity Titanium-Aluminum Alloys. *Trans.* AIME (1953) **197**, pp. 267-272; JOURNAL OF METALS (February 1953).

[18] W. M. Parris, P. D. Frost, and J. H. Jackson: Heat Treatment of High Strength Titanium-Base Alloys. *Trans.* ASM (1954) **46**, pp. 568-586.

[19] W. M. Parris, L. L. Hirsch, P. D. Frost, and J. H. Jackson: Development of Titanium-Base Alloys. To be published; Battelle Memorial Institute Reports to Materials Laboratory, Wright-Patterson Air Force Base (1952-1953).

[20] C. W. Phillips and J. C. Tobin: Phase Transformation and Heat-Treatability of Titanium Base Alloys. To be published; University of Michigan Final Report to Watertown Arsenal, WAL 401/81-18.

[21] W. Rostoker, D. J. McPherson, D. J. DeLazaro, and M. Hansen: Structural Changes of Commercial Titanium and Titanium Base Alloys on Heat Treatment. To be published; Armour Research Foundation Reports to Flight Research Laboratory (1951-1953).

[22] H. W. Worner: Heat Treatment of Titanium-Rich Titanium Iron Alloys. *Journal* Inst. of Metals (1951-1952) **80**, pp. 213-216.

[23] J. H. Hollomon and L. D. Jaffe: *Ferrous Metallurgical Design.* (1947) pp. 70-75, 182. New York. John Wiley and Sons.

[24] D. J. DeLazaro and W. Rostoker: Influence of Oxygen Content on Transformations in a Titanium Alloy Containing 11 Per Cent Molybdenum. *Acta Metallurgica* (1953) **1**, pp. 674-678.

# Recrystallization Textures of a Cold-Rolled Aluminum Single Crystal

by Y. C. Liu and W. R. Hibbard, Jr.

**An aluminum single crystal cold-rolled from (110) [1$\bar{1}$2] essentially retains its initial orientation after 99.6 pct reduction in thickness. The orientation of the recrystallized grains of this material can be described in terms of crystallographic rotations about principal poles of deformation texture.**

DURING the study of the recrystallization of a copper single crystal cold-rolled from a (110) [1$\bar{1}$2] initial orientation, the orientation of the recrystallized grains could be derived by a 30° rotation of the orientation of the cold-rolled matrix about its <111> poles.[1] The present investigation was undertaken to extend the work done on copper[1] to an aluminum crystal also cold-rolled from a (110) [1$\bar{1}$2] initial orientation.

## Experimental Procedure

The procedure of this experiment was similar to that reported for copper.[1] An aluminum (99.998 pct) single crystal rod* 1½ in. in diameter was grown in a thermal gradient furnace.[2] A rectangular specimen was cut with a surface ground parallel to the (110) plane. After the disturbed surface was etched off in Tucker's reagent, the rolling plane was about 3° from the (110) plane, as determined by the Laue back-reflection technique.[3] The specimen (1.20x 1.004x0.6787 in. thick) was then rolled along the [1$\bar{1}$2] direction. The final thickness was 0.0028 in., giving a reduction in thickness of about 99.6 pct.

Specimens were cut from the rolled strip with scissors, and approximately ⅛ in. of disturbed metal was removed with Tucker's reagent. The rolling edge remained intact.

The specimens were sandwiched between two graphite plates and annealed in a lead or lead alloy bath which was electrically heated. Pole figures were constructed using the techniques previously described.[3]

Specimens were electrolytically polished[4] and etched with 47 pct $HNO_3$, 50 pct HCl, and 3 pct of 48 pct HF. The electrolytic polishing method and etching reagent employed for aluminum specimens were not entirely satisfactory and the microstructures could not be studied in any detail.

## Results and Discussion

The octahedral pole figure of cold-rolled aluminum strip is plotted in Fig. 1. The <111> poles spread in the transverse direction approximately 8° for the highest intensity areas.

The spread in the transverse direction can be related to a rotation about two <110> directions lying in a plane containing the rolling direction and rolling plane normal. The two <110> directions and a scale of rotation for the <111> poles are shown in Fig. 2. The amount of rotation is consistent for three of the four <111> poles, about 35° to 40°. The discrepancy for the fourth pole is believed to be due to limitations of the film technique. Alternate inter-

* Kindly furnished by Dr. E. C. Burke, now with The Dow Chemical Co.

Y. C. LIU, Junior Member AIME, formerly Graduate Student, Yale University, is Research Associate, New York University, New York, and W. R. HIBBARD, JR., Member AIME, formerly Associate Professor of Metallurgy, Yale University, New Haven, Conn., is associated with Metallurgy Research Dept., Research Laboratory, General Electric Co., Schenectady.

Discussion of this paper, TP 3976E, may be sent, 2 copies, to AIME by Jan. 1, 1956. Manuscript, Sept. 13, 1954. Philadelphia Meeting, October 1955.

This paper is based on a portion of a thesis by Y. C. Liu submitted, in partial fulfillment of the requirements of the degree of Doctor of Engineering, to the Faculty of Yale University.

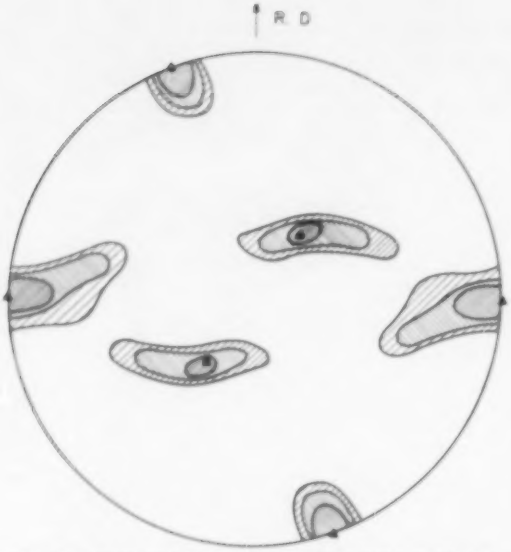


Fig. 1—Octahedral pole figure of an aluminum single crystal cold-rolled 99.6 pct reduction in thickness from the (110)[112] orientation. Triangle represents octahedral poles of (110)[112] orientation.

pretations such as 1—rotation about the rolling direction as an axis or 2—rotation about the <111> poles near the rolling direction as an axis result in larger discrepancies with the four central areas. The interpretation of rotation about the <110> axes fits the data best.

As indicated in the investigation on copper,[1] these two <110> poles are the slip directions with the highest resolved shear stress for the cold-rolling of a specimen with a (110) [$1\bar{1}2$] orientation.[7]

The spread about these two <110> directions might result from the 3° deviation of the initial orientation of the specimen from the {110} plane. Lutts and Beck[6] report that a rolled single crystal would preserve its original orientation with "remarkably little scatter" if the initial orientation of the specimen was prepared within one degree of the (110) [$1\bar{1}2$] orientation.

A microstructural study of the specimen annealed 300 sec at 300°C revealed no sign of recrystallization and the resultant pole figure is the same as Fig. 1. The reluctance of this aluminum specimen to recrystallize may be attributed to the "easy" flow for single crystals rolled in this orientation as proposed in the case of copper.[1] This characteristic behavior was also observed by Lutts and Beck.[6] The specimen which had been annealed 300 sec at 400°C was found to be fully recrystallized, based on microscopic examination.

The pole figures plotted for specimens annealed 300 sec at 400°, 500°, and 600°C exhibit essentially the same general characteristics, as shown in Fig. 3, with only slight variations in intensity. The 30° rotations reported in the case of copper[1] did not fit these textures.

However, 40° rotations about the three* <111> poles (AI, AII, and AIII of Fig. 5) of the deformed matrix was found to develop part of the recrystallization texture (open symbols in Fig. 3).

The 40° rotations about <111> poles of the deformed structure has also been reported for the recrystallization of cold-rolled polycrystalline, high purity (99.90 pct) aluminum, and compressed commercial aluminum single crystals.[5, 6]

The rotations in this investigation were found to be unidirectional, as indicated in Fig. 5. The resulting poles were found generally to satisfy most intense areas in the pole figures, but some of the denser regions (crosses in Figs. 3 and 5) still were not included. It was found that the remaining intense area could be included from orientations obtained by 30° unidirectional rotations about the three <110> poles (A-1, A-2, and A-5) indicated in Fig. 5.

The orientations derived from 30° rotations about two of the <110> poles, A-1 and A-2 of Fig. 5, were also used to rationalize the transverse spread in the deformation texture. By comparing Figs. 2 and 5,

* It should be noted that rotations about the <111> pole in the transverse direction are not required to rationalize the textures.

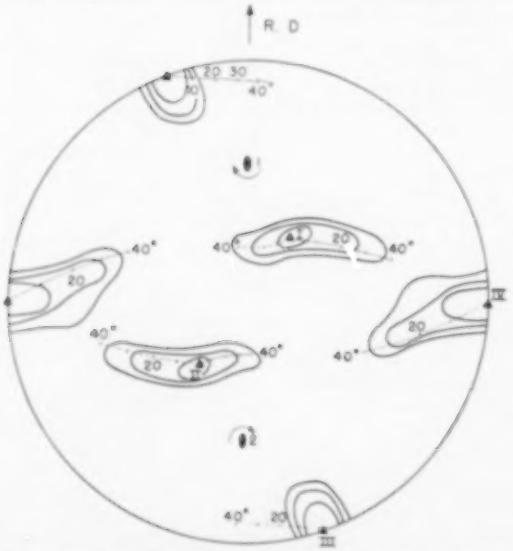


Fig. 2—Octahedral pole figure, same as shown in Fig. 1 with a scale of rotation about dodecahedral poles 1 and 2.

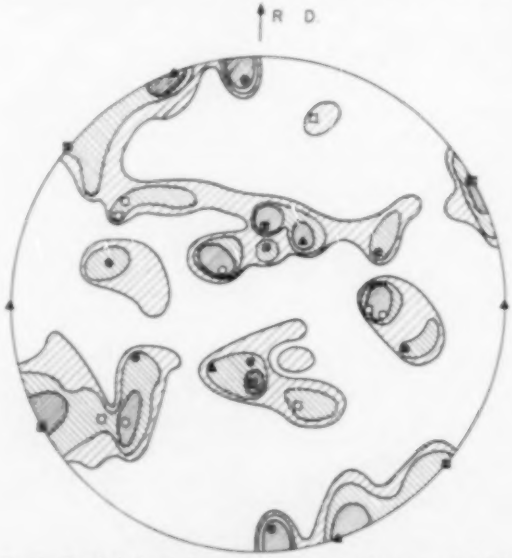


Fig. 3—Octahedral pole figure of aluminum specimen annealed 300 sec at 500°C. For symbols, see Fig. 5.

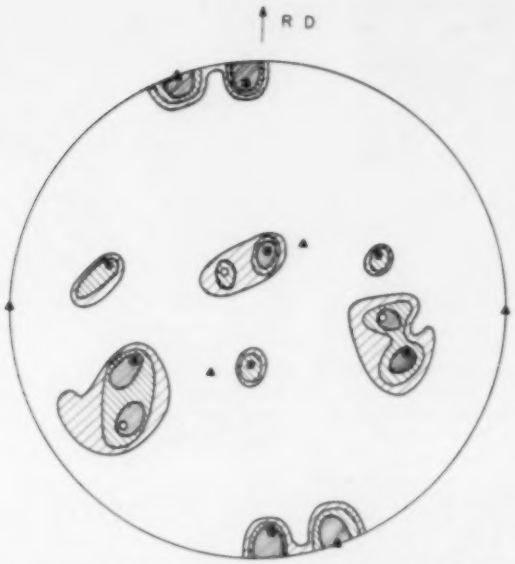


Fig. 4—Octahedral pole figure of aluminum specimen annealed 300 sec at 650°C. For symbols, see Fig. 5.

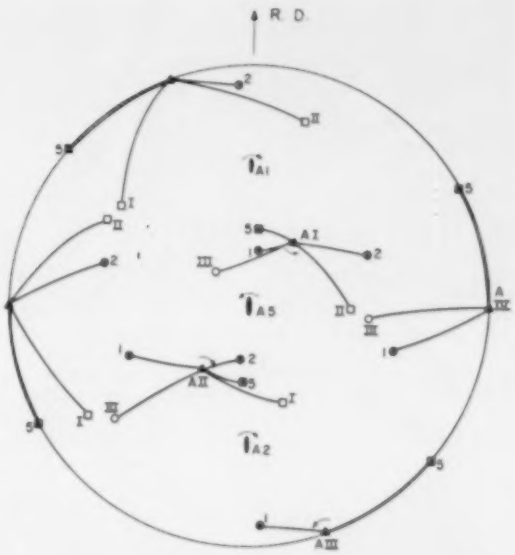


Fig. 5—Ideal octahedral orientations resulting from the recrystallization rotations about poles AI, AII, AIII, A1, A2, and A5. Numbers indicate poles of rotation (prefix *A*) or new orientations derived from these poles of rotations (no prefix).

it can be seen that both rotations are clockwise, in the manner indicated. It is suggested that the recrystallized grains related to the two <110> poles may be obtained from material which is present in the spread toward the transverse direction in the deformation texture.

The reason for the dodecahedral pole A-5 acting as an axis of rotation is not understood. This pole is symmetrically oriented between the other two participating dodecahedral poles, but the resolved shear stress in this direction during deformation is zero. However, it is possible that deformation involving the poles A-1 and A-2 might produce nuclei or growth areas, which can be related effectively to pole A-5, although they are actually the resultant of duplex deformation on the other two poles.

Fig. 4 is the pole figure plotted for the specimen annealed 300 sec at 650°C. Many of the orientations in Fig. 3 (squares) are not found in Fig. 4, and the only orientations developed (circles in Figs. 3 and 4) are those which can be related to one of three poles, namely, octahedral pole AIII or dodecahedral poles A-1 and A-2 (Fig. 5). The persistence of orientations with these poles as centers of rotation after high temperature annealing might be interpreted in terms of a high intensity of deformation on these planes or in these directions. This heavier deformation might result in early nucleation and growth of these grains at 650°C before the other orientations are formed. Those orientations indicated by the encircled crosses in Fig. 4 are present also in the fringe areas of the deformation texture and might have survived as a result of recrystallization in the same orientation and preferential growth with relation to the high intensity areas 30° away, previously present as the triangles in Figs. 1 and 3.

Intense areas related to <111> poles derived from a 40° rotation about <111> pole AIV in Fig. 5 are missing from the pole figures in Figs. 3 and 4. The absence of orientations from these rotations is believed to be associated with the fact that during rolling the resolved shear stress in this plane was zero, and thus it was probably not active in the deformation process.[4]

## Summary

1—A high purity aluminum single crystal (99.99 pct) was cold-rolled on the (110) plane in the [1$\bar{1}$2] direction. The resulting deformation texture showed that besides the retention of its original orientation, a spread in the transverse direction was present.

2—Annealing at 300°C produced no evidence of recrystallization, indicating that the cold-rolled single crystal is more reluctant to recrystallize than comparable polycrystalline aluminum.

3—After annealing at 400° to 600°C, the orientations of recrystallized grains can be expressed in terms of rotational reorientations described as (referring to the (110) [1$\bar{1}$2] orientation): 40° unidirectional rotation about three of the four octahedral poles and 30° unidirectional rotation about three dodecahedral poles.

4—Only three of the seven orientations resulting from the foregoing rotations are present after recrystallization at 650°C.

Discussion of this paper, if any, will appear in JOURNAL OF METALS, May 1956, and in AIME Metals Branch *Transactions*, Vol. **206**, 1956.

## References

[1] Y. C. Liu and W. R. Hibbard, Jr.: *Trans.* AIME (1953) **197**, p. 672; JOURNAL OF METALS (May 1953).
[2] E. C. Burke and W. R. Hibbard, Jr.: *Trans.* AIME (1952) **194**, p. 295; JOURNAL OF METALS (March 1952).
[3] A. B. Greninger: *Trans.* AIME (1936) **122**, p. 74.
[4] P. A. Jacquet: *Le Polissage Electrolytique des Surfaces Metallique et ses Applications.* (1948) Paris. Tomé.
[5] N. K. Chen and C. H. Mathewson: *Trans.* AIME (1952) **194**, p. 501; JOURNAL OF METALS (May 1952).
[6] P. A. Beck and H. Hu: *Trans.* AIME (1949) **185**, p. 627; JOURNAL OF METALS (September 1949).
[7] W. R. Hibbard, Jr. and M. K. Yen: *Trans.* AIME (1949) **185**, p. 126; JOURNAL OF METALS (February 1949).
[8] A. H. Lutts and P. A. Beck: *Trans.* AIME (1954) **200**, p. 257; JOURNAL OF METALS (February 1954).

# Cleavage Steps on Zinc Monocrystals: Their Origins And Patterns

by John J. Gilman

**Examination showed that characteristic cleavage step patterns are observed on the cleavage surfaces of undeformed, slipped, bent, twinned, compressed, and indented zinc crystals; and the effect of temperature is discussed. *Dimples* were seen to produce cleavage steps in a treelike pattern in otherwise undeformed crystals. The steps seem to originate when cracks intersect screw dislocations.**

IT has been known for a long time that the path of fracture in polycrystals may be discontinuous (see Jaffe, Reed, and Mann[1] for review). Recently, Kies, Sullivan, and Irwin[2] have proposed, and given evidence, that crack propagation is discontinuous within individual crystals as well. Other evidence has been given by Low.[3]

When discontinuous cracks within a crystal join together to make a macrocrack, the lamellae between each set of two cracks are torn somewhere, forming small *cliffs*. These cliffs appear as lines when the cleavage surface is observed microscopically.[4, 5] The lines have been called vein, tree, and riverlike markings by various authors, and they have sometimes been mistaken for *fissures*.[5] The descriptive term *cleavage steps* is used in this paper.

Cleavage steps vary in height over a wide range of values, from molecular dimensions[6] to 10$\mu$ and larger. Kies, Sullivan, and Irwin,[2] as well as George,[7] have shown that the gross cleavage step patterns for plastics, polycrystalline metals, and for monocrystals are sometimes similar. Thus, they depend mostly on the mechanical variables that prevail during cleavage and are relatively insensitive to the structure of the material. For example, parabolic markings[2, 7, 8] sometimes result when cracks open up ahead of, and not coplanar with, the main crack front. If the advance crack has the same velocity as the main crack, their intersection line is a parabola, otherwise it is a hyperbola or an ellipse.[9] The patterns are strongly affected by differences in crack velocities. This results in *chevron* patterns which point to the place of origin of the main crack.

It is the purpose of this paper to demonstrate the existence of a mechanism of cleavage step formation which is a continuous rather than a discontinuous process. Also, certain characteristic step patterns are described, and the strong effect of temperature is shown.

J. J. GILMAN, Junior Member AIME, is associated with Research Laboratory, General Electric Co., Schenectady.

Discussion of this paper, TP 3997E, may be sent, 2 copies, to AIME by Jan. 1, 1956. Manuscript, Sept. 16, 1954. Philadelphia Meeting, October 1955.

The specimens were zinc monocrystals (grown from 99.999+ pct pure metal). These were cleaved at room temperature and at −196°C.

### Results and Discussion

Cleavage step patterns are highly variable from point to point on a given specimen, as well as from one specimen to another. Although the patterns shown in the photographs are typical, they have been selected for graphic illustration.

Figs. 1a and 1b compare undeformed crystals that were cleaved at −196°C and room temperature, respectively. Cleavage at room temperature (Fig. 1b) resulted in a higher density of high steps (dark black lines) and enhanced the visibility of the fine background markings.

Deformation by simple slip caused no marked change in the step patterns until the glide strain reached about 1.0. But, as Fig. 1c shows, the density of high cleavage steps was greatly increased by large glide strains. Corrugations lying perpendicular to the slip direction may also be seen in Fig. 1c. These are caused by deformation bands. The cleavage resistance of the crystal of Fig. 1c was very high compared to undeformed crystals (estimated by the force on a needle required for cleavage).

Striking and varied cleavage step patterns were observed on bent crystals. Two characteristic patterns that were observed on crystals bent at 25°C, and cleaved by reverse bending at −196°C, are shown in Figs. 2a and 2b. The first, Fig. 2a, consists of *V*-shaped lines similar to the parabolas of other materials.[8, 9] Fig. 2b shows a pattern that is the equivalent of Fig. 1a, consisting of faint background lines with a few higher step markings. Cleavage of bent crystals at room temperature resulted in Figs. 2c and 2d. Now, the cleavage step lines show a strong tendency to follow one of two perpendicular paths. In Fig. 2c (bent once), many of the cleavage step components that lie parallel to the bend axis are assembled into irregular lines. In Fig. 2d (bent twice), the cleavage steps again tend to consist of two perpendicular components, but neither of the components is assembled into lines. Also, the step density is higher.

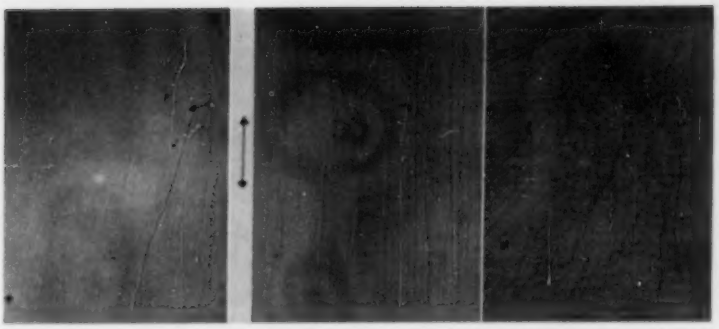

Fig. 1—Micrographs show cleavage steps on specimens both undeformed or deformed by simple slip. X100. Area reduced approximately 30 pct for reproduction.

a—Cleavage face resulted when as-grown zinc crystal was cleaved at —196°C.

b—This cleavage face resulted when as-grown zinc crystal was cleaved at room temperature. The arrow indicates the direction of crack motion.

c—Cleavage face of zinc crystal cleaved at —196°C with ~ 2.4 tensile glide strain; the slip direction was vertical. The crack originated off the upper right-hand corner of the photograph.

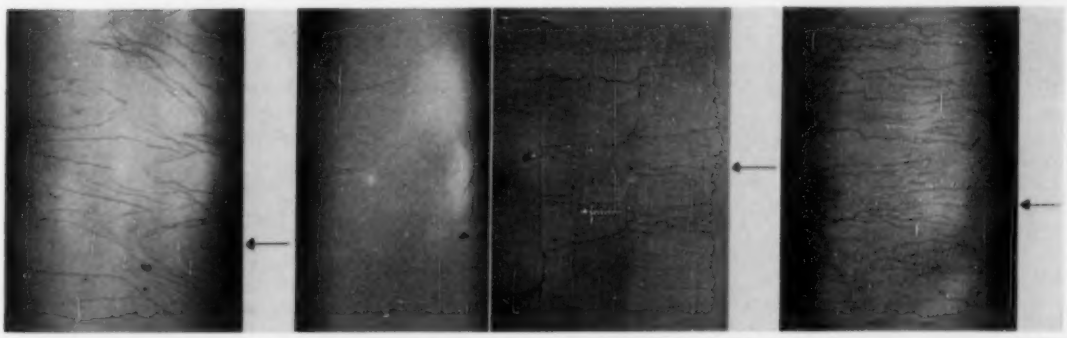

a—Cleavage surface shown is that of a crystal which was bent at room temperature and then cleaved by reverse bending at —196°C. The radius of curvature was 2.2 mm. The arrow indicates the direction of crack motion.

b—The cleavage surface and treatment were similar to those for the crystal shown in *a*, but a different crystal was used. The radius of curvature was 6.9 mm.

c—Cleavage surface shown is that of a crystal which was bent at room temperature and then cleaved by reverse bending at room temperature. The arrow indicates the direction of crack motion.

d—Cleavage surface shown is that of a crystal which was bent, unbent, and bent at room temperature; then it was cleaved at room temperature. The arrow indicates the direction of crack motion.

Fig. 2—Cleavage steps shown were observed on specimens deformed by bend gliding. The bed axis was vertical for all the figures and the close-packed direction was horizontal. *a*, *c*, and *d*: X100; *b*: X50. Area reduced approximately 30 pct for reproduction.

Fig. 3 shows the myriad of steps found on the cleavage plane of twin bands. The crystal ($\chi_o = 0°$, $\lambda_o = 0°$) had been loaded in tension. At 5.7 kg per sq mm, it twinned and almost simultaneously cleaved through the twins.

Compression parallel to the cleavage planes also produced an alteration in the step markings (Fig. 4). The compression resulted in a high density of *wiggly* step lines as shown in the photograph and increased the crystal's cleavage resistance.

Torsional strain about the hexagonal axis caused no characteristic change in the cleavage steps of otherwise undeformed crystals. It is not known, however, whether cleavage occurred along active slip planes.

Figs. 5a and 5b show cleavage step patterns that formed at *dimples* produced by indentation normal to the cleavage plane.[10] These specimens were cleaved immediately after indentation. Annealing prior to cleavage (5 min at 350°C) markedly reduced the numbers of fine branches in the trees, although the dimples remained present (Fig. 5c).

An important result that may be deduced from Fig. 5 is that cleavage steps sometimes originate at screw dislocations. Fig. 6 shows how a plane crack

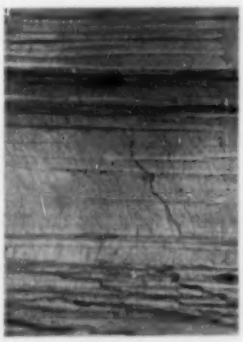

Fig. 3—Cleavage steps on the basal planes of twins are shown. The crystal was loaded in tension at room temperature until it twinned and then cleaved on the basal planes of the twin. X100. Area reduced approximately 30 pct for reproduction.

that intersects a screw dislocation becomes jogged and leaves a cleavage step behind it. It is believed that a crack, upon contacting screw dislocations lying in a dimple, breaks up into segments lying on various planes. As the segmented crack moves, its many elementary steps join together, forming larger steps until a few very large steps remain at the far side of the dimple. Probably only the larger steps are visible.

Fig. 4—Cleavage steps after compression parallel to cleavage planes are shown. The specimen was compressed ~ 1 pct parallel to the arrow and the close-packed direction. The stress was ~ 10 kg per sq mm, and the specimen was cleaved at —196°C. The arrow indicates the direction of crack motion. X100. Area reduced approximately 30 pct for reproduction.

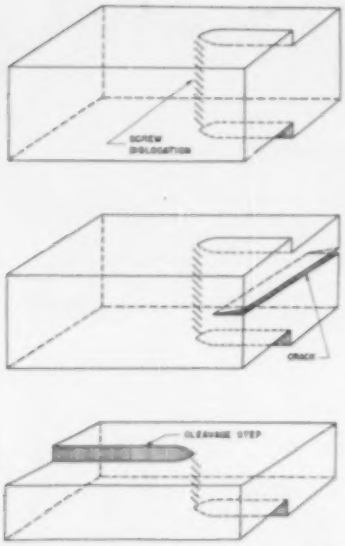


a—Crystal with a screw dislocation is shown before cleavage starts.

b—Cleavage has begun in the crystal.

c—Lower portion of the crystal is shown after cleavage.

Fig. 6—Three schematic diagrams illustrate the sequence in the production of a cleavage step when a crack crosses a screw dislocation.

The union of two elementary steps yields a higher step only if the elementary steps have the same sign. Otherwise, partial or total annihilation occurs. A striking case of step annihilation is shown in Fig. 5b. Here almost the entire step pattern disappeared when the crack left the dimple. Thus, the numbers of positive and negative screw dislocations that were intersected must have been about equal. This formed two large steps of opposite sign which annihilated at the *V* in the figure (oblique illumination verified that the steps had opposite signs).

Additional evidence of the foregoing mechanism was obtained as follows: One end of a crystal was twisted at 25°C. The axis of twisting was parallel to the specimen axis and lay in the basal plane parallel to a [1210] direction. The specimen was cleaved on the basal plane at —196°C, starting from the untwisted end. As the crack entered the twisted end of the crystal, many steps appeared gradually on the cleavage surface.

It is concluded that cleavage steps in zinc, as well as in other crystals, originate in at least two ways: The first is the discontinuous mechanism,[2] and the second is the screw dislocation mechanism being discussed here.

The reason why cleavage steps of opposite sign annihilate one another is that free surfaces are thereby eliminated. The attractive forces that cause this would be difficult to determine analytically, but they are readily demonstrated in an analogy: Two adjacent cuts in a foil will run together and annihilate if the tab between them is pulled. Contemplation of this analogy shows how the attraction between the cuts arises.

On the other hand, when two steps of the same sign unite, only an edge is eliminated. Therefore, attractive forces between two steps of the same sign are probably small, and they unite only when the geometry of the advancing crack front causes them to meet. Hence, in Fig. 1b, the steps run parallel over large distances, whereas near the dimples of Fig. 5 the steps run together.

The effect of prestrain on step density (Fig. 1c) is believed to result from screw dislocations introduced during the prestrain. The well known effects of prestrain and temperature on fracture stress are believed to result in part from the effects of these variables on step densities. The steps increase the effective surface energy of a crack and thereby increase the stress needed to make it grow.

## Summary

Characteristic cleavage step patterns that are observed on the cleavage surfaces of undeformed,

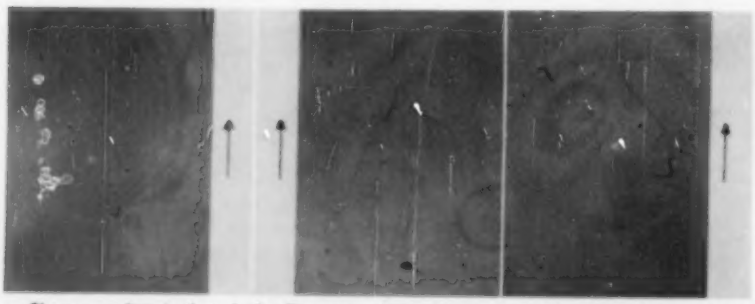

a—Cleavage surface is that of a specimen punched normal to the basal plane and then cleaved at —196°C. The arrow indicates the direction of crack motion.

b—Cleavage surface and conditions of treatment were similar to those for the crystal shown in *a*, but a different crystal was used. The arrow indicates the direction of crack motion.

c—Cleavage surface is that of a crystal specimen punched normal to the basal plane and then heated 5 min at 350°C, and then cleaved at —196°C. The arrow indicates the direction of crack motion.

Fig. 5—Cleavage steps at the dimples caused by punching are shown. *a*: X50; *b* and *c*: X100. Area reduced approximately 30 pct for reproduction.

slipped, bent, twinned, compressed, and indented zinc crystals were presented. The effect of temperature was also shown.

*Dimples*, in otherwise undeformed crystals, produce cleavage steps in a treelike pattern. It is believed that the steps originate when cracks intersect screw dislocations.

Discussion of this paper, if any, will appear in JOURNAL OF METALS, May 1956, and in AIME Metals Branch *Transactions*, Vol. **206**, 1956.

### References


[1] L. D. Jaffe, E. L. Reed, and H. C. Mann: Discontinuous Crack Propagation—Further Studies. *Trans.* AIME (1949) **185**, p. 683; JOURNAL OF METALS (October 1949).

[2] J. Kies, A. Sullivan, and G. Irwin: Interpretation of Fracture Markings. JOURNAL OF METALS (1950) **2**, p. 1090; also, *Journal of Applied Physics* (1950) **21**, p. 716.

[3] J. R. Low: The Relation of Microstructure to Brittle Fracture. *ASM Symposium* Cleveland (1953).

[4] J. Holden: Plastic Deformation Features on Cleavage Surfaces of Metal Crystals. *Philosophical Magazine* (1952) **43**, p. 976.

[5] C. Zapffe: Fractographic Structures in Zinc. *Metal Progress* (1947) **51**, p. 428.

[6] S. Tolansky: *Multiple-Beam Interferometry*. (1948) Oxford. Oxford University Press.

[7] W. George: Nucleation and Growth of Flow and Fracture Markings. *Industrial Engineering Chemistry* (1952) **44**, p. 1328.

[8] C. A. Zapffe, F. K. Landgraf, and C. O. Worden: Fractographic Study of Cast Molybdenum. *Trans.* AIME (1949) **185**, p. 616; JOURNAL OF METALS (September 1949).

[9] C. Zapffe and F. K. Landgraf: Fractographic Examination of Tungsten. *Trans.* ASM (1949) **41**, p. 396.

[10] D. C. Jillson: An Experimental Survey of Deformation and Annealing Processes in Zinc. *Trans.* AIME (1950) **188**, p. 1009; JOURNAL OF METALS (August 1950).


# Discussion — Iron and Steel Division*

*New York Meeting, February 1954*


Manganese Modification of the Fe-S-O System (paper by D. C. Hilty and Walter Crafts. JOURNAL OF METALS, September 1954, p. 959) ..... 1255

Slag-Metal-Graphite Reactions and the Activity of Silica in Lime-Alumina-Silica Slags (paper by James C. Fulton and John Chipman. JOURNAL OF METALS, October 1954, p. 1136) ..... 1257


*Chicago Meeting, February 1955*


Ionic Nature of Liquid Iron-Silicate Slags (paper by M. T. Simnad, G. Derge, and I. George. JOURNAL OF METALS, December 1954, p. 1386) ..... 1261

Oxygen Solubility and Oxide Phases in the Fe-Cr-O System (paper by D. C. Hilty, W. D. Forgeng, and R. L. Folkman. JOURNAL OF METALS, February 1955, p. 253) ..... 1258


*TP 4098C

## Manganese Modification of the Fe-S-O System

by D. C. Hilty and Walter Crafts

*DISCUSSION, C. B. Post and J. V. Russell, Chairmen*

**John Chipman** *(Massachusetts Institute of Technology, Cambridge, Mass.)*—After looking over the authors' shoulders for several years and after many discussions on the interesting diagrams of the types shown, it is a pleasure to see a formal paper published on this subject. There can be no doubt of the practical usefulness of the concepts shown. Inclusion formation in steel is such a highly complex matter that any system for understanding the subject is bound to be welcomed by those who must work with steels and who see in their day-to-day experience the good and evil effects of inclusions.

A feature of the work with which the discusser has been concerned, and which he would now like to attempt to explain, is the relation between the schematic diagrams which the authors use and the phase diagrams for related systems. Obviously, the authors' diagrams are in no sense complete phase diagrams. However, there is a relation between this type of diagram and the true phase diagram, and the understanding of this relation ought to help in understanding the general picture which the authors are presenting.

Consider the authors' Fig. 4, which shows the liquidus relations in the Fe-Mn-S-O system. To show the complete relations between temperature and composition in these four ternary systems would require four triangular prisms, the vertical axes of which would represent temperature. The four triangles of Fig. 4 represent basal projections of certain lines from the four prismatic phase diagrams. Readers of the paper are all more or less acquainted with this type of projection and its usefulness and limitations are generally understood.

In order to concentrate on the interesting parts and to minimize the less interesting features, the composition scale may be shifted to de-emphasize regions containing gaseous sulphur and oxygen. Such a diagram is shown in Fig. 16, which is a distorted version of the authors' Fig. 4. Here the oxide of iron is wüstite, denoted by W, and it is to be noted that between W and MnO lies the entire MnO-FeO "binary" system. Similarly, between MnS and FeS lies another binary whose

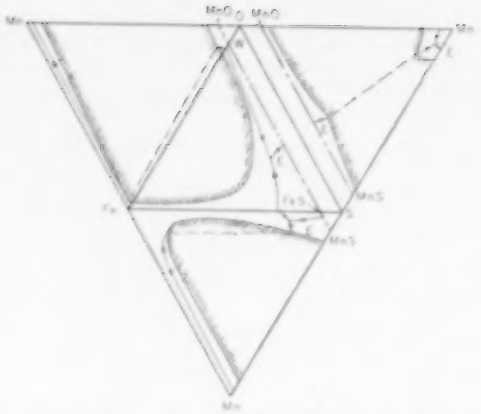


Fig. 16—Diagram of the liquidus relations in the Fe-MnS-O system (Fig. 4) has been modified so that regions containing gaseous sulphur and oxygen have been de-emphasized.

phase diagram would be almost invisible on the scale to which it has been reduced.

Now to take this distortion one step further: Move both the MnS and the FeS out to the point S. The investigator can no longer distinguish between MnS and FeS but the binary system is still there and must not be overlooked in the next step. Similarly, between wüstite and MnO there is a binary system which must not be forgotten but which is represented entirely at one point in the diagram and called simply "oxide." The lines showing the phase fields of the three external systems are distortions of those shown in the authors' Fig. 4. However, the central triangle now requires different treatment. The original Fe-S-O diagram must be erased and in its place something else substituted.

To fill the temporarily vacant central triangle, one proceeds as follows: Fold the three external triangles along the edges of the internal triangle, making a tetrahedron with manganese at the top. The space within this tetrahedron is now filled by a complex of lines representing intersections of various phase regions. Certain features within this complex are of especial interest and it can at least be imagined how they would look if data were available for their construction. For example, four ternary eutectics might be expected to be found in this system. One of these is

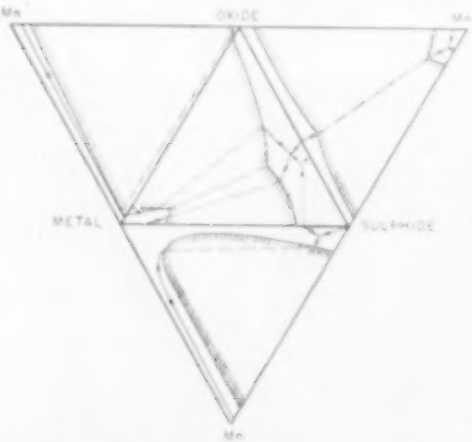


Fig. 17—Schematic Fe(Mn)-S-O diagram has been slightly modified to show the existence of one more of the ternary eutectics.

undoubtedly close to the manganese apex of the tetrahedron as the authors have pointed out. The others may be expected to be somewhat closer to the binary eutectics which are known.

To project these features upon the temporarily vacant triangle, imagine a point source of light at the apex of the tetrahedron and let it cast shadows on the base. The investigator must select now from the multiplicity of shadows those features in which he is particularly interested from the standpoint of the problem in hand, and he must mark these out upon the basal triangle. This is essentially what the authors' diagram amounts to. It is shown as the central triangle of Fig. 17, slightly modified to show the existence of one more of the ternary eutectics, but otherwise identical with the authors' Fig. 6.

**Nev A. Gokcen** *(Michigan College of Mining and Technology, Houghton, Mich.)*—Eq. 1 on p. 960 is an approximate form of the following relationship[14]

$$-\Delta F^{\circ} = R\,T \ln N = -\Delta H_{m} + T\,\Delta S_{m} \qquad [4]$$

where $\Delta S_{m} = -\Delta H_{m}/T_{m}$ and therefore

$$RT \ln N = \Delta S_{m}\,(T - T_{m}). \qquad [5]$$

When the difference between $T$ and $T_{m}$ is small, the following approximation, hence Eq. 1, is valid

$$R\,T \ln N = R\,T_{m} \ln N.$$

Since $T_{m}$ is considerably larger than $T$ for the case considered by the authors, Eq. 1 is not applicable. Their Eqs. 2 and 3 should therefore be replaced by

$$4.575T \log N = 6\,(T - 2058) \qquad [6]$$

$$4.575T \log (1\text{-}N) = 6\,(T - 1893). \qquad [7]$$

Simultaneous solution of these equations yields $N = 0.422$ (37.3 pct) and 1601°K (1328°C) rather than the authors' values of 40 pct and 1230°C, respectively.

It should be emphasized that entropies of fusion of sulphides and oxides of the same metal may differ considerably. For example,[15,16] $\Delta S_{m}$ is 4.6 for the compound FeO and 3.4 for FeS, $\Delta S_{m}$ is 1.99 for ZnO and 4.74 for ZnS, and $\Delta S_{m}$ is 8.9 for $Cu_2O$ and 3.9 for $Cu_2S$. Hence, the assumption that the entropies of MnO and MnS are equal is, at best, a rough approximation for the present purpose. A difference of two in the values of entropies would yield considerably different results in these calculations.

The most important source of error in the application of Eq. 4 is, however, the deviation from ideal behavior. It is rather impossible to expect ideality in the vicinity of $N = 0.5$ in a eutectic system. It can be shown by calculation that for each component a deviation of 0.2 in the activity coefficient of unity for an ideal system would change the eutectic temperature nearly 100°C.

Actually, there is no necessity in this case for such calculations by the application of an equation which is not expected to yield reliable results in the absence of thermodynamic data, since Andrew, Maddocks, and Fowler[17] have obtained a phase diagram for the MnO-MnS system and found that the eutectic occurs at 50 pct and 1280°C. Thus, the authors' preference of their incorrect calculations of the eutectic point over the experimental results of Andrew et al.[18] is without justification.

**D. C. Hilty** *(authors' reply)*—The authors are indebted to Professor Chipman for his contribution toward clarification of the rather complex visualization process by which Fig. 6 may be obtained. With certain modifications, the authors derived Fig. 6 very much as he has described.

It is agreed that there are four ternary eutectics in this system, namely: 1—metal-oxide-MnS, 2—metal-oxide-FeS, 3—metal-MnS-FeS, and 4—oxide-MnS-FeS. Only three of these are shown in Fig. 4 and in Dr. Chipman's Fig. 16. The fourth, the oxide-MnS-FeS eutectic, lies in the plane through the MnO-FeO-FeS-MnS

points of the tetrahedron formed by folding the external triangles of Fig. 4 along the edges of the internal triangle. In Fig. 6 and Dr. Chipman's Fig. 17, therefore, it will fall on the oxide-sulphide side of the metal-oxide-sulphide diagram. Since it is not encountered in compositions in equilibrium with metal, its presence has not been indicated. In reality, the broken line initiating from the oxide-sulphide side of the internal triangle in Fig. 17 represents this eutectic. Consequently, the eutectic suggested by the intersection of the broken lines in this triangle is actually the quaternary eutectic. Obviously, the difficulties of representing this quaternary eutectic so that it can be readily visualized are manifold.

N. A. Gokcen is correct with regard to the specific applicability of Eq. 1 in relation to the one he proposes. As was pointed out in the paper, however, and as has been re-emphasized by Gokcen, the other uncertainties involved are such that either calculation gives merely a rough approximation of the MnS-MnO eutectic. For the authors' purpose, on the other hand, a rough approximation is entirely adequate for development of the qualitative diagram and the different results of the two calculations are relatively unimportant in that they cause no significant change in the qualitative diagrams of Figs. 3, 4, and 6. It is enough that the uncertain diagram of Andrew, Maddocks, and Fowler, Gokcen's equation, and the authors' approximation give order of magnitude agreement on this minor point.

[16] S. Glasstone: *Thermodynamics for Chemists*. (1947) p. 340. New York. D. Van Nostrand Co.
[17] Rossini *et al.*: Selected Values of Chemical Thermodynamic Properties. *Circular 500* National Bureau of Standards (1952).
[18] K. K. Kelley: Heats of Fusion of Inorganic Substances. *Bulletin 393* U. S. Dept. of Interior, Bureau of Mines (1936).

---

## Slag-Metal-Graphite Reactions and the Activity of Silica in Lime-Alumina-Silica Slags

by James C. Fulton and John Chipman

*DISCUSSION, Gerhard Derge and John F. Elliott, Chairmen*

**R. C. Shnay** *(Dept. of Mines and Technical Surveys, Ottawa, Ont., Canada)*—The statistical methods used by Prof. Chipman and Dr. Fulton to estimate the accuracy of their chemical analysis results, p. 1138, appear open to question. The definition of standard deviation is given by the authors as

$$\sigma = \frac{\sqrt{\Sigma(x_i - \bar{x})^2}}{n}$$

where $x_i$ is the differences between pairs, $\bar{x}$ is the average difference, and $n$ is the number of pairs. This definition should actually be given as

$$\sigma = \frac{\sqrt{\Sigma(x_i - \mu)^2}}{\sqrt{N}}$$

where $\mu$ is the mean of the whole population and $N$ is the total number of individuals in the population.

The standard deviation is a population parameter and the population mean must be known to compute this parameter. This is very seldom possible, since the whole population must be measured before the mean $\mu$ can be computed. Therefore, in order to compute confidence intervals or test hypotheses, the function

$$s = \sqrt{\frac{\Sigma(x_i - \bar{x})^2}{n-1}}$$

must be used.

In this case, $\mu$ is replaced by its estimate $\bar{x}$ and $s$ is in turn an estimate of the standard deviation.

The difference between population parameters and the estimates calculated from samples can best be illustrated in the following way:

To find the average height $\mu$ of all men in North America, all the men could be measured. Since this is obviously impractical, a sample, e.g., 1000 men, could be measured. The average height $\bar{x}$ of the 1000 in this sample can then be used to estimate the average height of the male population of North America. The standard deviation of this population, if desired, can be estimated by means of the quantity

$$s = \sqrt{\frac{\Sigma(x_i - \bar{x})^2}{n-1}}$$

where $x_i$ is the height of the individuals in the sample and $n$ is the sample size, 1000.

In the paper under discussion, the population could be said to consist of the differences between all possible pairs that can be taken from the material. If all the possible pairs had been taken and analyzed, the necessary information would be obtained and the accuracy would not need to be estimated by means of confidence intervals. Obviously, this could not be done and the pairs are really a sample of the whole population.

Confidence intervals are computed from samples in order to define the degree of uncertainty involved in the estimate of the population mean. To define a confidence interval for the mean of a normally distributed population, the following quantity is used

$$t = \frac{\bar{x} - \mu}{\sqrt{\frac{\Sigma(x_i - \bar{x})^2}{n(n-1)}}}.$$

This quantity is distributed by the Student's t distribution. The tabulated values are substituted for t, leaving $\mu$ the only unknown. For example, a 90 pct confidence interval is defined by

$$\bar{x} - t_{0.90}\sqrt{\frac{\Sigma(x_i - \bar{x})^2}{n(n-1)}} < \mu < \bar{x} + t_{0.90}\sqrt{\frac{\Sigma(x_i - \bar{x})^2}{n(n-1)}}.$$

Since the accuracy of the sample mean (as an estimate of the population mean) increases with the sample size, the t distribution approaches the normal distribution as the sample size approaches infinity. In other words, for tables of the normal distribution to be used in defining a confidence interval, a very large sample must be taken. In the paper under discussion, the authors have used tables of the normal distribution. The factor two which was used to multiply the quantity $\sigma$ (as defined in the paper) is too small. The error in this case is greatest when only a small number of pairs were taken.

The aggregate effect of these errors is all in one direction. The estimates of error are too low. Even had the statistical analysis been carried out correctly, the procedure of taking duplicates only for master slags or where the first value appeared to be in error is questionable. It is difficult to justify any general conclusions on this basis.

Since all the necessary data do not appear to have been given, revised values for the confidence intervals cannot be computed. In any case, it seems doubtful

that the objections raised in this discussion invalidate the general conclusions reached by the authors. However, revised calculations of the confidence intervals would give a better idea of the extent of sampling or analytical errors and thus of the precision of the experiment as a whole.

**James C. Fulton** and **John Chipman** *(authors' reply)*—Mr. Shnay has focused attention on the statistical methods used by the authors. First, it should be pointed out that there was a typographical error in the original manuscript of the paper. In the definition of a sample $\sigma$, repeated by Mr. Shnay from the paper, the square root sign over the $n$ in the denominator was omitted in manuscript.

Mr. Shnay has suggested that confidence limits be set on the universe mean using an estimate of $\sigma$ of the universe based upon sample values. This approach to the problem is usual procedure when it is desirable to work with confidence limits on the mean. However, in the authors' paper, an attempt was made to set tolerance limits on the population, which is a problem in individual values rather than mean values.

Table X. Values of $\bar{x} + 2\sigma$ and $\bar{x} \pm ts_{\bar{x}}$

| Variable | n, No. of Pairs | $\bar{x}$, Mean Difference | $s_x$, Sample | $\bar{x} + 2\sigma$ | $\bar{x} \pm ts_{\bar{x}}$, 95 Pct Confidence Interval |
|---|---|---|---|---|---|
| $SiO_2$ | 94 | 0.25 | 0.16 | 0.57 | 0.25±0.03 |
| CaO | 35 | 0.27 | 0.18 | 0.63 | 0.27±0.06 |
| 10 pct $Al_2O_3$ | 19 | 0.18 | 0.14 | 0.46 | 0.18±0.07 |
| 20 pct $Al_2O_3$ | 45 | 0.51 | 0.34 | 1.19 | 0.51±0.10 |
| 0 to 8 pct Si | 6 | 0.02 | 0.02 | 0.06 | 0.02±0.02 |
| 8 to 15 pct Si | 13 | 0.10 | 0.08 | 0.26 | 0.10±0.05 |
| 15 to 24 pct Si | 28 | 0.23 | 0.19 | 0.61 | 0.23±0.08 |

Table X shows a tabulation of data for the terms $\bar{x} + 2\sigma$ for individual values and $\bar{x} + ts_{\bar{x}}$ for mean values. The values of $\bar{x} + 2\sigma$ were calculated by the method outlined on p. 1139 of the paper. The values of $\bar{x} + ts_{\bar{x}}$ were calculated according to the interval

$$\bar{x} - t_{\alpha,n}\sqrt{\frac{\Sigma(x_i - \bar{x})^2}{n(n-1)}} < \mu < \bar{x} + t_{\alpha,n}\sqrt{\frac{\Sigma(x_i - \bar{x})^2}{n(n-1)}}$$

as suggested by Mr. Shnay. It is the use of $\bar{x} + 2\sigma$ that has been questioned.

It is quite unlikely that the individual differences are normally distributed. A histogram of 94 samples for $SiO_2$ indicates a skew parent population. Under these conditions, a different function should be applied. Such refinement of the statistical analysis would be beyond the scope of the paper. However, assuming that the parent population has a unimodal distribution as suggested by the histogram, an inequality of the Camp-Meidell type could be used.

## Oxygen Solubility and Oxide Phases in the Fe-Cr-O System

by D. C. Hilty, W. D. Forgeng, and R. L. Folkman

*DISCUSSION, Gerhard Derge and R. D. Hindson, Chairmen*

**Nev A. Gokcen** *(Michigan College of Mining and Technology, Houghton, Mich.)*—The authors have attempted to identify the phases in equilibrium with liquid metal by making the false assumption that (p. 255) ". . . with sufficiently rapid cooling the primary inclusions are representative of the oxide phases in equilibrium with the metal at the time the solidification begins." It is illogical to consider that the inclusions represent equilibrium phases, since they are formed under a nonequilibrium condition created by supercooling. In addition, this assumption may readily be disproved by experimental observations as follows: 1—The inclusions in open hearth steels are certainly not representative of the slags with which the metal may be brought into equilibrium under laboratory conditions. 2—This discusser has examined inclusions in pure iron equilibrated with *only silica*, under carefully controlled atmospheres of $H_2O$ and $H_2$ mixtures at 1600°C, and found that the primary inclusions range progressively from grayish FeO inclusions to dark silicate and then to transparent silica inclusions as the silicon content of the metal increases from 0.006 to 6 pct, or as the oxygen content decreases from 0.07 to 0.002 pct, respectively. Thus, the composition of inclusions depends, among other factors, upon the degree of supersaturation with cooling and the concentration of the precipitating substances. 3—Pure liquid iron at 1550°C containing up to 0.2 pct O in inert crucibles, such as BeO and MgO, precipitates out wüstite inclusions no matter how fast the metal is cooled. It is obvious that these inclusions do not indicate that the metal was in equilibrium with wüstite, since below the saturation concentration, i.e., 0.2 pct O, wüstite is not present with liquid iron. Consequently, the contention that the authors have established slag phases and their composition in equilibrium with liquid metal must be rejected until conclusive and careful data on slag specimens are available.

It is stated qualitatively and loosely that (p. 259) "In general, X-ray diffraction examination of the previously mentioned slag samples confirmed the results of the inclusion examination with regard to existence, regions of stability, and disproportionating characteristics of the various oxide phases." Yet rigorous microscopical and chemical evidence with slag samples covering the entire range is not presented except the data on the low chromium range reported in Table VIII. The authors have never observed $Cr_3O_4$ in slag samples cooled in argon stream by contending that the argon atmosphere was oxidizing for the slag. If argon was slightly oxidizing, it could have been purified, or a large slag sample could have been taken to minimize errors from oxidation. The resulting slag samples, analyzed chemically, would then have provided evidence whether or not the formula $Cr_3O_4$ fits its composition. Accordingly, the existence of $Cr_3O_4$, claimed to be stable at high temperatures, requires further conclusive experimental investigations.

It is reported on pp. 260 and 261 that 1 to 2 hr after adding ferric oxide and chromium certain four runs still yielded excessively irregular results similar to the ones plotted in Fig. 1. This was attributed to a vague and inconceivable "persistent extra-equilibrium" condition and the four runs were therefore omitted arbitrarily from Table VI. The term "extra-equilibrium" is foreign to thermodynamics and must simply be rejected. The question arises then as to which set of their data truly represents equilibrium conditions in the absence of experimental evidence.

The establishment of dips and breaks in Fig. 12 would require data with less than ±3 pct scattering which is impossible to attain in high temperature research at present. Certainly the data semilogarithmically represented in Fig. 10, even after rejecting the so-called "extra equilibrium" runs, deviate several times more than ±3 pct and therefore do not justify the dips and breaks. Further, it is necessary that on the dotted lines, which are the loci of breaks in the isothermal equilibrium lines, two slag phases must be in equilibrium with liquid metal. This was not established by the examination of slag samples.

Finally, interpretation of data presented herein is

entirely in disagreement with the more careful investigation of Chen and Chipman.[8]

**J. C. Fulton** *(Allegheny Ludlum Steel Corp., Brackenridge, Pa.)*—The authors are to be congratulated on their exhaustive study and lucid discussion of the Fe-Cr-O system. These data resolve some of the questions that remained unanswered from previous investigations of this subject. X-ray measurement of oxide structures and the construction of a phase diagram help to establish a fundamental background with which stainless steel producers can apply these solubility data to steelmaking problems.

The identification of a distorted spinel and $Cr_2O_3$ should abbreviate much of the work in evaluating inclusions found in commercially pure chromium alloys. It would appear that the characteristic metallic particles formed upon disproportionation of $Cr_2O_3$ could be used for routine identification of this particular type of inclusion.

The chronological outline of the paper was used to advantage in explaining the scatter of their early data due to supersaturation with oxygen. Mere mentioning of this observation could not have brought out their point nearly as well as does Fig. 13 on p. 265. These results emphasize the important role of temperature in controlling oxygen content.

An interesting commercial application of these data is readily visualized for straight chromium steels containing more than 10 pct Cr, the minimum in the oxygen solubility curves. At chromium concentrations above this value, iron acts as a deoxidizer, as was mentioned in connection with Fig. 14. A means of taking advantage of this result is to adjust the chromium content of the bath, so that at the end of the slag reduction period it contains somewhat less than the desired tap analysis. That is, for a final analysis of 17 pct (type 430), the preliminary should be 12 to 14 pct. In this way, the oxygen activity will be maintained at a higher level and the oxygen solubility at a lower level throughout the reduction period than as if all chromium were initially present. These two factors should improve the elimination of oxygen from the bath during the reduction period.

A further advantage of this procedure is that the late addition of chromium to meet the specification acts as a cooling agent late in the melting cycle. This cooling in the presence of the proper concentration of manganese and silicon aids in the formation of fluid deoxidation products which can coalesce into large enough particle size to rise to the slag.

As with most modifications of melting practices, when certain features are stressed too heavily, other compensating factors appear. There is a tendency for furnace time to increase and, of course, much of the success of the process depends upon the cleanliness of the late ferroalloy addition.

Allegheny Ludlum has found that this procedure leads to better strip surface with respect to lines produced by inclusions in the steel breaking through the surface when rolling to thin sections. The use of the low chromium preliminary procedure has shown an improvement on not only straight chromium but also Cr-Ni steels. With the variation in facilities and end product that exists between shops, this practice would necessarily require evaluation prior to its adoption.

**C. E. Sims** *(Battelle Memorial Institute, Columbus, Ohio)*—This excellent work, painstakingly done, advances the understanding of oxygen relations to molten ferrous alloys another step. Of particular interest is the oxide phases found to be in equilibrium with the molten Fe-Cr alloys. Previously, there was considerable circumstantial evidence to indicate that the lower oxygen oxides are the likely phases to be in equilibrium with molten metals, but concrete evidence was lacking except for a few cases. It is known, for instance, that wüstite is in equilibrium with oxygen-saturated molten iron and it is the oxide phase which precipitates from iron. During cooling it tends to disproportionate into iron and $Fe_3O_4$.

The close proximity of a refractory oxide with a molten alloy does not guarantee equilibrium even after some period without change. An Fe-Cr alloy melted in a crucible of $Cr_2O_3$, for example, may not actually contact the $Cr_2O_3$ but be separated by a thin layer of lower oxide which is in equilibrium with the metal. The scale on heated iron is mostly $Fe_2O_3$, but on the outside, in contact with air, there is a thin layer of $Fe_3O_4$, while inside where it contacts the base is a layer of wüstite. On the other hand, it seems axiomatic that a material precipitated from solution is in equilibrium with the solution at the precipitation instant. The precipitated phase, of course, may be unstable and change later.

The evidence is convincing that the oxide in equilibrium with the Fe-Cr-O system of high chromium content is $Cr_2O_3$. If this be so and the analogy of the Fe-O system is considered, might there be a similar condition in other systems such as the Fe-Si-O and Fe-Al-O systems, if these are inspected closely enough?

**D. C. Hilty, W. D. Forgeng,** and **R. L. Folkman** *(authors' reply)*—The authors are compelled to disagree categorically with most of Professor Gokcen's comments. With regard to his concluding statement that the interpretation of the data is in entire disagreement with the earlier investigation of Chen and Chipman, reference should be made to oral comments by Prof. Chipman at the time this paper was presented and to Professor Chipman's recent publication[11] in which he took the opportunity to re-examine the Chen and Chipman work and bring it into complete accord with the present authors' results.

The method employed to identify the oxide phases in equilibrium with the metal at the time solidification began has become normal procedure in high temperature phase-equilibria studies. It has been described by Howe[10] and Tammann[16] among others and has been successfully applied by numerous investigators both in this country and abroad. Short of direct observation at the high temperatures involved, it seems entirely logical to have recourse to this well known technique of microscopic examination of specimens rapidly cooled from those temperatures. While admittedly indirect, the information derived by such a technique has proved indispensable in establishing the upper regions of phase diagrams which otherwise can be estimated only on the basis of thermodynamic calculations predicated on purely arbitrary assumptions of the phases present.

The breaks in the oxygen solubility curves were confirmed by the observations of different nonmetallic phases on either side of the breaks. The curves cannot be constructed in any other way without compromising the data.

With respect to the statement, "the authors have never observed $Cr_2O_3$ in slag samples . . . ," they have, in fact, made numerous observations of the presence of $Cr_2O_3$ in slags from high chromium melts and regret that the contrary was erroneously inferred.

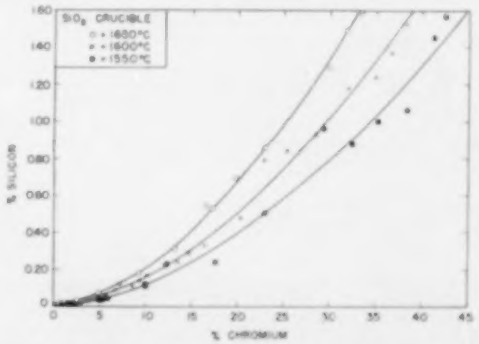


**Fig. 20—Curves and data points show chromium and silicon contents of liquid Fe-Cr-Si alloys in the presence of both chromium oxide slags and silica.**

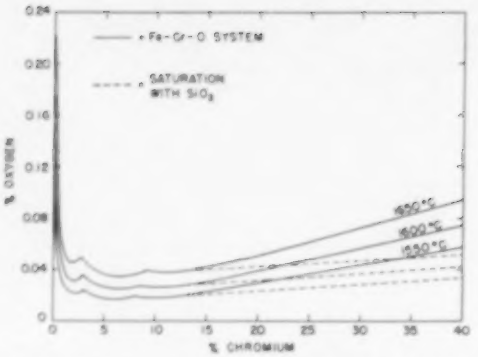


Fig. 21—Diagram shows the effect of sufficient silicon to produce saturation with silica on the oxygen solubility in the Fe-Cr-O system.

The authors appreciate Professor Gokcen's criticisms, even though they have recorded extensive disagreement with them. It is recognized that this disagreement may stem from a fundamental difference in viewpoint in the respective approaches to the physical aspects of problems in physical chemistry. In the field of process metallurgy, the strictly thermodynamical approach sometimes prefers to describe the state of a system in terms of numerical constants without regard to the physical natures of the phases present. This approach can be quite useful provided it does not ignore the existence of specific physical entities that can be readily seen and recognized. On the other hand, a purely physical approach that disregards the basic concepts of thermodynamics can also lead to erroneous interpretations. It is only by combination of empirical observations and theoretical considerations that phase relations in complex systems can be rationalized. This latter course is particularly essential for understanding the mechanism of inclusion formation in alloy systems and is the one the authors have followed.

Dr. Fulton's remarks on this paper are most gratifying. The authors are especially pleased that immediate commercial application of their data was forthcoming. They suggest, however, that practical application of these fundamental results to the production of stainless steels be approached cautiously. The data should be directly applicable at the end of the oxidizing period in stainless steel heats, but other elements, such as silicon, manganese, etc., that are normally present during the slag reduction and finishing stages may further complicate matters, especially with regard to inclusion evaluation.

An indication of the influence of silicon is given by Figs. 20 and 21, derived from observations of Fe-Cr-O alloys melted in silica crucibles. Fig. 20 shows the chromium and silicon contents of liquid metal saturated with both chromium oxide-rich slag and silica, and Fig. 21 illustrates a preliminary evaluation of the effect of these conditions on oxygen solubility. It can be inferred from these diagrams that silicon may substantially modify the composition and structure of the oxide phases—and therefore the inclusions—but the specific nature of such modification must be established by further investigation.

The authors thank Mr. Sims for his interest and his helpful comment. Coming from one who has had a major interest in this and similar problems for so many years, his remarks are especially significant. The question of conditions analogous to those the authors have described in the paper existing in other systems such as Fe-Si-O and Fe-Al-O is an interesting one upon which to speculate. Certainly the understanding of these systems is incomplete, and the existence of such conditions would help to explain some of the anomalous behavior frequently observed. Since the authors can do no more than speculate on this possibility, however, they will reserve judgment until tangible evidence is developed.

[11] J. Chipman: Atomic Interaction in Molten Alloy Steels. *Journal* Iron and Steel Inst., London (1955) 180, No. 2, pp. 97-106.
[12] H. M. Howe: *The Metallography of Steel and Cast Iron.* (1916) p. 202. New York, McGraw-Hill Book Co. Inc.
[13] G. Tammann: *Lehrbuch Der Metallographie.* (1921) p. 185. Leipzig, Leopold Voss.

---

# Discussion — Extractive Metallurgy Division*

*New York Meeting, February 1954*

Equilibrium Pressure Measurements Above ZnS from 680° to 825°C (paper by C. Law McCabe. JOURNAL OF METALS, September 1954, p. 969) 1260

*Chicago Meeting, February 1955*

Ionic Nature of Liquid Iron-Silicate Slags (paper by M. T. Simnad, G. Derge, and I. George. JOURNAL OF METALS, December 1954, p. 1386) 1261

* TP 4096D.

---

## Equilibrium Pressure Measurements Above ZnS from 680° to 825°C

by C. Law McCabe

*DISCUSSION, T. B. King and H. H. Kellogg, Chairmen*

**Philipp Gross** *(Fulmer Research Institute Ltd., Stoke Poges, England)*—As pointed out by the author, any better agreement between experimental and calculated

values cannot possibly be expected; the results must therefore be interpreted as practically complete dissociation of ZnS vapor.

In the experiments with graphite addition, the reaction rate was too low to give any effects. If reaction of any sulphide with added graphite occurs, effusion experiments can be interpreted only if equilibrium inside the vessel is established. In this case, the weight loss will *always* be changed by graphite addition. In the case of true evaporation, the vapor pressure is not affected; but by the establishment of the heterogeneous equilibrium between solid metal sulphide and graphite, formation and evaporation of metal and carbon sulphide will occur and increase the weight loss. In the case of sulphide dissociation, the apparent evaporation will be repressed by the metal vapor resulting from the reaction with graphite but, owing to this reaction, the total weight loss will increase. If, however, two solid sulphides are used simultaneously, of which one or both do not dissociate, the result for each of the effusing metal sulphides is independent of the presence of the other and the total weight loss equals the sum of the single values. If the sulphides both dissociate, they influence each other, the total weight loss being smaller than the sum of the single values, and if one of the sulphides has a decidedly greater dissociation pressure than the other, it very much depresses effusion of the latter.

Experiments in which the effused vapor is absorbed or condensed and analysed are much more likely to have decisive results than simple weight loss experiments. In every particular case, the effect can easily be calculated on exactly the same basis which the discusser adopted for the calculation of the dissociation pressure of ZnS, i.e., thermodynamic equilibrium inside the effusion vessel in which the gas mixture is, in general, not of stoichiometric composition and effusion from the vessel in stoichiometric proportions.

Note: on p. 971 of the paper under discussion, Dr. Philipp Gross' name was misspelled.

**C. Law McCabe** *(author's reply)*—The remarks by Dr. Gross are correct. His suggestion to study the effusion rate of two solid sulphides together and to compare it to the sum of the effusion rate for each individual sulphide has merit and should be tried. The use of carbon as an aid to species determination is limited not only by the point brought out in the paper, the slow rate of formation of the appropriate carbon sulphide, but also by the point raised by Dr. Gross.

## Ionic Nature of Liquid Iron-Silicate Slags

by M. T. Simnad, G. Derge, and I. George

*DISCUSSION, R. Schuhmann, Jr. and D. J. Girardi, Chairmen*

**Dr. W. A. Fischer** *(Max-Planck-Institut, Düsseldorf, Germany)*—The discusser has read with great interest the paper by Simnad, Derge, and George. Inasmuch as their conclusions agree quite well with those of F. Sauerwald and G. Neuendorff in 1925[15] and those of W. Geller[16] in 1940, the authors' attention is called to these earlier papers.

**Tryggve Baak** *(Royal Institute of Technology, Stockholm, Sweden)*—The authors are to be congratulated for having tackled such a difficult work as measurements of current efficiency in melts of the FeO-$SiO_2$ system. The method used is extremely practical and can without doubt be applied to other silicate melts.

The discusser would like to call attention to a paper by Esin and Schurygin[17] who have worked on the same system and have found values in agreement with those in the paper. The only significant difference is related to pure iron oxide melts (FeO+$Fe_2O_3$), where values up to 33 pct current efficiency have been reached.

In a study of the degree of ionic conductance in fayalite melts,[18] the discusser has found 98 pct ionic conductance which can, in practice, be put equal to 100 pct, since in the computations the iron has been considered as ferrous.

Concerning the measurements of transport numbers, it must be emphasized, however, that the method used will not give transport numbers. The reason is obvious and the authors are referred to an analogous experiment, which was performed by Schwartz[19] who was able to show that it is impossible to determine transport numbers in ionic melts in this way. Furthermore, Jost[20] discussed this problem and stated that, in melts of this type, there are not, unlike solids and liquid solutions, any frame of reference to which changes in concentration can be referred. After electrolysis, there are no observable changes due to the existence of transference numbers, differing for the different types of ions. If a frame of reference is introduced, artificially, by the choice of suitable electrodes, the apparent transport numbers are directly influenced, the numbers being calculated with respect to this frame of reference.

To this must be added that under special circumstances[2] it is possible to create a frame of reference. When the material being used is $Co_2SiO_4$ and a small quantity of CoO is added, then the oxide can be used as a frame of reference. Of course, this method may be applied to other orthosilicates.

This discussion will in no way deny that the $Fe^{2+}$ ions are the main carrier of the current which can be concluded already, from a geometric point of view, because of the sizes of the ions. It is intended that the discussion only draw attention to some minor points in a very able work.

**M. Simnad, G. Derge,** and **I. George** *(authors' reply)*—The work reported in the two papers referred to by Dr. Fischer was not very extensive but the conclusions agree with some of the authors'.

Dr. Baak has raised several interesting points. It is satisfying to learn that his results on the degree of ionic conductance in fayalite melts confirm the high degree of ionization which the authors have observed. His comments on the transport number measurements would have been valid for a fayalite melt where the composition $2FeO \cdot SiO_2$ corresponds to that of the anodic reaction product, namely

$$SiO_4^{4-} + 4e \rightarrow SiO_2 + O_2$$
$$O_2 + 2Fe \rightarrow 2FeO$$
$$SiO_2 + 2FeO \rightarrow 2FeO \cdot SiO_2 \text{ (fayalite)}.$$

In the authors' experiments on transport number measurements, the melt was always saturated with silica at 1400°C and had a composition of 60 pct FeO and 40 pct $SiO_2$, whereas the FeO content of fayalite is 70 pct. Hence, FeO can be used as a frame of reference, just as Dr. Baak has skillfully used CoO in $2CoO \cdot SiO_2$ for the same purpose. Additional experiments are in progress in order to demonstrate this more conclusively.

The authors have also measured the mobility of $Fe^{++}$ ions in these melts by employing radioactive iron anodes. The results prove quite definitely that the $Fe^{++}$ ions migrate with a high mobility.

[15] F. Sauerwald and G. Neuendorff: *Ztsch. für Elektrochemie* (1925) 31, p. 643.
[16] W. Geller: *Ztsch. für Elektrochemie* (1940) 46, p. 277.
[17] O. A. Esin and P. M. Schurygin: *Doklady Akad. Nauk, SSSR* (1954) 94, p. 1145.
[18] T. Baak: *Acta Chem. Scandinavica* (1954) 8, p. 166.
[19] K. G. Schwartz: *Ztsch. für Elektrochemie* (1939) 45, p. 740.
[20] W. Jost: *Diffusion in Solids, Liquids, and Gases.* (1952) p. 466. New York. Academic Press.

# Discussion — Institute of Metals Division*


Effect of the Structure of Dislocation Boundaries on Yield Strength (paper by J. Washburn. JOURNAL OF METALS, May 1955, p. 675) 1262

*Chicago Meeting, November 1954*

Stress-Strain Characteristics and Slip-Band Formation in Metal Crystals: Effect of Crystal Orientation (paper by F. D. Rosi. JOURNAL OF METALS, September 1954, p. 1009) 1263

Viscosity and Density of Liquid Lead-Tin and Antimony-Cadmium Alloys (paper by H. J. Fisher and A. Phillips. JOURNAL OF METALS, September 1954, p. 1060) 1264

Some Characteristics of the Isothermal Martensitic Transformation (paper by C. H. Shih, B. L. Averbach, and M. Cohen. JOURNAL OF METALS, January 1955, p. 183) 1265

*Chicago Meeting, February 1955*

Vanadium-Zirconium Alloy System (paper by J. T. Williams. JOURNAL OF METALS, February 1955, p. 345) 1266

Magnesium-Rich Corner of the Magnesium-Lithium-Aluminum System (paper by J. A. Rowland, Jr., C. E. Armantrout, and D. F. Walsh. JOURNAL OF METALS, February 1955, p. 355) 1267

Effect of Zinc Content on the Rolling Texture and Annealing Texture of Alpha Brass (paper by A. Merlini and P. A. Beck. JOURNAL OF METALS, February 1955, p. 385) 1267

On the Relationship of Texture Changes of Cold-Rolled Face-Centered-Cubic Metals During Recrystallization (paper by Y. C. Liu and W. R. Hibbard, Jr. JOURNAL OF METALS, February 1955, p. 381) 1270

Preferred Orientations in Beta-Annealed Zirconium (paper by J. H. Keeler and A. H. Geisler. JOURNAL OF METALS, February 1955, p. 395 1271

Contribution of Crystal Structure to the Hardness of Metals (paper by W. Chubb. JOURNAL OF METALS, January 1955, p. 189) 1272

Study of a New Mode of Plastic Deformation in Zinc Crystals (paper by J. J. Gilman. JOURNAL OF METALS, January 1955, p. 206) 1273

Viscous Flow of Copper at High Temperatures (paper by A. L. Pranatis and G. M. Pound. JOURNAL OF METALS, May 1955, p. 664) 1274

Study of the Effect of Boron on the Decomposition of Austenite (paper by C. R. Simcoe, A. R. Elsea, and G. K. Manning. JOURNAL OF METALS, January 1955, p. 193) 1275

Isoembrittlement in Chromium and Molybdenum Alloy Steels During Tempering (paper by G. Bhat and J. F. Libsch. JOURNAL OF METALS, February 1955, p. 330) 1276

A Study of the Microstructure of Titanium Carbide (paper by H. Blumenthal and R. Silverman. JOURNAL OF METALS, February 1955, p. 317) 1277



* TP 4100E.


## Effect of the Structure of Dislocation Boundaries on Yield Strength

by Jack Washburn

**P. L. Pratt** *(University of Birmingham, Birmingham, England)*—The author has measured the hardening effect of isolated edge and screw dislocation boundaries in a remarkably elegant manner, and he proposes that the detailed structure of the boundary determines its effectiveness as a barrier to slip although "there are still unknown details of the distribution which may be extremely important." On p. 678 the author states "that for a good crystal (one having a yield of about 30 psi) a change in annealing temperature from 300° to 400°C resulted in a negligible shift in the level of the stress-strain curve." Is this in agreement with the results of the earlier paper by Li, Washburn, and Parker[2] in which such a change of temperature produced notable hardening in crystals with a yield of about 30 psi? Or were these earlier crystals, of the same nominal purity, less perfect than those used in this work?

The experiment illustrated in Fig. 15, p. 681, shows that the boundary has sharpened after annealing at 400°C, the temperature at which the hardening effect first becomes apparent. Did the author verify that no sharpening of the boundary occurred at, say, 300°C where no hardening was found? This would seem to be an important check on the proposed mechanism, especially since zinc of this purity should polygonize at temperatures well below 400°C within the annealing times used here. There seem to be at least two alternative explanations which could fit these facts:

1—The boundary may sharpen at 300°C or even lower temperatures but be unable to contribute greatly to the hardening until jogged by thermal vacancies and other impurity atoms after 400°C anneal. This mechanism, discussed in the earlier paper,[2] is believed to account for the thermal hardening observed by Blank[3] in NaCl, as stated elsewhere,[1] and by results from recent experiments which tend to confirm this view.

2—The dislocations in the diffuse boundary may be locked by impurity atoms at 300°C and thus only sharpen the boundary at 400°C with the aid of thermal vacancies. In this case it would be difficult to distinguish between the two sources of hardening (sharpening or jogging), using metal of this purity.

**Jack Washburn** *(author's reply)*—The author wishes to thank Dr. Pratt for his discussion. In connection with his first comment, it should be pointed out that the temperature of testing in the present series of experiments was −196°C, whereas, in the earlier experiments he referred to,[2] it was 20°C. Therefore, the yield values should not be directly compared. It is likely that the crystals used in the present work were initially more perfect macroscopically than the large shear specimens used previously. The small size of the test section in the kink specimens made it possible to select regions of the large crystals, from which they were acid-cut, that were free of observable small angle boundaries. The sharpening of a microscopically diffuse boundary such as that in Fig. 15 begins in zinc of this purity well below 300°C. However, it is probably not justified to conclude that because a boundary looks sharp under the microscope it has attained the ideal structure. The author agrees with Dr. Pratt that jogging of dislocation lines is one of the structural features of a small angle boundary that should be important in determining its strengthening effect. More detailed information concerning the changes in boundary structure as a

function of annealing time and temperature is necessary before it will be possible to say what structural change is most important.

[16] F. Blank: Ztsch. für Physik (1930) 61, p. 727.
[17] R. W. Cahn: Ref. 22, Supplemento al Nuovo Cimento (1953) 10, p. 359.

## Stress-Strain Characteristics and Slip-Band Formation in Metal Crystals: Effect of Crystal Orientation

by F. D. Rosi

*DISCUSSION, W. A. Backofen and W. M. Baldwin, Chairmen*

**Bernard Jaoul** *(Centre de Recherches Métallurgiques, Ecole des Mines, Paris, France)*—Experiments on single crystals of aluminum (99.99 pct purity) and aluminum alloys (0.2 pct Si or 0.4 or 1.0 pct Cu) of varying orientation lead to the following results which are slightly different from those presented by Dr. Rosi:

1—All the stress-strain curves, including the curves obtained with those crystals which have their axes on the zone [100]-[111] or close to the [100] or [111] directions, have a first plastic stage where concavity is turned upward. However, the extent of stage I becomes very small when two slip systems occur; see Fig. 24. It must be noted that a very small amount of deformation during the handling of the specimens makes the easy glide disappear if this easy glide is limited.

2—A continuous photographic recording of the curves permits a very fine observation of their shape. Fig. 25 shows that the curves could be separated into two types from their behavior patterns at the beginning of straining. These types are: A—curves showing a yield point even in *pure* aluminum, a type of behavior that is general for the crystals that are strained without kink bands; and B—curves showing no yield point, a behavior that occurs when the glide is only on one plane and when kink bands occur. This type of curve becomes very rare when the aluminum is alloyed.

3—With aluminum, a parabolic hardening but no linear strain hardening occurred after the easy glide. The inflection point was taken as the limit of stage I. This limit is always at the same shear stress (Fig. 24) but the shear strain varies within very large limits, from 1.4 to 8 pct in pure aluminum. This variation depends only on the importance of the second slip system or of bands of secondary slip. Qualitative observations of the deformation microstructure seem to show that the relative importance of the two slip systems remains constant during the straining. For the orientations where kink bands occur—close to [110]—the initial shape of the curves seems to indicate that these kink bands are formed at the beginning of deformation.

4—As in silver and copper, the impurities in aluminum increase stage I by a large amount. This is shown in Table VIII where the values are within an accuracy of ±10 g per sq mm for $\tau_0$ and ±30 g per sq mm for $\tau_i$, except for some anomalies, especially near [111] and [100].

5—The uniform shape of the curve that was obtained leads to the following considerations: The increase of hardening seems to be related only to the importance of the second slip system and, thus, to the number of intersecting dislocations forming jogs or sessile dislocations. These faults in the structure can stop the progress of the dislocation loops from the sources. The number of such barriers should increase with deformation; and the faster the increase, the greater becomes the importance of the second system. With such an hypothesis, the shape of stage I of the shear stress ($\tau$) vs shear strain ($\gamma$) curve can be represented by a uniform logarithmic formula

$$\tau = \tau_0 - \frac{C}{L_{n^2}} \ln\left(1 - \frac{\gamma}{2\gamma_i}\right)$$

where $C$ is the work hardening in stage I ($C = \tau_i - \tau_0$).

This relation fits the experimental results very well, whatever may be the orientation of the crystal.

Then Schmid and Boas' law can be extended to the plastic range in the following way: The shear stress corresponding to a given fraction of the shear strain at the inflection points is independent of the orientation, except for the crystals near [111] or [100].

6—This relation is valid up to a critical shear stress $\tau_i$ where the internal stresses are such that the dislocations can proceed across the barriers. This critical shear stress is much smaller in aluminum than in copper and silver, as can be seen by comparing Dr. Rosi's curves and those in Fig. 24. The smaller critical shear stress for aluminum may be due to the fact that the barriers are less stable in aluminum.[18]

The mechanism at the end of stage I does not include a phenomenon of diffusion of impurities. Al-0.4 pct Cu specimens were strained at various rates (from 0.005 to 50 pct per min). The yield point was changed but the value of the shear stress $\tau_i$ remained the same: $\tau_i = 680 \pm 10$ g per sq mm. This leads to the belief that the microstructure of deformation has to change with purity—the number of barriers has to be smaller when the metal is less pure. Perhaps the amount of fine slip seen by D. Kuhlmann Wilsdorf on pure aluminum is smaller when the amount of impurities increases, so that the number of barriers decreases.

A comparable mechanism has been found in polycrystals,[19] but it is less clear because partly hidden

Table VIII. Data on the Shear Stress vs Shear Strain Curves

| | $\tau_0$,* G per Sq Mm | $\tau_i$,† G per Sq Mm | n | $\gamma_i$,‡ Pct |
|---|---|---|---|---|
| 99.99 pct Al | 65 | 250 | 40 | 5.0 |
| Al-0.2 pct Si | 180 | 400 | 6 | 10.2 |
| Al-0.4 pct Cu | 210 | 680 | 20 | 9.8 |
| Al-1.0 pct Cu | 390 | 1220 | 3 | 20.5 |

* $\tau_0$ is the mean critical elastic shear stress.
† $\tau_i$ is the shear stress at the inflection point averaged over n curves.
‡ $\gamma_i$ is the shear strain (extent of stage I) for a common orientation: $\chi = 42°$ and $\lambda = 44°$.

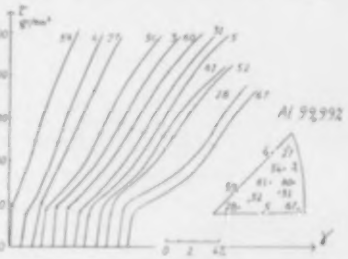

Fig. 24 — Plot of shear stress vs shear strain curves for 99.99 pct Al shows the shape of the curves and location of the inflection point.

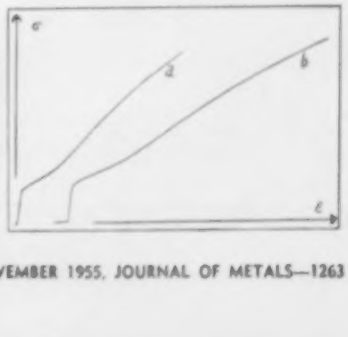

Fig. 25 — Recorded stress-strain curves for 99.99 pct Al have been reproduced to show the two types: a—those with a yield point and b—those without a yield point.

by the hardening due to boundaries. However, from a scrutiny of the curves, a change of curvature has been found at a critical strain that has been called *transition point*. The corresponding strain $\epsilon_p$ increases when the amount of impurities increases, as in the single crystals, following the relation

$$\epsilon_p = k\, x^{1/2}$$

where $x$ is the atomic concentration.[47] For the strain $\epsilon_p$ in polycrystals, something breaks down within the metal which allows the deformation to proceed, using a smaller rate of hardening. It seems that the phenomenon is the same as in single crystals.

[46] A. Seeger and G. Schöck: *Acta Metallurgica* (1953) 1, No. 5, p. 519.
[47] C. Crussard and B. Jaoul: *Révue de Métallurgie* (1950) 47, No. 8, p. 589.
[48] B. Jaoul: *Publication Scientifique et Technique du Ministère de l'Air* Paris (1954) No. 290.

## Viscosity and Density of Liquid Lead-Tin and Antimony-Cadmium Alloys

by H. J. Fisher and A. Phillips

*DISCUSSION, Howard Scott and Paul Gordon, Chairmen*

**Paul G. Bastien** and **M. Darmony** *(Ecole Centrale des Arts et Manufactures, Paris, France)*—The discussers have studied with much interest the excellent experimental work of the authors on viscosity and density of liquid Pb-Sn and Sb-Cd alloys.

Since the discussers are conducting research on the viscosity and castability of alloys, they would like to propose the following:

*Pure Metals:* The measure of viscosity $\eta$ by means of the damping of an oscillating vessel containing the liquid, suspended from a torsion wire, has been carried on either 1—by the use of a hollow sphere[41, 42] or 2—by the use of a hollow cylinder.[5, 31, 32, 33, 43]

In another way, some workers[44, 45] have experimented with the Margules-Couette's design, in which a cylinder moves in a uniform rotation around a second coaxial cylinder suspended from a torsion wire. The torsion deviation $a$ measures the viscosity $\eta$ of the liquid between the two cylinders.

Until now, there was a disagreement between the methods using a sphere and those using a cylinder.

The curve $\log \eta$ vs $1/T$ was a straight line even in the vicinity of the freezing point when a sphere was employed; while, in the case of a cylinder, a deviation from the linear rule was noticed in a range of a few °C's above the freezing point. This deviation suggested the existence of an unstable crystalline structure in the liquid phase near the freezing point. The results of Fisher and Phillips and those of Gebhardt and his research group, with an oscillating cylinder, confirm the validity of the linear rule down to solidification.

Therefore, it is permissible to think, along with some authors,[46] that the deviations from the linear rule are results of imperfections of the tests, i.e., impurities of the liquid studied, temperature gradients, etc.

*Alloys:* The results obtained by Fisher and Phillips contradict those of Jones and Bartlett.[16] For the former authors, the alloys have not any appreciable variation in the limit of solid solubility (except, perhaps, to 1°C above the liquidus); whereas, for the latter authors, there is a maximum of viscosity for the same concentration. Accordingly, it seems that it is now too early to decide in favor of the rule relating the viscosity of an alloy and its equilibrium diagram.

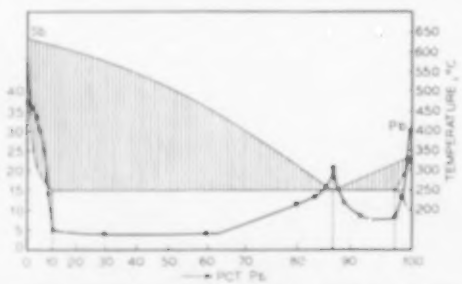


Fig. 18—Diagram shows that castability varies inversely with the interval of solidification for antimony and lead.

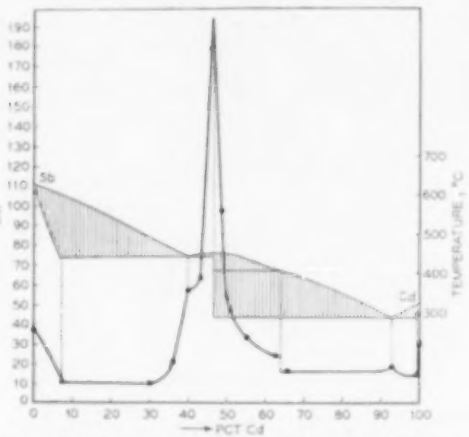


Fig. 19—Castability-composition curves of Portevin and Bastien for the Sb-Cd system show that there is little interdependence between viscosity and castability when compared with the viscosity-composition curves of Fisher and Phillips.

The authors of the paper gave the results of experiments carried on at 1°C above the liquidus. Therefore, this supposes a good knowledge of the curves of the equilibrium diagram to an accuracy of about 1°C. The discussers would be particularly interested to know if the authors have recently plotted, with a better accuracy, the equilibrium diagram of the materials studied; and, in this case, they would be very grateful to have an estimate of the precision of their methods of plotting.

*Viscosity and Castability:* The influence of the composition on the viscosity allows a useful comparison between the viscosity $\eta$ as an elementary physical property and the castability $A$ which is a complex property of foundry, depending, too, on other elementary factors (factors depending on the metal, factors relating to the mold and the contact between the mold and the casting, factors defining the casting conditions, etc.).

One of the discussers,[47] after systematic study with Portevin, has established the rules that relate the castability to the equilibrium diagram. He concluded that castability varied inversely with the interval of solidification, shown in Fig. 18, and he thought that the castability was nearly independent of viscosity.

A comparison between the viscosity-composition curves shown by Fisher and Phillips and the castability-composition curves of Portevin and Bastien for the Sb-Cd system, Fig. 19, shows that there is little interdependence between viscosity and castability.

In the particular case of the compound SbCd, a maximum of $\eta$ would be accompanied logically by a minimum of $A$, if the castability was principally dependent

on $\eta_i$ which is not true. On the contrary, Fig. 19 shows that a very pronounced maximum of castability corresponds to this definite compound.

Therefore, it is not possible to explain the sudden increase of castability near the eutectic and the definite compound as a function of viscosity.

**H. J. Fisher** and **A. Phillips** *(authors' reply)*—The precision of the potentiometer used in determining the liquidus temperature was 0.1 $\mu$v. The degree of uncertainty of the calibrated Pt—Pt-Rh thermocouple used was well within the order of ±0.5°C. U. S. Bureau of Standards calibration metals were checked to within ±0.2°C of their rated melting points.

Study of the physical properties of liquid metals and the fundamental factors influencing liquid metal flow has admitted applied and theoretical interest. It is, however, still difficult to establish a direct correlation between the viscosity, which is a specific physical property of a metal, and its castability, which is a complex function of many not easily controlled or evaluated factors such as: 1—latent heat effects, 2—surface tension at the metal/mold interface, 3—rate of heat abstraction, 4—variation of thermal conductivity of the alloy with composition, 5—restraining influence of the solidifying metal on flow through the channel, and 6—degree of supercooling possible with certain metals, e.g., antimony.

Even if the authors disregard all the foregoing influences except that from the latent heat of fusion of the SbCd compound, calculation[46] indicates that a relatively large temperature increase is possible in the liquid alloy immediately in the vicinity of the alloy undergoing freezing. This would prolong the time available for the liquid alloy to remain fluid and give rise to a relatively greater castability in comparison to that of the antimony or the cadmium.

On a weight basis, it can be shown that the heat released during freezing of 1 g of the SbCd alloy is sufficient to raise the temperature of 1 g of liquid alloy by approximately 410°C. Thus, on a relative basis, 1 g of the SbCd alloy on freezing releases enough heat to raise the temperature of 1 g of adjacent liquid SbCd alloy approximately 116°C higher than would be 1 g of liquid antimony or 240°C higher than 1 g of liquid cadmium.

The latent heat of fusion, $L_{SbCd}$, of the intermetallic compound SbCd can be well approximated from the following expression

$$L_{SbCd} = (x(L_{Cd}) + y(L_{Sb}) - \Delta H_{SbCd}) \text{ cal per gram-atom}$$

where $x$ and $y$ are mol fractions of cadmium and antimony, respectively; $L_{Cd}$ is the latent heat of fusion of cadmium and $L_{Sb}$ is the latent heat of fusion of antimony, both in cal per gram-atom; and $\Delta H_{SbCd}$ is the heat of formation of SbCd, —1800 cal per gram-atom.[46]

[41] E. N. de C. Andrade and Y. S. Chiong: *Proceedings* Physical Soc. (1936) **48**, p. 247.
[42] E. N. de C. Andrade and E. R. Dobbs: *Proceedings* Royal Soc. (1952) **211A**, p. 12.
[43] Y. S. Chiong: *Proceedings* Royal Soc. (1936) **157**, p. 264.
[44] E. Gebhardt and G. Wormag: *Ztsch. für Metallkunde* (1951) **42**, p. 353; (1952) **43**, No. 4, p. 106.
[45] E. Gebhardt, M. Becker, and E. Tragner: *Ztsch. für Metallkunde* (1953) **44**, No. 6, p. 379.
[46] B. R. T. Frost: *Progress in Metal Physics*. (1954) **V**, p. 102. London, Pergamon Press.
[47] P. Bastien: *Revue de Métallurgie* (1934) **31**, p. 270.
[48] R. A. Oriani: Private communication.
[49] C. Wagner: *Thermodynamics of Alloys*. (1952) p. 84. Boston, Addison-Wesley Press.

## Some Characteristics of the Isothermal Martensitic Transformation

by C. H. Shih, B. L. Averbach, and Morris Cohen

*DISCUSSION, E. S. Machlin and J. K. Stanley, Chairmen*

**D. Turnbull** *(General Electric Co., Schenectady)*—The discusser has analyzed some of the authors' isotherms in order to discover how well they can be described by an analytical relation of the form

$$x = at^n \qquad [3]$$

where $x$ is the volume fraction of the specimen transformed to martensite, $t$ is the time, $a$ is a temperature-dependent constant, and $n$ is a constant—possibly temperature independent. Eq. 3 is the limiting form, for $x \to 0$, of the more general relation

$$x = x_i[1 - \exp(-bt^n)] \qquad [4]$$

where $x_i$ is the limiting volume fraction of the specimen that transforms to martensite by a single mechanism and $a = bx_i$. It seems likely that the formation of isothermal martensite is complicated in the later stages by secondary processes, and also the decrease in size of martensite crystals due to "partitioning" becomes more important as the reaction progresses.[15] Therefore, the interpretation of the dependence of $x$ on time may be less complicated the smaller is $x$.

The dependence of log $x$ on log $t$ for the various isotherms included in the insert of the authors' Fig. 1 is shown in Figs. 8 and 9. The coordinates of the plotted points were calculated from $x = f(t)$ readings obtained from a X4 enlargement of the insert. When $x \gtrsim 0.03$, the relation between log $x$ and log $t$ is approximately linear, in agreement with Eq. 3. The best values of $n$ are indicated in the figures and range between 2.3 and 3.0, there being no marked trend with temperature. For $x > 0.03$, the transformation rates at a given temperature decrease more rapidly with increasing $x$ than demanded by either Eqs. 3 or 4 with a single $n$ value (to test Eq. 4, $x_i$ was set equal to 0.25 to 0.30).

Thus, as $x \to 0$, $n$ appears to have a limiting value between 2 and 3 but nearer to 3. However, the experimental error is relatively large for small values of $x$ and it is likely that the uncertainty in $n$ is of the order of ½ unit. Further, a particular analytical relation between $x$ and $t$ does not by itself establish a unique interpretation of the kinetic process.

However, a plausible interpretation of the kinetics that is consistent with the observed $x = f(t)$ relation and that can be tested by microstructural observations will be suggested. Suppose that transformation starts at a number $N$ per unit volume of sites that are primary nuclei immediately upon the establishment of the transformation temperature and that $N$ is not affected by time at this temperature. An initial martensite crystal disturbs, perhaps by plastic deformation, a volume surrounding it. Secondary sites within this disturbed volume are now promoted to martensite nuclei but an average time $\tau$ must elapse before a site within a disturbed region becomes a nucleus. Thus a disturbed zone may propagate from the center of a primary nucleus with a velocity, $a$. New martensite crystals nucleate at the periphery of the zone and thus sustain its continued propagation. This phenomenon would be quite like the "burst" phenomenon reported for Fe-Ni alloys but with a much greater time constant for the individual events constituting the burst. If this picture is correct, isolated colonies of martensite crystals should be observed to grow (via the formation of new crystals at their periphery) and finally impinge upon one another.

Assuming that a colony is spherical in shape, its volume $v$ after a time $t$ should be

$$v = x_i(4\pi/3)a^3(t - \tau)^3 \qquad [5]$$

and correcting for impingement as in the treatment of Johnson and Mehl,[15] an expression relating the martensite fraction, $x$, to $t$ is obtained that is formally identi-

cal with Eq. 4 with

$$b = (4/3)\pi N a^3 \quad [6]$$

$$n = 3.0. \quad [7]$$

The meaning of $a$ is more clearly indicated by the expression

$$a = pv_s(\lambda/\tau) \quad [8]$$

where $p$ is the number of secondary sites per unit volume, $v_s$ is the increase in volume of the disturbed zone due to formation of one martensite crystal, $\lambda$ is the mean spacing of martensite crystals within a colony, and $\tau$ is the mean time for formation of a martensite crystal within a disturbed region.

The fact that $n$ is usually less than three and tends to decrease as the transformation progresses might be accounted for if there is a spectrum of time constants for the secondary sites (as the authors have suggested for the primary sites). Also, if the concentration of preferred sites were greater near the surface, it would follow that impingement would be complete at the surface sooner than throughout the volume. Thus, the transformation rate would be less than predicted by Eq. 4. In the event that all the preferred sites are in the vicinity of the surface, $dx/dt$ should decrease continually after surface impingement. Thus Cech and Hollomon's results can be accounted for if it is assumed that at the start of their measurements the specimen was encased by a thin surface shell in which impingement of martensite colonies was complete and if this shell then grew inward without the nucleation of any additional primary sites in the interior of the specimen.

The discusser would like to have the authors' opinion on whether or not the interpretation that he has suggested is consistent with the microstructural changes that accompany the transformation.

There is strong evidence from other investigations (e.g., Machlin and Cohen[14]) that martensite nuclei form, in bulk specimens at least, at preferred sites. However, the fact that the authors' energy of nucleation, $\Delta F_n$, is smaller than the values calculated from Fisher's analysis is irrelevant to the question of preferred nucleation, since $\Delta F_n$ (or $n_c$) is a disposable parameter in the authors' treatment. In fact, general nucleation would be at least as important as singularity nucleation in the authors' experiments unless the free energy barrier to general nucleation is substantially *larger* than the 10 to 27 kcal per gram-atom that they calculate.

It is not clear whether the authors intend to imply (see point 4 of their summary) that preferred site

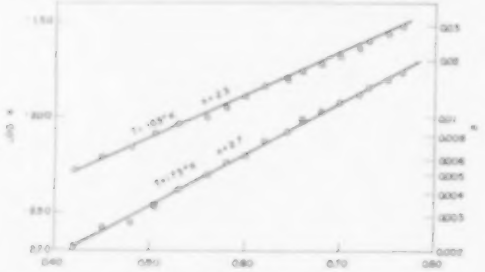

Fig. 8—Dependence of log $x$ on log $t$ for the various isotherms included in the insert of Fig. 1 is shown.

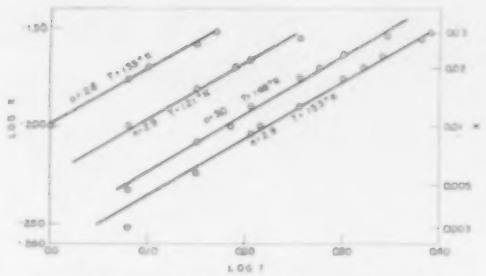

Fig. 9—Dependence of log $x$ on log $t$ for the various isotherms included in the insert of Fig. 1 is shown.

nucleation (i.e., heterogeneous nucleation) is somehow inconsistent with classical nucleation theory. However, the phenomena of heterogeneous nucleation (whether in fluid or solid media) have been readily explained on the basis of the classical nucleation theory. Possible interpretations of heterogeneous nucleation in the martensite transformation, based on the classical nucleation theory, are developed in papers by Hollomon and Turnbull[12] and Fisher and Turnbull.[13]

**C. H. Shih, B. L. Averbach,** and **Morris Cohen** *(authors' reply)*— As suggested by Dr. Turnbull, the microstructures have been examined in the early stages of the isothermal martensitic reaction. Nucleation was observed at preferred sites, such as grain boundaries, twin boundaries, and existing plates of martensite. In the latter case, the effect looked somewhat like chain lightning. Spherical colonies or patches of geometric similitude were not developed. Thus, although the reaction was certainly autocatalytic, the assumption of isothermally advancing colonies was not supported by the metallographic observations. In other words, the critical conditions for Dr. Turnbull's analysis were not operative in the alloys studied here.

His explanation of the data published by Cech and Hollomon is interesting. If an initial layer of martensite was produced at the surface of their specimens because of manganese loss, it would seem that this hypothesis could be checked by metallographic examination. It is also worth mentioning here that Fisher has applied the classical theory of homogeneous nucleation to the martensitic transformation in these Fe-Ni-Mn alloys and has reported good agreement.

Clearly, a choice between homogeneous and heterogeneous nucleation cannot be made on the basis of $\Delta F_n$ values alone. The authors' point is that the concept of preferred nucleation sites is both consistent with the microstructural observations and leads to values of the nucleation energy that are at least as reasonable as those derived on the assumption of homogeneous nucleation. The authors would argue that the classical theory of homogeneous nucleation is actually weakened by its reported agreement with the martensitic kinetics in these alloys because the microstructures show that the nucleation is, in fact, heterogeneous rather than homogeneous.

[12] W. A. Johnson and R. F. Mehl: Trans. AIME (1939) 135, p. 416; Metals Technology (August 1939).
[13] E. S. Machlin and M. Cohen: Trans. AIME (1951) 191, p. 746; Journal of Metals (September 1951).
[14] J. H. Hollomon and D. Turnbull: *Progress in Metal Physics* (1953) 4, pp. 333-388. London, Pergamon Press.
[15] J. C. Fisher and D. Turnbull: *Acta Metallurgica* (1953) 1, p. 310.

## Vanadium-Zirconium Alloy System

by J. T. Williams

*DISCUSSION, D. J. McPherson and J. P. Nielsen, Chairmen*

**Rodney P. Elliott** *(Amour Research Foundation of Illinois Institute of Technology, Chicago)*—In conjunction with a program of investigation of the Laves-type phases, an alloy at the stoichiometric composition $ZrV_2$ was prepared by arc-melting techniques. Similar to the experience of the author, the powder pattern of this composition was greatly fogged; however, no difficulty

was experienced in assigning indices of the $MgCu_2$ structure to this pattern. The lattice parameter was calculated to be 7.43kX. Other lines were observed but were accounted for as hexagonal-close-packed zirconium or body-centered-cubic vanadium.

There is an equivalence of Miller indices for planes of equal interplanar spacing for the three Laves-type structures; by the absence or presence of lines, it is possible to establish which of the phases is present. For this reason, it should have been possible for the author to index the pattern of his $\gamma$-phase as isomorphous with the $MgZn_2$ structure, even though this structure as determined by Wallbaum is not correct. It has been positively established that $ZrV_2$ is isomorphous with $MgCu_2$ and not $MgZn_2$. Specimens of the $ZrV_2$ alloys were annealed at 200° intervals from 600°C upward but gave no indication of having any allotropic structures.

## Magnesium-Rich Corner of the Magnesium-Lithium-Aluminum System

by J. A. Rowland, Jr., C. E. Armantrout, and D. F. Walsh

*DISCUSSION, D. J. McPherson and J. P. Nielsen, Chairmen*

**David W. Levinson** *(Armour Research Foundation of Illinois Institute of Technology, Chicago)*—As is pointed out by the authors, Shamrai[9,10] reports the existence of a ternary intermediate phase, called $MgLiAl_6$, which was not found by Frost et al.[5] nor by the present study. All of these studies were concerned with compositions in the vicinity of the magnesium corner.

A study of phase relations in the system Mg-Li-Al carried on at Armour Research Foundation between 1952 and 1955, results of which have been submitted for publication, have confirmed the existence of the Shamrai compound (Fig. 11) at the composition 46 atomic pct Al, 31 atomic pct Li, and 23 atomic pct Mg. The structure of this compound was found to be cubic ($a_o = 20.2$Å). Micrographs showing the coexistence of the compound with the magnesium solid solution and with the magnesium solid solution and $Mg_{17}Al_{12}$ are given in Figs. 12 and 13. These alloys were quenched from 400°C and were found to be essentially unchanged at 300°C.

These data cannot be reconciled with the identification of phases given by the authors in Fig. 8.

With regard to the size and temperature variation of size of the (Mg) and (Mg) + $\beta$ phase fields, the work at Armour is in essential agreement with the data presented in this paper.

**J. A. Rowland, Jr., C. E. Armantrout,** and **D. F. Walsh** *(authors' reply)*—The authors are grateful to Mr. Levinson for the interest taken in their paper and particularly for having called attention to evidence which he has obtained indicating the existence of the ternary compound $MgLiAl_6$ in fields extending to the $\alpha$ magnesium solid solution area. In the authors' study of the alloys, no evidence of the presence of this compound was found in the magnesium corner of the equilibrium diagram. Because of the narrowness of the three fields in which the compound is said to exist, especially when considering the diagram in terms of weight percent composition, occurrence of $MgLiAl_6$ could easily escape detection.

The structure shown in Fig. 8 of the authors' paper does not resemble that of Mr. Levinson's micrograph, Fig. 13. In the former, a clear-cut distinction exists between the $Mg_{17}Al_{12}$ and the partially dissolved AlLi; whereas, the outlined white phase in the discusser's Fig. 13 appears surrounded by an irregular gray zone.

The authors are pleased to see that Mr. Levinson's work verifies in general a major portion of the diagram as presented in this paper, and they await with interest the publication of details of his research on the alloy system.

[10] F. I. Shamrai: *Izvestiya Akademii Nauk SSSR* Otdelenie Khimicheskikh Nauk (1947) No. 6, pp. 605-611; (1948) No. 1, pp. 83-94.

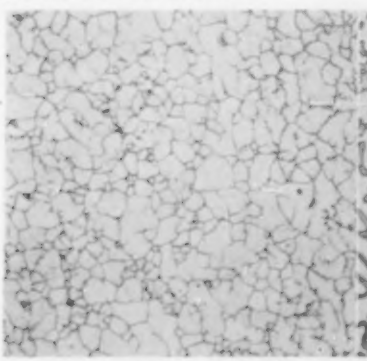

Fig. 11—Micrograph shows the existence of the Shamrai compound, the single phase $MgLiAl_6$. X250. Area reduced approximately 25 pct for reproduction.

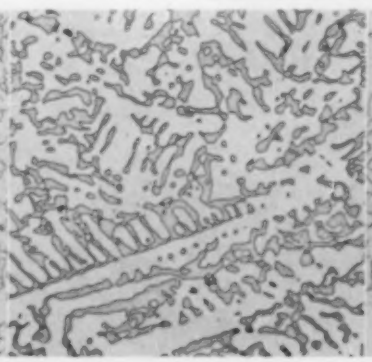

Fig. 12—Micrograph shows the coexistence of the Shamrai compound ($MgLiAl_6$) with magnesium solid solution (Mg). X250. Area reduced approximately 25 pct for reproduction.

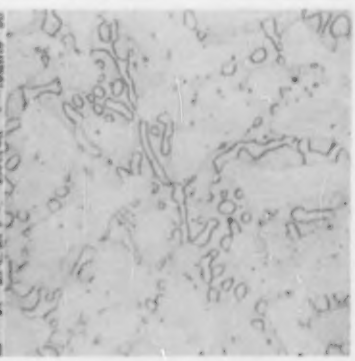

Fig. 13—Micrograph shows the coexistence of the Shamrai compound ($MgLiAl_6$) with magnesium solid solution (Mg) and $Mg_{17}Al_{12}$. X250. Area reduced approximately 25 pct for reproduction.

## Effect of Zinc Content on the Rolling Texture and Annealing Texture of Alpha Brass

by Alfonso Merlini and P. A. Beck

*DISCUSSION, G. Edmunds and W. R. Opie, Chairmen*

**Y. C. Liu** *(Research Div., New York University, New York)*—The authors apparently have not considered an important factor which must influence the observed

recrystallization texture, i.e., the presence of annealing twins. Annealing twins are quite profuse in brass and the number of twins per grain and the number of twin families per grain are increased with the addition of zinc to copper.[9] The effect of annealing twins on the recrystallization texture of brass should, therefore, be reflected in the recrystallization pole figures.

The 19 "ideal orientations" (indicated as 15 by the authors) were broken down into six groups designated as *A*, *B*, *C*, *F*, *M*, and *S*. The three orientations *A*, *B*, and *F* are in twin relationship, i.e., with orientation *A* as the parent orientation, orientations *B* and *F* are first order twins with respect to *A* about different octahedral planes. This is shown in Fig. 19. The orientation *A* can be related to the (110) [112] component of the deformation texture by a 22° rotation about octahedral pole III. Orientation *M* could also be related to the (110) [112] component by a 38° rotation about pole II, Fig. 19, as proposed by Dunn.[11] Orientation *C* is a cubic orientation which is related to the modified (358) [352] component of the deformation texture.[10] The assignment of orientation *S* seems to be doubtful. The locations of its octahedral poles are in low intensity regions. This orientation, however, can also be related to the modified (358) [352] component by a 22° rotation, as shown in Fig. 20. The orientations *C* and *S* should disappear in brass with higher zinc content, since both of them are related to the modified (358) [352] component of the deformation texture. On the basis of this analysis, the data appear to be in good agreement with the Liu and Hibbard rationalization.[10]

The authors stated that "such a theory would certainly have difficulty in accounting for the formation of the cubic texture . . . when the main deformation texture components become further and further removed from a <111> rotational relationship from the cubic orientation." The assignment of an ideal orientation to describe a component in a pole figure is usually very arbitrary, especially when the pole figure exhibits a large amount of scatter and many high intensity areas. In Fig. 2, for example, the positions of the four <111> poles of (145) [945] orientation are located at the intensity level of 725 (= 1450/2), 350, 500, and 390. The same tendency is also exhibited in Fig. 4. The data would be a little more self-consistent if they were explained on the basis of two components of the deformation texture.[12] The maximum near the rolling direction could be the pole which is associated with three orientations, one being the (110) [112] and others the modified (358) [352] orientations. The one near the transverse direction could be a superimposition of two adjacent maxima.* On this basis, the estimated amounts of individual components† of the deformation texture are shown in Table IV.

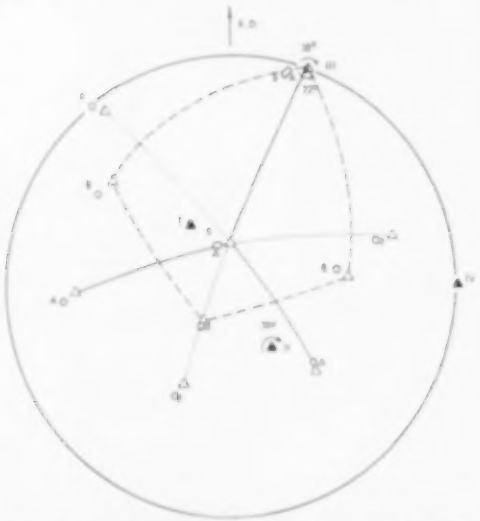

Fig. 19—Orientation relationships of *A*, *B*, *F*, and *M* with the (110) [112] component of the deformation texture are shown. Various symbols represent: circles, the octahedral poles for the respective orientations; solid triangles, the (110) [112] orientation; and open triangles, the orientations related to the (110) [112] orientation.

* It was observed that this maximum is almost always lower than it should be. This is better indicated in the case of 70:30 brass,[9] in which this maximum should be twice the intensity as plotted. This is because it is shared by both of the (110) [112] orientations. Following the trend in 70:30 brass, only the intensity of one orientation, instead of two, is considered in the present estimation.

† The total amount of each component in the deformation texture should be multiplied by two in the case of (110) [112] orientation and by four in the case of the modified (358) [352] orientation.

**Table IV. Estimated Amounts of Individual Components of the Deformed Textures**

| | (110)[112] | Modified (358)[352] |
|---|---|---|
| 3 pct Zn | 650 | 350 |
| 6 pct Zn | 550 | 200 |
| 10 pct Zn | 750 | 150 |

The amounts of recrystallization components of *A*, *B*, *F*, *M*, and *C* orientations were also estimated. Since some of intensity maxima in the <111> pole figures are associated with more than one orientation, the intensity levels in <200> pole figures were used. Where the intensity levels of the three cubic poles of a given orientation are not consistent, the pole intensity nearest to the center of the pole figure was used. It is assumed that the experimental error in this region is the least. The estimated amounts of individual components of recrystallization textures are as given in Table V. From this table, it is probable that the modified (358) [352] component existed in all of the brass strip, is decreased in amount with increasing zinc content, and is also similarly reflected in the recrystallization pole figures.

**Table V. Estimated Amounts of Individual Components of Recrystallization Textures**

| | Component Derived From Modified (358)[352], *C* | Components Derived From (110)[112] | | | | |
|---|---|---|---|---|---|---|
| | | *A* | *B* | *F* | *M* | Total* |
| 3 pct Zn | 100 | 80 | 80 | 60 | 45 | 970 |
| 6 pct Zn | 50 | 70 | 110 | 50 | 45 | 1010 |
| 10 pct Zn | 40 | 70 | 150 | 80 | 70 | 1340 |

* The total amounts of components *A*, *B*, *F*, and *M* should be multiplied by 4, 4, 4, and 2, respectively. This column shows the total amounts of components derived from the (110)[112] component of deformation texture.

As to the point mentioned by authors that the spread of the recrystallization texture should be roughly on the order of that of the deformation texture, according to his concept, the discusser thinks the whole problem still lies in the designation of "ideal orientation" for the deformation texture. In the deformation pole figures, the authors assigned only one orientation for the deformation texture so, naturally, there is quite a region of spread around the "ideal orientation." In the discusser's concept, two ideal orientations were assigned, as in Prof. Beck's previous investigation on copper.[8] This cuts down the spread markedly.

The discusser proposes the concept of two components of deformation texture of face-centered-cubic metals and considers that only one of them functions during annealing, on the basis that the recrystallization kinetics are a function of deformation texture.[13] Recent

Fig. 20—Orientation relationship between the orientation S and the modified (358) [352] component of the deformation texture is shown. Various symbols represent: open circles, the (338) [443] orientation and solid circles, the (125) [553] orientation.

work shows that the modified (358) [352] deformation texture recrystallizes at a lower temperature than would the (110) [112] component in copper.[9] This type of behavior was also observed recently in Si-Fe single crystals.[8]

The authors stated (Fig. 16) that the "ideal orientations" of the deformation textures vary with zinc content in a 22° range about one fixed octahedral pole, but that the "ideal orientations" of the components of recrystallization textures, except orientation *B*, do not vary appreciably with zinc content. (Orientation *S* is not discussed here, since the authors mention it only briefly.) This might indicate that orientations *A*, *F*, *M*, and *C* are all caused by some invariant in the deformation pole figure, which is not influenced by the addition of zinc; or the variant matrix, according to the authors' concept, does not influence the appearance of the recrystallization components of *A*, *F*, and *M*. (Orientation *C* should be excluded on the basis of "compromising textures," as the authors suggested.) Since the only thing which is constant throughout all the deformation pole figures, according to the authors, is the spread of minor intensities, it is, therefore, the spread matrix but not the major textured matrix which determines the recrystallization texture components *A*, *F*, and *M*. The more likely alternative is that the deformed matrix is an invariant, qualitatively.

It is difficult to understand the authors' contention that the minor spread in the deformation pole figure sometimes plays such a significant role in the occurrence of the main components of the recrystallization texture of brass and sometimes does not affect it at all, as in the case of copper. In comparing Fig. 2 with the pole figure plotted by Prof. Beck for copper,[9] the only difference that can be seen is a peripheral spread of intensity between 50 and 150 in Fig. 2. That this small difference will cause a sudden change from a single recrystallization texture of cubic orientation to a recrystallization texture of 19 components is difficult to understand. By assigning one "ideal orientation" for copper, the spread around the "ideal orientation" is much more predominant than the peripheral spread shown in Fig. 2. However, this spread around the "ideal orientation" seems to have no "appetite" to develop more components of recrystallization texture in copper. Fig. 6 shows a higher degree of peripheral spread than Fig. 2; however, the "ideal orientations" for the recrystallization texture components are only slightly changed but do not increase in number to more than 19. If two "ideal orientations" are assigned to the deformation texture, as Prof. Beck actually did in the case of copper,[9] the presence of another component of deformation texture, according to authors' reasoning, has much less influence on the recrystallization texture in comparison with the peripheral spread in Fig. 2.

It now appears, according to the oriented growth hypothesis, that both the peripheral spread as well as the major textured matrix should be considered as important. Under what condition is one more important than the other?

Prof. Beck suggested[9] that, according to the oriented growth hypothesis, it should be expected that there is a "sharpening effect." By comparing the recrystallization pole figures with corresponding deformation pole figures in the paper, this tendency cannot be observed.

**Alfonso Merlini** and **Paul A. Beck** *(authors' reply)*—As pointed out in the paper, orientations in the vicinity of (110) [1$\bar{1}$2] probably occur with considerable frequency in the rolling textures of copper and brasses from 0 to 30 pct Zn, representing an important orientation spread. The authors have, however, consistently refrained from considering an orientation as representing a texture *component*, unless at least two or three (preferably all) of the poles correspond to maxima in the pole figures. The two maxima on which each component is based in the present paper are listed in Tables II and III. From this point of view, the two (110) [1$\bar{1}$2] type orientations do not represent texture components in the 0, 3, and 6 pct Zn alloys, since only one pole of each actually corresponds to an intensity maximum. In a complex texture, such as the rolling textures of low brasses, there are many orientations with one pole at a maximum and some others at high intensity areas. The choice of any of these as a *component* is quite arbitrary. For instance, in the case of 3 pct Zn brass, the (110) [1$\bar{1}$2] orientation is a texture component only in a sense in which any one of a very large number of other orientations could also have been selected. The value of the rotational reorientations postulated by Dr. Liu on the basis of the (110) [1$\bar{1}$2] *components* may be, therefore, somewhat questionable. (Unawareness of the clear distinction between an orientation, such as *S*, admittedly somewhat arbitrarily selected as representative of a spread, and an orientation representing a main texture component based on at least two maxima may have misled Dr. Liu to the conclusion that the recrystallization textures reported in the paper have 19 components. As stated in the paper, the number of main components is 15.)

It is clear that the assignment of "ideal orientations" is in many cases not quite unique, even when at least two maxima are used as a basis. One of the difficulties encountered, which was also noted by Dr. Liu, is that the intensities corresponding to the various poles for a certain ideal orientation are often not consistent with each other. The discrepancies encountered are far greater than the probable experimental error of the measurements, and they should be considered as a necessary result of the great oversimplification involved in the attempt of describing a texture in terms of "ideal orientations," instead of statistical orientation distributions. For this reason, Dr. Liu's calculations of the intensities to be assigned to the various "texture components" he chose must be regarded with caution.

The question as to the effect of minor matrix texture components or spreads on the recrystallization texture, on the basis of oriented growth, may be perhaps answered on a qualitative level as follows: If the orientation of the minor component is such as to favor the growth of grains in orientations also favored by major texture components, its effect will not be felt. On the other hand, if a minor matrix component is unfavorable for the growth of recrystallized grains which are favored by major matrix components, an inhibiting

effect far out of proportion with the relative intensities of the minor matrix components in question may be expected.

[16] W. R. Hibbard, Jr., Y. C. Liu, and S. F. Reiter: *Trans.* AIME (1949) 185, p. 635; JOURNAL OF METALS (September 1949).
[17] C. G. Dunn: *Acta Metallurgica* (1954) 2, p. 386.
[18] Y. C. Liu and W. R. Hibbard, Jr.: *Trans.* AIME (1953) 197, p. 672; JOURNAL OF METALS (May 1953).
[19] Y. C. Liu: Unpublished data.
[20] P. K. Koh and C. G. Dunn: *Trans.* AIME (1955) 203, p. 401; JOURNAL OF METALS (February 1955).
[21] P. A. Beck and H. Hu: Discussion, *Trans.* AIME (1950) 188, p. 1057; JOURNAL OF METALS (August 1950).

## On the Relationship of Texture Changes of Cold-Rolled Face-Centered-Cubic Metals During Recrystallization

by Y. C. Liu and W. R. Hibbard, Jr.

*DISCUSSION, G. Edmunds and W. R. Opie, Chairmen*

**Paul A. Beck** *(University of Illinois, Urbana, Ill.)*—Since the "modified (358)[352] orientation," discussed by the authors, nearly coincides with the main deformation texture components near (123)[2$\bar{1}$1] found for aluminum and copper,[4] the reorientation referred to in the paper, corresponding to [111] rotations leading to the cube texture and to a recrystallization texture similar to the deformation texture, are essentially the same as those previously proposed[4] on the basis of the oriented growth analysis. Although the authors now attempt to justify the same reorientations on the basis of an oriented nucleation analysis, the first impression conveyed might be that the two approaches are fundamentally equivalent. However, on further thought, it appears that this is not the case. For instance, it is difficult to see how the oriented nucleation analysis, without additional ad hoc hypotheses, can account for the sharpness of the cube texture formed on annealing from a deformation texture having a wide orientation spread. Even if it is assumed that the nuclei have a definite crystallographic orientation relationship with the matrix, it is difficult to visualize how a nucleus orientation can be related to the orientation of any part of the matrix other than that immediately surrounding the nucleus. The picture of each nucleus having a definite orientation relationship with the microscopic portion of the matrix immediately surrounding it leads to a spread of nucleus orientations corresponding approximately to the spread of matrix orientations. The authors got around this difficulty by using only two of the continuum of orientations present in the deformed matrix, namely, the "modified (358)[352]" and the (110)[1$\bar{1}$2] as the basis for deriving nucleus orientations. It is, however, not clear why these two matrix orientations only should give rise to nuclei. On the other hand, on the basis of the oriented growth analysis, the observed annealing textures can be easily rationalized[6, 7] if it is assumed that they are dominated by crystals most favorably oriented for growth with respect to the matrix as a whole, including the various matrix texture components and spreads with which the recrystallized grain comes into contact in the course of its growth.

A difference arises between the two interpretations also in regard to the "phantom recrystallization texture components," which do not actually occur although they have the same orientation relationship with respect to one of the matrix texture components as the actual recrystallization texture. For instance, it is not at all clear on the basis of the oriented nucleation analysis why the cube orientation should be the only recrystallization texture component in highly rolled and annealed copper and why other crystallographically equivalent [111] rotations should not occur. On the basis of the oriented growth analysis, the unique role of the cube orientation is quite evident: it is the only orientation nearly ideally oriented for growth with respect to all four major deformation texture components.

The effect on the formation of the cube texture of a number of variables, such as the penultimate grain size, the final reduction of area in rolling, the final annealing temperature, and etching to a very small thickness prior to the final anneal, has been well established experimentally. Qualitative explanation of all these effects in terms of the oriented growth analysis has also been given.[20] It would be interesting to learn how these effects can be interpreted on the basis of the oriented nucleation analysis proposed by the authors.

The absence in 70-30 brass of the two (112)[1$\bar{1}$0] type recrystallization texture components, shown in Fig. 5 of the paper, is cited by the authors as a fact incompatible with the oriented growth analysis. As pointed out previously,[20] their conclusion would be undoubtedly correct if the rolling texture of $\alpha$ brass consisted only of the two components described by ideal orientations of the (110)[1$\bar{1}$2] type. It has been also pointed out, however, that actually the rolling texture of 70-30 brass includes a very intense orientation spread centered around the (110)[001] orientation and that the "phantom recrystallization texture" (112)[1$\bar{1}$0] is very far removed from an orientation favorable for growth with respect to the central part of this spread. Consequently, the absence of the (112)[1$\bar{1}$0] recrystallization texture in brass may be rationalized in terms of the oriented growth analysis on the basis of its orientation relationship with respect to the principal orientation spread in the rolling texture.

**Y. C. Liu** and **W. R. Hibbard, Jr.** *(authors' reply)*—There is no question that preferential grain growth plays an important part in the process of recrystallization. The question is, to what extent is this phenomenon operative in the development of a recrystallization texture? According to Dr. Beck, it is the sole factor in the development of the recrystallization texture.[4] The authors do not agree. The process as they see it is that, in addition to and prior to preferential grain growth, there is another process which provides nuclei for later growth. The mechanism of this process is related to the deformation mechanism. The resulting orientations of nuclei have a rotational reorientation relationship with respect to the deformed matrix, not due to growth but due to the deformation and recovery during their formation. Thus, the process provides nuclei which are related to the deformation process imposed on the matrix material. The authors agree with Dr. Beck that their viewpoints seem to be the same on the surface but are quite divergent in basic concepts.

Differentiation between these two concepts is extremely difficult; both of them provide evidence through the rotational reorientation relationship. In many cases, the experimental observations could be interpreted either way without any difficulty. For instance, the observation of eight equivalent components of recrystallization texture in a cold-rolled copper single crystal[7] was interpreted by Dr. Beck as a strong indication of the operation of his concept in this respect.[4]

The pole of rotation, according to the authors' analysis, is the pole of the active slip planes, but it is the pole of the most densely packed crystallographic plane according to Dr. Beck's concept.[4, 21] However, the most densely packed plane usually is also the slip plane, and the two concepts once again confuse each other. Nonetheless, a difference between these two concepts some-

times arises, such as the observed secondary orientation relationship about the cubic pole of the primary texture in cases such as are given in the paper.

Dr. Beck has raised an interesting question in connection with the orientation of the matrix immediately surrounding the nuclei on a microscopic scale. If the deformation texture is reasonably sharp, say, having a (358)[3$\bar{5}$2] orientation, Dr. Beck's suggestion for the formation of the cubic texture has a logical basis. However, as observed by Dr. Beck and his collaborators, the deformation texture of copper shows a large degree of scatter.[4] The question then arises what would happen in a microscopic region where matrix grains of other than (358)[3$\bar{5}$2] orientation are present? The grain of cubic orientation might be a "compromised" grain to grow in such a matrix. But this does not rule out the possibility that in this very region there could be another grain of the right orientation which possesses the "maximum grain boundary mobility" with respect to this microscopic region. Instead of a sharp cubic recrystallization texture, a certain degree of scatter, which depends on the orientation spread in the deformation texture, would be expected. According to the authors' concept, this situation does not constitute a problem, since all the recrystallized grains are not pre-existent but are derived from their corresponding deformed grains. Recrystallized grains of other than cubic orientation may not exist, either because there are no deformed grains to serve as the origin for these grains, or because the kinetics of recrystallization favors the formation of the cubically oriented nuclei.

The authors explained the sharpness of the cubic texture on the basis of two components of deformation texture[27] without any additional ad hoc hypotheses, as suggested by Dr. Beck. By comparing the spread around the octahedral pole *B* of the modified (358) [3$\bar{5}$2] orientation, Fig. 1 in the paper, with any octahedral poles of cubic texture in the pole figures plotted by Dr. Beck and his collaborators,[5,6] it would be seen that they are almost the same.

The suggestion of two components of deformation texture in copper was made on the basis of experimental observation. Although the suggestion of (110)[1$\bar{1}$2] orientation as the ideal orientation of one component of the deformation texture was made from pole figures derived by X-ray photographic methods,[2] similar indices were also used by Dr. Beck and his collaborators[5] to describe the component of the deformation texture in their quantitative pole figure. The most concrete observation of its existence was first made by Barrett and Steadmann[28] and it has been verified many times[7,29] that single crystals of this orientation will retain the orientation after high reduction in thickness and that all other orientations under investigation[29] are unstable during the course of cold-rolling. Barrett and Steadmann had also suggested the (358)[5$\bar{8}$3] orientation, which was later verified by Dr. Beck[4] with indices of (358)[3$\bar{5}$2]. Recent experiments carried out on copper single crystals of initial modified (358)[3$\bar{5}$2] orientation[30] indicated that this orientation is retained during rolling but with complications. There seems no doubt of the coexistence of these two components in the deformation texture of cold-rolled copper. The most important thing is that, by assuming the existence of these two components, it would be possible to rationalize the recrystallization texture in face-centered-cubic metals with both simplicity and a reasonable degree of self-consistency. No doubt, components of other orientations could also exist in the rolled strip. These minor components may or may not survive, depending upon the recrystallization kinetics which, as the authors suggested, are a function of the texture orientations as confirmed by recent work of Koh and Dunn[31] on rolled Si-Fe single crystals.

"Phantom recrystallization texture components" are a problem according to Dr. Beck's concept.[32,33] The two explanations offered by Dr. Beck,[32] as pointed out by Burke,[33] are either without evidence or support the concept of oriented nucleation. To the authors, this problem is simple. Since it is the deformation process and subsequent annealing which produces the conditions leading to the recrystallization nuclei, the active slip systems should be related to the choice of poles of rotation, together with the kinetics of the annealing process leading to the growth of the nuclei. The relation between poles of rotation and active slip planes was experimentally demonstrated by Maddin, Mathewson, and Hibbard[34] on brass single crystals and suggested by the authors' in the investigation of the recrystallization texture of copper single crystals. Accordingly, it would be expected that all crystallographically equivalent poles of rotation would *not* be equal unless there was equivalent slip on each corresponding plane.

As to the various factors that influenced the formation of the cubic texture, they might be explained according to the authors' concept on the basis of their effect on the number of grains in the (358)[3$\bar{5}$2] orientation prior to the final annealing, and their effect on the kinetics of recrystallization of the components present in the deformed material. Recent experiments carried out by one of the authors[30] suggested a doubt as to whether the cubic texture is precisely a cubic orientation or a combination of several near-cubic orientations. It looks as though more information about the cubic texture is needed before it can be rationalized in detail.

The authors are very glad that Dr. Beck offered his viewpoint on behalf of his concept concerning the analysis of the 70:30 brass texture in Fig. 5 of the paper. However, he does not show any evidence that the "phantom" (112)[1$\bar{1}$0] type of recrystallization component possesses "minimum grain boundary mobility" in order to prevent its growth to the spread matrix. On this basis—including the spread—the absence of the (112)[1$\bar{1}$0] component, particularly in the presence of the other components related to the (110)[1$\bar{1}$2] matrix (but not the spread), is still difficult to rationalize if all crystallographically equivalent orientations are considered.


[27] P. A. Beck: Notes on the Theory of Annealing Textures. *Acta Metallurgica* (1953) **1**, p. 230.
[28] P. A. Beck: Annealing of Cold Worked Materials. Advances in Physics. *Philosophical Magazine Supplement* (1954) **3**, p. 245.
[29] P. A. Beck: *Trans.* AIME (1952) **194**, p. 979; JOURNAL OF METALS (September 1952).
[30] P. A. Beck: *Trans.* AIME (1951) **191**, p. 475; JOURNAL OF METALS (June 1951).
[31] Y. C. Liu: Discussion, *Trans.* AIME (1955) **203**, p. 1267; JOURNAL OF METALS (November 1955).
[32] C. S. Barrett and F. W. Steadmann: *Trans.* AIME (1942) **147**, p. 57; METALS TECHNOLOGY (February 1942).
[33] B. E. Warren and B. L. Averbach: *Journal of Applied Physics* (1952) **23**, p. 497.
[34] Y. C. Liu: *The "Cubic Texture"* in Copper. Unpublished research.
[35] P. K. Koh and C. G. Dunn: *Trans.* AIME (1955) **203**, p. 610; JOURNAL OF METALS (February 1955).
[36] J. J. Becker: *Trans.* AIME (1951) **191**, p. 115; JOURNAL OF METALS (February 1951).
[37] J. E. Burke: *Trans.* AIME (1952) **194**, p. 263; JOURNAL OF METALS (March 1952).


## Preferred Orientations in Beta-Annealed Zirconium


by J. H. Keeler and A. H. Geisler


*DISCUSSION, G. Edmunds and W. R. Opie, Chairmen*

**J. B. Newkirk** *(General Electric Co., Schenectady)*—The discusser would like to suggest an additional explanation for the reversion of recrystallized $\alpha$ zirconium to its original texture on heat-treating at temperatures 40° to 70°C above the transformation.

It is fairly well established that, in a phase transformation $\alpha \rightleftarrows \beta$, stable $\alpha$-embryos can be retained in the temperature range of $\beta$-stability in cavities of suitable extraneous solids present in the system. These retained $\alpha$-embryos may nucleate the $\beta \rightarrow \alpha$ transformation when the system is returned to the range of $\alpha$-stability. If the active cavities are in solid particles which are firmly fixed within a solid crystal, it follows that the orientation of the $\alpha$-crystalline material within the cavities will determine the orientation of the new $\alpha$-lattice which is generated as the parent $\beta$-crystal transforms.

Cavities with a small conical angle can retain stable $\alpha$-embryos farther into the region of $\beta$-stability than can those with a larger conical angle. If the system is taken far enough into the $\beta$-region, no $\alpha$-embryos will be retained in cavities and this mechanism of preferred nucleation can no longer operate. A modified $\alpha$-texture based on random nucleation from the $\beta$-phase would then be expected. This is the behavior which the authors report.

**J. H. Keeler** *(author's reply)*—Dr. Newkirk's additional explanation for the reversion of recrystallized $\alpha$-zirconium to its original texture on heat-treating at temperatures 40° to 70°C above the transformation is appreciated. A critical experiment that would show which of four possible alternatives is responsible for the texture reversion would now be of interest.

[16] D. Turnbull: Kinetics of Heterogeneous Nucleation. *Journal of Chemical Physics* (1950) **18**, pp. 198-203.

---

## Contribution of Crystal Structure to the Hardness of Metals

by W. Chubb

*DISCUSSION, H. Y. Hunsicker and A. A. Burr, Chairmen*

**W. J. Bratina** *(University of Toronto, Toronto; now with Ontario Research Foundation, Toronto)*—Dr. Chubb has presented the temperature-hardness relationship for cobalt, iron, uranium, titanium, and zirconium; the hardness, determined as Dph, is plotted against the temperature on semilogarithmic coordinates. The elastic properties of titanium and zirconium have been investigated in this laboratory employing the internal friction method and it appears interesting to compare the temperature variation of the hardness for these two metals with the variation of their torsion (shear) modulus. Of special interest are the inflections in the hardness values at approximately 500° and 400°C for titanium and zirconium, respectively, and the abrupt changes at the allotropic transformation temperature (Figs. 5 and 7 of the paper). Similar inflection points in some other metals have been discussed previously[7-10] and very recently.[11]

The variation of torsion modulus with the temperature is shown for titanium in Fig. 8, where the values for titanium TMC Ti-75A are shown, but the specimen has absorbed certain amounts of gases (mostly oxygen) during the experiment despite a vacuum of $5 \times 10^{-4}$ mm Hg. This contamination, expressed as atomic percentage of oxygen, amounts to 0.80. The temperature variation of torsion modulus for pure TMC Ti-75A up to 700°C has been reported elsewhere.[12] In zirconium it was necessary to investigate the high temperature region separately[13] to prevent excessive contamination. In the graphs the value $G_t/G_{20}$ is plotted, where $G_t$ and $G_{20}$ are the torsion modulus $t°$ and 20°C, respectively. The first significant deviation from the linearity

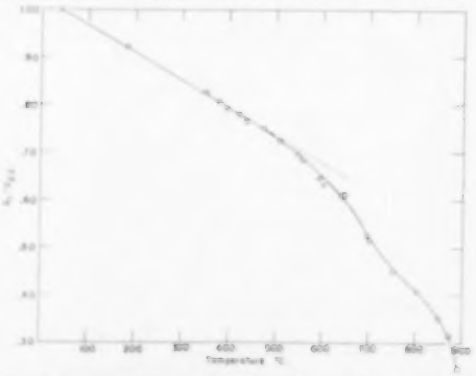

Fig. 8—Curve and data points show the variation of torsion modulus with temperature in titanium.

in the case of well annealed polycrystalline specimens begins in the temperature region where, according to the theory of anelasticity, the grain boundary relaxation phenomena become significant. The second marked decrease is in the allotropic transformation temperature region.

Comparing the $G_t/G_{20}$ and log (Vhn) vs temperature curves for titanium (or zirconium), certain coincidence in the temperature where the first inflection appears is apparent, especially if the scatter of the experimental data is taken in consideration. This would suggest, at first sight, that this inflection in hardness values might also be caused by the presence of grain boundaries, since in both cases polycrystalline specimens have been employed. On the other hand, in the internal friction experiments, mostly well annealed specimens are used which differ greatly from the lattice conditions found close to the indentation area in hardness tests; it would appear that cold-worked and partially annealed polycrystalline specimens would be a better approach. A number of internal friction experiments has been done on such specimens, for example, by Ké[14] on aluminum and very recently by Köster et al.[15] on copper; the effects of cold work and annealing have been studied. In general, data of internal friction experiments seem to indicate that the first inflection point in the hardness vs temperature curve in titanium and zirconium might be due to more or less complex action of various interfaces within the specimen. Some of them, such as grain boundaries, are present in the specimen originally and some are introduced by plastic deformation and subsequent recovery processes, if any. This seems to explain also well known experiments on single copper crystals[16] where a similar inflection in the hardness vs temperature curve has been observed as in polycrystalline material.

It is to be expected that the physical properties would change if the crystal structure is changed; therefore, the inflection point in hardness and torsion modulus curve in the allotropic transformation range is no surprise. More interesting is that both hardness and torsion modulus attain lower values in the $\beta$ phase, as can be seen from the data for zirconium[10] and can be concluded for titanium from Fig. 8, although in this case the measurements were not extended into the $\beta$ region. However, the reason for this drop might be different. Dr. Chubb has shown that the decrease in the hardness values is due to the body-centered-cubic crystal structure which is always a softer structure when it is involved in an allotropic transformation. The decrease in the torsion modulus is not very clear. It would be interesting to investigate from this point of view the values for iron, where the first inflection in the log (Vhn) vs temperature curve corresponds quite closely to the inflection in the torsion modulus curve,[10]

but the $\gamma$ phase shows an increase in hardness compared to the $\alpha$ phase.

In Fig. 5 the hardness value for higher purity titanium shows a slower decrease with the temperature than for less pure titanium; finally they meet at the inflection point. Perhaps this effect can be attributed to the surface contamination, since the vacuum was not very high? Similar conditions as in iron of different purity, Fig. 4, might be expected.

**W. Chubb** *(author's reply)*—Dr. Bratina's contribution to this subject is greatly appreciated, and the author is in agreement with Dr. Bratina's interpretation of the inflections at 400° and 500°C in zirconium and titanium. His observation that grain boundary relaxation phenomena become significant in the region of the hardness inflection is particularly interesting. Other phenomena that occur near this temperature are stress relief, recrystallization, and the disappearance of cold work in creep. In all cases, the temperature associated with these phenomena can be shifted by alloying, but in no case that this writer knows of can impurities or lack of impurities cause these phenomena to disappear.

As Dr. Bratina points out, the data seem to indicate that the inflection point is due to complex action of interfaces within polycrystalline specimens. The author is of the opinion that all these phenomena are best understood in terms of the mechanistic *theory of dislocations*. The "interfaces" then become simply barriers to the movement of dislocations, whatever form they may take. At low temperatures, the movement of dislocations is restricted by these barriers; high stresses are necessary to cause plastic deformation; "cold work" results from plastic deformation; and the energy absorbed by the oscillation of dislocations between barriers (as manifested by "internal friction") is small. As the temperature of the metal is raised, the kinetic energy of the atoms increases; the jump frequency of vacant lattice sites increases; and the rate of self-diffusion increases. Presently, as the temperature is raised, it is found that, when the potential energy of a small stress is superimposed upon the kinetic energy of vibration of the atoms, the combination is sufficient to cause barriers to diffuse out of the path of dislocations or for the effective size of the barriers to be reduced so that dislocations may climb over the barriers. At such a temperature, stress relief, disappearance of cold work in creep, and the onset of "grain boundary" relaxation (caused by the absorption of energy as dislocations cycle over barriers) are observed. This writer feels that the inflection point at about 400°C in the hardness curves for iron, titanium, and zirconium may be regarded as that point at which stress relief is occurring so rapidly that it occurs during the time of indentation. Therefore, this inflection should occur at temperatures slightly above that for long time stress relief, disappearance of cold work in creep, and grain boundary relaxation. Tentative confirmation of this theory is to be found by comparing the inflection point found by Dr. Bratina, Fig. 8, with that found by hot hardness, Fig. 5. It appears that the latter occurs 50°C higher than the former.

Recrystallization is related to these phenomena only to the extent that diffusion is necessary before nucleation and grain growth can occur. The factors of amount of cold work, time, and temperature of treatment must be taken into consideration before recrystallization can be related to the hot hardness inflection.

Melting is related to these phenomena to the extent that as the temperature is raised the kinetic energy of vibration of the atoms increases, the free energy of formation of the solid increases, the stability of the solid decreases, and the free energy of formation of the liquid decreases. As Dr. Westbrook has demonstrated,[7] metals usually melt at a temperature such that the absolute temperature for melting and the absolute temperature for the inflection point can be related by a factor of about 0.55. However, if a transformation occurs, the high temperature allotrope becomes more stable than the low temperature allotrope; thus, the free energy of the solid is decreased, and the melting point may be pushed to a higher temperature than would be expected if there were no transformation.

With respect to the modulus of iron, W. Koster has reported values for the effect of temperature upon the dynamic moduli of a large number of metals including cobalt, iron, thallium, and zirconium.[11] He found that the moduli of cobalt, iron, and thallium increased and that the modulus of zirconium decreased at the transformation temperatures. The behavior of thallium as reported by Köster seems to be anomalous, since it would indicate that the binding energy of body-centered thallium is greater than that of close-packed thallium. Unpublished data by R. E. Maringer show that the modulus of uranium varies in the same manner as the logarithm of hardness. A plot of the modulus of uranium vs temperature could easily be mistaken for Fig. 6 of this paper.

The author cannot agree with Dr. Bratina that surface contamination is responsible for the intersection of the two curves for titanium in Fig. 5. If the iodide titanium sample had become contaminated during the test at moderate temperatures, it surely would have become more contaminated at higher temperatures, and the sharp drop in hardness at the transformation would not have been observed. The curve for RC-55 titanium (which incidentally is somewhat purer than Ti-75A titanium) might be taken as an example of material slightly contaminated with oxygen. The curves shown in Fig. 5 illustrate the well known fact that oxygen raises the transformation range of titanium but is not very effective in strengthening titanium at slightly elevated temperatures.

[10] Discussion of ref. 7. *Trans.* ASM (1953) 45, p. 243.
[11] E. D. Kunat: *Metallen* (1954) 9, p. 23.
[12] J. N. Pratt, W. J. Bratina, and B. Chalmers: *Acta Metallurgica* (1954) 2, p. 203.
[13] W. J. Bratina and W. C. Winegard: To be published. *Trans.* AIME.
[14] T. S. Kê: *Trans.* AIME (1950) 188, pp. 575, 581; JOURNAL OF METALS (March 1950).
[15] W. Köster, L. Bangert, and W. Lang: *Ztsch. für Metallkunde* (1955) 46, p. 84.
[16] J. Engl and G. Heidtkamp: Cited in ref. 7.
[17] T. S. Kê: *Trans.* AIME (1948) 176, p. 448; METALS TECHNOLOGY (June 1948).
[18] W. Köster: *Ztsch. für Metallkunde* (1948) 39, p. 1.

## Study of a New Mode of Plastic Deformation in Zinc Crystals

by J. J. Gilman

*DISCUSSION, C. S. Roberts and F. L. Vogel, Chairmen*

**P. L. Pratt** *(The University of Birmingham, Birmingham, England)*—The deformation markings studied in this paper are "believed to be the same thing as the *micro kink bands* observed by Holden[2] and by Pratt[3]" (p. 212). The term *micro kink bands*, attributed incorrectly to these two authors, "seems to be inept to this author because there is a qualitative and a quantitative difference between $\mu$-bands and ortho kink bands" (p. 213). On the surface, these markings may appear to be similar but, without a small amount of photographic evidence and within the body of the crystal, it is difficult to see this similarity. The fine and coarse kinks studied by Pratt were related to the buckling of the compressed side of a bent specimen and, as indicated in Figs. 15a and 15b, they failed to cross the



nature are continued for a time longer than about 60

Is Fig. 1 a scale drawing of the apparatus used? If so,

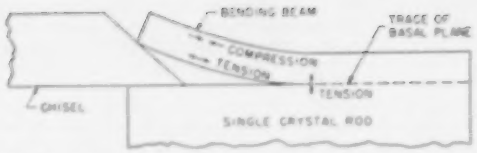


Fig. 15a—Diagram shows the stress system during cleavage of a thin flake.

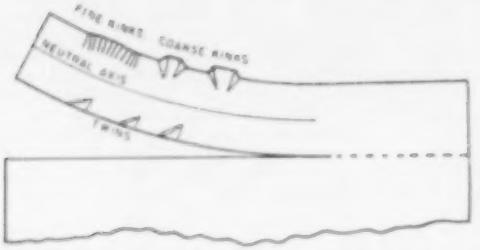


Fig. 15b—Section through the thin cleavage flake shows deformation.

neutral axis of the specimen. Figs. 13 and 14, however, indicate that the $\mu$-bands run from one side of the specimen to the other, with no macroscopic buckling of the specimen, and it is difficult to correlate this model with Fig. 4 and with the observation that buckling accounts for the maximum in the stress-strain curve, Fig. 3 (although the author does state on p. 213 that, despite Figs. 3 and 4, there was no "macro bending." The dislocation model proposed in Fig. 14 appears to be an early stage in the development of a normal deformation band, as discussed by Cahn[9] and by Mott,[10] and can hardly permit plastic buckling on the scale of Fig. 4. The dislocation model for the coarse kinks (and probably the fine kinks also) of Fig. 15 is shown in Fig. 16 in which edge dislocations of opposite sign lie in two kink planes meeting below the surface of the crystal. These dislocations might well come from Frank-Read sources lying between the two kink planes, and their density in the kink plane is inversely proportional to the local radius of curvature of the bent beam (i.e., proportional to their distance from the neutral axis). It seems possible to describe the buckling of a compressed rod by means of a simple contraction of this model, and this process would outwardly appear to suppress ortho kinking on a macroscopic scale by permitting local relaxations of the buckling stress distributed along the specimen.

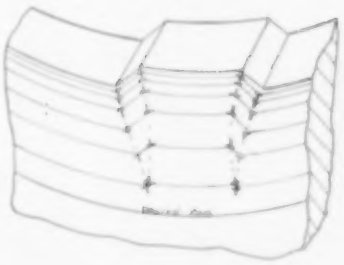

Fig. 16—The dislocation model for coarse kinks, Fig. 15, is shown in the diagram, in which edge dislocations of opposite sign lie in two kink planes that meet below the surface of the crystal.

Johnson[11] has said, "Every man has a right to utter what he thinks truth, and every other man has a right to knock him down for it." If, in fact, these $\mu$-bands are the same as the earlier deformation markings, perhaps the term *micro deformation band* and the title of the paper, *Study of a New Mode of Plastic Deformation in Zinc Crystals*, might also seem inept.

**J. J. Gilman** *(author's reply)*—Little is to be gained at this time by a discussion of the terminology that was used in the paper. This is a matter of opinion, and the author has no strong feelings in the matter. However, until the true nature of the *new mode* of deformation becomes clear, the author thinks that it is unwise to draw an analogy between it and normal kinking.

The author based his conclusion that the $\mu$-bands of his paper are the same thing as the "fine kinks" of Pratt on the facts that both are found only upon compression parallel to the basal planes of zinc and both have the same crystallographic geometry. Admittedly, the microscopic *appearance* of the markings is not exactly the same. In the author's opinion, this is a result of strain rate differences.

Apparently, a misunderstanding exists in connection with Fig. 4. This figure shows a crystal that had been completely buckled. However, as is indicated in Fig. 3, macroscopic buckling did not begin until an appreciable amount of plastic flow had already occurred, and most of the paper is concerned with happenings during the prebuckling stages of deformation. Thus, there is no inconsistency between Fig. 4 and Figs. 13 and 14.

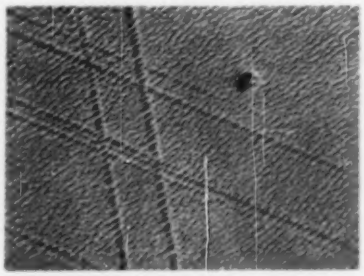

Fig. 17 — Micrograph shows etched $\mu$-bands in a zinc crystal. X1000. Area reduced approximately 45 pct for reproduction.

Additional evidence has recently been obtained which shows conclusively that $\mu$-bands, and probably fine kinks, are qualitatively different from normal kink bands. This evidence has been obtained by means of a special etching technique that will be described in detail elsewhere. Fig. 17 shows the characteristic appearance of etched $\mu$-bands. They consist of regularly spaced pits that are oval in shape and have their major axes lying parallel to basal planes. Clearly, the dislocation distribution of Fig. 16 is inconsistent with the etched structure.

On the other hand, the etched structure of Fig. 17 is not clearly related to the dislocation distribution of Fig. 14b, although this distribution is not ruled out. The author thinks the nature of $\mu$-bands is not clear at the present time, and they should be viewed with an open mind. They may be a type of *deformation band*, they may be very fine twins, or they may be caused by unidirectional pyramidal glide. Perhaps the discusser, or the author, will be able to prove which possibility is correct at some future date.

[9] N. F. Mott: *Proceedings Physical Soc.* B (1951) 65, p. 729.
[10] J. Boswell: *Life of Johnson*. (1791).

## Viscous Flow of Copper at High Temperatures

by A. L. Pranatis and G. M. Pound

*DISCUSSION, C. S. Roberts and F. L. Vogel, Chairmen*

**A. P. Greenough** *(University College, Swansea, England)*—The paper provides further experimental evidence for the validity of the theory developed by Herring. However, it also recalls a problem still to be solved in this type of work. When experiments of this

nature are continued for a time longer than about 60 hr, the reproducibility of the results becomes very bad. This was noticeable in the work which Greenough published;[9] and his further work since then, which has not been published, has not revealed the cause. In view of this, it is interesting to examine closely Fig. 2 of the paper under discussion.

It is not clear from the text what accuracy is being claimed for the measurements. Assuming that the length in the specimens can be measured to ±0.0003 in., a change in length can be measured to ±0.0006 in., and therefore the strain on a 4 in. gage length can be measured to ±0.00015.

It should be possible to make any of the plotted points lie on the line by a movement corresponding to changing the strain by less than ±0.00015. At first sight, the last point plotted for specimens KL-F and KL-G does not fulfill this criterion, but in each case a small change in the position of the plotted line removes the discrepancy without introducing any inconsistency. Have the authors had any experience with the behavior of their specimens over periods of longer than 60 hr?

In this connection, Tamman and Boehme[10] found that the deformation of their foils apparently ceased after about 15 min. However, it appears that in this case the foils would recrystallize on heating and that the accuracy of the experiments would be insufficient to detect the deformation of the annealed specimens if the final grain diameter were of the order of 0.005 in., as would be expected. The discusser is unable to comment on the work of Sawai and Nishida,[10, 11] which he has so far seen only in abstract form.

Is Fig. 1 a scale drawing of the apparatus used? If so, was any check made of the temperature distribution over the length of the specimen during a test? There must have been a fairly steep temperature gradient between the bottom of the specimen and the glass wool. Was the temperature inside the copper chamber uniform? Finally, what precautions were taken to prevent the copper pins from sintering to the container during the course of a run?

**A. L. Pranatis** and **G. M. Pound** (*authors' reply*)—The authors wish to thank Dr. Greenough for his interesting comments.

In all specimens strained for periods of time longer than 60 to 100 hr, strain rates unmistakably decreased but not to the extent that a limiting strain could be assigned. No explanation is offered beyond the suggestion of possible saturation of grain boundaries with vacancies. In several instances of long time straining, specimens broke intergranularly. The intergranular cavitation recently reported by Greenwood, Miller, and Suiter[17] is brought to mind. However, the specimens were not carefully examined at the time and no grain boundary porosity can be reported.

The Kanthal furnace windings were spaced on an Inconel furnace tube to provide a hot zone that extended several inches above and below the specimen. Temperatures along the length of the specimen did not vary more than 1°.

Graphite smears at the copper interfaces were used to prevent the loosely fitting copper parts from welding together, often successfully.

[17] J. N. Greenwood, D. R. Miller, and J. W. Suiter: *Acta Metallurgica* (1954) 2, p. 250.

## Study of the Effect of Boron on the Decomposition of Austenite

by C. R. Simcoe, A. R. Elsea, and G. K. Manning

*DISCUSSION, D. Turnbull and D. J. Blickwede, Chairmen*

**Harry Udin** (*Massachusetts Institute of Technology, Cambridge, Mass.*)—The authors are to be congratulated for a fine piece of experimental work. Particularly valuable is their confirmation of the high surface activity of boron in steel, which has been suspected for austenite[16] and has been demonstrated experimentally for liquid steel.[17]

It is reasonably well established that the predominant influence of boron on hardenability lies in inhibition of ferrite nucleation brought about by boron adsorption on the austenite boundaries, with consequent lowering of the boundary free energy. However, the explanations for the effect of austenitizing temperature and for the inversion with increasing boron content are by no means clear. The authors assume that small additions of boron lower the strain energy at austenite grain boundaries by occupying high energy sites. Further additions are forced into less favorable sites in the boundary, thereby increasing the strain energy. That such atoms would attempt to enter the grain boundaries is extremely doubtful and probably not very important.

Nucleation theory is based on the free energy of an interface and not on the strain energy contribution to free energy. On this basis, the authors' arguments, as illustrated schematically by their Fig. 16, are untenable. Gibbs[18] proved that for a solvent-solute system

$$\Gamma = -(\delta\gamma/\delta\mu)_T$$

where $\Gamma$ is surface excess of the solute, $\gamma$ is surface energy, and $\mu$ is the chemical potential of the solute. This is a thermodynamic statement, holding independent of the atomistic model of the mechanism of solute adsorption.

Fig. 16 shows $d\gamma/dc$ positive over the range *A-P*. Rewriting Gibbs' isotherm in the form

$$\Gamma = -(\delta\gamma/\delta c)(\delta c/\delta\mu)$$

it is seen that this can only happen if $\Gamma$ or $dc/d\mu$ becomes negative, a highly unlikely state of affairs. For $\Gamma$ to swing negative would require that the ratio of boron concentration at the boundaries to boron concentration in the austenite crystals change from >1 to <1. This would appear impossible at boron levels of $0.000x$ pct and would, further, invalidate the authors' Figs. 17 and 18 and any reasoning based thereon. $dc/d\mu$ can be negative only if the activity of the boron decreases with increasing concentration. This is patently impossible for a system nearing boron saturation.

A more likely explanation can be made on the basis of two more probable assumptions:

1—Boundary energy increases with increasing temperature. This is the rule rather than the exception in solvent-solute systems where the solute is highly surface active. It is brought about by desorption of the solute, so it would be expected that the hardenability decreases at high austenitizing temperatures, followed by a gradual increase upon cooling to and holding at lower temperatures, as the desorbed boron diffuses back to the boundaries.

2—The solubility of boron in austenite is nil. (This again is the rule for highly surface active solutes). Boron exists in supersaturated solution in austenite only because of the difficulty of nucleating the boride precipitate. When the boron content is made high enough to permit this precipitation, the dissolved boron is quickly stripped from both the grains and the grain boundaries, and the hardenability reverts toward normal. In terms of Fig. 16, this would mean that points *A* and *P* both coincide with the minimum of the

curve, but the precipitate is not detected at low boron concentrations.

**C. R. Simcoe, A. R. Elsea,** and **G. K. Manning** *(authors' reply)*—The intermediate position of the boron atom between the size of the usual interstitial solute atom and the substitutional atom poses a problem to any explanation of the effect of boron on hardenability in steel. The explanation preferred by Udin, who extends the customary thermodynamic treatment for liquid solutions to the case of solid solutions, is not as straightforward as he would have it appear.

The statement that "nucleation theory is based on the free energy of an interface and not on the strain energy contribution to free energy" is puzzling. It is true that Becker in his early papers used a simplified model of nucleation in solid solutions, in which the strain energy term was assumed negligible. Later refinements of solid-state nucleation theory, however, include strain energy considerations. Mehl and Dube[9] discussed the role strain energy plays in nucleation and concluded that it must be taken into account.

It may be of interest to point out that, in the Fe-Fe$_2$B system[10] at 850°C, the distribution coefficient changes from $<1$ to $>1$ as the boron concentration increases. As for the improbability of $dc/d_{a_i}$ being negative, several examples exist of a decreasing activity with increasing concentration. For example, work on the Au-Ni system at Massachusetts Institute of Technology[11] has shown this effect.

A necessary part of Udin's suggested mechanism is that the solubility of boron in austenite be nil—that boron be present in austenite in a supersaturated state. He suggests that, once conditions become such that precipitation occurs, "the dissolved boron is quickly stripped from both the grains and the grain boundary." If Udin's view were correct, it would follow that once precipitation of the boron compound had occurred the effect on hardenability would be permanently lost. Certainly a precipitate cannot be dissolved in a solvent in which the solubility is nil. Yet it is known that the boron precipitate does redissolve when steel is subsequently heated to the austenite temperature range. In fact, if it did not redissolve, the boron effect would never have been observed. All rolled, forged, or annealed steels are cooled (prior to hardening) in a manner that must insure precipitation of the boron compound. In general, the boron effect is realized regardless of prior treatment. The only known cause for loss of the boron effect is oxidation of the boron. Udin's suggested mechanism, therefore, appears to the authors to be untenable.

[9] J. C. Fisher: Influence of Boron on Hardenability of Steel. Trans. AIME (1954) **200**, p. 1146; Journal of Metals (October 1954).
[10] Y. A. Klyachko et al.: *DAN SSR* (1950) 72; Butcher Translation No. 2669.
[11] S. Glasstone: *Thermodynamics for Chemists*. (1947) 1st Ed., p. 245. New York, D. Van Nostrand and Co.
[12] C. C. McBride, J. W. Spretnak, and R. Speiser: A Study of the Fe-Fe$_2$B System. Trans. ASM (1954) **46**, p. 517.
[13] L. L. Seigle, M. Cohen, and B. L. Averbach: Thermodynamic Properties of Solid Nickel-Gold Alloys. Trans. AIME (1952) **194**, p. 1322; Journal of Metals (December 1952).

## Isoembrittlement in Chromium and Molybdenum Alloy Steels During Tempering

by Gopalkrishna Bhat and Joseph F. Libsch

*DISCUSSION, D. Turnbull and D. J. Blickwede, Chairmen*

**B. C. Woodfine** *(General Electric Co. (of England) Ltd., Erith, Kent, England)*—Although the authors claim that for the AISI 5140 steel an attempt to relate the hardness and transition temperature at long tempering times leads to results opposite those proposed[4] to explain the embrittlement of the plain carbon steel, Fig. 7 shows that, for the specimens of the AISI 5140 steel tempered at 1200° and 1260°F (650° and 680°C) for both long and short times, there is a very good correlation between hardness and transition temperature. This, in fact, leads to a similar conclusion with regard to the embrittlement at 1200° and 1260°F as was reached for the carbon steel, i.e., that the embrittlement is the result of ferrite grain growth. At lower temperatures, 800° to 1000°F (425° to 540°C), the embrittlement of the AISI 5140 steel is almost certainly due to intergranular temper embrittlement and would not be expected to show a correlation with hardness. At 1110°F (590°C), the results in Fig. 7 and Fig. 3 show that the two modes of embrittlement overlap with the intergranular embrittlement reaching a maximum after about 1 hr and then decreasing, while the ferrite grain growth embrittlement begins to be apparent after

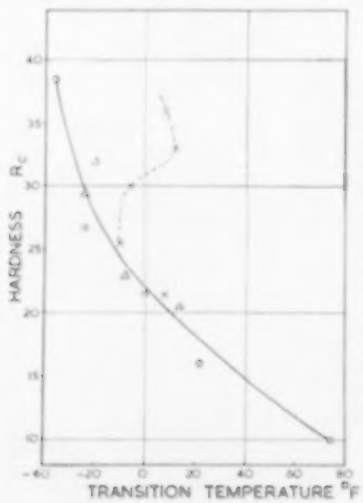


**Fig. 7—Good correlation between hardness and transition temperatures results in specimens of AISI 5140 steel tempered at 1200° and 1260°F (650° and 680°C) for both long and short times. Symbols represent: circles, 1260°F; triangles, 1200°F; and crosses, 1100°F (590°C).**

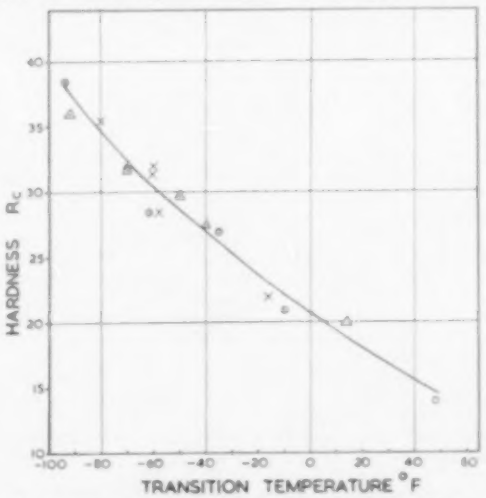


**Fig. 8—In specimens of AISI 4047 steel, the close correlation between hardness and transition temperature extends to specimens embrittled at 1100°F (590°C) as well as those embrittled at 1200° and 1260°F (650° and 680°C). Symbols represent: circles, 1260°F; triangles, 1200°F; and crosses, 1100°F.**

Table V. Results of High Temperature Tempering Treatments on Development of Embrittlement in an Ni-Cr Steel Quenched Initially from 850°C (1560°F)

| Treatment | Transition Temperature, °C | Embrittlement, °C |
|---|---|---|
| Tempered at 650°C (1200°F) for 1 hr | −59 | |
| Tempered at 650° + 500°C (930°F) for 32 hr | +137 | 196 |
| Tempered at 650°C (1200°F) for 50 hr | −52 | |
| Tempered at 650° + 500°C (930°F) for 32 hr | +56 | 108 |

about 10 hr. For the short times at 1100°F where the increase in transition temperature was due to intergranular temper embrittlement, the results do not fall on the hardness/transition temperature curve obtained for the higher temperatures, Fig. 7; but for the longer times where the embrittlement is presumably entirely the result of ferrite grain growth, the points fit the curve very well.

With the molybdenum steel which shows very little susceptibility to intergranular temper embrittlement, the close correlation between hardness and transition temperature extends to those specimens embrittled at 1100°F as well as those embrittled at 1200° and 1260°F, Fig. 8. Thus, for the molybdenum steel, it is suggested that the embrittlement at temperatures above 1100°F is entirely due to ferrite grain growth and that from Fig. 4 this form of embrittlement would appear to overlap with intergranular temper embrittlement at 1100°F.

If the suggestion advanced previously in the discussion to explain the authors' data is correct, examination of the relevant specimens should reveal: 1—that the brittle fracture of specimens embrittled at above 1150°F (620°C) for the AISI 5140 steel and 1100°F (590°C) for the AISI 4047 is entirely cleavage, 2—that the brittle fracture of specimens embrittled below these temperatures is partly or wholly intergranular, and 3—that for specimens embrittled just below lower critical temperature there is good correlation between transition temperature and ferrite grain size.

In regard to the authors' comment that the high temperature tempering treatment may influence the subsequent development of embrittlement at 900° to 1000°F (480° to 540°C), this has, in fact, been observed.[5] With an Ni-Cr steel quenched initially from 850°C (1560°F), the results given in Table V were obtained.

These results show that for this steel increasing the tempering time at 650°C (1200°F) from 1 to 50 hr only gives a slight increase in transition temperature due to ferrite grain growth, but that the same treatment has a very pronounced effect on the subsequent development of intergranular embrittlement at 500°C (930°F).

**Gopalkrishna Bhat** and **Joseph F. Libsch** (*authors' reply*)—Mr. Woodfine's interpretation of the authors' data leads to the same conclusions presented in the paper. For example, for the AISI 5140 steel two distinct regions of embrittlement occur: 1—just below the lower critical temperature and 2—in the region 800° to 1000°F, the two modes of embrittlement overlapping in the temperature range 1100° to 1150°F.

The authors object, however, to the use of a hardness vs transition temperature plot for interpreting these data, since this would in effect appear to relate the transition temperature to the hardness per se, while, in fact, Mr. Woodfine relates the embrittlement at 1200° to 1260°F to the basic structural change involving ferrite grain growth. Since this structural change is continuous with temperature and time, it would be expected that there would be a continuous change in hardness in the absence of noncontinuous structural changes having a marked influence on the transition temperature. As stated in the paper, an attempt to relate the hardness per se to the transition temperature over the whole range of isothermal embrittling temperatures (including 1000° to 900°F, etc., not shown by Mr. Woodfine) does not provide any definite relationship.

The authors are pleased to note that Mr. Woodfine's data indicate the influence of embrittlement just below the critical temperature upon subsequent embrittlement in the region 900° to 1000°F. More extensive experiments in the authors' laboratory, conducted in an effort to distinguish the two modes of embrittlement defined in the paper, likewise indicate a pronounced decrease in rate and degree of embrittlement at 900° to 950°F in an Ni-Cr steel after prior embrittlement just below the lower critical temperature.

## A Study of the Microstructure of Titanium Carbide

by Herman Blumenthal and Ronald Silverman

*DISCUSSION, H. H. Hausner and G. T. Horne, Chairmen*

**Claus G. Goetzel** (*Sintercast Corp. of America, Yonkers, N. Y.*)—The authors are to be congratulated on the fine piece of work they have done on such a difficult problem as the study of cemented titanium carbide. It is precisely the kind of investigation carried out by them which is needed to shed light on the very complex reactions and mechanisms involved in the sintering of this type of material.

The discusser would like to ask the authors several questions, the answers to which could possibly further help in understanding some of the findings reported. Why did they concentrate their work on a composition containing only 20 pct binder? Material of this type has been found to be extremely brittle and therefore of little interest as a possible material for commercial applications in jet engine blades and the like.

In the discusser's experience, the binder content also has some bearing on the microstructure and it would be interesting to compare such structures of low binder material with material prepared under identical conditions but containing binder phase in the order of 40 to 60 pct. Undoubtedly, the texture would show some difference. Not only would the spacing between the individual carbide grains be greater in general, but also the shape of the carbide grains may be different. The discusser has found that high binder materials generally tend to have more spheroidized titanium carbide grains. Such type of grains, in the discusser's opinion, would be more desirable for a commercial product because they would yield materials of greater ductility and mechanical and thermal shock resistance, thanks to a reduction of internal notch effects.

It is hard to bring into agreement the apparently porous nature of most of the micrographs shown by the authors with their statement that most of the specimens were virtually 100 pct dense. Is it possible that the dark areas which are predominant in some of the micrographs are not porous but graphite precipitates or inclusions?

There is also a question whether the coring reported is real or a relief effect. If the latter is true, there should be a hardness gradient apparent from the core of the grain to the case. Microhardness measurements, if possible on such a relatively fine grain size, would be most desirable as a means of finding at least a partial answer to this question.

Finally, it should be mentioned that experience with cemented titanium carbides and other cermets has shown that transverse rupture strength data are often misleading and much influenced by specific testing conditions. While room temperature transverse rupture

data are meaningful in such brittle materials as cemented tungsten carbide whose field of application lies at relatively low temperature levels, the same cannot be said for materials which are to perform at temperatures above 1600°F. A variant, the modulus of transverse rupture test at elevated temperatures, i.e., 1600° to 2000°F, is an improvement, since it gives information on the load-carrying capacity and deformability of the material at the higher temperature level. However, the method and rate of loading as well as the size of the specimens are critical, and greatly different properties can be established by varying the testing conditions. Thus, there is no reliable translation to short time tensile strength or stress-to-rupture tests, more conventional for high temperature alloys.

In addition to the desirability of having information on hot tensile strength and stress-to-rupture strength of materials of the type discussed in this paper, it is also of great importance that their capacity to take sudden stresses and shocks is known and related to their microstructure. Conventional impact tests have been scaled down to take into account the much lower impact properties of the cemented titanium carbides and related materials, as compared to superalloys in commercial use today. In view of the fact that the impact properties of the titanium carbide materials are much more sensitive to structural changes than, for example, the static stress-rupture properties, it would be most interesting to have the authors continue their fine work and establish a relation between the different effects noted in the microstructure with the impact strength of the material. It should be kept in mind that work of the type discussed in this paper must, by necessity, remain academic as long as it does not lead to a clear road to a marked improvement of the obvious shortcomings of this type of material for commercial applications in the high temperature field.

**John C. Redmond** (*Kennametal Inc., Latrobe, Pa.*)—The authors have presented an interesting study of the effect of some variables on the microstructure and properties of cemented titanium carbide compositions. However, it is to be regretted that the study was so limited as to the processing variables investigated and the criteria used to evaluate the effects of variables. The conclusions drawn cannot be applied to all titanium carbide-base cermets but are valid only for the narrow range investigated.

Titanium carbide-base cermets which have transverse rupture strengths in excess of 250,000 psi are now being produced commercially, whereas the authors refer to "the high transverse rupture strength of 179,000 . . ." for their specimens produced with titanium carbide material *B*. Even with the same material *A* used by the authors and the same chemical composition, viz, 20 pct Ni binder, strengths in excess of 200,000 psi are being obtained regularly. This indicates that many variables not investigated by the authors, such as final particle size of the ball-milled mix, pressing lubricant, and many other variables, as well as the effect of various binder compositions, have large effects. Thus, the results with the different titanium carbide materials might be in quite a different order of merit.

The transverse rupture strength was, in the early stages of cermet development, a satisfactory criterion for judging the merits of compositions. However, for many uses for which cermets are being considered, other factors are far more important. A very important property is impact resistance. For a given transverse rupture strength, threefold variations in impact strength have been observed and these variations have been found to be related to microstructure. High temperature strength, as measured, for example, by the stress-to-rupture test, is a necessity and can vary greatly with transverse rupture strength. All of these factors and more must be taken into account when evaluating titanium carbide-base cermets.

**Herman Blumenthal** and **Ronald Silverman** (*authors' reply*)—This paper is the offspring of a research project, the aim of which was to investigate the effect of raw material production variables on the properties of titanium carbide. Investigation of the influence of a variation in binder content was not within the scope of the project. The intention was to compare commercial grades of titanium carbide and determine their properties as functions of production procedure and chemical composition. For this reason, the initial pieces were made without any binder. When it was found that this was not feasible, first 10 and finally 20 pct binder were added. The latter amount was used as a standard composition in this investigation. This relatively low binder content was deliberately chosen in order not to cover up the characteristics of the original titanium carbide. A higher binder content might easily have leveled off those differences which the authors were eager to demonstrate. The fact that different grades of titanium carbide, with 20 pct binder, show different structures proves that this leveling off did not occur. Angular grains cannot be considered to be characteristic of 20 pct binder content; the authors found that pieces containing 40 to 60 pct binder did not always show spherical grains. Depending on the nature of the binder, these pieces showed either spherical or rectangular grains with rounded edges.

The preparation of specimens for microscopic investigations often leads to difficulties. Grinding and polishing were sometimes troublesome. During these operations, particles were often ripped out, causing the appearance of porosity in dense pieces. Densities were determined by water displacement or pycnometrically when the pieces were small. Chemical analyses showed little or no free carbon; the materials were very pure.

As far as coring is concerned, the authors are quite sure that this phenomenon is not a relief effect. Specimens were repolished and re-etched up to six times and the effect was still there. Furthermore, it always appeared in certain materials after certain treatments and never in others. Some micrographs show up to 10 pct of the total consisting of this condition. If this would be another phase and not titanium carbide, it should show up in X-ray patterns, which it never did. The suggestion to test the hardness gradient was considered but was given up as too time-consuming.

Transverse rupture strength was used as a representative physical property because it is so easy to determine and because it is very sensitive to changes in microstructure. There is no reason why another physical property could not be used instead if it is as sensitive to microstructure changes as is transverse rupture strength. It would be interesting to find out if similar relationships exist between microstructure and other properties, especially elevated temperature properties, such as the relationship shown between microstructure and transverse rupture strength. Such basic research is necessary in order to overcome the shortcomings of this type of material for commercial applications.

It must be admitted that, as far as processing variables are concerned, this investigation was quite limited. The aim was, however, to compare the products of various manufacturers under the same conditions. No claim was made that the conditions used were optimum conditions. Better physical properties were obtained by using the best conditions for each material. This, however, did not permit proper comparison. Such a determination of optimum conditions, while very valuable, would have involved an additional investigation for which there was not enough time.

The reason for using transverse rupture strength as a criterion has been explained before. From a commercial point of view, impact resistance of titanium carbide-base materials is undoubtedly more important, but the aim of this project was primarily to improve the basic understanding of this material. This paper does not attempt to give a final evaluation of the investigated grades of titanium carbide. For such a commercial evaluation, elevated temperature and impact tests would, of course, be necessary.

**Appreciation is gratefully acknowledged to the following organizations whose support has helped to make possible AIME's extensive publications program of metallurgical research:**

Allis-Chalmers Mfg. Co.
Aluminum Co. of America
American Brake Shoe Co.
American Iron & Steel Institute
American Metal Co. Ltd.
American Smelting & Refining Co.
American Zinc, Lead & Smelting Co.
Anaconda Co.
Battelle Memorial Institute
Bridgeport Brass Co.
Bunker Hill & Sullivan Mining & Concentrating Co.
Calumet & Hecla, Inc.
Cerro de Pasco Corp.
Clevite Corp.
Climax Molybdenum Co.
Consolidated Coppermines Corp.
Consolidated Mining & Smelting Co. of Canada Ltd.
Copper Range Co.
Crane Co.
Cyprus Mines Corp.
Dow Chemical Co.
Wilbur B. Driver Co.
Electro Metallurgical Co., div. of Union Carbide & Carbon Corp.
Engineering Foundation
Ford Motor Co.
Freeport Sulphur Co.
General Electric Co.
General Motors Corp.
Handy & Harman
Howe Sound Co.
Hudson Bay Mining & Smelting Co. Ltd.
International Nickel Co., Inc.
Kennecott Copper Corp.
Magma Copper Co.
P. R. Mallory & Co., Inc.
Mallory-Sharon Titanium Corp.
Metal Hydrides, Inc.
Miami Copper Co.
Molybdenum Corp. of America
National Lead Co.
New Jersey Zinc Co.
Newmont Mining Corp.
Noranda Mines, Ltd.
Phelps Dodge Corp.
Raytheon Mfg. Co.
Rem-Cru Titanium Inc.
Revere Copper & Brass Inc.
St. Joseph Lead Co.
Texas Gulf Sulphur Co.
Titanium Metals Corp. of America
U. S. Smelting, Refining & Mining Co.
Vanadium Corp. of America

# NUCLEAR METALLURGY

All the Papers at a Symposium
Conducted by

**INSTITUTE OF METALS DIVISION**
**AMERICAN INSTITUTE OF MINING AND METALLURGICAL ENGINEERS**

October 17, 1955

**Power Reactors** by Alvin M. Weinberg

**Problems in Materials for Nuclear Power** by John P. Howe

**Plutonium Metal** by E. R. Jette

**Physical Metallurgy of Thorium** by H. A. Wilhelm and B. A. Rogers

**Physical Metallurgy of Uranium** by Frank G. Foote

**Price: $3.75**

AIME 29 W. 39th St., New York 18, N. Y.

Please send me a copy of Nuclear Metallurgy. Enclosed is Check ☐; Money Order ☐ for $..... (AIME members may be billed.)

• AIME Members, 50% Discount on All Books.

Name .....

Address .....

City and Zone ..... State .....

Nonmember Foreign Orders, Add 30c for Mailing